The Functional Roles of pH-sensing G protein-coupled receptors in Intestinal Inflammation

by

Edward Joseph Sanderlin

November, 2018

Director of Dissertation: Li Yang, PhD

Department: Internal Medicine

The inflammatory microenvironment in inflammatory bowel disease (IBD) is complex, replete with microbial byproducts, complement, leukocytes, and resulting inflammatory cytokines. Parallel to these microenvironmental factors are protons, which are produced in excess due to altered metabolism of infiltrated leukocytes and local ischemia. Immune cells and intestinal microvasculature exist in the acidic, inflamed microenvironment and in turn alter their function in response to the acidic pH. Currently, only little is known how cells sense extracellular acidity and subsequently alter the inflammatory response. Recently, a class of proton-sensing G protein-coupled receptors (GPCRs) have emerged as functional pH-sensors, expressed in either leukocytes or vasculature, and are capable of altering immune cell inflammatory programs in response to acidic pH. These family members include GPR4, OGR1 (GPR68), TDAG8 (GPR65), and G2A (GPR132). Our group has uncovered a novel role for GPR4 in mediating endothelial cell (EC) inflammation in response to acidic pH. GPR4 activation in ECs have resulted in increased vascular adhesion molecule expression and functionally mediates leukocyte-EC interactions which are essential for the leukocyte extravasation process. Proton-sensors GPR65 and GPR68, however, are not expressed in ECs but are highly expressed in myeloid and lymphoid cells. GPR65 and GPR68, therefore, has been shown to mediate both pro- and anti-inflammatory responses in leukocytes in response to acidic pH. GPR132, however, has been described as a promiscuous GPCR, capable of responding to protons, bioactive lipids, and oxidized free fatty acids. Evidence suggests GPR132

is highly expressed in immune cells and plays important roles in immunity and the inflammatory response.

Several lines of evidence suggest loss of pH homeostasis is associated IBD and could correspond to the degree of inflammation. For these reasons we sought to investigate the functional roles of pH- sensors GPR4, GPR65, and GPR132 in the regulation of intestinal inflammation. We utilized the acute and chronic dextran sulfate sodium (DSS)- induced experimental colitis mouse model with GPR4-null, GPR65-null, or GPR132-null mice. Our results indicate GPR4 contributes to intestinal inflammation in both acute and chronic DSS-induced colitis models likely though mediating leukocyte infiltration into the intestinal mucosa. Furthermore, a novel GPR4 antagonist was capable of inhibiting acute intestinal inflammation, suggesting GPR4 could be a valuable therapeutic target in colitis. Conversely, GPR65 reduces intestinal inflammation in the chronic DSS-induced colitis model. *In vitro* studies using bone marrow derived macrophages suggest GPR65 regulates macrophage functions. Lastly, GPR132 genetic deficiency was evaluated in two generations of GPR132 knockout mice in intestinal inflammation. Our results suggest GPR132 functions to reduce intestinal inflammation in the DSS-induced colitis mouse model. Further studies need to be performed to fully evaluate the role and mechanism of GPR132 in intestinal inflammation.

Overall, this dissertation work highlights the emerging roles of pH-sensing GPCRs in the regulation of intestinal inflammation and implicates these receptors as valuable therapeutic targets in the remediation of intestinal inflammation.

The Functional Roles of pH-Sensing G protein-coupled receptors in Intestinal Inflammation

A Dissertation

Presented to the Faculty of the Department of Internal Medicine

East Carolina University

In Partial Fulfillment of the Requirements for the Degree

Doctor of Philosophy in Interdisciplinary Biological Sciences

Edward Joseph Sanderlin

November, 2018

The Functional Roles of pH-sensing G protein-coupled receptors in Intestinal Inflammation

by

Edward Joseph Sanderlin.

APPROVED BY:

DIRECTOR OF DISSERTATION: _____
Li Yang, Ph.D.

COMMITTEE MEMBER: _____
Yan-Hua Chen, Ph.D.

COMMITTEE MEMBER: _____
Mark Mannie, Ph.D.

COMMITTEE MEMBER: _____
Heng Hong, MD, Ph.D.

COMMITTEE MEMBER: _____
Kvin Lertpiriyapong, DVM, Ph.D.

COMMITTEE MEMBER: _____
Mary Jane Thomassen, Ph.D.

IDPBS BIOMEDICAL SCIENCE PROGRAM DIRECTOR: _____
Li Yang, Ph.D.

DEAN OF THE GRADUATE SCHOOL: _____
Paul J. Gemperline, PhD

DEDICATION

To my wife, Mallory Sanderlin. Also, to my loving parents Ed and Jackie Sanderlin. Finally, to my dear friends Kirk and Linda Burtch.

ACKNOWLEDGEMENTS

I would like to thank all current and former Yang lab members, as well as all collaborators for their careful and patient instruction and work. Particularly, thanks are deserved to Ivy Dong and Calvin Justus for their dedicated time to teach me basic laboratory techniques and bring me up to speed my first two years of this program. I would also like to thank Joani Zary for teaching and assisting in tissue sectioning, of which was a heavy work burden. Many thanks are deserved for Hematology and Oncology administrative assistants, namely Glenda and Delores, for providing so many needs of mine. Lastly, I wish to acknowledge the exceptional mentorship of Dr. Yang, who provided me daily instruction and helped frame my mind to think as a scientist. I am truly grateful I found your lab.

TABLE OF CONTENTS

LIST OF FIGURES

LIST OF ABBREVIATIONS

5-ASA	5-aminosalicylic acid
AAALAC	Association for Assessment and Accreditation of Laboratory Animal Care
AC	Adenylyl cyclase
APC	Antigen presenting cell
Arg1	Arginase 1
ASIC(s)	Acid-sensing ion channel(s)
ATF1	Activating transcription factor 1
ATF6	Activating transcription factor 1
Agr2	Anterior gradient protein 2 homolog
BCR-ABL	BCR-ABL fusion gene
BID	bis in die (twice a day)
BMDC	Bone marrow derived dendritic cell
BMDM	Bone marrow derived macrophage
C5a	Complement component 5a
cAMP	Cyclic adenosine monophosphate
CCL 2,5,7,20	C-C motif chemokine ligand 2,5,7,20
CD 3,4,8,18,45	Cluster of differentiation 3,4,8,18,45

CD11b	Cluster of differentiation b/c
cDNA	complementary DNA
CHOP	C/EBP Homologous Protein
CM	centimeter
CO_2	Carbon dioxide
COX-2	Cyclooxygenase-2
CrD	Crohn's disease
CREB	cAMP responsive element binding protein 1
CSF2	Colony stimulating factor 2
CX3CL1	C-X3-C motif chemokine ligand 1
CXCL1,2,3,6	C-X-C motif chemokine ligand 1,2,3,6
DAI	Disease activity index
DAPI	4′,6-diamidino-2-phenylindole
DC	Dendritic Cells
DMSO	Dimethyl sulfoxide
DNA	Deoxyribonucleic acid
DRG	Dorsal root ganglion
DSS	Dextran sulfate sodium salt

EAE	Experimental autoimmune encephalomyelitis
EC	Endothelial cell
EdU	5-ethynyl-2’-deoxyuridine
EPAC	Exchange protein activated by cAMP
ER stress	Endoplasmic reticulum stress
E-selectin	SELE
FBS	Fetal bovine serum
FDA	Food and Drug Administration
FIZZ1	RELM alpha
FOV	Field of view
Gα s,q,12/13	G protein alpha s,q,12/13
G2A	G2 accumulation
GALT	Gut-associated lymphoid tissue
GC	Germinal center
GFP	Green fluorescent protein
GM-CSF	Granulocyte-macrophage colony-stimulating factor
GPCR	G protein-coupled receptor
GPR4	G protein-coupled receptor 4

GPR65	G protein-coupled receptor 65 (TDAG8)
GPR68	G protein-coupled receptor 68 (OGR1)
GPR132	G protein-coupled receptor 132 (G2 accumulation)
GPR4 antagonist 13	NE 52-QQ57
GWAS	Genome-wide association study
H&E	Hematoxylin and eosin
HCO_3^-	Biocarbonate ion
HETEs	hydroxyeicosatetraenoic acids
HEV	High endothelial venule
HMVEC	Human microvascular endothelial cells
HMVEC-L	Human microvascular endothelial cells from lung
HODE	Hydroxyoctadecadienoic acid
HPAEC	Human pulmonary artery endothelial cells
HUVEC	Human umbilical vein endothelial cells
IBD	Inflammatory Bowel Disease
ICAM-1	Intercellular adhesion molecule 1
ICC	Immunocytochemistry
IFNγ	Interferon gamma

IgA	Immunoglobulin A
IgG2a	Immunoglobulin G2a isotype
IHC	Immunohistochemistry
IL- 1-6, 8-10	Interleukin - 1-6, 8-10
IL1A-B	Interleukin 1A-B
IL-12,17,21,22	Interleukin-12,17,21,22
ILF	Isolated lymphoid follicle
IMECs	Intestinal microvascular endothelial cells
IP3	Inositol triphosphate
IRE1	Inositol-requiring enzyme 1
IRES	Internal ribosome entry site
KO	Knockout
LFA-1	lymphocyte function-associated antigen-1
LPC	Lysophospatidylcholine
LPS	Lipopolysaccharide
M0	Naïve macrophage
M1	Classically activated macrophage
M2	Alternatively activated macrophage

MAdCAM-1	Mucosal vascular addressin cell adhesion molecule 1
MAPK	Mitogen-activated protein kinases
MCAFs	Medium-Chain Fatty Acids
M-CSF	Macrophage colony-stimulating factor
MG	Milligram
MLN	Mesenteric lymph node
mRNA	Messenger ribonucleic acid
NF-κB	Nuclear factor kappa-light-chain-enhancer of activated B cells
NK cells	Natural killer cells
NOD2	Nucleotide-binding oligomerization domain-containing protein 2
NS	Not significant
OGR1	Ovarian cancer G-protein-coupled receptor 1
ORMDL3	Orosomucoid like 3
PAMPs	Pathogen-associated molecular pattern
PBS	Phosphate buffered saline
PCR	Polymerase chain reaction
PDE4	Phosphodiesterase 4
PECAM-1	Platelet endothelial cell adhesion molecule

PERK	Protein kinase RNA-like endoplasmic reticulum kinase
pH	Power of hydrogen
PKA	Protein kinase A
PKC	Protein kinase C
PLC	Phospholipase C
PMN	Polymorphonuclear
PPRs	Pattern recognition receptors
P-selectin	SELP
PS-GPCR	Proton-sensing G protein-coupled receptor
PTGS2	Prostaglandin-endoperoxide synthase
qPCR	Quantitative real-time polymerase chain reaction
Rho	Ras homolog gene
RNA	Ribonucleic acid
ROCK	Rho-associated protein kinase
RORγT	Retinoic acid-related orphan receptor γT
shRNA	Short hairpin ribonucleic acid
SMAα	Smooth muscle actin-α
TDAG8	T cell death-associated gene 8

TGFβ	Transforming growth factor beta
Th1	T helper 1
Th2	T helper 2
Th9	T helper 9
Th17	T helper 17
TLR4	Toll-like receptor 4
TNBS	Trinitrobenzenesulfonic acid
TNFα	Tumor necrosis factor alpha
Treg	T regulatory cells
TRP	Transient receptor potential
UC	Ulcerative Colitis
UPR	Unfolded protein response
VCAM-1	Vascular cell adhesion protein-1
VLA-4	Very Late Antigen-4
WT	Wild type
XBP1	X-box binding protein 1

Chapter I: Introduction

Portions of this chapter are modified and reprinted from Cell Health and Cytoskeleton, 7, 99-109 (2015)

A. The Inflammatory Response

The inflammatory response is initiated for the removal of an infectious agent, in response to antigenic stimuli, or when there is injury to tissue. Once the inflammatory stimulus is recognized by the host, leukocytes are recruited to the site where the pathogenic agent resides and is subsequently removed. This process of removal is tightly regulated for the resolution of the inflammatory response followed the repair of damaged tissues and subsequent return of appropriate tissue functions.

These responses to inflammatory stimuli can be divided into two broad categories, namely the acute and chronic inflammatory response. The differences between the acute and chronic inflammatory response is largely due to both the duration and pathological features displayed during the inflammatory response. Acute inflammation predominately includes components of the innate immune system. The innate immune system provides a rapid-onset and nonspecific initial defensive response. These indiscriminate defensive mechanisms broadly include physical barriers to pathogens such as dermal tissues and mucosal barriers. Biochemical responses can also be employed such as complement and lysozyme. Vasculature in the inflammatory loci will also dilate resulting in inflammatory exudate containing soluble factors such as antibodies and complement for the dilution and removal of pathogens. Cellular constituents involved in the innate immune response include neutrophils, monocytes, macrophages, dendritic cells, and natural killer cells. Macrophages and dendritic cells are critical

during the innate immune response. Macrophages and dendritic cells are capable of recognizing distinct microbial patterns by pattern recognition receptors (PPRs) such as toll-like receptors (TLRs), NOD-like receptors (NLRs), and C-type lectin receptors (CLRs). TLR4 activation can result in the NF-κB intracellular signaling pathway which will result in the production of pro-inflammatory cytokines TNF-α, IL-1, and IL-6 [1, 2]. These pro-inflammatory cytokines initiate host defense mechanisms for the removal of pathogen. Provided the pathogenic insult is insufficiently cleared, the innate immune response will have served to mount and augment the adaptive immune response through the uptake of antigen by antigen presenting cells. In addition to mediating the innate response, macrophages and dendritic cells can provide the link between the indiscriminate innate immune response with a specific, highly efficient acquired immune response. These phagocytes uptake pathogen and process the antigen for the presentation to T-cells.

Naïve T-cells can develop, in part, to type I or type II CD4+ T helper cells. The T-cell subsets are characterized by the cytokines produced upon activation and are dependent on the inflammatory microenvironment during antigen stimulation [3-5]. Activated antigen presenting cells can secrete IL-12 and IL-18 which will progress naïve T-cells toward the T helper 1 (Th1) phenotype which will subsequently increase IFNγ and in turn augment macrophage pro-inflammatory and cytolytic CD8+ T cell function. Furthermore, Th1 cells will activate neutrophils through lymphotoxin secretion and also promote B cell production of IgG_{2a} which is involved in microbial complement binding and opsonization. Activated T cells will differentiate to Th2 cells when stimulated with IL-2 and IL-4 where the predominate effector cells are eosinophils, mast cells, and B-cells. Th2 cells will produce IL-4 and IL-13 which is involved in inhibiting the pro-inflammatory phenotype of macrophages through alternative activation.

Additional studies have provided new and comprehensive insights into $CD4^+$ T helper cell subsets. Studies found that naïve $CD4^+$ T cells in the presence of TGFβ and IL-6 can develop T cells which produce IL-17, IL-21, and IL-22 under the influence of the RORγ+ transcription factor and are subsequently termed Th17 cells [6-9]. Th17 cells have been implicated in many chronic inflammatory diseases such as rheumatoid arthritis, multiple sclerosis, psoriasis, and inflammatory bowel disease [9]. Collectively Th1, Th2, and Th17 are termed T effector cells and are central to the adaptive immune response for the removal of antigen. Furthermore, additional T cell subsets have been identified and include Th9 which secrete high levels of IL-9 [10-12].

However, continual inflammatory responses by these discrete inflammatory cell constitutes presents an unchecked inflammatory response which will result in tissue injury and subsequently impaired organ function if not regulated [13]. $CD4^+$ T cells can also differentiate into another T cell subset in the presence of TGFβ. This T cell subset has been shown to increase the secretion of IL-10, which has anti-inflammatory functions in adaptive immunity. IL-10 can downregulate the pro-inflammatory functions of Th1 cell activity, NK cells, and macrophages. Furthermore, IL-10 deficiency in animals has been associated with the development of autoimmune diseases. Additionally, this T cell subset increases the secretion of regulatory cytokine TGFβ. These cells are known as T regulatory cells and serve to suppress the inflammatory response for the maintenance of homeostasis [14, 15].

Having observed a rudimentary overview of the cellular basis of the inflammatory response, one critical step in the inflammatory response is getting the immune cells to the site of inflammation to exert these described functions. Without this process there will be no "response" provided by leukocytes to the inflammatory stimulus. This multistep process is critical for the

passage of neutrophils, monocytes, and T-cells to the sites of inflammation for the removal of pathogen. If host vasculature exists in injured or infected tissues then inflammatory mediators such as histimine, acidity, pro-inflammatory cytokines (e.g. TNFα), or pathogen associated molecular patterns such as LPS will activate endothelial cells (ECs) [16].

Activation of endothelial cells results in the movement of P-selectin from intracellular Weibel-Palade bodies to the luminal membrane surface. P-selectin will interact with the complementary leukocyte ligand P-selectin glycoprotein 1. P-selectin interaction with ligand will initiate the capture of the leukocyte to the endothelium and allow the subsequent rolling of the leukocyte along the venular endothelium. Another molecule expressed on the activated ECs is E-selectin which will bind to corresponding ligand ESL-1 on leukocytes. E-selectin mediates a slower rolling of captured leukocytes along the endothelium when compared to P-selectin. Rolling leukocytes will activate through the interaction of chemokine expression on ECs with the respective chemokine receptor expressed on the leukocyte. Next, VLA-4 and LFA-1 integrin expression on the rolling leukocytes will result in the firm adhesion to vascular cell adhesion molecule-1 (VCAM-1) and intercellular adhesion molecule-1 (ICAM-1) on ECs, respectively. Once the interaction occurs, the leukocytes are firmly adhered to the endothelium and will locomote to the junction between ECs for diapedesis to occur where CD31 (PECAM-1) is highest expressed. CD31-CD31 interactions between leukocytes and ECs will mediate the transmigration of the leukocyte between EC-EC junctions. The migrating leukocyte will then traverse the basal lamina where matrix metalloproteases will resolve the ECM facilitating leukocyte extravasation into the interstitial space [16-20] (Figure 1.1).

Taken together, the immune system is a tightly regulated and highly complex defense against infectious agents or damage to tissue. When in homeostasis, the immune response is

capable of both broad and targeted elimination of pathogenic stimuli followed by the appropriate resolution and the coordination of tissue repair. However, sometimes these processes can be frustrated, resulting in unchecked chronic inflammation as observed in numerous diseases of which include inflammatory bowel disease.

B. The Mucosal Immune System and Inflammatory Bowel Disease

The gastrointestinal tract has been described as an immunological wonder. The intestinal mucosa is the site of tightly regulated "physiologic" inflammation. The intestinal mucosal lumen comes into contact with antigen from commensal microorganisms and food derived protein. It is estimated 10^{12} commensal bacteria exist per milliliter of colonic content. The mucosal immune system is therefore involved in the process of distinguishing pathogenic bacteria from commensal microorganisms and foreign, non-harmful food proteins. The intestinal epithelial barrier serves as a physical barrier whereby energy-dependent absorption/secretion occurs and restricted passive movement of intestinal solute from the lumen to intestinal tissues. The epithelium also serves as a mediator of relative physical barriers which are distinct from cells and cellular junctions involved in intestinal homeostasis. These relative physical barriers are predominately developed from a variety of epithelial and subepithelial types [21]. These relative barriers include mucin secretion, secretory IgA, and HCO_3^- secretion at the luminal surface [22]. Intestinal mucin is involved in the aggregation of luminal bacteria for clearance as well as in the peristaltic movement of antigen loaded luminal content for removal. Secretory immunoglobulin IgA is involved in binding to pathogens and pathogenic antigen secretions for elimination.

The intestinal epithelium also serves as a barrier between luminal content and a compartment for the mucosal immune system. Immune cells are both scattered throughout the intestinal mucosa as well in highly organized compartments known as the gut-associate

lymphoid tissues (GALT). These secondary and tertiary lymphoid tissues include the mesenteric lymph nodes, Peyer's patches, and isolated lymphoid follicles (ILFs) and serve to mount inflammatory responses. Scattered immune cells are predominately located in the epithelium or lamina propria of the intestine. The predominate immune cell type in the intestinal epithelium are the intraepithelial cytotoxic T-cells. The lamina propria contains mostly macrophages, dendritic cells, mast cells, plasma cells, eosinophils, and high numbers of CD4+ and CD8+ T-cells. These effector T-cells and innate immune cells scattered throughout the epithelium and lamina propria are also kept in check through several tolerogenic mechanisms including the generation of T regulatory cells, lymphocyte anergy, and antigen experienced T-cell apoptosis [22-24].

Taken together, the intestinal epithelium barrier and mucosal immune system work in concert to prevent pathogenic organism infiltration and to maintain mucosal tolerance to harmless luminal antigen. However, some of these described functions of the mucosal immune system can be influenced by alternate environmental conditions, microbiota dysbiosis, and genetic factors resulting in a pathological intestinal immune response. These attributing factors, in conjunction with responding mucosal inflammation, have resulted in a chronic inflammatory disease localized in the gastrointestinal tract tissues which has been termed inflammatory bowel disease (IBD).

IBD can take two separate, yet distinct forms in the gastrointestinal tract. These two forms include Crohn's disease (CrD) and Ulcerative colitis (UC) [25]. CrD and UC can be distinguished by the localization of aberrant inflammation. CrD can affect any portion of the gastrointestinal tract from the mouth to rectum discontinuously. Furthermore, CrD is characterized by transmural inflammation. UC, however, is confined to the colon mucosa with particular disease activity in the rectum [26]. Clinical manifestations of IBD are based on the

disease severity and localization. Generally, gastrointestinal manifestations include severe abdominal pain, bloody mucoid stool, diarrhea, body weight loss, anemia, fever, and chronic fatigue. Currently, in the United States there are approximately 1-1.3 million people with IBD [27]. The incidence of CrD and UC is rising in prevalence and is higher in westernized countries as well as those of Caucasian and Ashkenazic Jewish origins [27]. UC is moderately higher in males, while CrD is slightly more frequent in females.

In addition to the common clinical manifestations from localized intestinal inflammation, IBD also displays extraintestinal manifestations of inflammation [28, 29]. The mouth, ocular, hepatobiliary, cutaneous, pancreatic, pulmonary, hematological, genitourinary, and musculoskeletal systems are sites of associated inflammatory disorders. Furthermore, patients with IBD are at higher risk for the development of colorectal cancer [30].

The etiology of IBD is currently unclear and the factors involved in disease onset are complex and multifactorial [31]. Simultaneous interactions between the environment, genetics, immune system, and microbiome appears to contribute to the development of IBD. Environmental factors such as diet, smoking, social stresses, and geography are correlated to disease development. Microbial dysbiosis has also been shown to contribute to the pathogenesis [25, 27, 32-34]. Pathological immune responses to normal flora or during dysbiosis can result in IBD. Some of these unchecked inflammatory responses are owing to genetic factors. Genome wide association studies (GWAS) have associated numerous genetic variants in distinct genomic loci with the susceptibility for IBD development. The IBD susceptibility gene candidates span a wide range of cellular and immunological processes. Genetic risk loci are associated with oxidative stress, ER stress, cell migration, intravesicular trafficking, apoptosis, immunological tolerance, lymphocyte regulation, epithelial barrier function, and innate mucosal immune cell

function [35-37]. Collectively, influences from environmental changes, genetics, and microbial diversity can contribute to a pathological inflammatory response from the mucosal immune system and disrupt the normal mucosal immune cell function equilibrium.

Innate immunity is involved in IBD pathogenesis. First, defects in the mucosal epithelial barrier can result in heightened permeability of luminal solutes and microbes into the lamina propria. As mentioned above, GWAS studies have implicated the epithelial barrier in IBD pathogenesis as genetic variants in genes involved in epithelial junction proteins (e.g E-cadherin and Zonula occuldens-1). Defective barrier functions have also been demonstrated in colonic biopsies of IBD patients [22, 38]. Innate immune cells such as macrophages, dendritic cells, and neutrophils are also involved. Macrophages and dendritic cells have been characterized from patients with IBD and shown to have heightened expression of pattern-recognition receptors (PPRs) such as TLRs and NOD-like receptors [32, 39, 40]. Interestingly, and not surprisingly, genetic risk loci for IBD include PPRs such as NOD2 and TLR4. In line with these observations, augmented secretion of pro-inflammatory cytokines such as IL-6, TNF-α, IL-12, IL-18, IL-23, and IL-1β are observed from macrophages and dendritic cells in the mucosa of IBD patients and can contribute to the stimulation of pathological adaptive immune responses in patients with IBD [32, 39, 40]. Under these distinct cytokine milieus observed in IBD tissues, antigenic stimulation of naïve T-cells by APCs can result in an imbalance of the Th1-Th2 paradigm. Reports have indicated patients with CrD have elevated levels of IFNγ and IL-2 which are indicative of a Th1 mediated adaptive immune response [41]. The Th1 mediated pro-inflammatory cytokines can further augment the innate immune cells, such as macrophages, for heightened inflammatory functions. Conversely, colon tissues from patients with UC have elevated levels of, IL-4, IL-5 and IL-13 which are indicative of a pronounced Th2 response [41]. Mucosal T-cells isolated

from UC patients displayed cytokine profiles associated with the Th2 cells. In line with these observations, CrD has classically been termed a Th1 mediated disease while UC was categorized as a Th2 condition [42]. More recent studies have provided further characterizations of effector T cell contribution to IBD. Elevated Th17 cells have been observed in colon samples from patients with both CrD and UC. The Th17 associated cytokine production has been reported to stimulate the inflammatory functions of infiltrated neutrophils as well as the promotion of Th1 differentiation. Some studies claim Th17 cells have an equally involved in both CrD and UC. However, the majority of studies seem to indicate Th17 mediated immunopathogenesis is more prominent in CrD and less in UC [6, 8, 9, 40].

As described above, much effort has been given to the investigation of mucosal barrier function and aberrant immune cell functions in IBD, however, significantly less effort has been given to the investigation of the intestinal microvascular contribution to the pathology of IBD. Vascular endothelial cells (ECs) regulate both the type and quantity of leukocytes migrating into tissues. As described above, a tightly regulated process is involved for the recruitment and migration of leukocytes into the intestinal tissues for the exertion of dysregulated IBD-associated characteristic inflammation. Intestinal microvascular endothelial cells (IMECs), therefore, are not passive participants in the disease progression. Numerous studies have characterized IMECs isolated from chronically inflamed intestinal tissues from patients with CrD and UC. These ECs have shown higher expression of cellular adhesion molecules such as VCAM-1 and MAdCAM-1 and subsequently result in enhanced leukocyte adherence *in vitro* and *ex vivo* [43-45]. Moreover, IMECs isolated from chronically inflamed intestinal tissues from patients with IBD displayed heightened expression of chemokine expression following IFNγ and TNF-α stimulation when compared to control IMECs [43-45]. These results have provided the intestinal microvasculature

as a central mediator contributing to intestinal inflammation through the hyper-adhesive phenotype observed. In addition to leukocyte adhesion aspects, IMECs have been shown to contribute to IBD pathology through enhanced angiogenesis, disorganized and defective vascular networks, increased coagulant potential, and vaso-occlusive phenomena [43-45].

In summary, IBD is a chronic inflammatory disease characterized by aberrant inflammatory responses in the mucosa of the intestine. These pathological inflammatory responses are owing to distinct cellular constituents involved in the dysregulation of the innate and adaptive immune system, among others. As our understanding of the immunopathogenesis of IBD has progressed, so too has our advancement in therapeutic intervention.

C. Therapeutic Landscape of IBD

As the exact etiology of IBD is unknown, there is no singular treatment that can cure IBD. As such, current therapeutic intervention for IBD predominately focuses on symptomatic improvement. Currently, conventional therapy for IBD includes 5-aminosalicylates (5-ASAs), steroids, and immunomodulating drugs [39, 46, 47]. 5-ASAs are front-line therapy for UC patients, however, CrD patients show a limited response. The mechanism of action of 5-ASAs are currently unclear, however, in order for 5-ASAs to be effective the agent must come in contact with the mucosal epithelium of the intestine. Corticosteroids are also utilized to induce remission of active IBD and have shown high effectiveness. However, corticosteroids are unable to maintain remission states and also provide adverse side effects during prolonged use such as life-threatening infection. Immunomodulatory drugs, namely Thiopurines and methotrexate are effective in both CrD and UC to achieve remission from active disease activity. These drugs, however, present significant potential for adverse effects as the mechanism of action centers on the impedance of DNA synthesis. More recently, non-conventional therapy has emerged.

Biologics, such as anti-TNF and anti-α4β7 antibodies have provided substantial progress in IBD therapy. Anti-TNF therapy is used for the induction of remission and maintenance for IBD by targeting a central pro-inflammatory cytokine to the immunopathology of IBD [48]. However, provided the advancements with this biologic, ~30% of patients do not respond to anti-TNF therapy and ~50% develop immunogenicity and lose responsiveness [48]. These patients often are initiated on anti-integrin (α4β7) which prevents leukocyte firm adhesion to MAdCAM-1 on intestinal microvascular endothelial cells.

The current therapeutic landscape is limited in scope and efficacy. Due to advances in our understanding of the immunopathogenesis of IBD, advanced treatment options have arisen for patients with IBD. However, these treatment options are not effective for all IBD patients, present significant adverse effects, and can result in reduced efficacy over treatment course as is observed in anti-TNF therapy. Additionally, chronic use of anti-TNF therapy has been associated with increased risk of lymphoma in some patients. Further investigation into the underlying mechanisms of IBD are warranted for the development of novel IBD therapeutics.

D. Acidosis, Inflammation, and IBD

A common and poorly investigated feature observed within the inflammatory loci and IBD is a loss of pH homeostasis. Immune cells, vascular endothelial cells, and therapeutic agents exist and function within the inflamed microenvironment and associated pH homeostasis loss. Understanding this central feature of the inflammatory microenvironment and implication in IBD pathogenesis is ideal for the further delineation of immune cell dysfunction and subsequent therapeutic development in response to acidic pH.

Cellular metabolism produces acid as a byproduct. Metabolism of each glucose molecule by glycolysis generates two pyruvate molecules. Under anaerobic conditions the metabolism of pyruvate results in the production of the glycolytic end product lactic acid, which has a pKa of 3.9. Lactic acid is deprotonated at the carboxyl group and results in one lactate ion and one proton at physiological pH. Under aerobic conditions pyruvate is converted into acetyl-CoA and CO_2 in the mitochondria. CO_2 in water forms a chemical equilibrium of carbonic acid and bicarbonate, an important physiological pH buffering system. The body must maintain suitable pH for proper physiological functions. Some regulatory mechanisms to control systemic pH are respiration, renal excretion, bone buffering, and metabolism [49-52]. The respiratory system can buffer the blood by excreting carbonic acid as CO_2 while the kidney responds to decreased circulatory pH by excreting protons and electrolytes to stabilize the physiological pH. Bone buffering helps maintain systemic pH by Ca^{2+} reabsorption and mineral dissolution. Collectively, it is clear that several biological systems require tight regulation to maintain pH for normal physiological functions. Cells utilize vast varieties of acid-base transporters for proper pH homeostasis within each biological context [53-56]. Some such transporters are H^+-ATPase, Na^+/H^+ exchanger, Na^+-dependent $HCO_3^-/C1^-$ exchanger, Na^+-independent anion exchanger, and monocarboxylate transporters. Cells can also maintain short-term pH homeostasis of the intracellular pH by rapid H^+ consuming mechanisms. Some such mechanisms utilize metabolic conversions that move acids from the cytosol into organelles. Despite these cellular mechanisms that tightly maintain proper pH homeostasis, there are many diseases whereby pH homeostasis is disrupted. These pathological conditions are characterized by either local or systemic acidosis. Systemic acidosis can occur from respiratory, renal, and metabolic diseases and septic shock [49-52, 57]. Additionally, local acidosis is characterized in ischemic tissues, tumors, and chronically

inflamed conditions such as in asthma, arthritis, and inflammatory bowel disease caused by deregulated metabolism and hypoxia [58-64].

Acidic pH is a main characteristic of the inflammatory loci as numerous studies have shown that local tissue pH below 7.0, and sometimes even below 6.0, is detected in inflammatory diseases and alters cellular functions [63, 65-68]. The acidic microenvironment in inflamed tissue is predominately due to the increased metabolic demand from infiltrating immune cells. These immune cells increase oxygen consumption and glucose uptake for glycolysis and oxidative phosphorylation. When oxygen availability is limited, cells often undergo anaerobic glycolysis. This process generates increasing amounts of lactic acid, thereby creating a local acidic microenvironment within the inflammatory loci [63]. However, there are other factors that can contribute to the acidic inflammatory loci. Neutrophils are often the first responders to the site of inflammation for the elimination of a pathogen owing to bacterial overgrowth. These bacteria can acidify the inflammatory microenvironment due to the accumulation of short chain fatty acids as microbial metabolic by-products [69, 70]. Neutrophils and macrophages can attempt to eliminate these harmful bacteria through respiratory bursts, which can further acidify the microenvironment. Indeed, dysregulated local pH is a hallmark of inflamed tissues.

As mentioned above, loss of pH homeostasis is linked to inflammatory bowel disease. In addition to the reduced interstitial pH observed in inflamed tissues, reports have indicated the colonic lumen of patients with IBD are more acidic when compared to the normal bowel. As patients with IBD commonly suffer from diarrhea, it was proposed patients with IBD would have reduced ventilation of CO_2 due to frequent bicarbonate loss. Several groups have investigated the luminal and peri-mucosal colon pH values from normal and IBD affected patients. The

radiotelemetric capsule method or oral tube mounted electrodes were used for the measurement of the luminal pH of the bowel. Normal median luminal pH values for proximal and terminal small intestine are ~6.7 and ~7.5, respectively. The ascending and descending normal colon median luminal pH values are ~5.88 and ~6.12, respectively. However, several reports have found the cecum/ascending colonic luminal pH is reduced during active colitis beyond what is observed under normal conditions [71-76]. One study showed patients with UC had luminal pH values as low as 2.3 and 3.4 [72]. Other reports showed a more moderate reduction of luminal pH between ~4.7 and ~5.5 [74]. These observations suggest the loss of pH homeostasis in IBD could be an indicator of IBD severity and occurrence. Some reports, however, have provided conflicting results. One group has reported that patients with active UC have elevated luminal pH values when compared to control [74, 75]. Further studies have claimed that there is no alteration in colonic luminal pH during active UC [77]. Regardless, the consensus seems to indicate loss of pH homeostasis in the intestine exists in IBD and might contribute to disease activity.

The reduced pH typical of inflamed tissue, and observed in active IBD, highlights a poorly understood mechanism of how leukocytes and non-immune cells in the inflamed acidic tissue microenvironment can sense changes in microenvironmental acidity and subsequently modulate their function. This provides a role for cellular pH sensing mechanisms in the regulation of intestinal inflammation.

E. Proton-Sensing (PS) GPCR Family Members

Acidosis is a stress for the cell and this stress commonly exists in the inflamed microenvironment. The ability of the cell to sense and modulate activity for adaptation to the stressful environment is critical. There are several mechanisms whereby cells sense acidosis and

modulate cellular functions to facilitate adaptation. Cells can detect extracellular pH changes by acid sensing ion channels (ASICs) and transient receptor potential (TRP) channels [78]. Apart from ASIC and TRP channels, extracellular acidic pH was shown to stimulate inositol polyphosphate formation and calcium efflux [79, 80]. This suggested the presence of an unknown cell surface receptor that may be activated by a certain functional group, namely the imidazole of a histidine residue. The identity of the acid-activated receptor was later unmasked by Ludwig et al as a family of proton-sensing G protein-coupled receptors (GPCRs). This group identified human ovarian cancer GPCR 1 (OGR1) which upon activation will produce inositol phosphate and calcium efflux through the G_q pathway [81]. These pH-sensing GPCR family members include GPR4, GPR65 (TDAG8), and GPR68 (OGR1). The proton-sensing GPCRs sense extracellular pH by protonation of several histidine residues on their extracellular domain. These receptors are capable of activation within the physiological pH range (7.32-7.42). However, peak activation of these receptors can occur between pH 6.4-7.0. The activation of these proton-sensing GPCRs facilitates the downstream signaling through the $G_{q/11}$, G_s, and $G_{12/13}$ pathways. GPR65, GPR4, and GPR68 have been shown to couple to the G_s and $G_{12/13}$ while GPR4 and GPR68 can also couple to $G_{q/11}$ (Figures 1.2-1.3)[82].

The family of pH-sensing GPCRs have distinct expression profiles. GPR4 is highly expressed in vascular-rich tissues such as the lung, liver, kidney, and soft tissues. In line with these observations, GPR4 is predominately expressed in vascular endothelial cells. Recent studies have shown GPR4 is also expressed in neurons of the retro-trapezoid nucleus (RTN) and white adipose tissue [82]. GPR65 expression is highest in leukocyte rich tissues like the spleen, bone marrow, and lymph nodes owing to the predominate expression in immune cells. GPR65 is expressed in both the myeloid and lymphoid derived cells. Recent studies have also provided a

role for GPR65 expression in neurons [82]. GPR68 is expressed broadly in various tissues such as lymph nodes, lung, and spleen. GPR68 has been investigated in the immune system as GPR68 is expressed in dendritic cells, macrophages, neutrophils, and T-cells. However, GPR68 is also expressed on and has regulatory functions in fibroblasts, dorsal root ganglia, osteoclasts, and cardiomyocytes [82].

Given the diverse expression of the pH-sensing GPCR family and distinct G-protein activation status, each member has been implicated in a variety of physiological systems. Studies have provided roles for GPR65 in respiratory (asthmatic inflammation), nervous (nociception and panic disorders), skeletal (bone resorption/density) and immune system (leukocyte inflammatory response). GPR68 has been studied in the cardiovascular (cardiomyocyte viability), renal (acid/base homeostasis), respiratory (inflammatory airway remodeling), gastrointestinal (intestinal homeostasis), skeletal (bone acid sensing), and endocrine (insulin secretion) systems. Furthermore, GPR4 has been investigated in the nervous (CO_2 chemosensing), endocrine (insulin sensitivity), renal (acid-base balance), cardiovascular (blood vessel stability and integrity), and immune system (endothelial inflammation) (Figure 1.3) [82]. As each member of these GPCRs are pH sensitive and are implicated in the immune system, this presents a role for the pH-sensing GPCR GPR65 (TDAG8) and GPR4 in inflammation and immune cell function (Figure 1.3). Further analysis of their role in the inflammatory response is warranted.

Similar, yet distinct from GPR65 and GPR4 is GPR132 (G2A or G2 accumulation). GPR132 is both highly and broadly expressed on immune cells yet is classified as a weak proton sensor [83]. This feature has caused many to exclude GPR132 from the pH-sensing GPCR family. Originally, GPR132 was identified as a DNA damage and stressed- induced GPCR that

was highly expressed on B cells and thymocytes [84]. Initial studies centered on the evaluation of GPR132 in tumorigenesis as GPR132 was identified as a BCR-ABL target gene [84]. GPR132 was consequently shown to function as a tumor suppressor though mediating cell cycle arrest and accumulation in the G2/M phase. Later studies found that aged GPR132 KO mice developed an autoimmune syndrome characterized by heavy leukocyte infiltration into numerous tissues [85]. Additionally, this study found GPR132 deficient T cells are hyperresponsive to TCR activation and subsequently had heightened T cell proliferation. Taking these two studies together, it could be proposed GPR132 regulates inflammation though the inhibition of cellular activation and proliferation. Even with the subsequent progressive understanding of the role of GPR132 in several cellular functions, there remains significant controversy over the endogenous ligands for GPR132. Lysophosphatidylcholine (LPC) was initially reported to have high affinity for the GPR132 receptor [86]. However, these data could not be reproduced, and the article was retracted. Additional studies suggested LPC mediates GPR132 signaling not through direct ligand binding to GPR132, but rather though redistribution of GPR132 membrane localization and intracellular sequestration [87]. Regardless, numerous studies have shown that there is a link between LPC and GPR132 activity. Further studies found GPR132 was a pH-sensitive GPCR after increased intracellular inositol phosphate could be observed when GPR132 was overexpressed [88]. Later studies, however, suggested GPR132 proton-sensing capabilities were dispensable when compared to family members GPR65, GPR4, and GPR68 [83]. These studies concluded GPR132 was an acid sensor, although weak. More recently, additional ligands have been identified for GPR132 of which include lactate, certain oxidized free fatty acids (9-HODE, 5-,8-,9-,15-HETE), and several bioactive lipids (LPC and commendamide) [89-93]. Many of

these endogenous ligands are present in the inflammatory loci and implicate GPR132 in the inflammatory response.

F. PS-GPCRs GPR4, GPR65, GRP68, and GPR132 in Inflammation

Numerous studies have shown GPR132 plays important roles in inflammation. As mentioned briefly above, an early study suggested GPR132 was involved in the maintenance of immune homeostasis by observing GPR132 KO mice developed a progressive late-onset autoimmune syndrome. Following this study, both pro- and anti-inflammatory roles have been provided for GPR132 in various immune cell populations. For example, GPR132 knockdown resulted in reduced chemotaxis of T lymphoid cells to LPC [94]. In an atherosclerosis mouse model, GPR132 provided a pro-atherogenic role as reduced atherosclerotic lesions were observed in the knockout mice [95]. However, GPR132 deficiency in monocytes have been shown to increase IL-1β, IL-6, and IL-8 in response to *Propionibacterium acnes* infection [96]. Furthermore, studies have shown GPR132 deficiency resulted in reduced efferocytosis of dying neutrophils [97], enhanced macrophage activation and accumulation in an atherosclerosis mouse models [95], reduced LPC mediated chemotaxis of macrophages to apoptotic cells [98], a late onset autoimmune syndrome in mice [85], and reduced M2 macrophage phenotypes in response to lactate [92]. Another study proposed GPR132 activity in the dorsal root ganglia (DRG) functioned to reduce inflammatory hyperalgesia and subsequently reduces inflammatory cell infiltration into inflamed tissues [99].

GPR65 was originally identified by cloning as an orphan GPCR which was observed to be upregulated during thymocyte apoptosis [100, 101]. It was demonstrated that GPR65 inhibited pro-inflammatory cytokine secretion, which includes IL-6 and TNF-α, in mouse peritoneal macrophages upon activation by extracellular acidification. This cytokine inhibition was shown

to occur through the G_s-cAMP-protein kinase A (PKA) signaling pathway [102, 103]. Treatment with dexamethasone, a potent glucocorticoid, increased GPR65 expression in peritoneal macrophages. Following dexamethasone treatment, there was an inhibition of TNF-α secretion in a manner dependent on increased expression of GPR65 [104]. Furthermore, a GPR65 agonist, BTB09089, was able to inhibit macrophage LPS-induced pro-inflammatory cytokine expression and anti-CD3 splenocyte stimulation [105]. Another study investigated the role of GPR65 and acidosis in microglia inflammatory responses [106]. GPR65 was shown to reduce IL-1β secretion through the G_s/cAMP/PKA pathway. Additional studies showed GPR65 deletion reduced myocardial infraction-induced inflammation through inhibiting resident macrophage secretion of CCL20, a chemokine for γδT cells [107]. Another study found genetic deletion of GPR65 reduced a type II collagen-induced mouse arthritis model [105, 108]. Furthermore, GPR65 deletion was investigated in the experimental autoimmune encephalomyelitis mouse model. The data showed GPR65 reduced disease severity presumably through invariant natural killer T cells [109].

However, other reports provide a pro-inflammatory role for GPR65 during inflammation. GPR65 was reported to increase eosinophil viability in the acidic microenvironment by reducing apoptosis through the cAMP pathway [110]. As eosinophils are central in asthmatic inflammation and allergic airway disease, GPR65 may play a role in increasing asthmatic inflammation. Notably, GPR65 appears to be involved in regulating Th17 pathogenicity. One paper demonstrated that the absence of GPR65 reduced the promotion of IL-17A cells *in vitro* [111]. Furthermore, this group reconstituted WT and GPR65 KO $CD4^+$ T-cells into RAG deficient mice and observed the loss of GPR65 in $CD4^+$ T-cells protected mice from experimental autoimmune encephalomyelitis (EAE). Another study analyzing transcriptome

signatures of Th17 cells involved in spondyloarthritis proposes GPR65 expression in Th17 cells likely contributes to enhanced GM-CSF expression and subsequent spondyloarthritis disease severity [112].

These studies demonstrate that the modulation of inflammation by GPR65 is complex and is highly relevant to cell type and biological context. GPR4, however, appears to regulate the inflammatory response primarily through the mediation of vascular endothelial cell activation. Endothelial cells compose blood vessels that often penetrate acidic tissue microenvironments, especially in the inflammatory loci. Among the pH-sensing GPCR family, GPR4 has the highest expression in endothelial cells. Several studies have demonstrated GPR4 can regulate EC inflammatory responses and has been presented as a key regulator for EC inflammatory responses in acidic tissue microenvironments [113, 114]. Our group has demonstrated in a variety of human endothelial cells that GPR4 can induce EC inflammation through upregulating pro-inflammatory cytokine production, adhesion molecule expression, and increasing monocyte-EC interaction in response to acidic stimulation. Microarray analysis revealed human umbilical vein endothelial cells (HUVECs) with endogenous (HUVEC/vector) or overexpressed (HUVEC/GPR4) GPR4 expression upregulated a variety of pro-inflammatory cytokines and chemokines (CXCL1, CXCL2, CXCL3, CXCL6, CX3CL1, CCL2, CCL5, CCL7, CCL20, CSF2, IL1A, IL8) when stimulated by acidic pH. Additionally, adhesion molecules such as E-selectin, VCAM-1, and ICAM-1 were also upregulated by GPR4 activation. Other genes in the TNF pathway, NF-KB pathway, and ER stress genes were shown to be regulated by GPR4. However, the distinct G-protein pathways involved in the regulation of these discrete target genes remain to be fully elucidated.

One key regulator of the inflammatory response is leukocyte recruitment to the site of inflammation through host vasculature, firm adhesion of leukocytes to the blood vessel wall, and leukocyte extravasation into the inflamed tissue. Our group demonstrated acidosis/GPR4 increases adhesion of leukocytes to ECs *in vitro* through a GPR4-dependent manner [113]. Taken together, acidosis/GPR4 increases expression of cytokines, chemokines, and adhesion molecules that subsequently increase EC-leukocyte adhesion *in vitro.*

Similar to GPR4 is GPR68 in that acidosis-induced activation results in enhanced inflammation. However, GPR68 is not reported to be expressed in endothelial cells as GPR4, but rather is expressed immune cells. Studies have shown that GPR68 contributes to macrophage and dendritic cell inflammation [82, 102, 115, 116]. Notably, GPR68 has been implicated in increasing intestinal inflammation through macrophage inflammatory programs [116, 117].

Altogether, the proton sensing GPCR family memebers provide differential regulation of the inflammatory response through mutual acid sensing capabilities. However, the role of acid sensing for GPR132 remains to be investigated. GPR65 and GPR132 predominately demonstrates function in the inhibition of the inflammation whereas GPR4 activation exacerbates inflammation through mediating leukocyte trafficking to sites of inflammation. As described previously, the chronic inflammation mediated by activated inflammatory cells and endothelial cells are two central features of the immunopathology of IBD and were initially delineated using a variety of animal models.

G. Murine Models for IBD Study

Murine models have been integral for the investigation of the underlying mechanisms and pathogenesis of IBD. The overall goal of IBD animal models is to closely mimic human IBD

pathology, however, no single animal model can achieve this feat. To-date, several classes of IBD animal models have been used complete with their subsequent advantages and disadvantages. There are several modes of induction of experimental IBD. These models broadly include chemical induction, genetic modification (e.g. IL-$10^{-/-}$), and adoptive transfer to an immunocompromised host (e.g. $CD45RB^{hi}$ to SCID or $RAG1^{-/-}$ mice) for the inducible or spontaneous development of intestinal inflammation [118]. However, chemical induction of experimental colitis is the most widely used approach owing to predictable disease induction that can be easily paired with genetically modified mice to evaluate the role of a certain gene in the immunopathology of colitis. The most common chemical agents used are dextran sodium sulfate (DSS) and trinitrobenzene sulfate (TNBS). DSS works to disrupt the intestinal epithelium for the allowance of luminal content (bacterial antigen and food proteins) to enter the mucosa and elicit both an innate and adaptive inflammatory response [119-122]. DSS-induced colitis is achieved by dissolving DSS, usually between 2-4% into the drinking water of mice. DSS is a sulfated polysaccharide that can link with medium-chain-length fatty acids (MCFAs) on the colonic epithelial mucosa and form nanometer-sized vesicles. These vesicles can bind to the colonic epithelial cells and reduce epithelial barrier functions and subsequently increase mucosal inflammation [119]. Depending on the duration and concentration of DSS given to mice, models for acute, chronic, and relapse have been developed. Clinical and histopathological features of DSS-induced colitis have similarities to human disease. Clinical manifestations of DSS-induced colitis include mouse body weight loss, fecal blood and diarrhea, and anaemia [123]. Histologically, defects in colonic crypt architecture and epithelium are observed. Similarly, inflammatory cell infiltration is observed in the laminal propria and submucosa results in crypt abscesses and inflammation resembling features of human IBD [123].

H. Rationale for the investigation of PS-GPCRs in Intestinal inflammation

The aims of this dissertation are to delineate the functional roles of proton sensing GPCRs (GPR4, GPR65, and GPR132) in the regulation of intestinal inflammation. As the pH-sensing GPCRs are expressed in the gastrointestinal system and reports have shown the colonic tissue pH is reduced is active IBD, we sought to investigate the roles of these receptors during intestinal inflammation.

Previous studies have provided a role for GPR4 in mediating a pro-inflammatory response of endothelial cells in response to acidic pH [113, 124]. Also, studies have described intestinal microvasculature, which exist in the acidic inflammatory loci, as a key regulator of intestinal inflammation though regulating leukocyte trafficking to the gut. Based on these data, we hypothesized that GPR4 contributed to the pathogenesis of IBD through increasing leukocyte extravasation into colon tissues. We further hypothesized that pharmacological inhibition of GPR4 would alleviate intestinal inflammation.

Once leukocytes get into the intestinal tissues, they too exist in and contribute to local acidification, which can in turn alter their function. GPR65 and GPR132 have shown high expression on these leukocytes and can subsequently modulate their inflammatory programs. Previous reports suggest GPR65 and GPR132 have a predominate immunosuppressive role in response to endogenous ligands. These described roles of GPR65 and GPR132 in inflammation implicate them in the regulation of dysregulated leukocyte inflammation in IBD. We hypothesized that GPR65 and GPR132 serve to dampen the leukocyte inflammation though reducing the pro-inflammatory functions of leukocytes.

To test our hypothesis, we utilized the acute and chronic DSS-induced colitis mouse models combined with GPR4 knockout (KO), GPR65 KO, and GPR132 KO mice. This dissertation work provides a novel role for the class of pH-sensing GPCRs in the regulation of abnormal mucosal inflammation commonly associated with IBD.

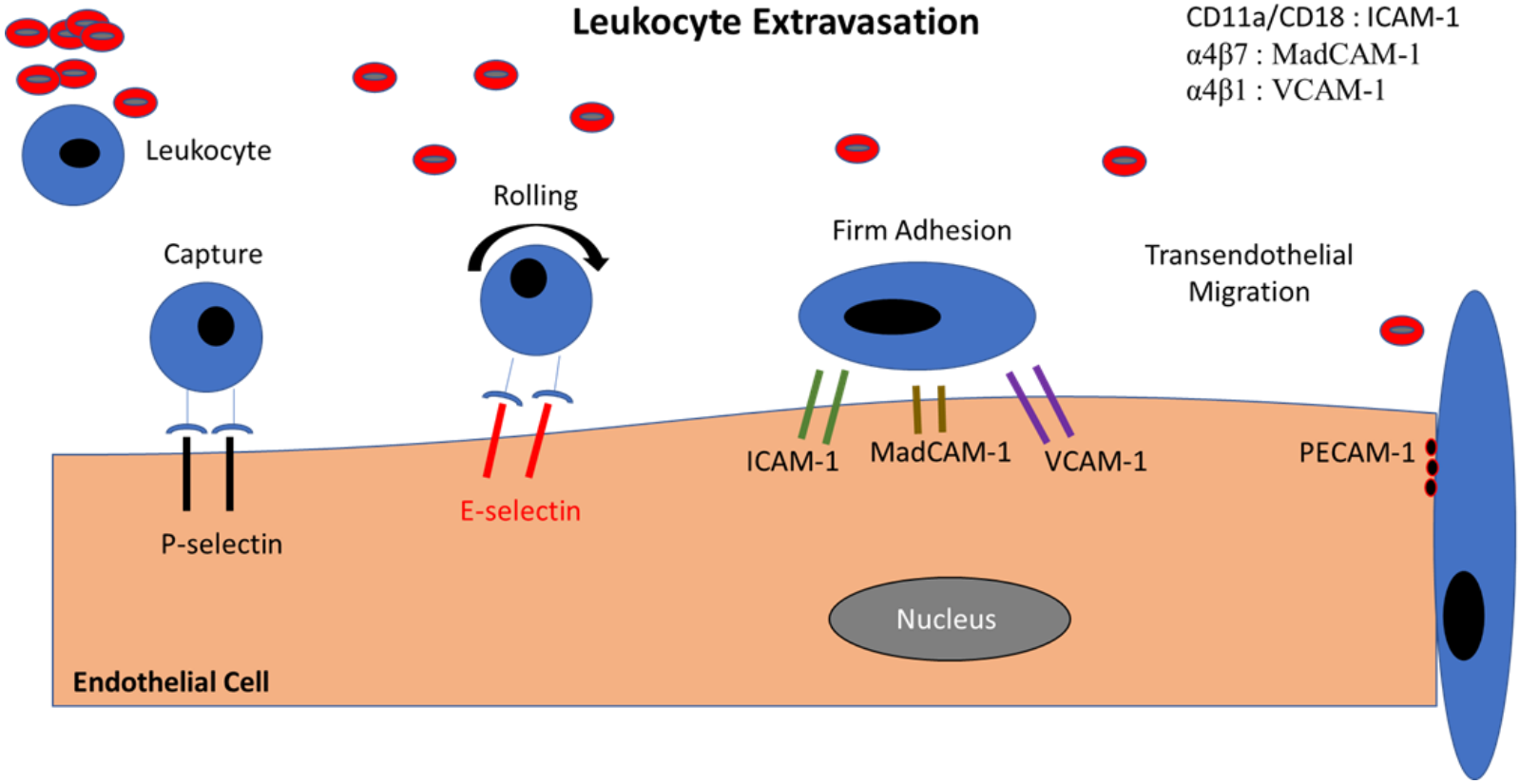
Leukocyte Extravasation
CD11a/CD18 : ICAM-1
α4β7 : MadCAM-1
α4β1 : VCAM-1
Leukocyte
Capture
Rolling
Firm Adhesion
Transendothelial Migration
P-selectin
E-selectin
ICAM-1
MadCAM-1
VCAM-1
PECAM-1
Nucleus
Endothelial Cell

Figure 1.1: A graphical representation of the leukocyte extravasation process.

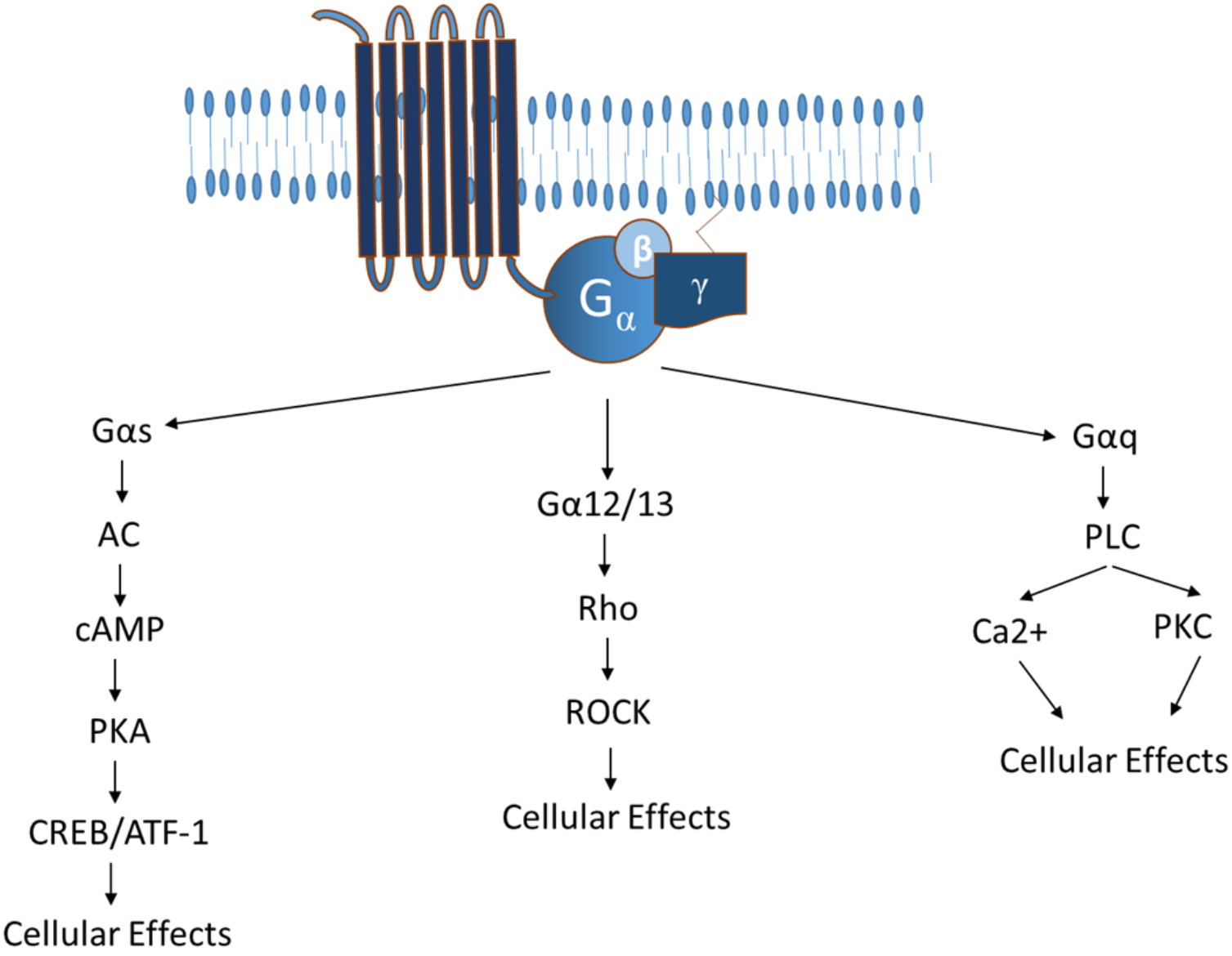
β
γ
Gα
Gαs
AC
cAMP
PKA
CREB/ATF-1
Cellular Effects
Gα12/13
Rho
ROCK
Cellular Effects
Gαq
PLC
Ca2+
PKC
Cellular Effects

Figure 1.2: A graphical representation of the G protein coupled receptor and their discrete signaling cascades of $G\alpha_s$, $G\alpha_q$, and $G\alpha_{12/13}$.

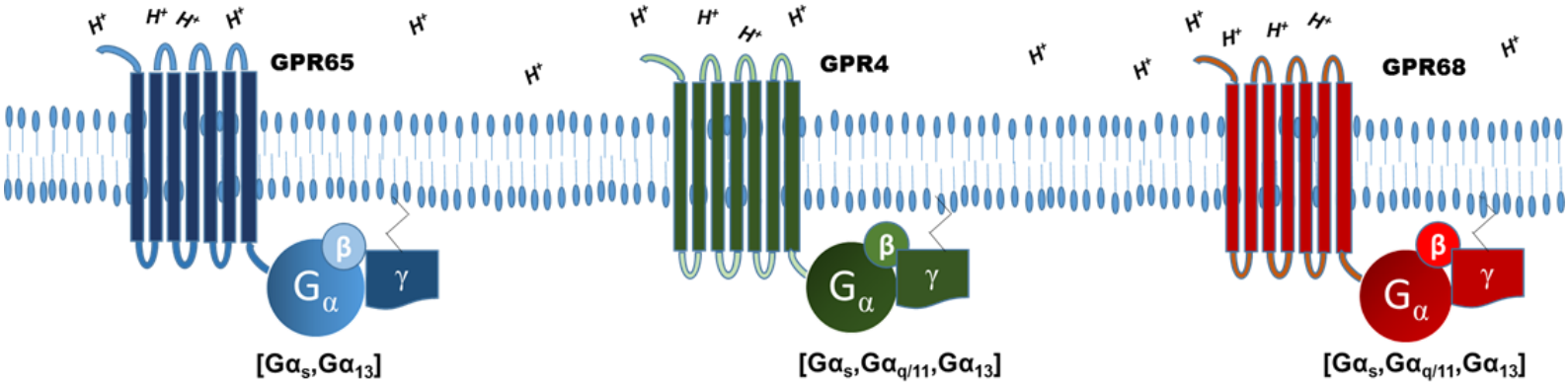

Predominately expressed in leukocytes	Predominately Expressed in Endothelial Cells	Predominately expressed in leukocytes
Immune System/Inflammation: Leukocyte inflammatory response **Respiration System:** Asthmatic Inflammation **Skeletal System:** Bone resorption/density **Nervous System/Nociception:** Hyperalgesia/Nutrient sensing/Panic disorders **Tumor Biology:** Tumor suppressing/promoting activities	**Immune System/Inflammation:** Endothelial inflammation **Cardiovascular System:** Blood vessel stability/integrity **Renal System:** Acid/base homeostasis **Nervous System/Nociception :** CO_2 chemosensing/blood pressure regulation/Hyperalgesia **Endocrine System:** Insulin sensitivity **Tumor Biology:** Tumor suppressing/promoting activities **Skeletal System:** Bone acid sensor	**Cardiovascular System:** Cardiomyocyte viability/vascular integrity **Renal System:** Acid/base homeostasis **Respiratory System:** Airway remodeling **Skeletal System:** Bone acid sensor/Enamel formation **Endocrine System:** Insulin secretion **Gastrointestinal System:** Intestinal homeostasis **Tumor Biology:** Tumor suppressing/promoting activities

Figure 1.3: A profile of the proton-sensing G protein-coupled receptors in each physiological system.

Chapter II: Materials and Methods

A. Summary

The functional role of the proton-sensing GPCRs were assessed by the chemical induction of acute and chronic experimental colitis using dextran sodium sulfate (DSS) in global GPR4, GPR65, and GPR132 knockout (KO) mice. KO mice were compared in all analyses to wild-type mice. Mouse clinical disease severity was assessed in conjunction with histopathological features of, and distinct cellular constituents contributing to, intestinal inflammation. Furthermore, molecular analysis was performed to evaluate the contribution of inflammatory gene and protein expression in colon tissues. Complementary to our approach for investigating the roles of the pH-sensing GPCRs in intestinal inflammation are our efforts to further delineate the effects of acidic pH-induced GPR65 activation. We evaluated the function of GPR65 activity in wild-type and GPR65-null bone marrow derived macrophages, bone marrow derived dendritic cells, and thymocytes *in vitro*. The methods employed in this dissertation work will provide a comprehensive analysis of colitis disease severity and illuminate potential contributions to inflammation by the proton-sensing GPCR family members in the experimental colitis mouse models.

B. Materials and methods contributing to the investigation of pH-sensing GPCRs in intestinal inflammation.

B.1. Dextran sodium sulfate (DSS)-induced acute and chronic experimental colitis mouse model

All experiments were carried out in 9 week old male and female wild-type, GPR4-deficient, GPR65-deficient, and GPR132-deficient mice. GPR4 deficient mice and wild-type

littermates were generated as previously described and were backcrossed into the C57BL/6 background for 11 generations [125]. GPR65-deficient mice were previously generated and backcrossed into the C57BL/6 background 9 generations [126]. Finally, G2A-deficient mice were generated as previously described and backcrossed 12 and 14 generations into the C57BL/6 background [85]. The mice were maintained specific pathogen-free of exogenous murine viruses, ectoparasites, endoparasites, and Helicobacter. Mice were housed in an Association for Assessment and Accreditation of Laboratory Animal Care (AAALAC)-accredited facility under environmental conditions of a 12:12 light/dark cycle, temperature maintenance at 22 ± 1°C and relative humidity range of 30-70%. Mice were group housed in microisolator caging on corncob bedding and provided tap water and pelleted diet (ProLab 2000, Purina Mills) ad libitum. Acute colitis was induced by the addition of 3% (w/v) Dextran Sulfate Sodium Salt (DSS) [36,000-50,000 M.Wt, Lot# Q1408, MP Biomedical] to drinking water. Mice were treated with 3% DSS or water for seven consecutive days, with a replenishment of 3% DSS or water every two days. For GPR4 antagonist 13 administration during acute chemical colitis induction, the small molecule was suspended in 0.5% methylcellulose/ 0.5% Tween 80/ 99% water. On day one, mice were orally gavaged with either vehicle or 30mg/kg GPR4 antagonist 13 (provided by Novartis) in the morning followed by addition of 3% DSS into the drinking water in the afternoon. On days two through six, mice were orally gavaged with vehicle or GPR4 antagonist 13 BID. On day seven mice were euthanized for tissue collection and macroscopic disease indicator measurement. For chronic DSS-induced colitis, mice drank 3% DSS solution or water ad libitum. To cycle between moderate and severe inflammation, mice were given 3% DSS in tap water or tap water alone for 4 cycles. Each cycle constituted 5 days of 3% DSS (severe inflammation) followed by 2 days of water (moderate inflammation). Following the fourth cycle,

water was switched back to 3% DSS for 2 final days. Mouse body weight and clinical phenotypic scores were assessed daily during the treatment period and tissue was collected at the end of the treatment period. Animal studies were performed according to the randomized block experimental designs that can increase the power and reproducibility [127]. All animal experiments were approved by the Institutional Animal Care & Use Committee of East Carolina University, Greenville, North Carolina and were in accordance with the Guide for the Care and Use of Laboratory Animals administered by the Office of Laboratory Animal Welfare, NIH.

B.2 Clinical phenotype scoring

Assessment of colitis severity was determined using the clinical parameters of body weight loss and fecal score. Each day stool was collected from mice and assessed for presence of blood and stool consistency. Fecal scoring system consisted of the following: 0= normal, dry, firm pellet; 1= formed soft pellet with negative hemoccult test, 2= formed soft pellet with positive hemoccult test; 3= formed soft pellet with visual blood; 4= liquid diarrhea with visual blood; 5= no colonic fecal content; bloody mucus upon necropsy. Presence of micro blood content was measured using the Hemoccult Single Slides screening test (Beckman Coulter).

B.3 Collection of tissue for histology and molecular analysis

After the acute or chronic treatment time course of DSS, mice were euthanized and the entire gastrointestinal tract was removed. The colon length was measured in centimeters from anus to ileocecal junction, then detached from the cecum. The colon was then washed with phosphate buffered saline (PBS) to remove fecal matter. Distal colon tissues were resected commencing from the anus and promptly snap frozen in liquid nitrogen for storage at a -80°C freezer for RNA analysis. The remaining colon tissue was fixed in 10% buffered formalin for

further histological analysis. The cecum was also cleaned of all fecal matter and fixed in 10% buffered formalin for histological studies. The mesenteric lymph nodes were isolated. The lymph nodes most proximal to the cecum were used for size measurement and histological analysis. Lymph node length (L) and width (W) were measured to calculate the volume of each lymph node using the formula $(L \times W^2)\ \pi/6$. Once the measurements were taken, the lymph nodes were fixed using 10% buffered formalin and processed for histological analysis. Spleens were collected and measured for weight.

B.4 Histopathological scoring

Five µm sections of colon and cecum tissue segments were stained with hematoxylin and eosin (H&E) for analysis. Two independent board-certified pathologists, with expertise in animal or human pathology, analyzed colon and cecum sections in a blind fashion. Pathologists analyzed and scored sections for histopathological features commonly observed in IBD tissues. Scoring criteria and methodology were conducted as previously reported with minor adaptations [128]. Each pathologist used complementary, yet distinct scoring systems for histopathological analysis. Briefly, the criteria used by the veterinary pathologist for histopathological changes included a scoring system from one to four, wherein a score of four was most severe. The veterinary pathologist assessed and scored the degree of inflammation, epithelial defects, crypt atrophy, epithelial hyperplasia, and dysplasia. Each cecum and colon section was assessed for each parameter and the sum of each parameter was presented as total histopathological score per mouse. The scoring criteria used by the human pathologists included the individual assessment of each parameter including inflammation, area of leukocyte infiltration, crypt damage, and edema. The score for each parameter was multiplied by a factor corresponding to the degree of overall intestinal tissue involvement. The sum of all parameters for each mouse provided the

total histopathological score. For in-house histopathological analysis, distal, middle, and proximal colon segments were evaluated by an operator blind to sample identification according to previously published criteria with minor modifications [129]. Briefly, each colon segment was evaluated in four recurring locations. Each location was evaluated for leukocyte infiltration, epithelial damage, and mucosal architecture distortions. The leukocyte infiltration score included severity scores of 1= mild, 2= moderate, and 3= severe with regard to both degree and location of cellular infiltrates. The mucosal architecture score included 1= focal epithelial erosions, 2= focal ulcerations, and 3= extended ulcerations. The sum score of these parameters represents the histopathological score of severity. In-house histopathological evaluation was performed under the oversight of trained pathologists. For the assessment of colonic fibrosis, colon segments were stained with picrosirius red and Masson's Trichrome stains for fibrosis analysis and graded for pathological fibrosis as previously described with minor adaptations under the supervision of pathologists.

B.5 Isolated lymphoid follicle quantification

Cecum and colon tissue was collected as described above and serial histological sections were stained with hematoxylin and eosin (H&E). Using a light microscope, cecum tissue sections were scanned using 4× and 10× objective lenses and isolated lymphoid follicles (ILFs) were counted. Colon sections were scanned from proximal to distal on longitudinal sections using 4× and 10× objective and ILFs were counted. The entire colon section was then measured in centimeters. ILF number is presented as ILFs per centimeter of colon section length. ILFs in the cecum are presented as ILFs per cecum in tissue sections.

B.6 Immunohistochemistry

Immunohistochemistry was performed on serial sections of 5-μm paraffin-embedded cecum, lymph node, and colon tissue sections. All colon, cecum, and mesenteric lymph node sections were de-paraffinized and hydrated from 100% ethanol to water followed by antigen retrieval using Tris-EDTA pH 9.0 with 0.1% Tween 20. Slides were incubated in antigen retrieval buffer for 18 minutes at 99 °C followed by blocking of endogenous peroxidase activity. Tissue sections used to analyze GFP expression in GPR4 KO, GPR65 KO and GPR4 heterozygous mice were incubated with primary goat polyclonal against green florescent protein (GFP) overnight at 4°C (Abcam, ab6673, 1:1000). The IHC system (Anti-goat HRP-DAB Cell and Tissue Staining Kit, R&D Systems, Minneapolis, MN) was used which employs a peroxidase-conjugated streptavidin as a colorogenic component. For the MAdCAM-1 (Abcam, 1:500, ab80680) antibody, the rat VECTASTAIN ABC HRP kit was used (Vector laboratories). For VCAM-1 (Abcam, ab134047, 1:100), E-selectin/CD62E (Abcam, ab18981, 1:1000), F4/80 (Invitrogen, 1:500, SP115), CD3 (Abcam, 1:1000) or αSMA (Abcam, 1:1000) either the Superpicture 3rd Gen IHC Detection system or rabbit VECTASTAIN Elite ABC HRP kit was employed. When the Superpicture 3rd Gen IHC Detection system was used, endogenous mouse IgG in blood serum was blocked using the Mouse on Mouse blocking reagent (Vector Laboratories, Burlingame, CA) followed by blockade with 10% normal serum. Tissues were incubated with primary antibodies overnight at 4°C and then recombinant secondary antibody incubation occurred followed by DAB (3,3'-diaminobenzidine). The rabbit VECTASTAIN Elite ABC HRP kit (Vector laboratories) was used according to the manufacture's protocol with the addition of AVIDIN/BIOTIN block (Invitrogen). Slides were then dehydrated and mounted.

Pictures were taken with a Zeiss Axio Imager A1 microscope or Zeiss AxioImager.M2 with Axiocam 503 digital color camera.

B.7 Immunocytochemistry

Wild type and GPR65 KO bone marrow derived macrophages (BMDMs) and bone marrow derived dendritic cells (BMDCs) were assessed for specific pan macrophage and dendritic cell markers, respectively. ICC was performed as previously described [113, 114]. Briefly, cells were fixed with 4% paraformaldehyde, permeabilized with PBS + 0.1% tween 20, and blocked with 10% normal serum. Primary antibodies specific for CD11b (1:500, MA1-10080) and CD11c (1:500, MA11C5) were incubated for 1hr at room temperature with either BMDMs or BMDCs, respectively. Cells were washed with PBS and incubated with secondary antibodies conjugated to Alexa Fluor 488 against the primary antibodies of respective host species. Nuclei was stained with DAPI. BMDM and BMDC purity was assessed by calculating the present positive cells for either CD11b or CD11c with respect to the total cell number per field of view.

B.8 Mucosal inflammatory Cell Quantification for the DSS-induced colitis mouse model

Colon tissue sections were randomly selected from WT-DSS, GPR65 KO-DSS, and GPR4 KO DSS mice. The absolute numbers of polymorphonuclear neutrophils, F4/80- positive macrophages, CD4-positive T cells, CD8-positive cells, myofibroblast α-SMA, and CD3-positive T cells were counted from high-power (400× magnification) pictures taken from 5-10 random fields per distal colon section in a blind manner as previously described [128]. Neutrophils were quantified by their distinct polymorphonuclear morphology by H&E staining under guidance of board certified pathologists (H.H. and Q.C.). Distinct cellular constituents

quantified are indicated in figure legends. ImageJ software was utilized for counting of cells per high power field of view (FOV).

B.9 Blood vessel VCAM-1 and E-selectin intensity score and MAdCAM-1 positive vessel enumeration

After IHC was performed for VCAM-1 and E-selectin on colon tissue segments, VCAM-1 and E-selectin intensity was blindly assessed by two independent operators from distal, middle, and proximal segments. Scoring criteria included 1= none/minimal, 2= mild, 3= moderate, and 4= high signal intensity. Each tissue segment was completely evaluated using 10x and 20x objectives and subsequently scored for intensity. For MAdCAM-1 positive vessel enumeration, vessels were assessed from the distal, middle, and proximal colon segments and total MAdCAM-1 positive vessels were counted using 10x and 20x objectives. The total colon length was recorded in centimeters and results were shown as MAdCAM-1 positive vessels/centimeter.

B.10 Real-time RT-PCR and Western blotting

Total RNA and protein was isolated using the IBI Scientific DNA/RNA/Protein Extraction Kit (MidSci) and 500-1000ng of RNA were reverse transcribed using SuperScript II or Superscript IV reverse transcriptase (Invitrogen, Waltham, MA) and quantified using Nanodrop. TaqMan pre-designed primers-probe sets specific for target gene (Applied Biosystems) were used and are listed (Figure 2.1). Real-time PCR was performed in duplicate with a program of 50°C for 2 min, 95°C for 10 min followed by 40 cycles of 95°C for 15 sec and 60°C for 1 min, and the data was acquired and analyzed using the ABI 7300, ABI 7900HT, or QuantStudio 3 Real-Time PCR system. Data was analyzed using the $2^{-\Delta Ct}$ method or expression relative to control samples. The crohn's and colitis cDNA arrays were purchased from Origene

Technologies (catalog #CCRT102) and subjected to real-time PCR using specific primer-probes for human GPR4, GPR65, and β-actin. The primer and probe used for human GPR4 has been previously described [113, 114]. The cDNA array contained 47 samples including 7 normal, 14 Crohn's, and 26 ulcerative colitis intestinal samples from patients diagnosed with IBD. All de-identified sample information can be obtained through Origene Technologies (http://www.origene.com/qPCR/Tissue-qPCR-Arrays.aspx) and are published as a supplemental table (Supplementary Table 2) [128]. Following protein extraction, protein concentration was determined using the DC Protein Assay (Bio-Rad). The protein was separated by gel electrophoresis using 4-12% SDS-PAGE Bis-Tris Gels (Invitrogen). Protein was then transferred to a nitrocellulose membrane followed by probing with polyclonal goat IgG anti-mouse VCAM-1/CD106 (R&D Systems, #AF643). Protein expression of phosphorylated CREB and ATF-1 was assessed by western blot analysis and normalized to β-actin. Protein lysate was collected using RIPA lysis buffer supplemented with protease/phosphatase inhibitors and quantified using the Bradford assay. Western blot was performed as previously described above. The expression of phosphorylated phospho-CREB/AFT1 (Cell Signaling, #9197,) and β-actin (Cell Signaling, #4970) was analyzed by Western blotting and horseradish peroxidase (HRP)- conjugated secondary antibodies. Chemiluminescence signals were detected using the Amersham ECL Advance Western blotting detection kit. The western blot bands were subsequently quantified by densitometry using the imageJ software.

B.11 Bone marrow progenitor cell Isolation and differentiation

Wild-type and GPR65 KO mice ranging from 6-12 months of age were utilized to isolate thymocytes and collect bone marrow for macrophage and dendritic cell differentiation. Thymocytes were isolated from the thymus by gentle homogenization into RPMI media followed

by lysis of the red blood cells as previously described in detail [126]. Bone marrow derived macrophages (BMDMs) and dendritic cells (BMDCs) were differentiated from bone marrow progenitor cells as previously described [130-132]. Briefly, bone marrow was collected from the tibia and femur of WT and GPR65 KO mice and were differentiated into macrophages by culturing in 15% L-929 cell conditioned medium for seven days or dendritic cells by culturing in the presence of recombinant mouse GM-CSF for 6 days. BMDMs and BMDCs were cultured and assessed for purity based on distinct morphology and CD11b and CD11c expression, respectively. BMDMs and BMDCs were frozen in liquid nitrogen for further experimentation. Naïve BMDMs (M0) were either classically activated (M1) or alternatively activated (M2). Briefly, classical activation was achieved by the addition of 100ng/ml LPS and 50ng/ml IFNγ for 24hrs. Alternative activation occurred though the addition of 10ng/mL IL-4 for 24hrs.

B.12 *In vitro* pH treatments

Following the collection of thymocytes from the thymus gland, thymocytes were then suspended in RPMI media buffered to pH 7.4 or 6.4 for 3hrs to assess gene expression changes or 30min for western blot assessment of CREB/ATF-1 phosphorylation. BMDMs were cultured for 24hrs after thawing from liquid nitrogen to allow recovery. Naïve macrophages were then treated with DMEM media buffered to pH 7.4 and 6.4 for 3hrs to assess gene expression or 30min for CREB/ATF1 phosphorylation assessment by western blot. To assess gene expression changes in M1 and M2 BMDMs, cells were fully polarized to M1 and M2 for 24hrs and were treated with DMEM media buffered to pH 7.4 and 6.4 for 5hrs. BMDCs were treated for 3hrs in RPMI media buffered to pH 7.4 or 6.4 for 3hrs.

B.13 Cellular proliferation assay

WT and GPR65 KO BMDMs were cultured in macrophage conditioned medium (MCM) containing DMEM 10% FBS + 10ng/mL mrM-CSF for 24hrs. MCM was then removed and MCM buffered to pH 7.4 or 6.4 was added and BMDMs were incubated for 20hrs. Cells were then pulsed for 4hrs with EdU in pH-adjusted MCM using the Click-it EdU cellular proliferation kit. BMDMs were subsequently fixed, permeabilized, and labeled for EdU detection according to manufacturer's instructions for the Click-it EdU assay (Invitrogen). Nuclear localization was achieved by Hoechst staining. Representative pictures were taken from 5-10 locations with a 20x objective for the co-localization of Hoechst and EdU nuclear signal. Total cells were counted followed by total EdU positive cells from each field of view and the percent of proliferating cells were quantified using imageJ software.

B.14 Transwell migration assay

The cellular Transwell migration assay was performed as previously described with minor modifications [133]. Briefly, WT and GPR65 KO BMDMs were suspended in migration medium buffered to pH 7.4 or 6.4 at 1x10^6 cells/mL. 1x10^5 cells were added to the upper chamber of the Transwell insert and incubated at 5% CO_2 for 20 minutes. 600uL of migration medium buffered to pH 7.4 or 6.4 with or without 5ng/mL C5a was added to the lower chamber followed by 3hrs of incubation in 5% CO_2 atmosphere. Adherent cells attached to the bottom of the Transwell membrane were fixed in methanol and stained with DAPI solution. Five pictures were taken of the membrane with a 10x objective and migrated cells were quantified by counting DAPI signal using imageJ software.

B.115 Statistical analysis

All statistical analysis was performed using GraphPad Prism software. The unpaired t-test or Mann-Whitney test was used to compare differences between two groups. Correlation of gene expression was determined by the linear regression analysis. When comparing three or more groups with one independent variable the one-way ANOVA was used. When comparing three or more groups with two independent variables, the two-way ANOVA was used. The one-way or two-way ANOVA was followed by either the Tukey, Newman-Keuls, or Bonferroni post hoc tests. All statistical analysis performed is indicated in the figure legends. All comparisons are considered statistically significant where * $P < 0.05$, ** $P < 0.01$, and *** $P< 0.001$.

Gene	Species	TaqMan Assay ID
18S	Human	Hs99999901_s1
β-actin	Human	Hs01060665_g1
GPR65	Human	Hs002692477_s1
GPR65	Mouse	Mm02619732_s1
GPR68	Mouse	Mm01335275_m1
GPR4	Mouse	Mm00558777_s1
IL-1β	Mouse	Mm00434228_m1
TNF-α	Mouse	Mm00443258_m1
IL-6	Mouse	Mm00446190_m1
PTGS2	Mouse	Mm00478374_m1
IL-10	Mouse	Mm01288386_m1
CXCL2	Mouse	Mm00436450_m1
VCAM-1	Mouse	Mm01320970_m1
E-selectin	Mouse	Mm00441278_m1
ICAM-1	Mouse	Mm00516023_m1
MAdCAM-1	Mouse	Mm00522088_m1
Arginase 1	Mouse	Mm0047988_m1
FIZZ1	Mouse	Mm00445109_m1

Figure 2.1: A list of TaqMan primer-probe assays for gene expression studies.

Chapter III. The Role of GPR4 in the Regulation of Intestinal Inflammation

Portions of this chapter are modified and reprinted from Biochimica et Biophysica Acta - Molecular Basis of Disease, 2, 569-584 (2017).

A. Summary

GPR4 is a proton-sensing G protein-coupled receptor that can be activated by extracellular acidosis[113, 134, 135]. It has recently been demonstrated that activation of GPR4 by acidosis increases the expression of numerous inflammatory and stress response genes in vascular endothelial cells (ECs) and also augments EC-leukocyte adhesion [113, 114]. Inhibition of GPR4 by siRNA or small molecule inhibitors reduces endothelial cell inflammation. As acidotic tissue microenvironments exist in many types of inflammatory disorders, including inflammatory bowel disease (IBD), we examined the role of GPR4 in intestinal inflammation using a dextran sulfate sodium (DSS)-induced acute and chronic colitis mouse model. We observed that GPR4 mRNA expression was increased in mouse and human IBD tissues when compared to control intestinal tissues. To determine the function of GPR4 in intestinal inflammation, wild-type and GPR4-deficient mice were treated with 3% DSS for the development of acute or chronic colitis. Finally, We have assessed the function and efficacy of a GPR4 antagonist, 2-(4-((2-Ethyl-5,7-dimethylpyrazolo[1,5-a]pyrimidin-3-yl)methyl)phenyl)-5-(piperidin-4-yl)-1,3,4-oxadiazole (GPR4 antagonist 13, also known as NE 52-QQ57), within the colitis disease indication as a potential therapeutic for the remediation of intestinal inflammation. Our results showed that the severity of colitis was decreased in GPR4-deficient DSS-treated mice in comparison to wild-type DSS-treated mice in both the acute and chronic models. Clinical parameters, macroscopic disease indicators, and histopathological features were less severe in the DSS-treated GPR4-deficient mice than the DSS-treated wild-type mice. Histopathological

damage, leukocyte infiltration, and isolated lymphoid follicle (ILF) formation were reduced in intestinal tissues of DSS-treated GPR4-null mice. Finally, GPR4 antagonist 13 reduced disease severity and inflammation in mice when compared to vehicle control. Collectively, our results suggest GPR4 provides a pro-inflammatory role in the inflamed colon as the absence or pharmacological inhibition of GPR4 ameliorates intestinal inflammation in the DSS-induced experimental colitis mouse model.

B. Introduction

The pH-sensing G protein-coupled receptors (GPCRs) have emerged as a new class of receptors that are involved in sensing both local and systemic pH changes. Subsequently, these receptors have been implicated in various disease states and conditions associated with dysregulated pH homeostasis such as cancer, ischemia, metabolic acidosis, and inflammation [82, 135-137]. Family members of the pH-sensing GPCRs include GPR4, TDAG8 (GPR65), and OGR1 (GPR68). These receptors are capable of sensing protons in the extracellular milieu by the protonation of several histidine residues on their extracellular domains[81, 83, 138]. GPR65 and GPR68 are predominately, though not exclusively, expressed on leukocytes and provide various roles in the exacerbation or amelioration of a diverse set of diseases associated with inflammation and acidosis. GPR4, reciprocally, is highly expressed in vascular endothelial cells (ECs) and blood vessel rich tissues such as the lung, kidney, heart, and liver. Recently, GPR4 has been shown to mediate EC inflammatory responses to acidosis and is central for leukocyte-endothelium interaction.

In response to extracellular acidosis (increased extracellular proton concentration), GPR4 has been reported as a pro-inflammatory mediator in a variety of ECs [113, 114]. Both isocapnic and hypercapnic acidosis have been demonstrated to activate GPR4 and induce an inflammatory response in three types of primary endothelial cells, including human umbilical vein endothelial

cells (HUVECs), human pulmonary artery endothelial cells (HPAECs), and human lung microvascular endothelial cells (HMVEC-Ls) [113, 114]. The GPR4 mediated inflammatory response to acidosis encompasses the induction of adhesion molecules such as E-selectin (SELE), vascular cell adhesion molecule 1 (VCAM-1), and intercellular adhesion molecule 1 (ICAM-1) in ECs and subsequently increases the functional adhesion of leukocytes *in vitro*. In addition to adhesion molecules, GPR4 activation in ECs increases the expression of chemokines such as CCL20, CXCL2, and IL-8 (CXCL8) involved in the recruitment and activation of leukocytes [113]. Furthermore, GPR4 activity stimulates the induction of COX-2, NF-κB pathway genes, and stress responsive genes in ECs under acidic conditions [114]. These results collectively describe GPR4 as pro-inflammatory through increasing leukocyte-EC adhesion and subsequent extravasation into inflamed tissues. Therefore, GPR4 could potentially provide a role in the inflammatory response for host defense and the removal of pathogens or apoptotic cells in various tissues by the recruitment of leukocytes. If inflammation is not properly resolved, however, GPR4 could exacerbate inflammatory disorders.

Recently, a family of imidazo pyridine derivatives has been identified as exhibiting anti-inflammatory functions in ECs by reducing pro-inflammatory cytokine secretion, adhesion molecule expression, and leukocyte-EC adhesion through the inhibition of GPR4 [113, 114, 139]. In addition to chemical antagonists of GPR4, similar results were observed with use of siRNA inhibitors specifically targeting GPR4 expression [113]. Moreover, it has been shown that the expression of the GPR4 gene can be increased in ECs by inflammatory stresses such as cytokines (TNF-α) and reactive oxygen species (H_2O_2), which commonly exist in inflammatory bowel disease [140].

Inflammatory bowel disease is characterized by chronic, aberrant mucosal inflammation of the gastrointestinal tract [26]. There are two distinct disease subsets in which IBD can take form, namely, Crohn's disease (CrD) and ulcerative colitis (UC). The exact etiology of IBD is unknown, but a complex interaction between immunologic, environmental, microbiome, and genetic constituents is believed to contribute to the disease onset and continued progression. Both CrD and UC have distinct, yet overlapping clinical and histopathological features that are a result of altered mucosal homeostasis. The production of cellular metabolic byproducts contributes to an acidic inflammatory mucosal loci in IBD [63]. Indeed, an acidic inflammatory microenvironment is a hallmark of chronically inflamed tissue as numerous studies have shown that local tissue pH below 7.0, and sometimes even below 6.0, is detected in inflammatory diseases and alters cellular functions[62, 63, 66, 67, 141-143]. In addition to tissue acidosis in the gut, reports indicate that the lumen of the colon is more acidic in patients with IBD than patients without IBD [72-74, 76, 144]. As a result, host vasculature, leukocyte infiltrates, and stromal cells often function within an acidic tissue microenvironment and can in turn modulate the inflammatory response.

Inflammation in IBD is a conglomerate of gut associated pathologies, but one particular pathological hallmark is a hyper-dysregulated vascular inflammatory response in the gut [145]. Host vasculature is critical in mediating the extent of inflammation and subsequent tissue damage resulting from chronic inflammation. The inflammatory response requires the active passage of leukocytes such as neutrophils, monocytes, and lymphocytes to the site of inflammation through host vasculature. EC adhesion molecules and chemokines facilitate leukocyte complementary binding for firm adhesion and subsequent extravasation from the blood vessel wall into tissue. The endothelium therefore functions as a gate; either barring or

allowing the passage of inflammatory cells into inflamed tissue. Modulating the passage of leukocytes into tissue is an ideal target for IBD therapy. Currently, anti-adhesion biologics such as natalizumab and vedolizumab are used in the clinic for IBD patients [146]. Even though anti-adhesion therapies have proven efficacious in the clinical remission of IBD, there have been some limitations reported. For example, cases of progressive multifocal leukoencephalopathy (PML) have been observed in patients treated with natalizumab [147].

We hypothesize that endothelial GPR4 expression functions as a "gatekeeper" in regulating the extent of leukocyte infiltration into the inflamed colon. In this study, we observed that GPR4 mRNA expression was increased in the inflamed colon of human IBD samples as well as in a DSS-induced experimental colitis mouse model. GPR4 genetic deficiency and pharmacological inhibition reduced inflammation parameters such as clinical phenotype, histopathological score, leukocyte infiltration, ILF development, and adhesion molecule expression in vascular endothelial cells.

Altogether, our study has identified GPR4 as a potential regulator of intestinal inflammation and suggests that molecular responses to the acidic microenvironment in inflamed intestinal tissues may be a novel mechanism involved in IBD pathogenesis. A similar mechanism may also exist in other inflammatory disorders.

C. Results

C.1 GPR4 exacerbates intestinal inflammation in the acute DSS-induced experimental colitis mouse model.

In order to determine the functional role of GPR4 in intestinal inflammation, we chemically induced intestinal inflammation in wild type (WT) and GPR4 KO mice. By day 7, WT mice treated with DSS (WT-DSS) lost nearly 16% of body weight on average (Figure 3.1).

In comparison, GPR4 KO mice treated with DSS (GPR4 KO-DSS) had only a 7% reduction in bodyweight. The WT-DSS mice also had a fecal score more severe compared to GPR4 KO-DSS mice intermittently throughout the experiment (Figure 3.1B). On day 7 of the experiment, mice were euthanized and the colon length was evaluated as an indicator of the degree of colonic inflammation induced by DSS. GPR4 KO-DSS mice had less colon shortening compared to WT-DSS mice (Figure 3.1C, Figure 3.12). Additionally, mesenteric lymph nodes were isolated and measured to calculate the volume as an assessment of the response to inflammatory stimulation. GPR4 KO-DSS mice had a significant reduction in mesenteric lymph node expansion compared to WT-DSS mice (Figure 3.1D). Collectively, the clinical phenotype of gut inflammation was less severe in GPR4 KO-DSS mice compared to WT-DSS mice indicating GPR4 is pro-inflammatory. The DSS-induced colitis disease model causes very severe acute intestinal inflammation and tissue damage; subsequently, the partial recovery phenotype observed in the GPR4 KO-DSS mice is comparable to other studies showing an alleviation of the DSS-induced phenotype with mutant mice [148-150]. Additionally, we observed no sex dependent susceptibility to DSS in our experiments (Figure 3.12).

In conjunction with the clinical aspects of colonic inflammatory extent, severity was also assessed through histopathological analysis by both veterinary and medical pathologists. Common features of IBD were evaluated and scored such as the degree of inflammation, area of leukocyte infiltration, edema, epithelium damage, hyperplasia, dysplasia, and crypt damage for both the cecum and colon. Both independent pathologists, using distinct methodologies, arrived at the same observation that GPR4 KO-DSS mice were less severe when compared to WT-DSS mice in both the colon and cecum (Figure 3.2; Figure 3.13). Of particular interest, the degree of inflammation and area of leukocyte infiltration were reduced spanning from cecum and colon

tissues in the GPR4 KO-DSS mice compared to WT-DSS mice (Figure 3.2C-D). Interestingly, the degree of reduction in histopathological features of GPR4 KO-DSS mice were significantly greater in the cecum when compared to colon (Figure 3.2A-B). This observation could be due to the increased acidity in the cecum compared to the colon, thereby increasing GPR4 activity in the cecum.

To further address the reduction of leukocyte infiltration observed by pathologists in GPR4 KO-DSS mice compared to WT-DSS mice, we compared the number of neutrophils, macrophages, and T cells between WT and GPR4 KO colon tissues. We observed a significant increase in immune cell infiltrates in DSS-treated mice when compared to untreated mice. When comparing WT-DSS and GPR4 KO-DSS mice, there was a 20-30% reduction in the number of neutrophils (Figure 3.3A-C), macrophages (Figure 3.3D-F), and T cells (Figure 3.3G-I) in the inflamed colon tissues. These results indicate GPR4 may regulate leukocyte infiltration and potentiate intestinal inflammation.

Recently there has been growing interest in isolated lymphoid follicles (ILFs) and local gut immunity. ILFs predominately develop in the colon and are similar in structure and function as Peyer's patches (PP) in the small intestine with the major difference between PP and ILFs being the inducible nature of ILFs in response to inflammatory stimuli [151, 152]. Crosstalk between stromal cells, lymphoid tissue inducer cells (LTi), and immune cells (dendritic cells, T cells, B cells) are critical for ILF development and effector functions in the gut [153]. Increased development of ILFs in the colon is associated with increased intestinal inflammation and tissue damage [154, 155]. In keeping with these reports, we observed a significant increase in ILF development in WT-DSS mouse colons when compared to WT control colons (4.0 ILFs/cm vs. 0.8 ILFs/cm of colon section) (Figure 3.4A). Similar results were observed upon evaluation of

the cecum sections for ILFs (Figure 3.4B; Figure 3.14). The GPR4 KO-DSS mice, however, had no significant increase of ILF formation in both the colon and the cecum (Figure 3.4; Figure 3.14). The GPR4 KO-DSS mice had on average 1.1 ILFs per centimeter of colon section. ILFs could be observed spanning the proximal and distal sections of the colon. ILF density increased in areas of greater inflammation. As such, fewer ILFs were observed in the proximal regions of the colon compared to the distal colon where increased inflammation was visible. The GPR4 KO-DSS mice had an ILF number very similar to the WT-control mice in both colon and cecum. These results suggest GPR4 is critical for ILF formation in response to gut inflammation.

To further characterize the involvement of GPR4 in intestinal inflammation, we examined GPR4 mRNA expression in WT-DSS and WT-control mice by real-time PCR. Our results demonstrated that GPR4 mRNA expression was upregulated in the inflamed colonic tissue of WT-DSS mice by nearly 2.7 fold when compared to normal controls (Figure 3.5A). No GPR4 mRNA expression was detected in colon tissues of GPR4 KO mice, confirming the deficiency of GPR4 in the KO mice (data not shown). Furthermore, we measured the GPR4 mRNA expression in IBD and normal human intestinal tissues by real-time PCR. We used a cDNA array containing 7 normal colon, 26 active colitis, and 14 Crohn's tissue cDNA samples. We observed a ~4.7 fold increase of GPR4 mRNA expression in human colitis and Crohn's disease lesions compared to normal human intestinal tissues (Figure 3.5B). These data collectively demonstrate that GPR4 expression is increased in inflamed intestinal lesions and could be involved in the pathogenesis of the disease.

In order to characterize the expression pattern of GPR4 in the mouse colon and cecum, we performed immunohistochemistry for green fluorescent protein (GFP) as a surrogate marker for GPR4 due to the lack of an antibody that can reliably detect endogenous GPR4 protein.

GPR4-deficient mice were generated by replacing the GPR4 coding region with an internal ribosome entry site (IRES)-GFP cassette under the control of the GPR4 gene promoter as previously described [125]. Therefore, GFP expression in mouse tissues serves as a surrogate marker for endogenous GPR4 expression. GFP expression was predominately detected in the endothelial cells (ECs) of blood vessels, including arteries, veins, and microvessels of the cecum and colon in GPR4 KO untreated mice (Figure 3.6, Figure 3.17A-B). GPR4 heterozygous untreated mice had the same GFP expression pattern in the intestinal tissues as GPR4 KO untreated mice (Figure 3.16). Additionally, GFP expression could also be observed in microvessels adjacent to ILFs and the specialized high endothelial venules (HEVs) in mesenteric lymph nodes (Figure 3.6). GFP expression could not, however, be significantly detected in lymphatic endothelial cells (Figure 3.6A). In addition to GFP expression in ECs, GFP expression could be detected in histiocytes (macrophages) located in the sinus of the mesenteric lymph nodes (Figure 3.6F). No GFP signal could be detected in WT untreated control intestinal tissues, with the exception of background signal on the epithelium, luminal content, and adipose tissue (Figure 3.17). The GFP expression pattern is in accordance with previously published results showing that GPR4 is expressed in several types of cultured vascular endothelial cells and isolated monocytes/macrophages [98, 103, 114, 156]. The role of GPR4 in macrophages is currently unknown and further studies will need to be conducted in the future to elucidate the functional and molecular role of GPR4 in macrophages.

Upon examination of GFP expression in the inflamed colon and cecal tissues of GPR4 KO-DSS mice, similar localization of GFP in the endothelial cells of arteries, veins, microvessels, and HEVs could be observed as the GPR4 KO control mice (Figure 3.7). GFP expression could also be detected in mucosal macrophages in inflamed lesions of the GPR4 KO-

DSS mice as well as the sinus regions of the mesenteric lymph nodes (Figure 3.7B, F). In accordance with the WT untreated control tissues, no GFP signal could be detected in WT-DSS tissues with the exception of minor background staining of the luminal epithelium, luminal content, and adipose tissue (Figure 3.18).

Due to the localization of GPR4 in HEVs traversing lymphoid tissues such as mesenteric lymph nodes and in microvessels adjacent to ILFs in the mucosa, GPR4 could regulate lymphoid tissue expansion in a manner consistent with previous publications demonstrating GPR4 in ECs increases numerous cytokines, chemokines, and adhesion molecules regulating leukocytes interaction with ECs [113, 114]. GPR4 could be involved in increasing the passage of leukocytes critical for inflammatory responses in secondary and tertiary lymphoid tissues as is observed in GPR4 KO-DSS mice having reduced mesenteric lymph node volume (Figure 3.1D) and ILF development (Figure 3.4, Figures 3.14).

As previous GPR4 inhibitor and shRNA knockdown studies have shown that inhibition of GPR4 reduces the expression of adhesion molecules and numerous inflammatory genes in endothelial cell cultures, we sought to examine a selection of inflammatory genes expressed in WT and GPR4 KO whole colon tissue. Given the diverse cell population in the inflamed colon, coupled with the focal nature of IBD, inflammatory molecules such as VCAM-1, E-selectin and ICAM-1 can be expressed by a variety of stromal and immune cells in addition to endothelial cells. As GPR4 is expressed primarily in vascular endothelial cells, much of the detectable inflammatory molecule expression is derived from other cell types within the inflamed colon tissue and is not regulated by GPR4. Therefore, the effects of EC gene expression governed by GPR4 can be masked by gene analysis of whole tissue colon segments. In spite of this limitation, using real-time PCR analysis of whole colon tissue segments we observed the mRNA expression

of adhesion molecules E-selectin, ICAM-1, VCAM-1, and MAdCAM-1 modestly reduced (~15-30%), although not statistically significant with this sample size, in the GPR4 KO-DSS mouse colon compared to the WT-DSS colon (Figure 3.8A-D). In addition to adhesion molecule expression, mRNA levels of COX-2 were modestly reduced (~30%) in GPR4 KO-DSS mice whereas CXCL2 showed no difference between WT-DSS and GPR4 KO-DSS mice (Figure 3.8E-F). In addition to gene expression analysis, we examined the protein expression of VCAM-1 in whole colon tissues. We observed a similar trend in the reduction of VCAM-1 protein expression as noted in VCAM-1 gene expression (Figure 3.19, Figure 3.8B).

Furthermore, correlating GPR4 mRNA expression in WT-DSS colonic tissues to inflammatory gene expression, we were able to see a statistically significant positive correlation between increased GPR4 mRNA expression and inflammatory gene expression such as E-selectin and COX-2 (Figure 3.8G, L). With the exception of CXCL2; VCAM-1, ICAM-1, and MAdCAM-1 showed a trend in correlation with GPR4 mRNA expression that has not yet reached statistical significance given the current sample size (Figure 3.8K, H, I, J).

To further examine the effects of GPR4 within endothelial cells and overcome the limitations of whole tissue gene analysis, we performed immunohistochemistry to examine the expression of E-selectin and VCAM-1 in the vascular endothelium. Overall, the E-selectin and VCAM-1 protein expression was increased in the DSS-treated inflamed WT and GPR4 KO mouse intestinal tissues when compared to the non-treated control tissues. E-selectin was expressed in the vascular endothelium and some colon epithelial cells. One report confirms the expression of E-selectin in colon epithelial cells [157]. We observed ECs in GPR4 KO-DSS mouse colons and cecums had reduced E-selectin expression when compared to WT-DSS mice (Figure 3.9A-D, 3.10A-D). Immunohistochemical analysis of VCAM-1 revealed expression on a

variety of cell types in addition to the ECs within the inflamed colon and cecum. Expression could be observed in the mucosa, submucosa, and muscularis externa. Overall, total VCAM-1 expression was visibly reduced and less extensive in the GPR4 KO-DSS mice compared to WT-DSS mice, and an appreciable reduction in VCAM-1 signal could be discerned in the mucosal endothelial cells themselves within the colon and cecum tissues (Figure 3.9E-H, 3.10E-H).

Taken together, GPR4 appears to increase the expression of E-selectin and VCAM-1 in the inflamed colon and cecum based on immunohistochemical analysis. These data suggest GPR4 could increase intestinal inflammation through the regulation of endothelial inflammation and leukocyte infiltration into inflamed gastrointestinal tissues.

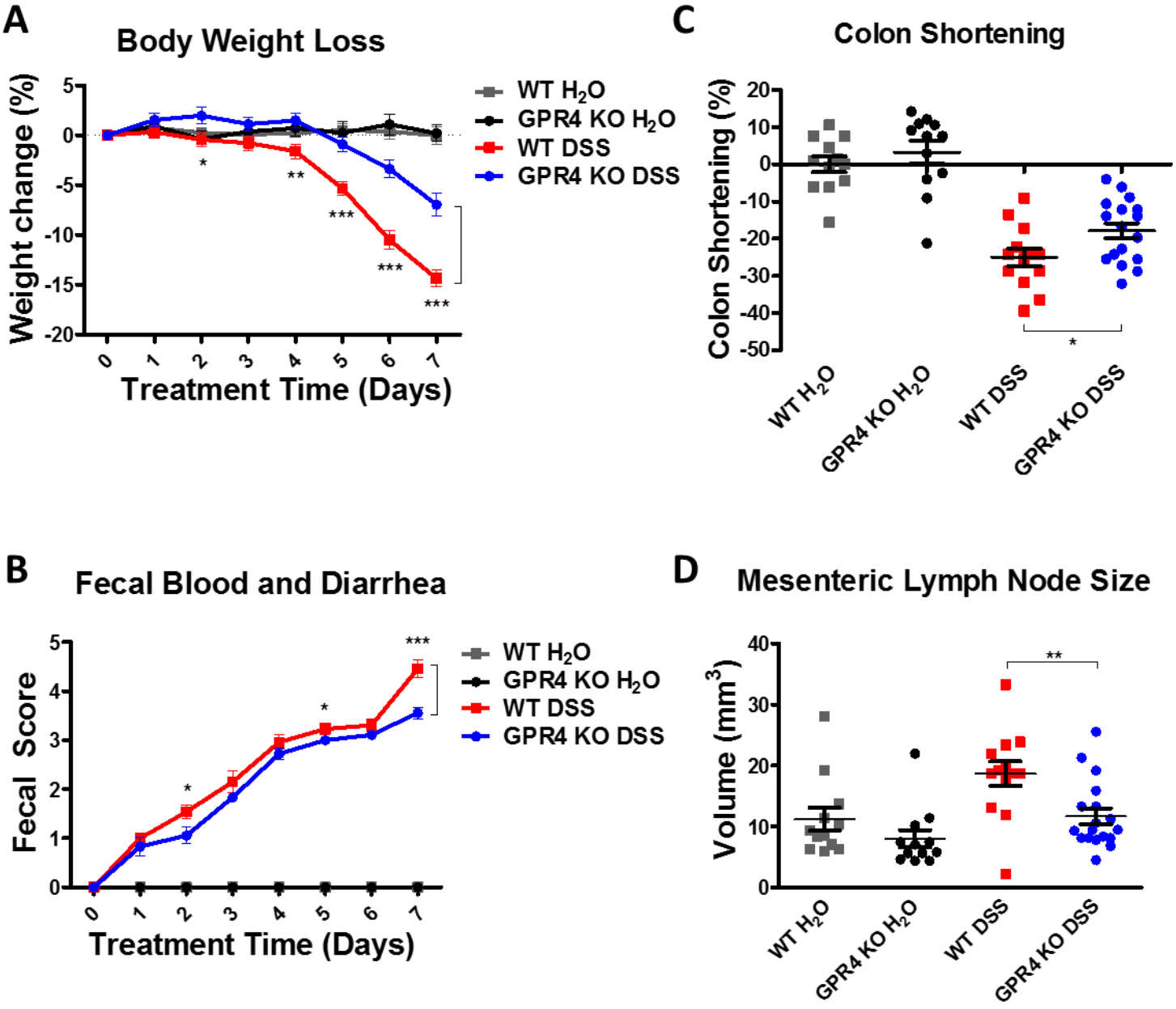
A
Body Weight Loss
Weight change (%)
Treatment Time (Days)
WT H2O
GPR4 KO H2O
WT DSS
GPR4 KO DSS
C
Colon Shortening
Colon Shortening (%)
WT H2O
GPR4 KO H2O
WT DSS
GPR4 KO DSS
B
Fecal Blood and Diarrhea
Fecal Score
Treatment Time (Days)
D
Mesenteric Lymph Node Size
Volume (mm3)

Figure 3.1. **Clinical phenotypes and macroscopic indicators**. To assess the extent of DSS-induced colitic inflammation in mice, we measured several parameters to gauge the disease severity in mice. We observed GPR4 KO-DSS mice had reduced disease severity when compared to WT-DSS mice. Clinical parameters of disease severity, including (A) body weight loss, (B) colon shortening, (C) fecal score and (D) mesenteric lymph node volume, were assessed in WT-control (n=12), WT-DSS (n=13), GPR4 KO-control (n=12), and GPR4 KO-DSS (n=18) mice. Each dot represents the data from an individual mouse. Data are presented as mean ± SEM and was analyzed for statistical significance using the unpaired *t*-test between WT-DSS mice and GPR4 KO-DSS mice or as indicated within graph. (*$P < 0.05$, **$P < 0.01$, *** $P< 0.001$).

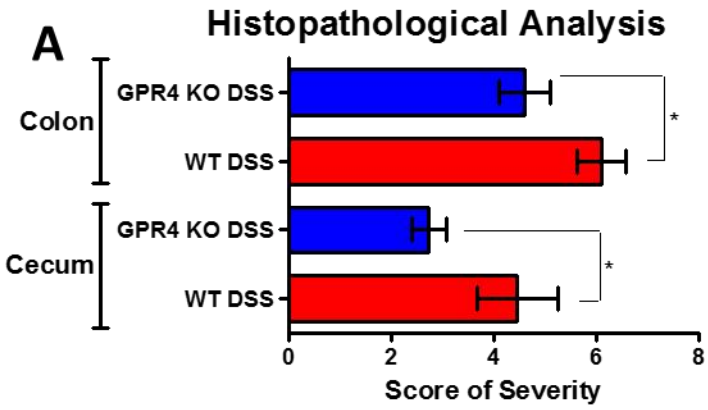
A
Histopathological Analysis
Colon
Cecum
GPR4 KO DSS
WT DSS
GPR4 KO DSS
WT DSS
*
*
0
2
4
6
8
Score of Severity

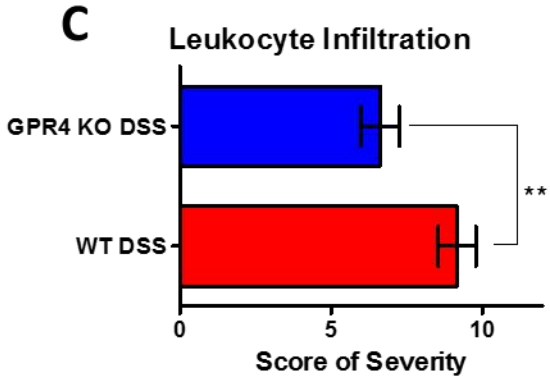
C
Leukocyte Infiltration
GPR4 KO DSS
WT DSS
**
0
5
10
Score of Severity

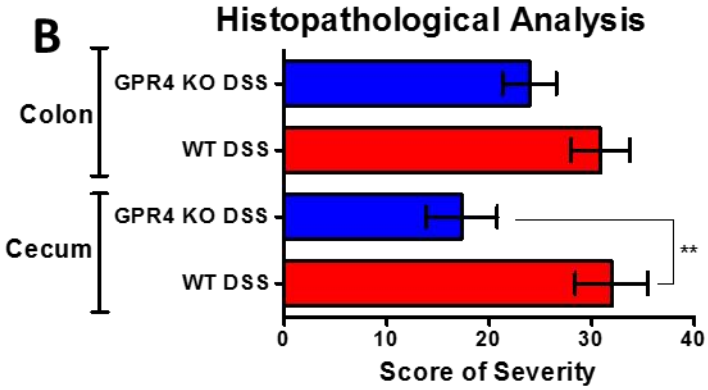
B
Histopathological Analysis
Colon
Cecum
GPR4 KO DSS
WT DSS
GPR4 KO DSS
WT DSS
**
0
10
20
30
40
Score of Severity

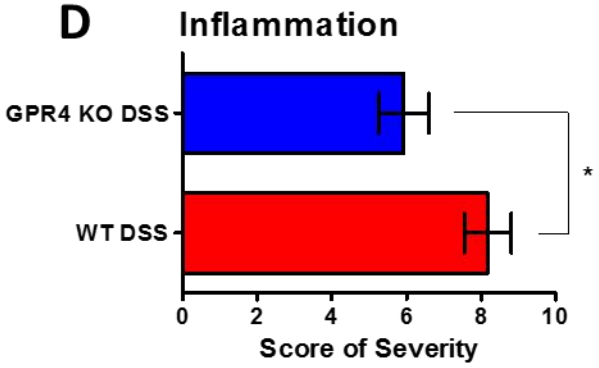
D
Inflammation
GPR4 KO DSS
WT DSS
*
0
2
4
6
8
10
Score of Severity

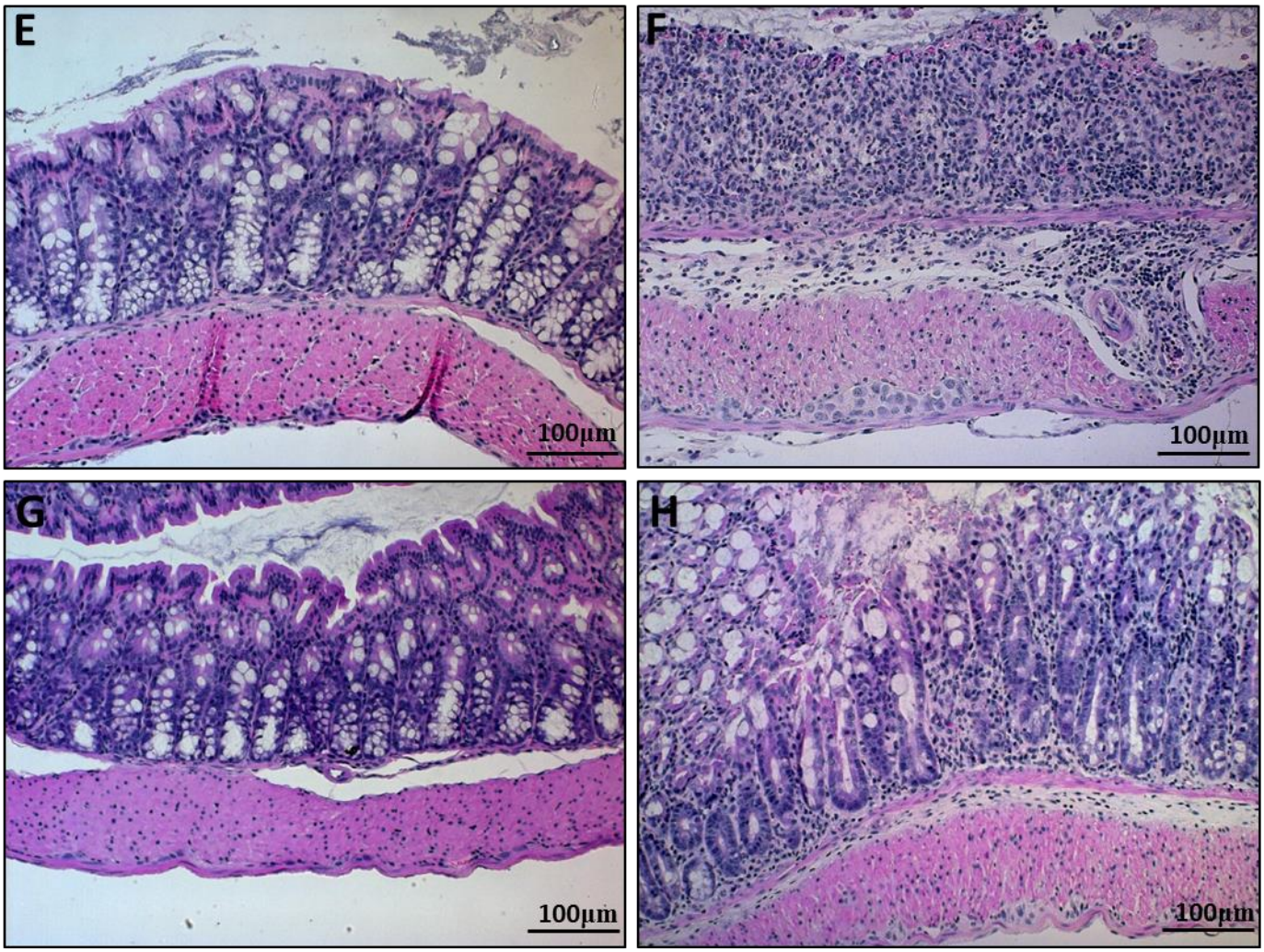
E
100μm
F
100μm
G
100μm
H
100μm

Figure 3.2. **Histopathological analysis of mouse colon and cecum**. Histological features of colitis were examined to further assess the degree of disease activity in the mice by veterinary and human pathologists using complementary, yet distinct scoring systems. Overall, GPR4 KO DSS mice had reduced histopathological scores in cecum and colon when compared to WT DSS mice. (A) Veterinary pathologist and (B, C, D) human pathologist assessment of colon and cecum. (C) Reduced leukocyte infiltration was observed spanning from the cecum to distal colon in GPR4 KO DSS mice compared to WT DSS mice. (D) Overall inflammation was reduced in GPR4 KO DSS mice compared to WT DSS mice in tissues spanning from the cecum to distal colon. Representative H&E staining pictures of colon in (E) WT control, (F) WT-DSS, (G) GPR4 KO control, and (H) GPR4 KO DSS using a 20× microscope objective. Data are presented as mean ± SEM and analyzed for statistical significance between WT-DSS and GPR4 KO DSS groups using the unpaired *t*-test. WT-Control (n=12), WT-DSS (n=13), GPR4 KO Untreated (n=12), and GPR4 KO DSS (n=18) tissues were used for analysis. (*$P < 0.05$, **$P < 0.01$)

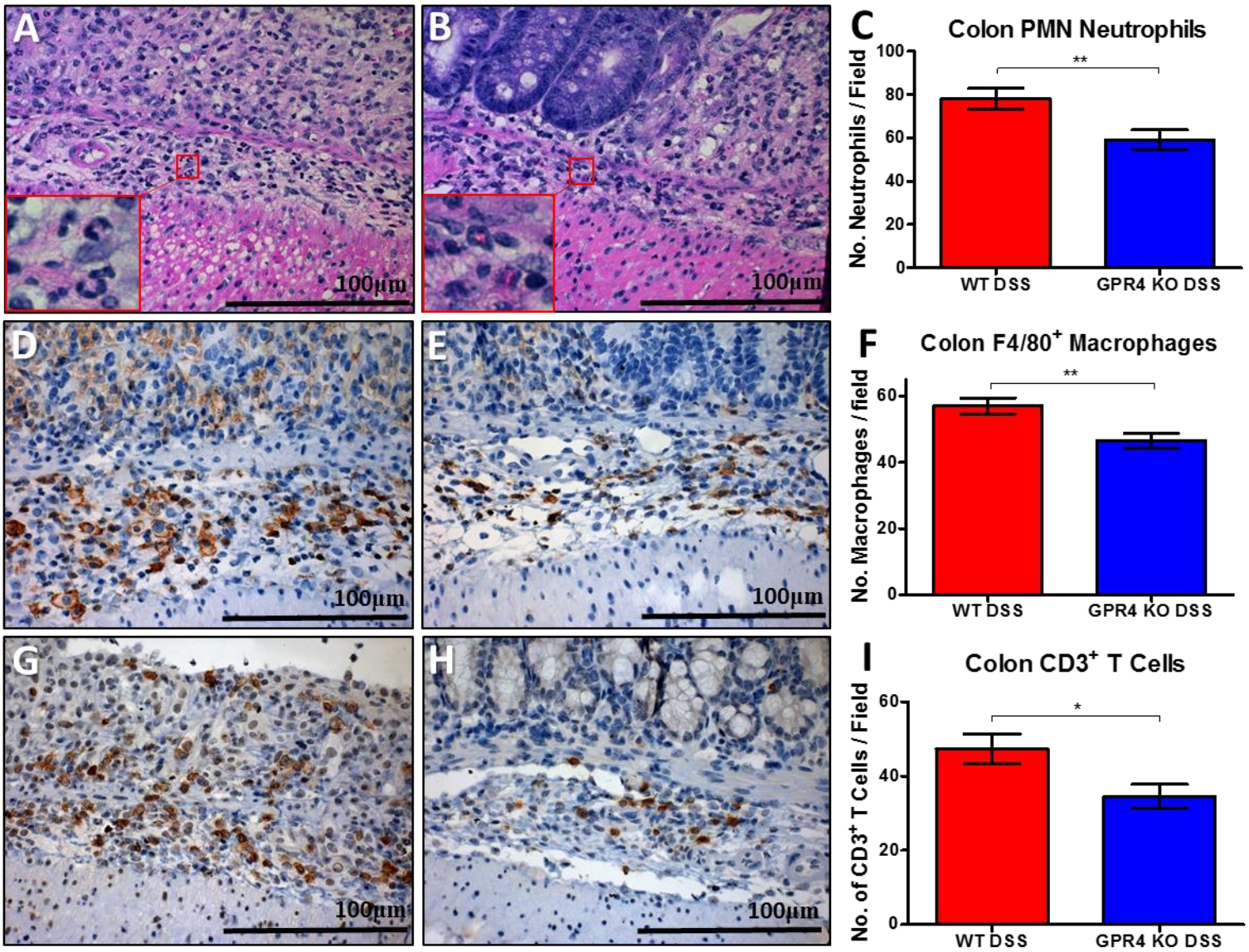
A
100µm
B
100µm
C
Colon PMN Neutrophils
No. Neutrophils / Field
100
80
60
40
20
0
**
WT DSS
GPR4 KO DSS
D
100µm
E
100µm
F
Colon F4/80+ Macrophages
No. Macrophages / field
60
40
20
0
**
WT DSS
GPR4 KO DSS
G
100µm
H
100µm
I
Colon CD3+ T Cells
No. of CD3+ T Cells / Field
60
40
20
0
*
WT DSS
GPR4 KO DSS

Figure 3.3. **Immune cell infiltrate quantification in colon mucosa**. GPR4 KO-DSS mice (n= 4-5) had reduced numbers of neutrophils, macrophages, and T cells in the mucosa of the colon compared to WT-DSS mice (n= 4-5). (Fig. 3A-C) Neutrophil quantification based on polymorphonuclear (PMN) morphology and cytoplasmic staining, (Fig. 3D-F) $F4/80^{+}$ macrophages, and (Fig. 3G-I) $CD3^{+}$ T cells. 40× microscope objectives. Statistical analysis was performed using the unpaired *t*-test between WT-DSS and GPR4 KO-DSS groups. (*$P < 0.05$, **$P < 0.01$)

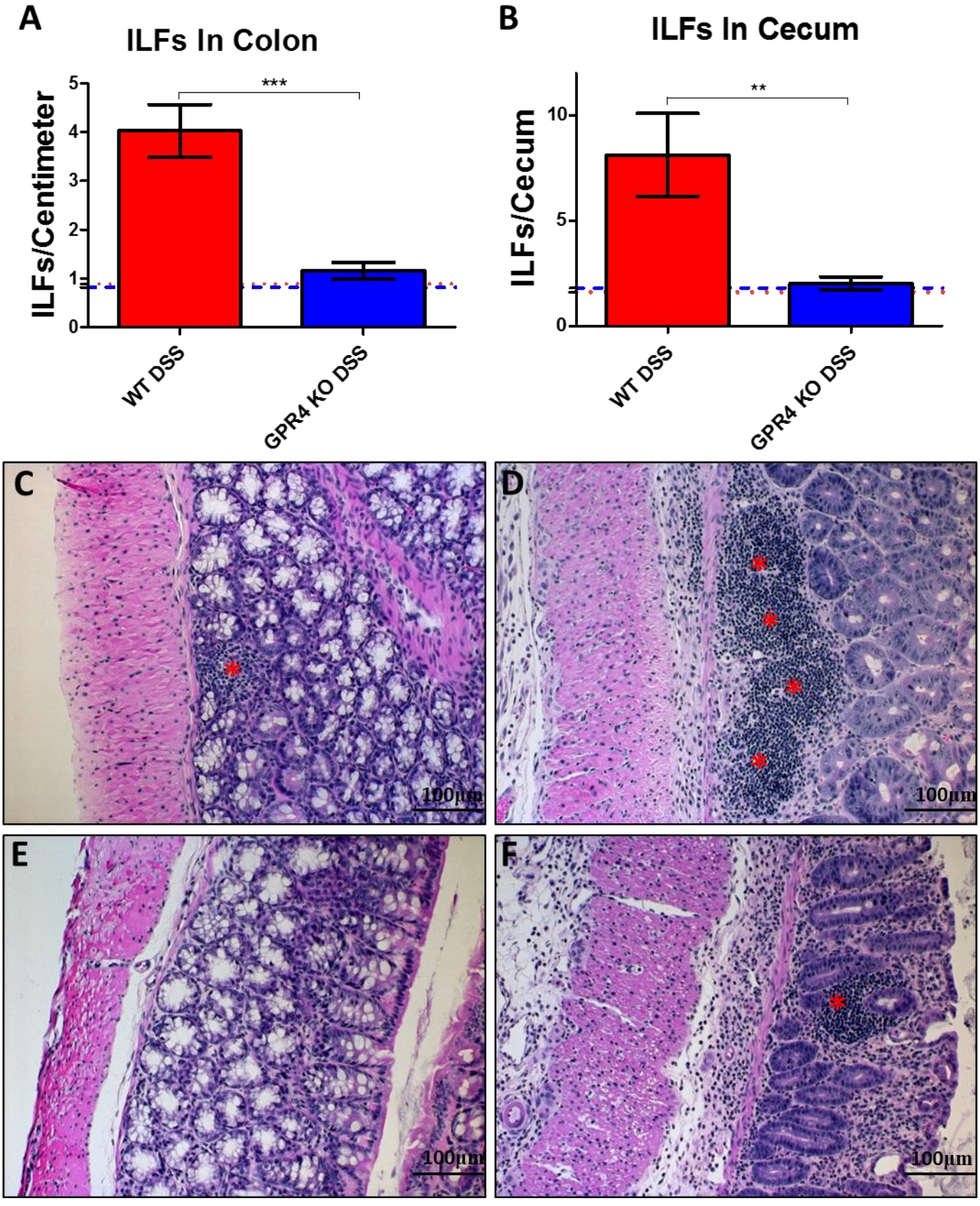
A
ILFs In Colon
ILFs/Centimeter
***
WT DSS
GPR4 KO DSS
B
ILFs In Cecum
ILFs/Cecum
**
WT DSS
GPR4 KO DSS
C
D
E
F
100µm

Figure 3.4. **Isolated lymphoid follicle (ILF) quantification and H&E staining of ILFs**. GPR4 KO DSS mice had reduced ILF number in the colon and cecum when compared to WT-DSS mice. ILF quantification in WT and GPR4 KO (A) colon and (B) cecum tissues. Representative H&E staining of ILFs in (C) WT control (n=12), (D) WT-DSS (n=13), (E) GPR4 KO control (n=12), and (F) GPR4 KO-DSS colons (n=18). Red asterisks indicate representative ILFs in colon tissue. Red and blue dotted lines indicate WT-control and GPR4 KO control ILF quantification, respectively (A-B). Data are presented as mean ± SEM. WT-Control (n=12), WT-DSS (n=13), GPR4 KO control (n=12), and GPR4 KO DSS (n=18) tissues were used for analysis. Statistical analysis was performed using the unpaired *t*-test between WT-DSS and GPR4 KO-DSS groups. (**$P < 0.01$, *** $P< 0.001$)

A

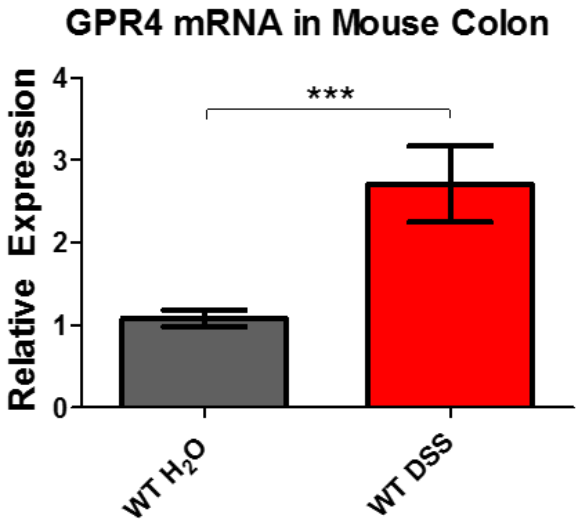
GPR4 mRNA in Mouse Colon
Relative Expression
4
3
2
1
0
***
WT H_2O
WT DSS

B

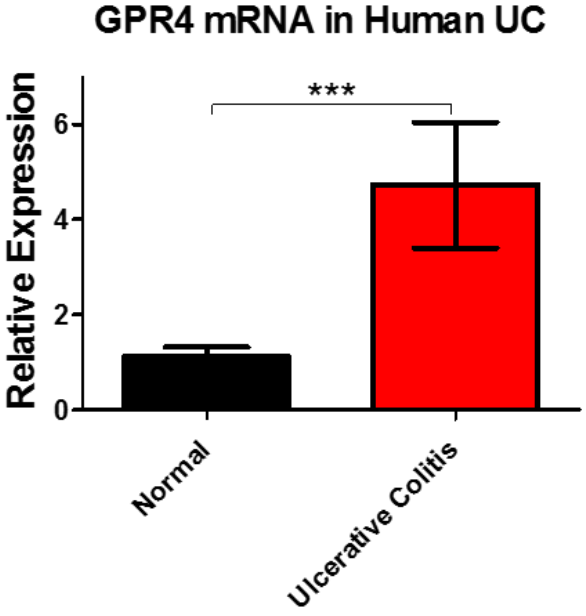
GPR4 mRNA in Human UC
Relative Expression
6
4
2
0
***
Normal
Ulcerative Colitis

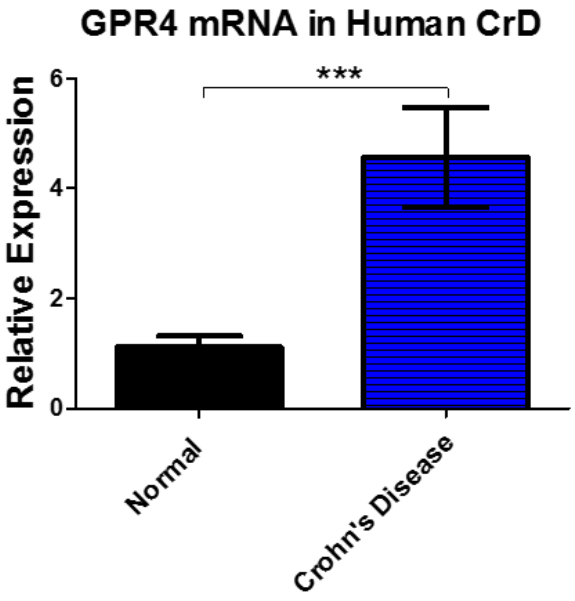
GPR4 mRNA in Human CrD
Relative Expression
6
4
2
0
***
Normal
Crohn's Disease

Figure 3.5. GPR4 mRNA expression in human and mouse inflamed intestinal tissues.

Expression levels of GPR4 in inflamed and non-inflamed intestinal tissues were assessed. GPR4 mRNA was increased in inflamed lesions of human and mouse intestinal tissues when compared to normal intestinal tissues. (A) GPR4 mRNA expression in mouse WT-DSS colonic tissue compared to WT-control tissues. (B) GPR4 mRNA expression in human normal (n=7), ulcerative colitis (n=26), and Crohn's intestinal tissues (n=14). Data are presented as mean ± SEM and analyzed for statistical significance using the (A) unpaired *t*-test and (B) nonparametric Mann-Whitney test. (*** $P< 0.001$)

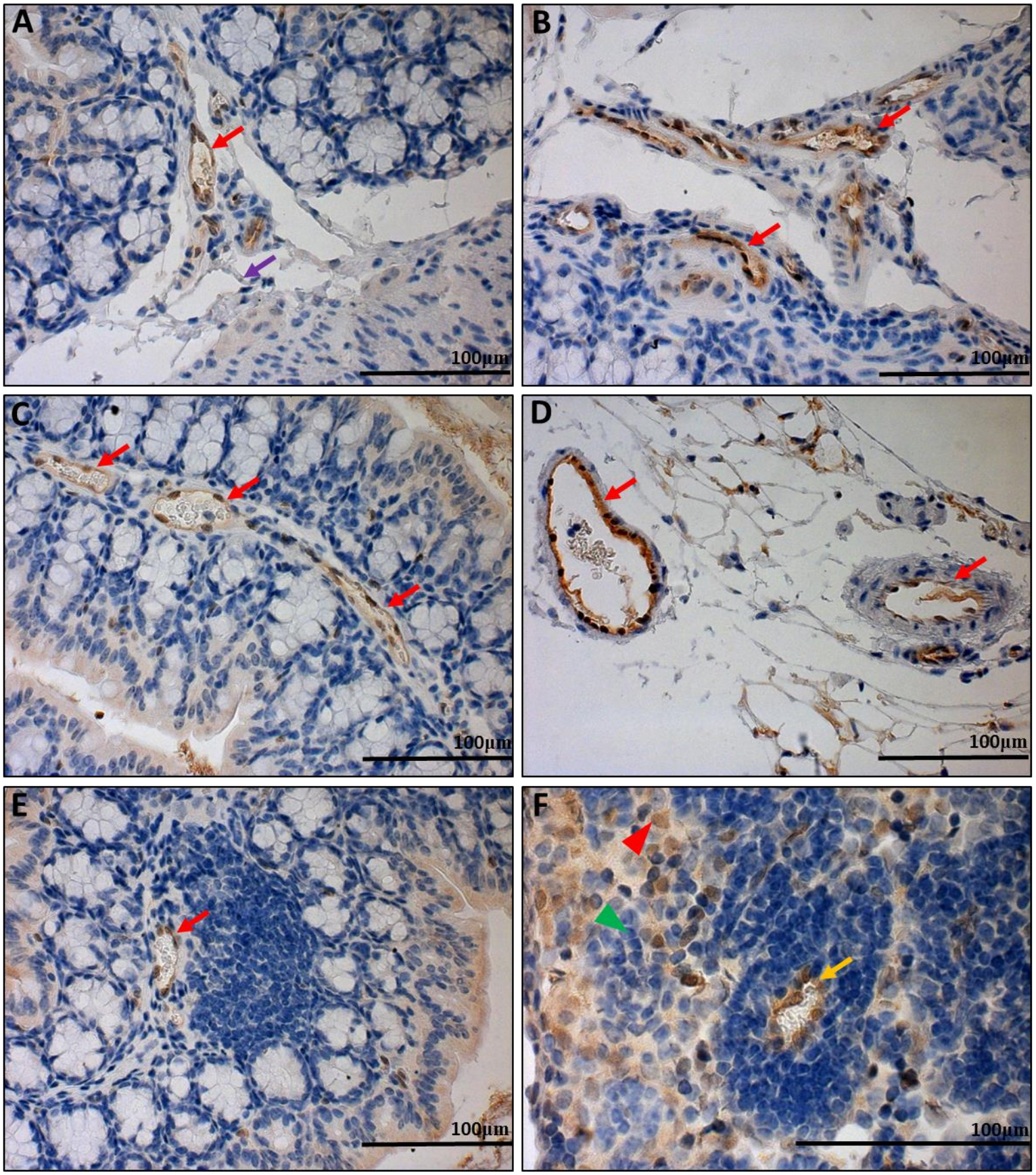
A
100µm
B
100µm
C
100µm
D
100µm
E
100µm
F
100µm

Figure 3.6. GFP knock-in as a surrogate marker for GPR4 expression in GPR4 KO control mouse colon and lymphoid tissues. To assess the localization of GPR4 in intestinal tissues, we performed IHC of GFP in intestinal and lymph tissues. GFP expression was visualized as brown signals in the intestinal microvascular endothelial cells, ex-mural blood vessels, and mesenteric lymph node high endothelial venules (HEVs). GFP expression was barely detectable in lymphatic ECs. (A-B) Colonic GPR4 KO-control mouse blood vessel, artery, and lymphatic vessel, (C) transverse fold microvessels, (D) ex-mural blood vessel and arteries, (E) microvessels adjacent to isolated lymphoid follicles, and (F) mesenteric lymph node HEVs and histiocytes. No GFP signal detected in WT untreated control tissues (Supplementary Fig. S7). (A-E) 40× and (F) 63× microscope objectives. Red arrow heads indicate histiocytes (macrophages) and green arrow heads indicates lymphocytes. Red arrows indicate blood vessels, yellow arrows indicate HEVs, and purple arrows indicate lymphatics.

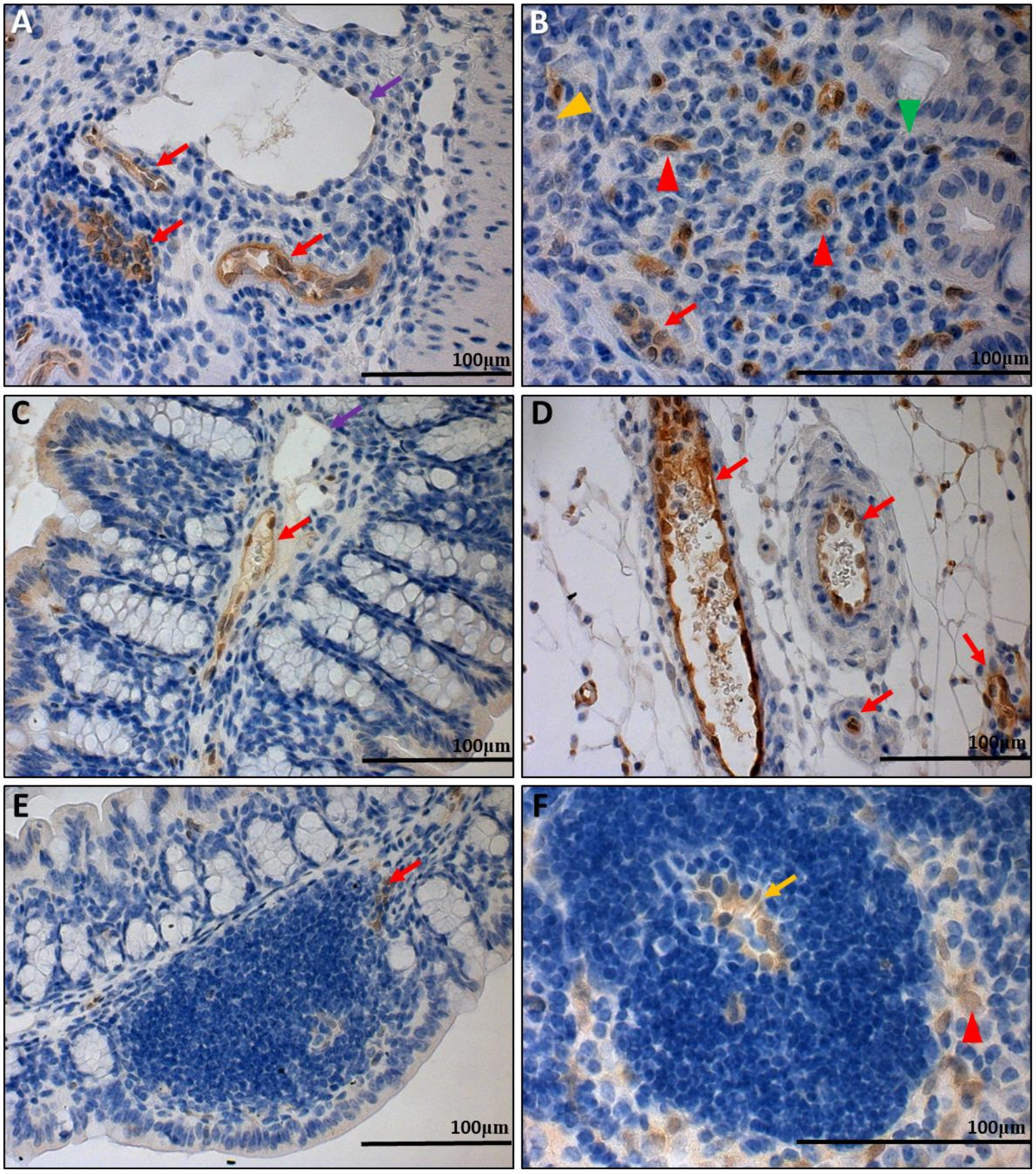
A
100µm
B
100µm
C
100µm
D
100µm
E
100µm
F
100µm

Figure 3.7. GFP knock-in as a surrogate marker for GPR4 expression in GPR4 KO-DSS mouse colon and lymph tissues. To examine the expression of GPR4 in inflamed intestinal tissues, we performed IHC of GFP in GPR4 KO-DSS tissues. GFP expression could be visualized as brown signals in the intestinal microvascular endothelial cells, ex-mural blood vessels, mesenteric lymph node HEVs, and macrophages. Minimal GFP could be detected in lymphatic ECs. (A) Colonic GPR4 KO-DSS blood vessel, artery, and lymphatic vessel, (B) macrophages in inflamed lesions, (C) transverse fold ECs, (D) ex-mural blood vessels, (E) isolated lymphoid follicle vessels, and (F) mesenteric lymph node HEVs and histiocytes. No expression of GFP could be detected in WT-DSS control tissues (Figure 3.17). (A-E) 40× and (F) 63× microscope objectives. Red arrow heads indicate macrophages, yellow arrow heads indicate neutrophils, and green arrow heads indicates lymphocytes. Red arrows indicate blood vessels, yellow arrows indicate HEVs, and purple arrows indicate lymphatics.

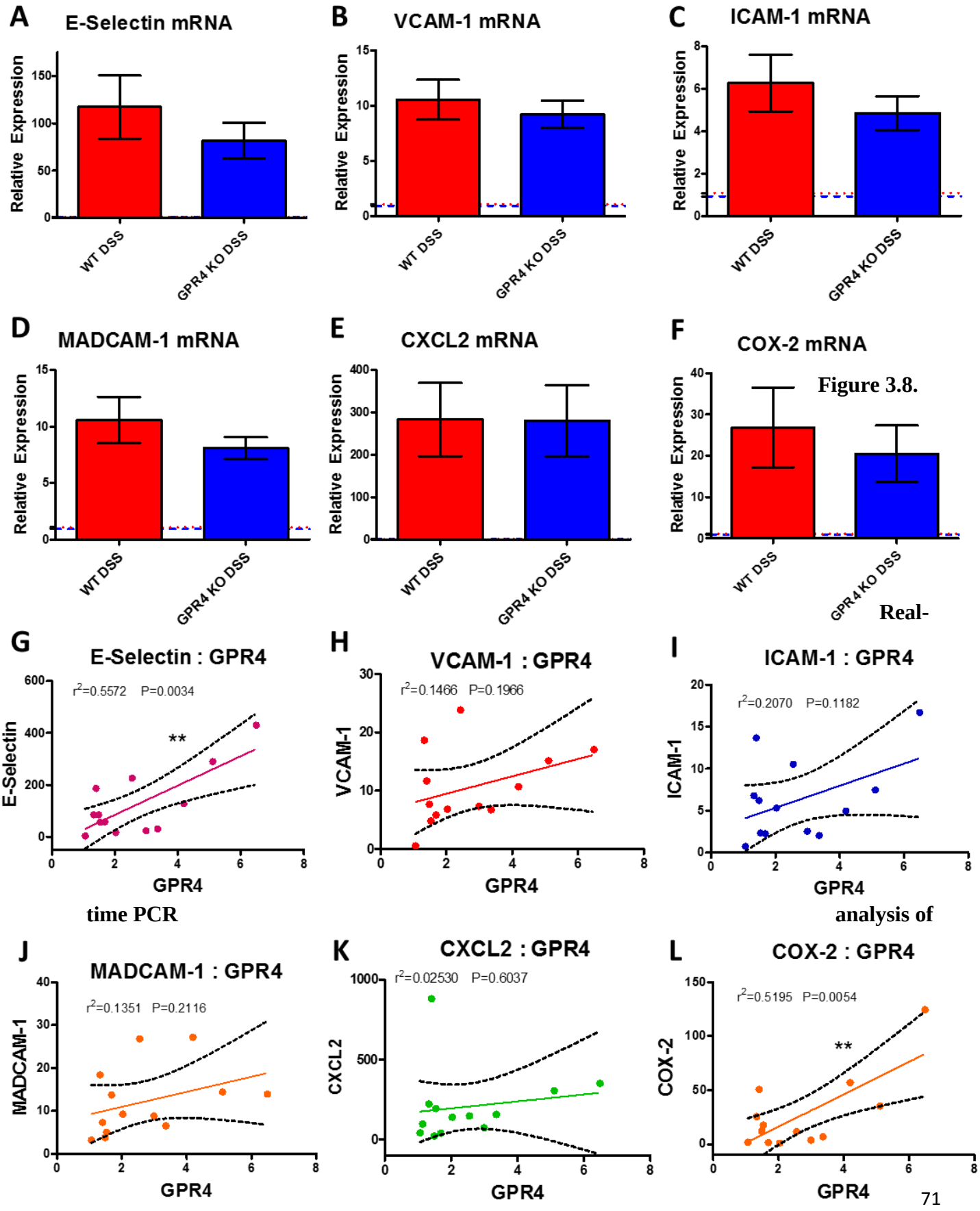

Figure 3.8. **Real-time PCR analysis of**

inflammatory gene expression and correlation with GPR4 expression. Inflammatory gene expression was evaluated in whole colon tissue segments to assess the contribution of GPR4, among other cells not regulated by GPR4, to inflammatory molecule expression. DSS induced the expression of the inflammatory genes in both WT-DSS and GPR4 KO-DSS colon tissues when compared to control colon tissues. GPR4 KO-DSS mice exhibited a trend of reduced pro-inflammatory gene expression when compared to WT-DSS mice, though not statistically significant. Adhesion molecules (A) E-selectin, (B) VCAM-1, (C) ICAM-1, and (D) MAdCAM-1 were analyzed along with chemokine (E) CXCL2, and inflammatory enzyme (F) COX-2. (A-F) Red and blue dotted lines indicate WT-control and GPR4 KO control quantification, respectively. Data are presented as mean ± SEM and analyzed for statistical significance using the unpaired *t*-test. WT-Control (n=12), WT-DSS (n=13), GPR4 KO-Control (n=12), and GPR4 KO DSS (n=18) were used for analysis. (G-L) To further characterize GPR4 regulated inflammatory gene expression, GPR4 mRNA expression was correlated with inflammatory gene expression from WT-DSS colon segments. Each dot represents the data from an individual mouse. GPR4 mRNA expression positively correlates with increased inflammatory gene expression when analyzing (G) E-selectin, (H) VCAM-1, (I) ICAM-1, and (J) MAdCAM-1, (K) CXCL2, and (L) COX-2. WT-DSS (n=13) tissues were used for gene expression correlation by linear regression analysis. (**$P < 0.01$)

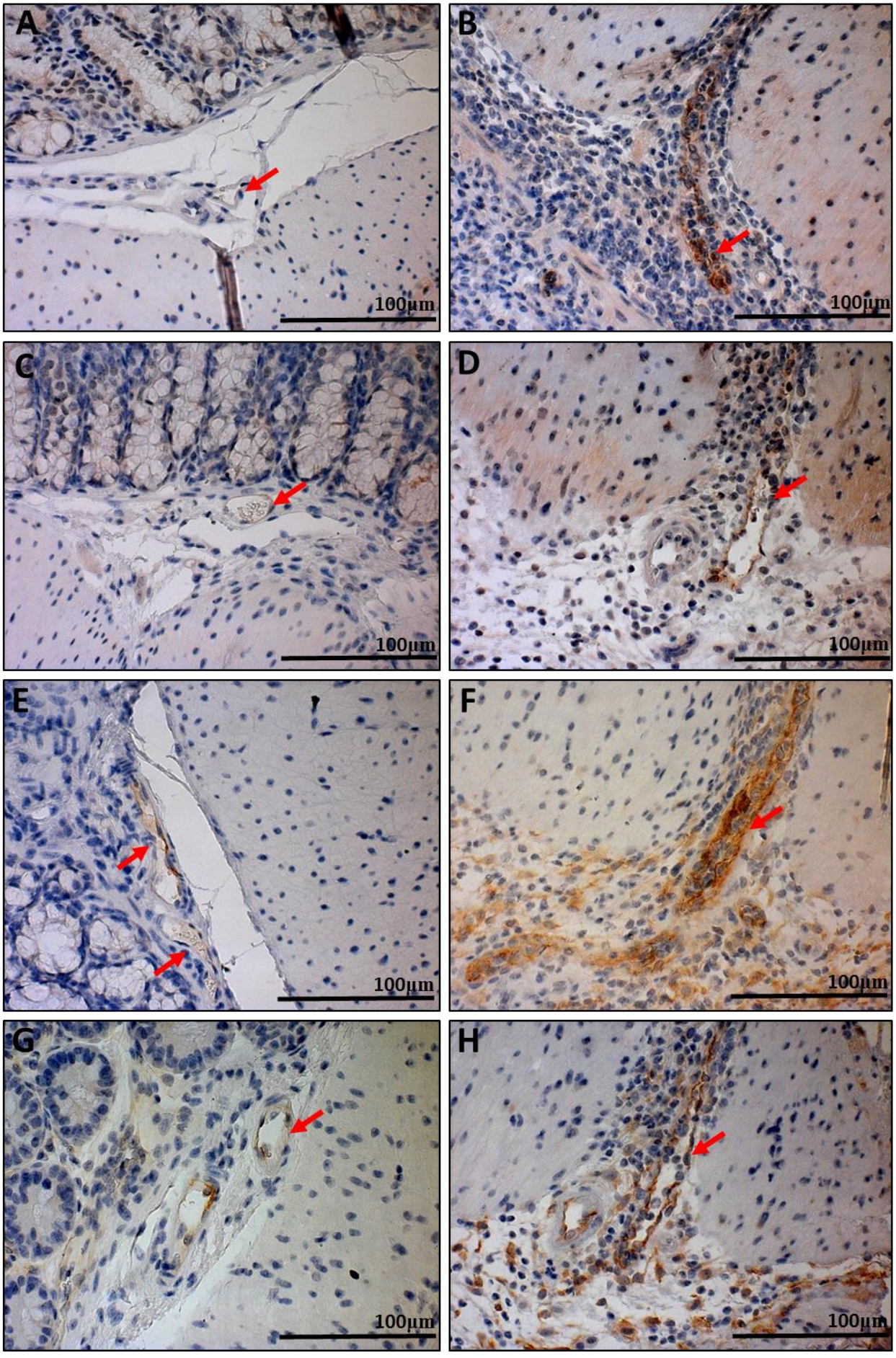
A
100µm
B
100µm
C
100µm
D
100µm
E
100µm
F
100µm
G
100µm
H
100µm

Figure 3.9. **Immunohistochemical analysis of E-selectin and VCAM-1 protein expression in mouse colon tissues**. As whole tissues are not ideal for analyzing endothelial cell specific gene expression, we performed IHC to analyze adhesion molecules E-selectin and VCAM-1 protein expression in ECs within the tissue. GPR4 KO-DSS mice have reduced E-selectin and VCAM-1 protein expression in colonic mucosal vasculature when compared to WT-DSS mice. E-selectin expression could be visualized as brown signals in (A) WT-control, (B) WT-DSS, (C) GPR4 KO-control, and (D) GPR4 KO-DSS colon tissues. VCAM-1 expression could be visualized in (E) WT-control, (F) WT-DSS, (G) GPR4 KO-control, and (H) GPR4 KO-DSS colon tissues. 40× microscope objective. Red Arrows indicate blood vessels.

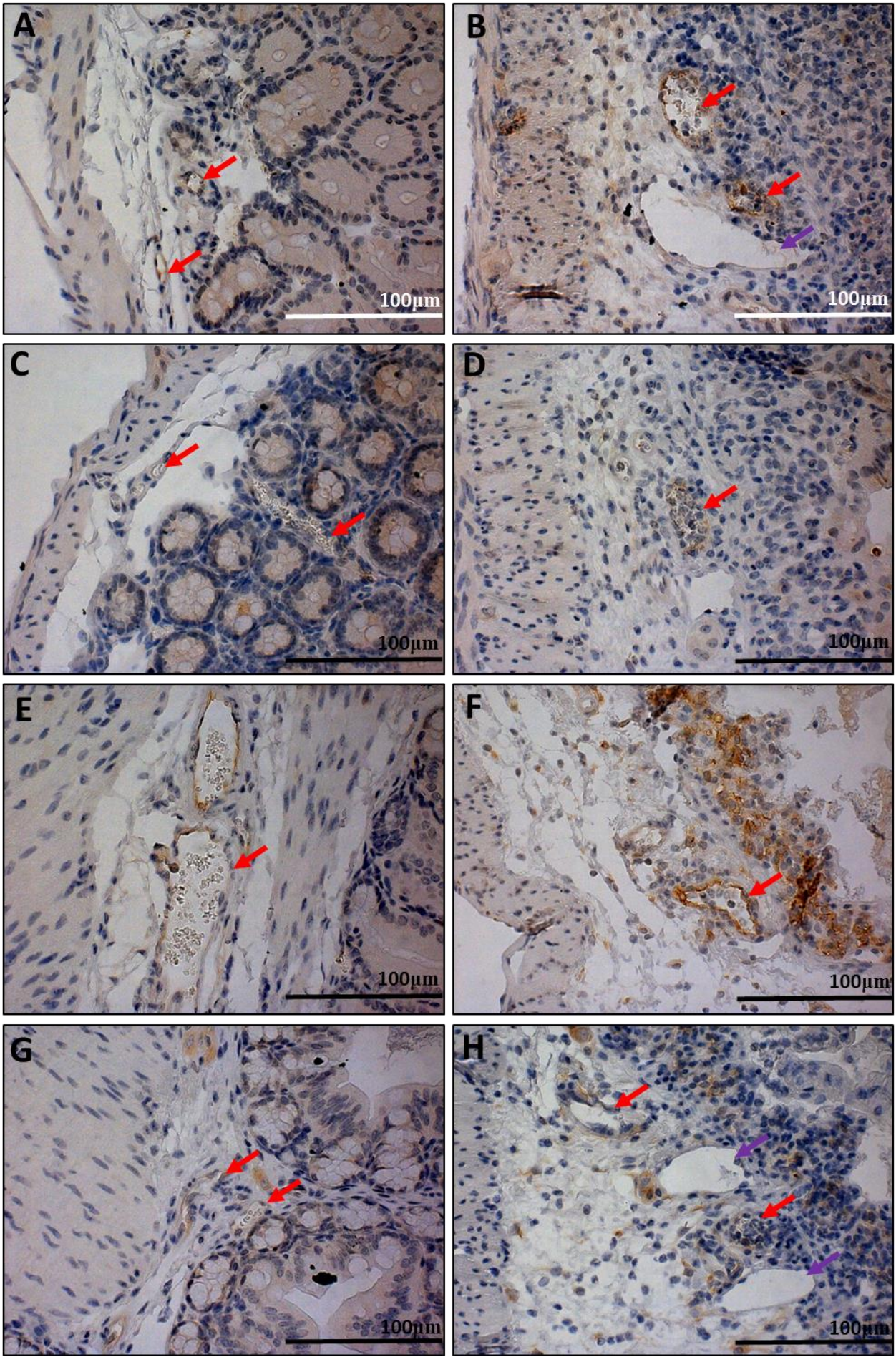
A
100µm
B
100µm
C
100µm
D
100µm
E
100µm
F
100µm
G
100µm
H
100µm

Figure 3.10. **Immunohistochemical analysis of cecum adhesion molecule expression in ECs**. In addition to the colon, cecum tissues were examined for adhesion molecule expression between WT and GPR4 KO mice. Similar to colon, GPR4 KO-DSS mice had a reduction in the expression of E-selectin and VCAM-1 in ECs. E-selectin protein expression could be visualized as brown signals in (A) WT-control, (B) WT-DSS, (C) GPR4 KO-control, and GPR4 KO-DSS mucosal blood vessels. VCAM-1 protein expression could be visualized in (E) WT-control, (F) WT-DSS, (G) GPR4 KO-control, and (H) GPR4 KO-DSS mucosal blood vessels. 40× microscope objective. Red Arrows indicate blood vessels.

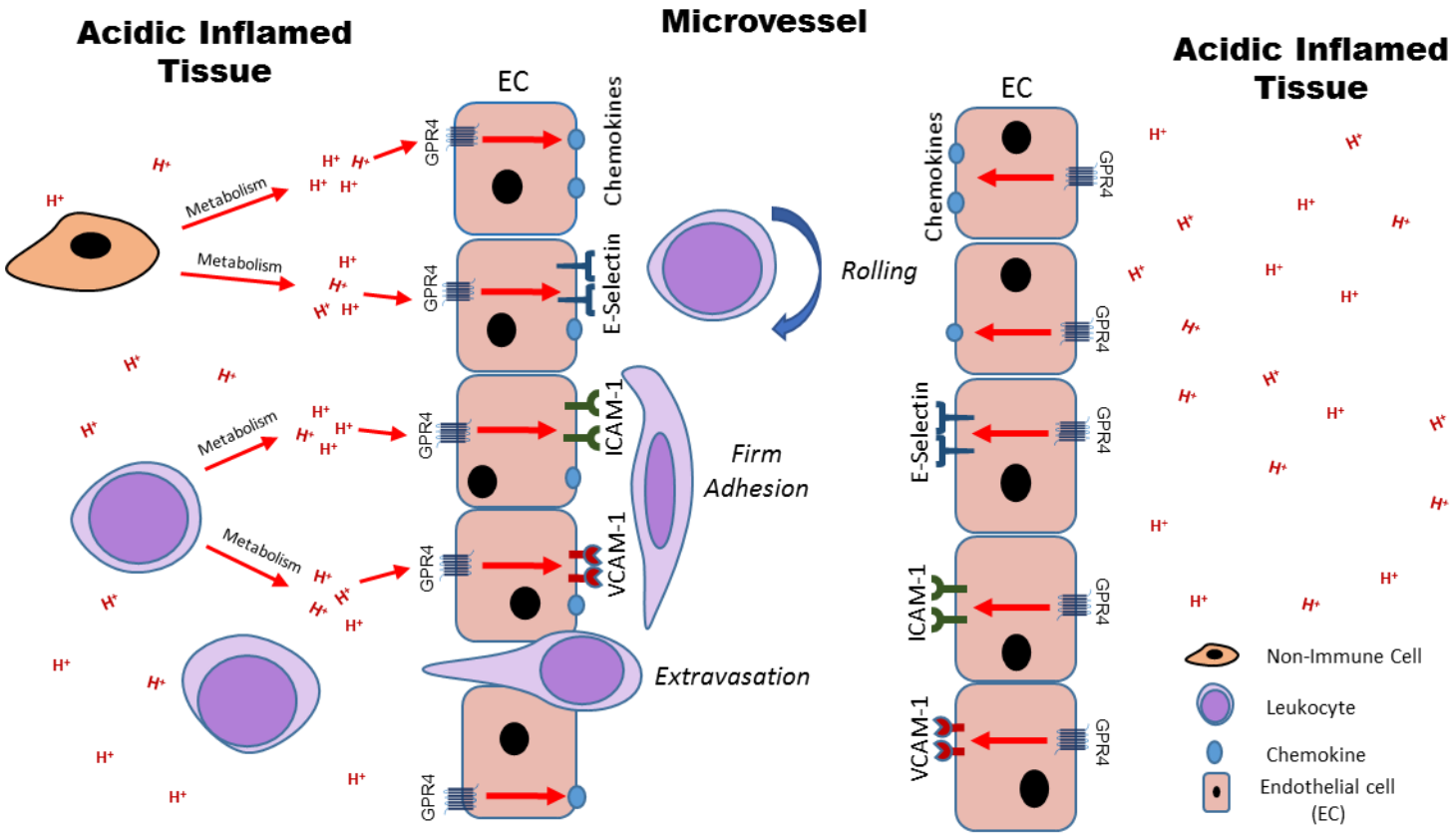
Acidic Inflamed Tissue
Microvessel
EC
Chemokines
GPR4
Metabolism
E-Selectin
Rolling
ICAM-1
VCAM-1
Firm Adhesion
Extravasation
Acidic Inflamed Tissue
Non-Immune Cell
Leukocyte
Chemokine
Endothelial cell (EC)

Figure 3.11. **Model of proposed mechanism for the governance of endothelial cell inflammatory responses by GPR4**. GPR4 can be activated by protons in the acidic microenvironment and increase the expression of adhesion molecules and chemokines for the recruitment and adherence of leukocytes to the endothelium. Increased leukocyte extravasation will occur into the inflamed tissue and potentiate local inflammation.

A

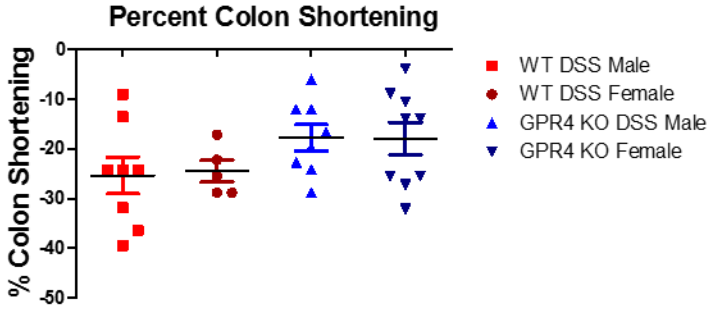
Percent Colon Shortening
% Colon Shortening
0
-10
-20
-30
-40
-50
WT DSS Male
WT DSS Female
GPR4 KO DSS Male
GPR4 KO Female

B

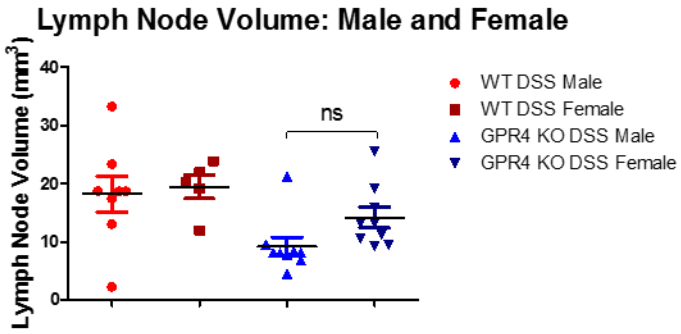
Lymph Node Volume: Male and Female
Lymph Node Volume (mm3)
40
30
20
10
0
ns
WT DSS Male
WT DSS Female
GPR4 KO DSS Male
GPR4 KO DSS Female

C

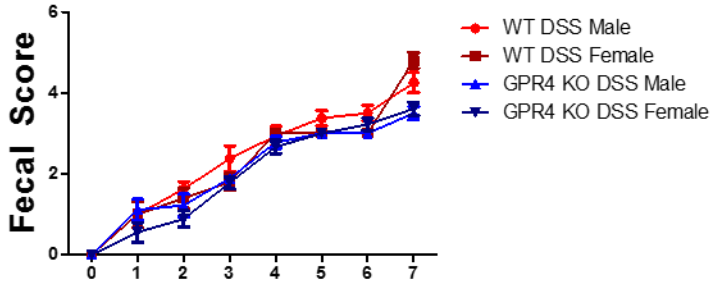
Fecal Score: Male and Female
Fecal Score
6
4
2
0
0 1 2 3 4 5 6 7
WT DSS Male
WT DSS Female
GPR4 KO DSS Male
GPR4 KO DSS Female

D

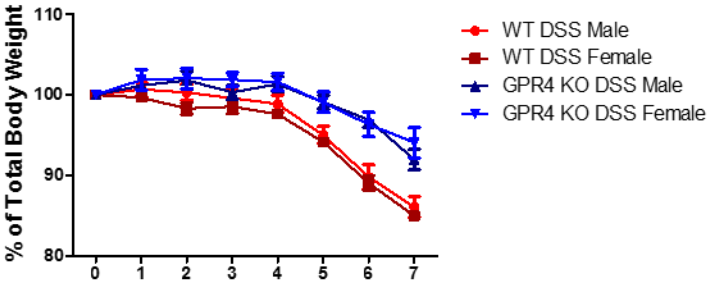
Body Weight Loss: Male and Female
% of Total Body Weight
110
100
90
80
0 1 2 3 4 5 6 7
WT DSS Male
WT DSS Female
GPR4 KO DSS Male
GPR4 KO DSS Female

E

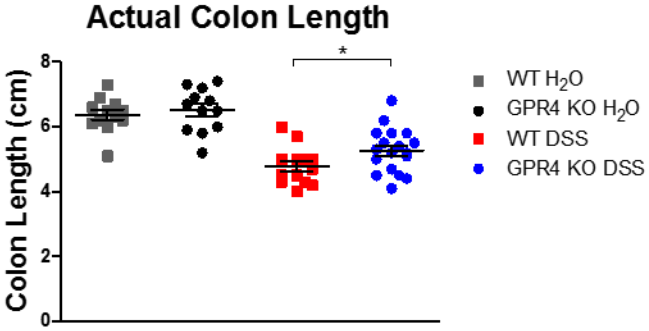
Actual Colon Length
Colon Length (cm)
8
6
4
2
0
*
WT H2O
GPR4 KO H2O
WT DSS
GPR4 KO DSS

Figure 3.12. Clinical phenotype and macroscopic disease indicators; male vs. female. (A) Percent colon shortening male vs. female mice, (B) mesenteric lymph node volume male vs. female mice, (C) fecal score male vs. female mice, and (D) percent body weight loss male vs. female mice. Actual colon length as a clinical parameter of intestinal inflammation. Colon lengths of WT control (n=12), WT-DSS (n=13), GPR4 KO control (n=12), and GPR4 KO-DSS (n=18) are presented in centimeters (E). Data are presented as mean ± SEM and analyzed for statistical significance using the unpaired *t*-test between two groups indicated on graph. *ns*: not significant.

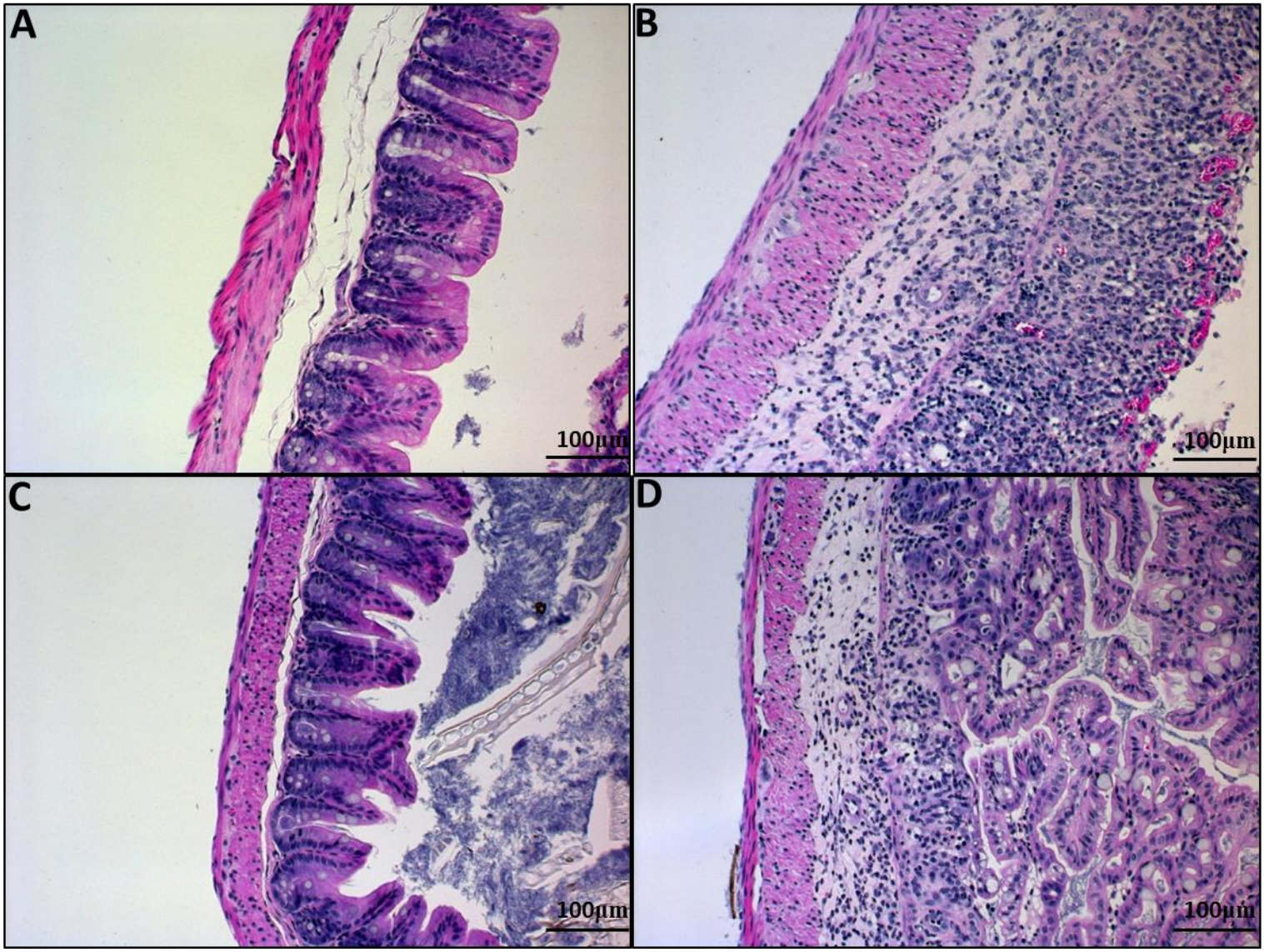
A
100µm
B
100µm
C
100µm
D
100µm

Figure 3.13. H&E representative pictures of cecum in (A) WT control, (B) WT-DSS, (C) GPR4 KO control, and (D) GPR4 KO-DSS. Histopathological features are reduced in GPR4 KO mice when compared to WT mice in cecum tissues. 20× microscope objective.

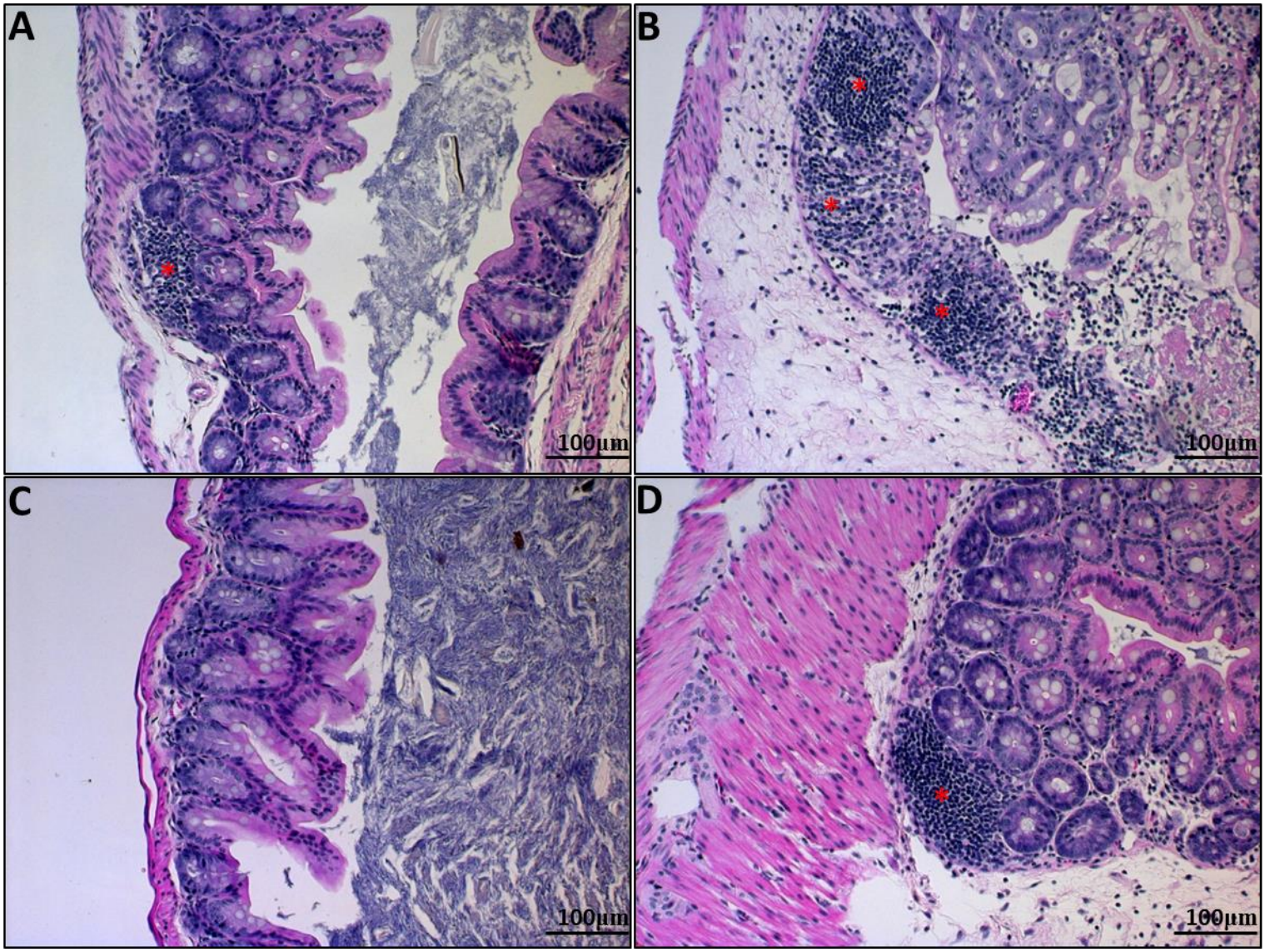
A
100µm
B
100µm
C
100µm
D
100µm

Figure 3.14. H&E representative pictures of ILFs in cecum. (A) WT control, (B) WT-DSS, (C) GPR4 KO control, and (D) GPR4 KO-DSS. GPR4 KO-DSS mice have reduced ILFs in cecum tissues when compared to WT-DSS mice. 20× microscope objective. Red asterisk indicates ILF.

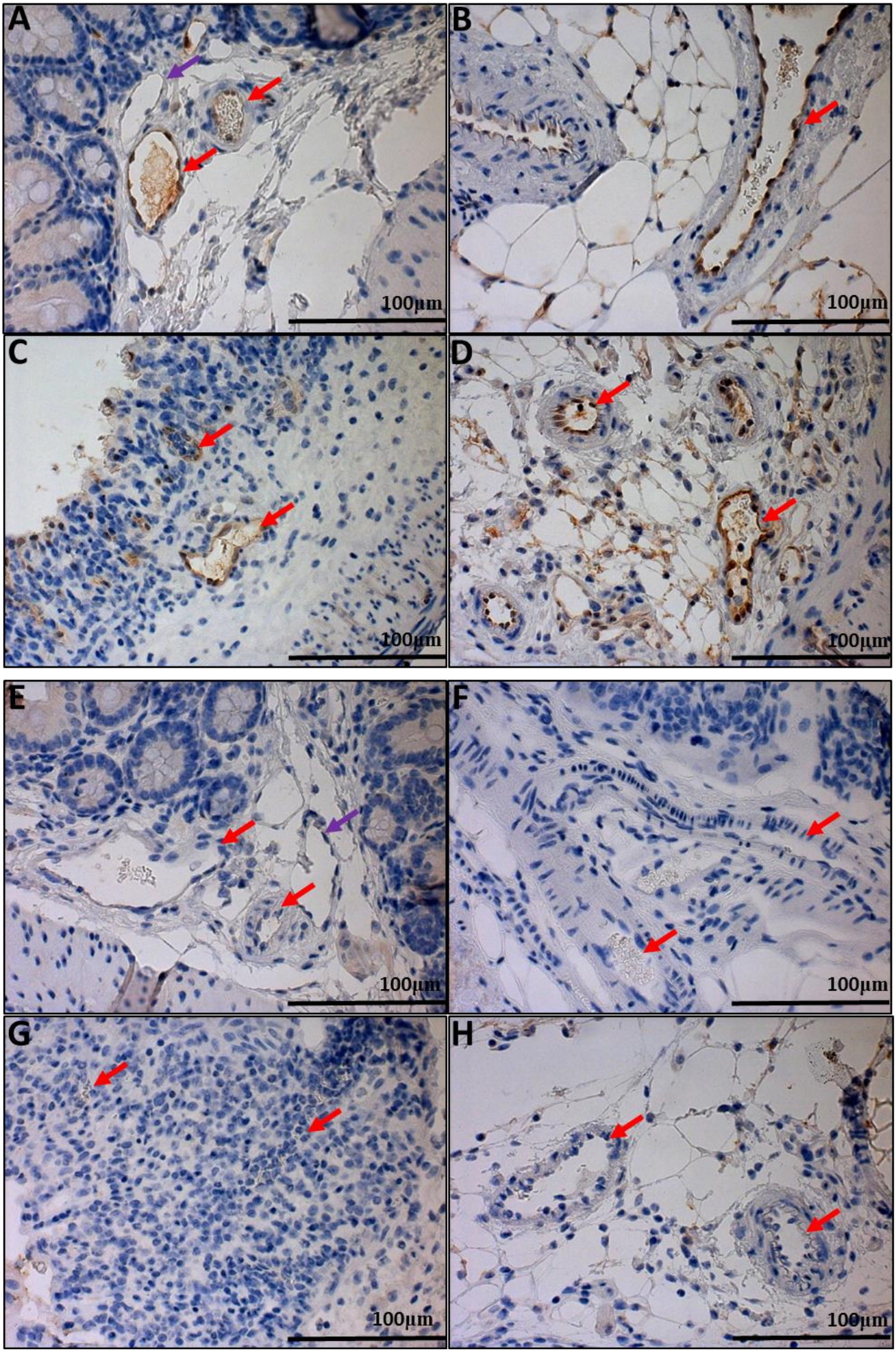
A
100μm
B
100μm
C
100μm
D
100μm
E
100μm
F
100μm
G
100μm
H
100μm

Figure 3.15. **GFP knock-in as a surrogate marker for GPR4 expression in GPR4 KO mouse cecum**. Immunolabeling of GFP was performed in GPR4 KO cecum tissue. Similarly to mouse colon tissue, GFP expression could be visualized in the intestinal microvascular endothelial cells, ex-mural blood vessels, arteries in both control and inflamed cecum tissues. Lymphatics had very low GFP expression. (A) GPR4 KO untreated cecum submucosa blood vessels and (B) ex-mural vessels compared to (C) inflamed GPR4 KO-DSS submucosa blood vessels and (D) ex-mural vessels. No GFP signal could be detected in (E-F) WT control untreated cecum tissues and (G-H) WT-DSS cecum tissues. 40× microscope objective. Red arrows indicate blood vessels and purple arrows indicate lymphatics.

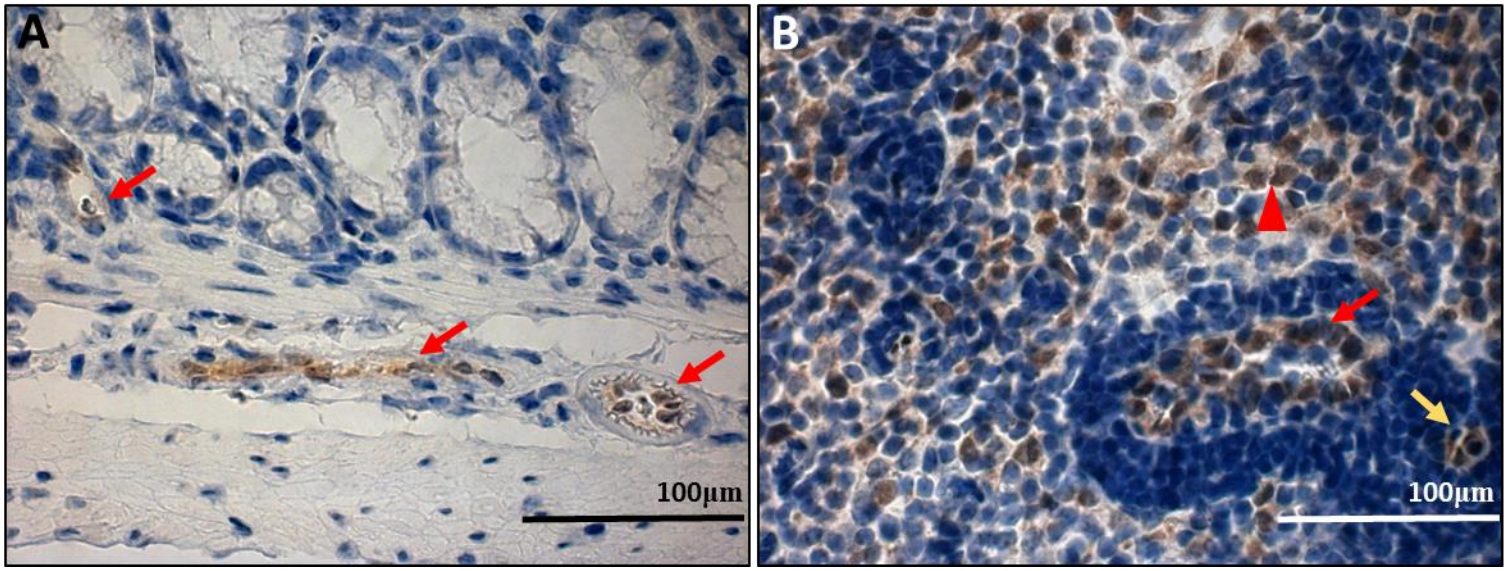
A
100µm
B
100µm

Figure 3.16. **GFP immunohistochemistry of GPR4 heterozygous mouse colon and mesenteric lymph node**. GFP expression can be observed in the same cell types observed in GPR4 KO homozygous mouse tissues. (A) GFP can be detected in colon blood vessels. 40× microscope objective. (B) GFP expression in the lymph node can be observed in resident histiocytes, blood vessels, and HEVs. 63× microscope objective. Red arrow heads indicate macrophages, red arrows indicate blood vessels, and yellow arrows indicate HEVs.

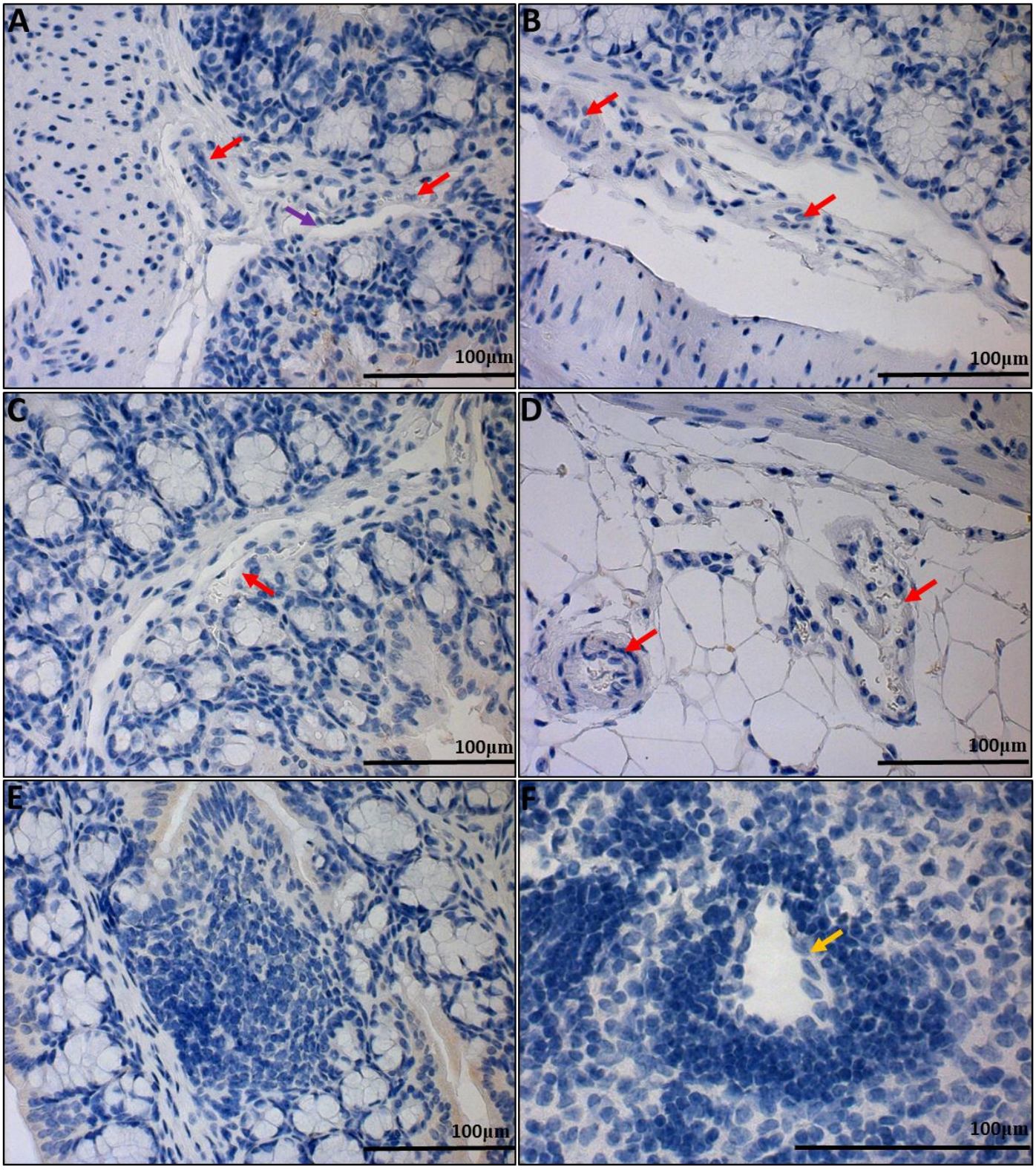
A
100µm
B
100µm
C
100µm
D
100µm
E
100µm
F
100µm

Figure 3.17. **GFP immunohistochemistry of WT control colon**. No visible GFP expression can be detected in tissues. Minor background staining could be observed on epithelium. (A-B) Submucosa, (C) transverse folds, (D) ex-mural, (E) isolated lymphoid follicles, (F) mesenteric lymph node HEV and resident macrophages. (A-E) 40× and (F) 63× microscope objectives. Red arrows indicate blood vessels, yellow arrows indicate HEVs, and purple arrows indicate lymphatics.

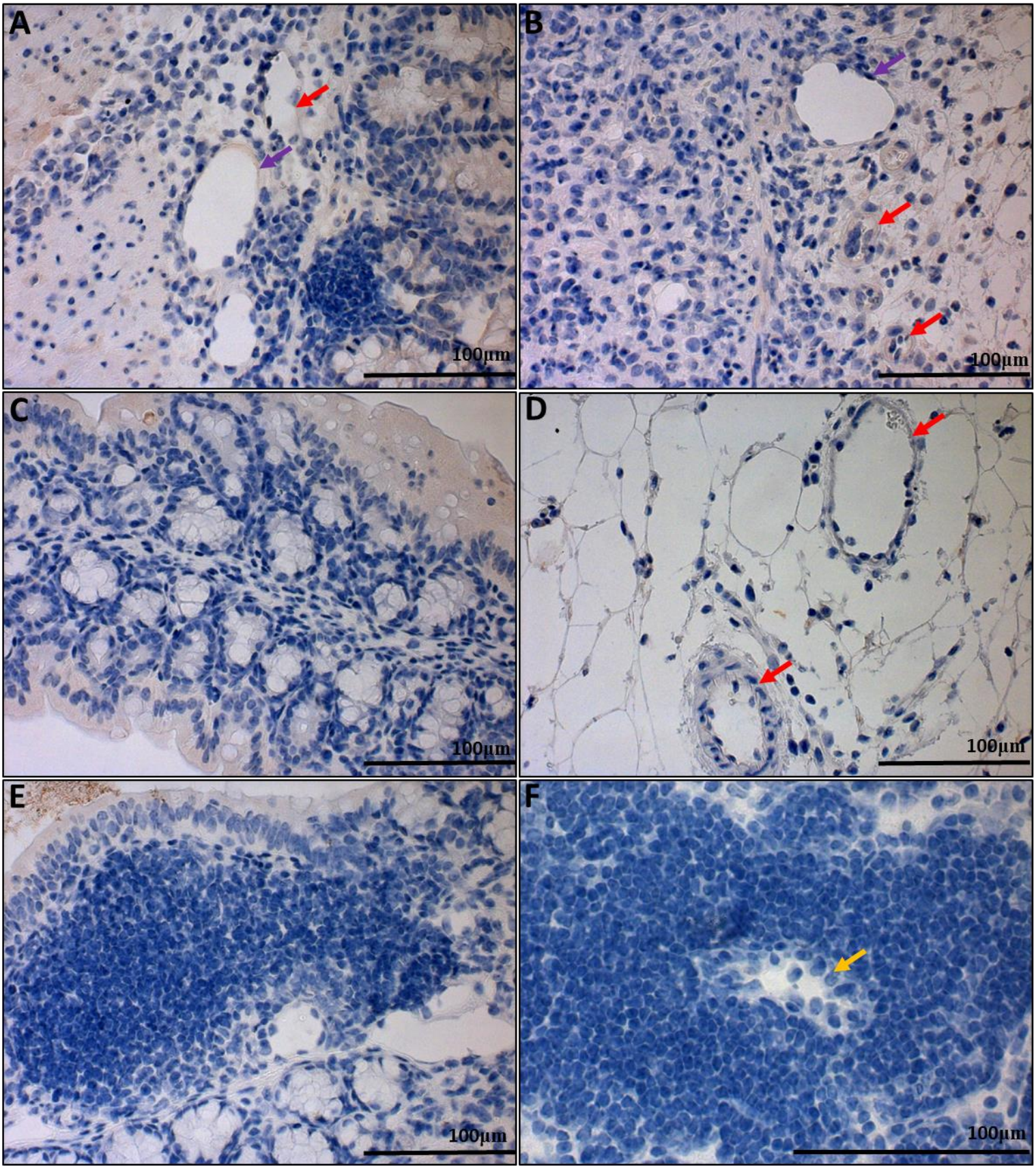
A
100µm
B
100µm
C
100µm
D
100µm
E
100µm
F
100µm

Figure 3.18. **GFP immunohistochemistry of WT-DSS treated colon**. No visible GFP expression can be detected in WT tissues. Minor background staining could be observed on epithelium, luminal content, and connective tissues. (A-B) Submucosa, (C) transverse folds, (D) ex-mural, (E) isolated lymphoid follicles, and (F) mesenteric lymph node HEV and resident macrophages. (A-E) 40× and (F) 63× microscope objectives. Red arrows indicate blood vessels, yellow arrows indicate HEVs, and purple arrows indicate lymphatics.

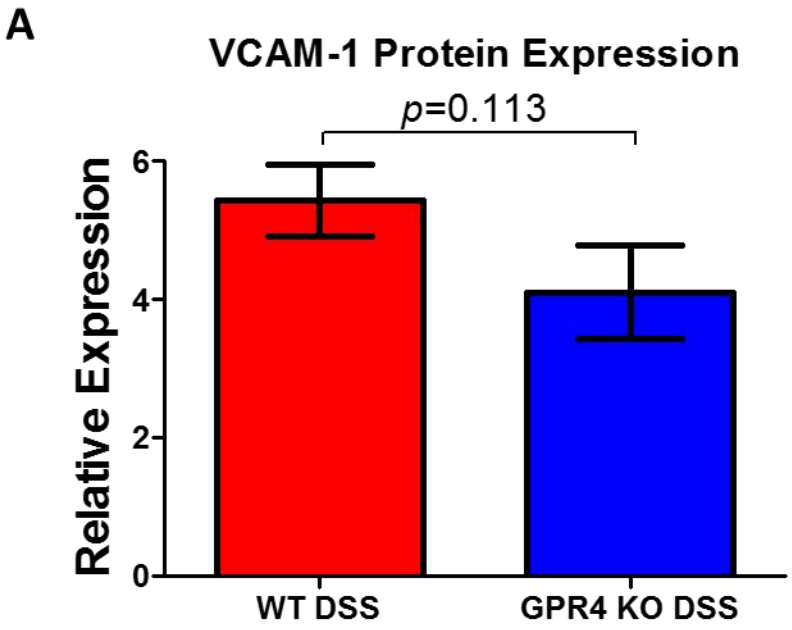
A
VCAM-1 Protein Expression
p=0.113
Relative Expression
6
4
2
0
WT DSS
GPR4 KO DSS

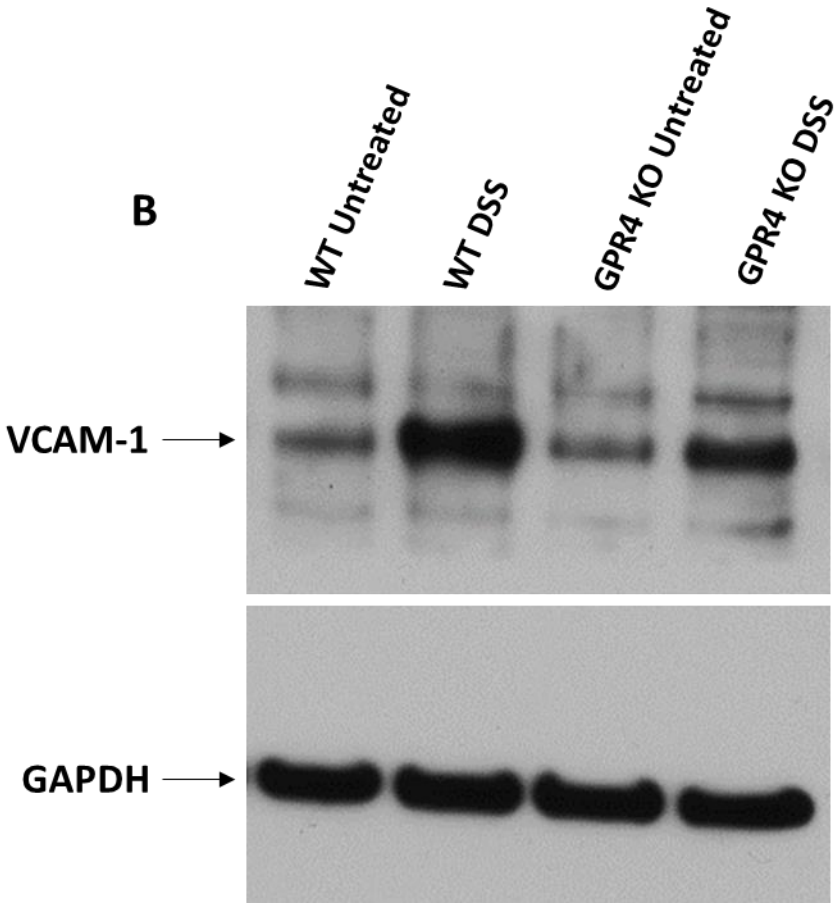
B
WT Untreated
WT DSS
GPR4 KO Untreated
GPR4 KO DSS
VCAM-1
GAPDH

Figure 3.19. **Western blot analysis of VCAM-1 protein expression in mouse colon tissues**. VCAM-1 protein expression was reduced in GPR4 KO-DSS (n=9) colon tissues when compared to WT-DSS (n=9), although not statistically significant (*P*=0.113). Target bands are indicated by an arrow. Red and blue dotted lines indicate WT-control (n=9) and GPR4 KO control (n=9) quantification, respectively. Data are presented as mean ± SEM and analyzed for statistical significance using the unpaired t-test between WT-DSS and GPR4 KO-DSS mice.

C.2 GPR4 potentiates intestinal inflammation in the chronic DSS-induced experimental colitis mouse model.

Wild-type (WT) and GPR4 KO mice were started on the chronic DSS-induced mouse colitis model consisting of 4 cycles of severe to moderate intestinal inflammation. During each day of the experiment, mouse bodyweight and fecal blood and diarrhea were analyzed and used to determine the disease activity index score. During cycle one, no obvious difference could be observed in disease activity between WT and GPR4 KO DSS-induced mice. However, beginning from cycle two through four GPR4 KO mice displayed less disease activity when compared to WT DSS-induced mice (Figure 3.20). No disease activity was observed in water control WT and GPR4 KO mice. Analyzing distinct clinical features of disease activity such as body weight loss and fecal blood and diarrhea scores, WT-DSS mice began to lose between 12-15% body weight following cycle one whereas GPR4 KO-DSS mice lost between 5-10% body weight though out all cycles (Figure 3.21). Fecal blood and diarrhea scores also indicated GPR4 KO-DSS mice were less clinically severe when compared to WT-DSS mice as GPR4 KO-DSS mice had reduced fecal blood and diarrhea scores (Figure 3.21).

Upon completion of all four cycles of the chronic DSS-induced colitis induction, macroscopic disease indicators were collected such as mesenteric lymph node (MLN) enlargement and colon length measurements. Interestingly, no significant differences were observed in MLN volume between WT and GPR4 KO DSS-induced mice as was observed in the acute DSS-induced mouse model (Figure 3.21). The colon length, however, indicated GPR4 KO-DSS mice had less colon shortening when compared to WT-DSS mice (Figure 3.21). Collectively, these results indicate GPR4 potentiates disease severity in the chronic DSS-induced mouse model.

Following the investigation of the clinical and macroscopic disease indicators for the assessment of the role of GPR4 in intestinal inflammation, we evaluated the degree of histopathology in the distal, middle, and proximal colon segments. Distinct parameters of colitis-associated histopathology were assessed such as leukocyte infiltration, edema, crypt loss, and architectural distortion to obtain a score of severity. WT and GPR4 KO water control mice displayed no observable histopathology (data not shown). However, GPR4 KO-DSS mice had reduced histopathology when compared to WT-DSS mice in the colon segments (Figure 3.22). Interestingly, leukocyte infiltration was reduced in the colon of GPR4 KO-DSS mice compared to WT-DSS mice which corroborates previous reports indicating GPR4 can increase leukocyte infiltration into inflamed intestinal tissues through upregulating endothelial cell adhesion molecules (Figure 3.22).

Isolated lymphoid follicles (ILFs) were also evaluated as an indicator of intestinal inflammation severity. Total ILFs were counted from distal, middle, and proximal colon segments and displayed as ILFs/centimeter of colon length. A trend in reduced ILF numbers could be appreciated in GPR4 KO-DSS mice when compared to WT-DSS mice, however, only the middle colon segment reached statistical significance (Figure 3.23).

Another distinct histopathological consequence is pathological fibrosis in chronically inflamed intestinal tissues. We observed heighted fibrotic development in mice with chronic DSS-induced colitis. The distal colon segment displayed the highest degree of fibrosis with a progressive reduction of severity from middle to proximal. A significant reduction could be observed in the GPR4 KO-DSS mice in the distal, middle, and proximal colon segments when compared to WT-DSS mice (Figure 3.24).

We next assessed the cellular constituents which may be contributing to the heighted inflammation observed in the DSS-induced mice when compared to GPR4 KO-DSS mice. Total $F4/80^+$ macrophages, $CD4^+$ T cells, and $CD8^+$ T cells were counted in the distal colon segment of WT-DSS and GPR4 KO-DSS mice. Consistent with total leukocyte infiltration scores, GPR4 KO-DSS mice had reduced numbers of $F4/80^+$ macrophages (~80 vs. 60), $CD4^+$ T cells (~85 vs. 75), and $CD8^+$ T cells (~75 vs. 38) cells per field of view in the distal colon when compared to WT-DSS mice, respectively (Figure 3.25).

In summary, GPR4 KO-DSS mice had reduced disease severity and intestinal inflammation when compared to WT-DSS mice in the chronic DSS-induced colitis mouse model. These results indicate GPR4 not only mediates acute intestinal inflammation, but also chronic intestinal inflammation.

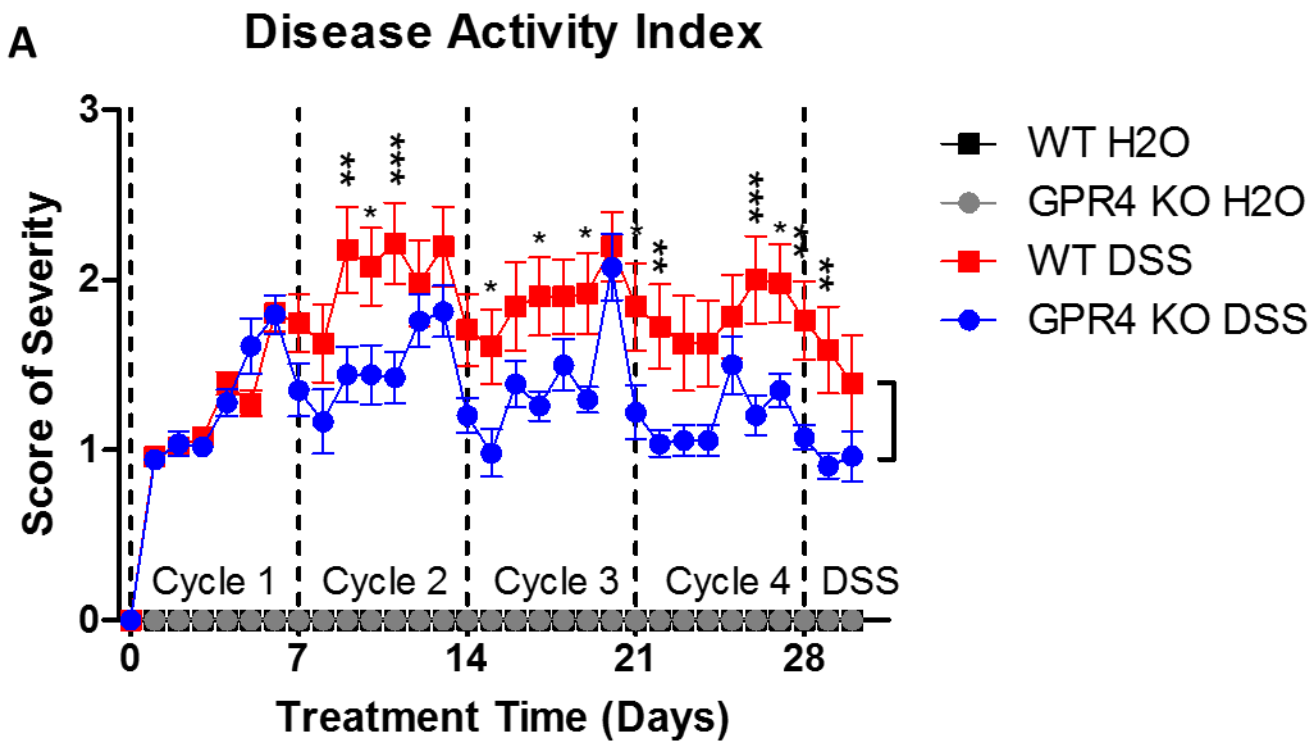
A
Disease Activity Index
Score of Severity
3
2
1
0
Cycle 1
Cycle 2
Cycle 3
Cycle 4
DSS
0
7
14
21
28
Treatment Time (Days)
WT H2O
GPR4 KO H2O
WT DSS
GPR4 KO DSS

Figure 3.20: **Disease activity index**. (A) GPR4 deficiency reduces disease activity in the chronic DSS-induced colitis mouse model. WT-untreated (n=14), WT-DSS (n=18), GPR4 KO-untreated (n=14), and GPR4 KO-DSS (n=18). Data are presented as mean ± SEM and was analyzed for statistical significance using the two-way ANOVA followed by Bonferroni post hoc between WT-DSS mice and GPR4 KO-DSS mice or as indicated within graph. (*$P < 0.05$, **$P < 0.01$, *** $P< 0.001$).

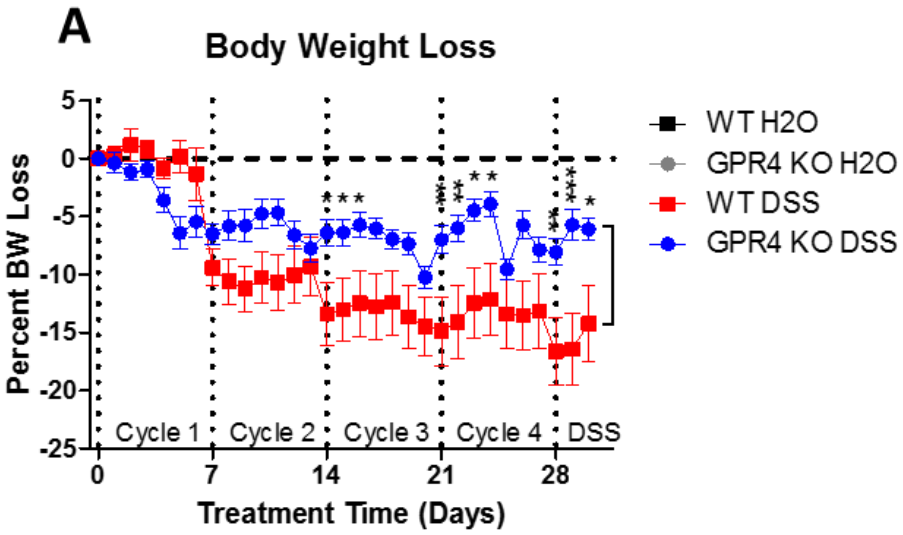
A
Body Weight Loss
Percent BW Loss
Treatment Time (Days)
Cycle 1
Cycle 2
Cycle 3
Cycle 4
DSS
WT H2O
GPR4 KO H2O
WT DSS
GPR4 KO DSS

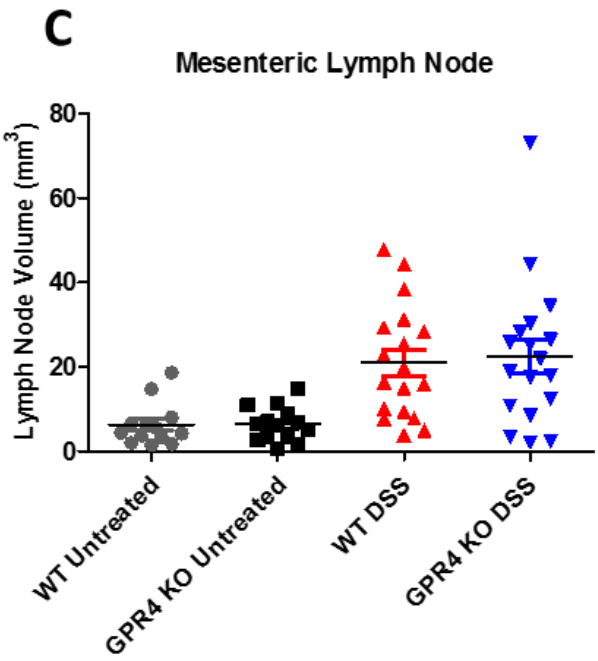
C
Mesenteric Lymph Node
Lymph Node Volume (mm3)
WT Untreated
GPR4 KO Untreated
WT DSS
GPR4 KO DSS

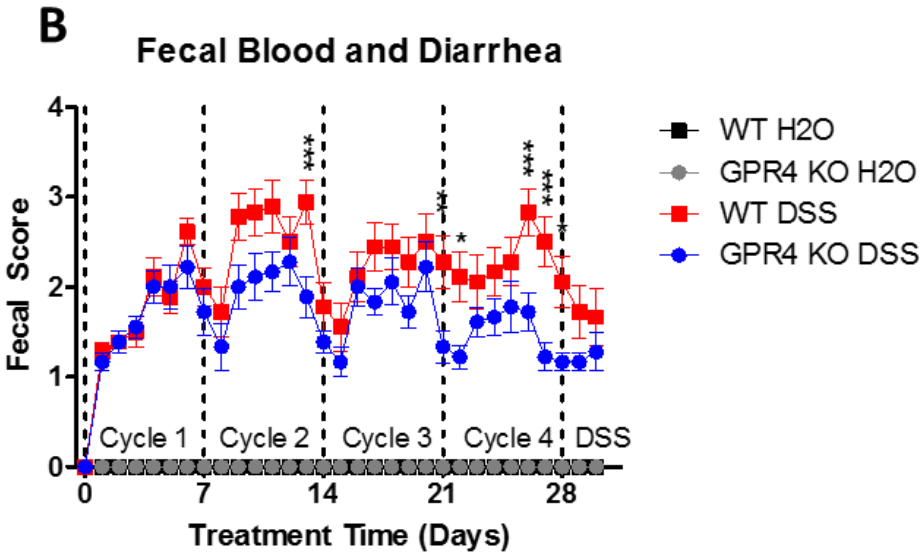
B
Fecal Blood and Diarrhea
Fecal Score
Treatment Time (Days)
Cycle 1
Cycle 2
Cycle 3
Cycle 4
DSS
WT H2O
GPR4 KO H2O
WT DSS
GPR4 KO DSS

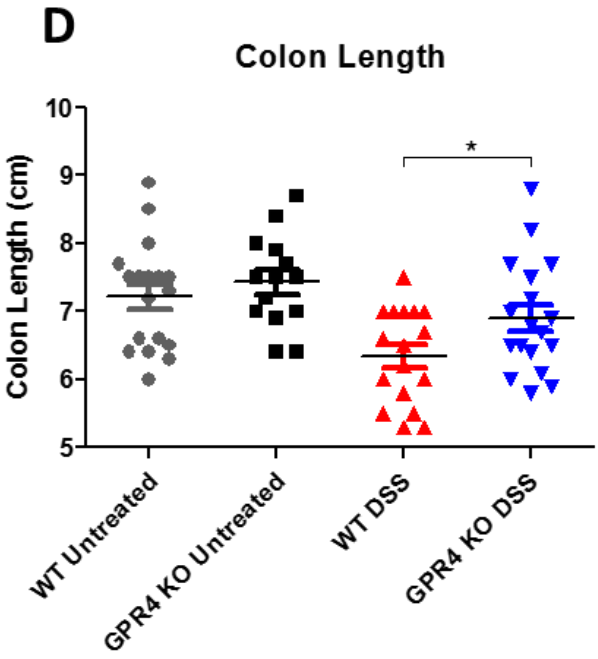
D
Colon Length
Colon Length (cm)
WT Untreated
GPR4 KO Untreated
WT DSS
GPR4 KO DSS

Figure 3.21: **Clinical phenotypes and macroscopic disease indicators**. GPR4 deficiency reduced (A) body weight loss and fecal blood and (B) diarrhea scores during intestinal inflammation. Additionally, (C) mesenteric lymph node volume and (D) colon length in centimeters were assessed as macroscopic disease indicators. WT-untreated (n=14), WT-DSS (n=18), GPR4 KO-untreated (n=14), and GPR4 KO-DSS (n=18). Data are presented as mean ± SEM and was analyzed for statistical significance using the two-way ANOVA followed by Bonferroni post hoc between WT-DSS mice and GPR4 KO-DSS mice or as indicated within graph. (*$P < 0.05$, **$P < 0.01$, *** $P< 0.001$).

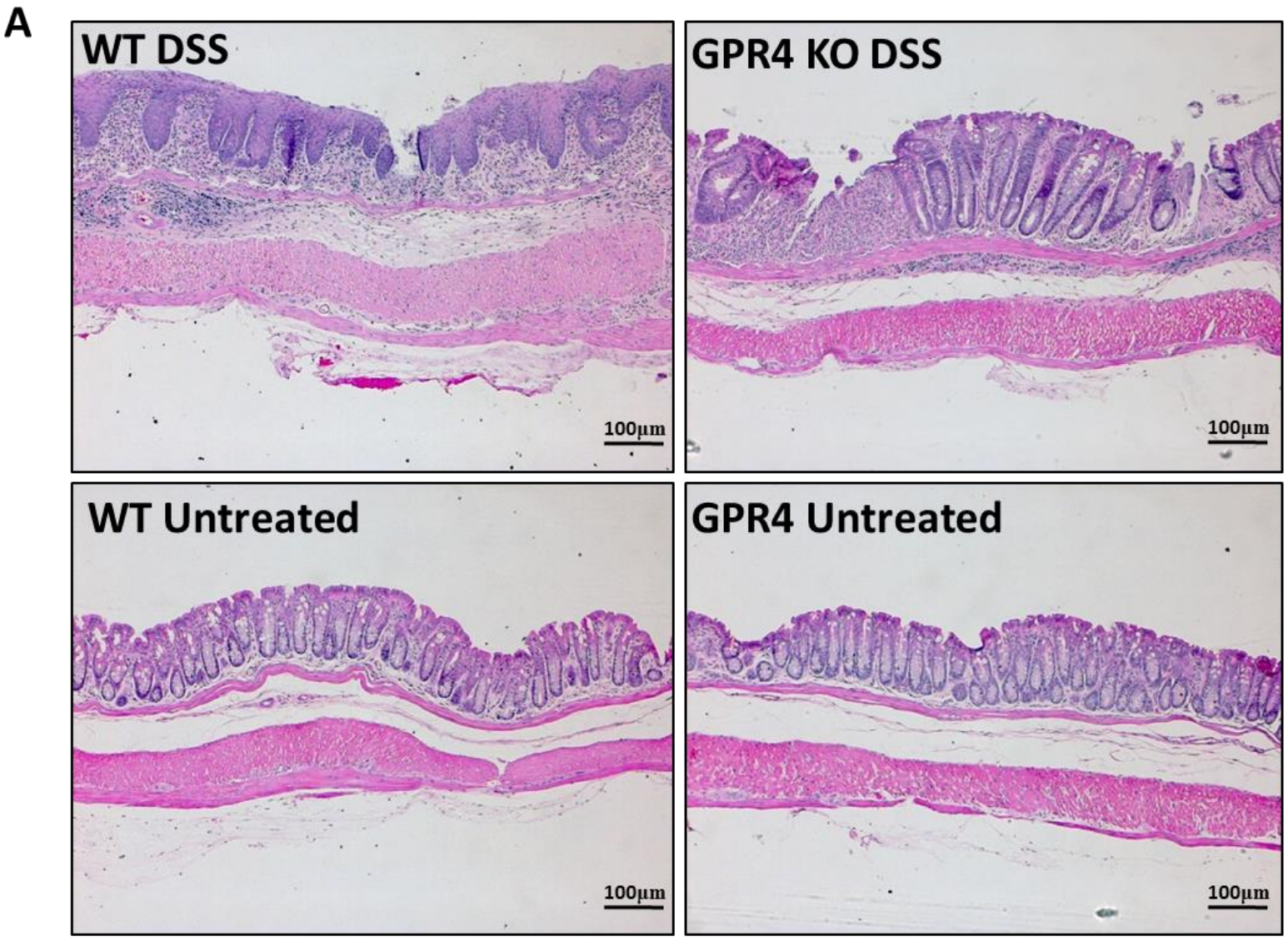
A
WT DSS
GPR4 KO DSS
WT Untreated
GPR4 Untreated
100µm
100µm
100µm
100µm

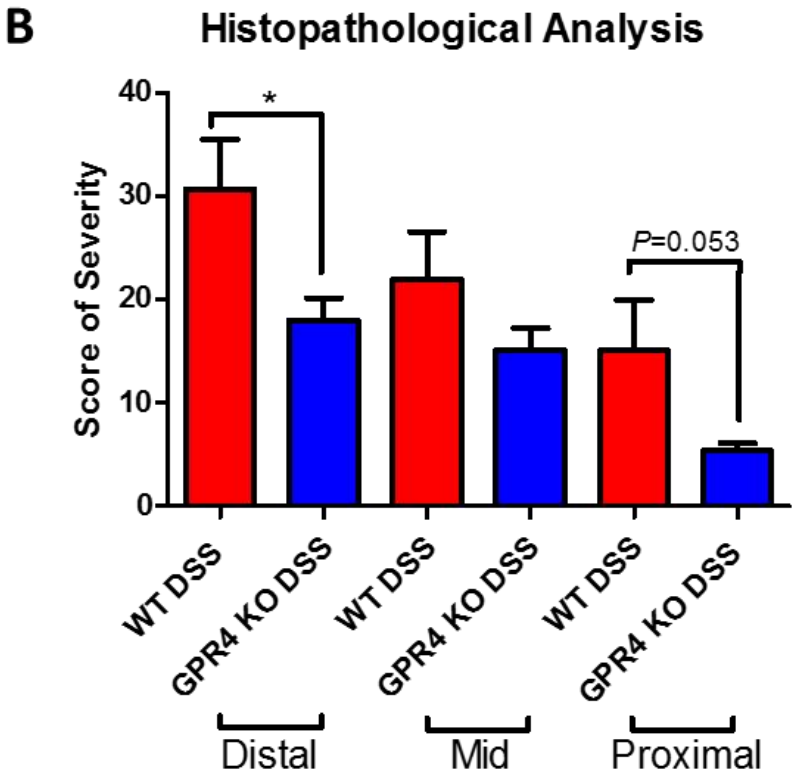
B
Histopathological Analysis
Score of Severity
40
30
20
10
0
*
P=0.053
WT DSS
GPR4 KO DSS
WT DSS
GPR4 KO DSS
WT DSS
GPR4 KO DSS
Distal
Mid
Proximal

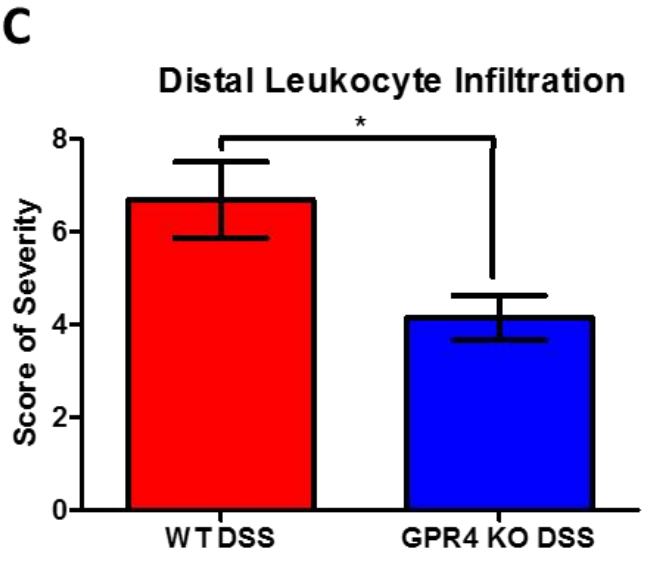
C
Distal Leukocyte Infiltration
Score of Severity
8
6
4
2
0
*
WT DSS
GPR4 KO DSS

Figure 3.22: **Histopathological analysis of colon tissues**. GPR4 knockout mice have reduced histopathology when compared to WT mice. (A) Representative images of reduced histopathological features and graphical representation of total (B) histopathology score of severity and (C) leukocyte infiltration. WT-untreated (n=14), WT-DSS (n=18), GPR4 KO-untreated (n=14), and GPR4 KO-DSS (n=18). Data are presented as mean ± SEM and was analyzed for statistical significance using the unpaired *t*-test between WT-DSS mice and GPR4 KO-DSS mice or as indicated within graph. (**P* < 0.05, ***P* < 0.01, *** *P*< 0.001).

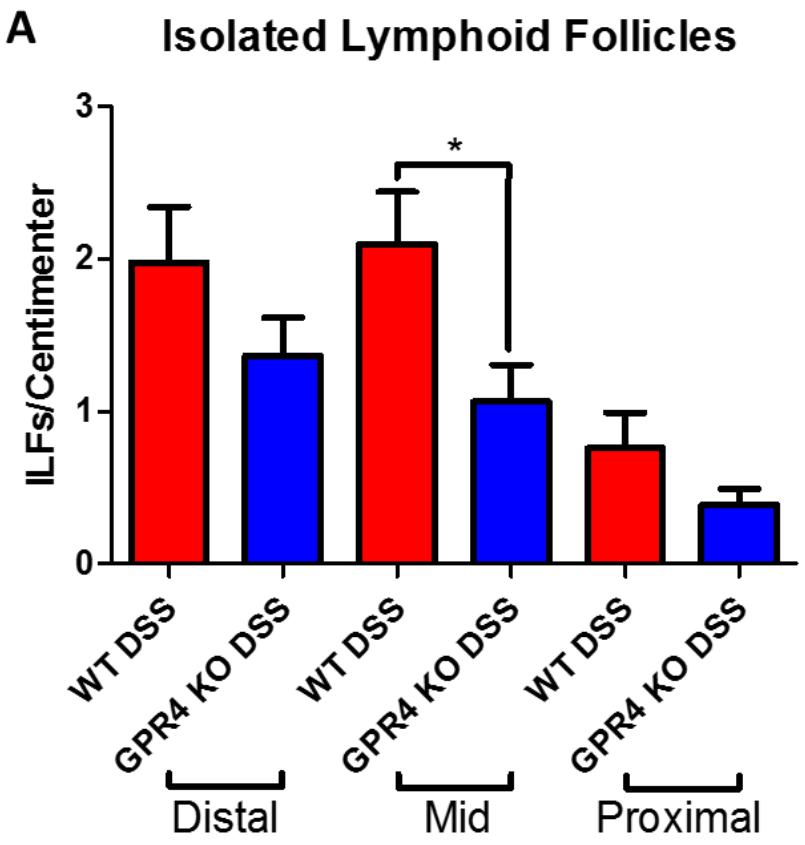
A
Isolated Lymphoid Follicles
ILFs/Centimenter
3
2
1
0
*
WT DSS
GPR4 KO DSS
WT DSS
GPR4 KO DSS
WT DSS
GPR4 KO DSS
Distal
Mid
Proximal

Figure 3.23: **Isolated lymphoid follicle development**. (A) GPR4 deletion results in fewer isolated lymphoid follicles when compared to WT mice. WT-untreated (n=14), WT-DSS (n=18), GPR4 KO-untreated (n=14), and GPR4 KO-DSS (n=18). Data are presented as mean ± SEM and was analyzed for statistical significance using the unpaired *t*-test between WT-DSS mice and GPR4 KO-DSS mice or as indicated within graph. (*$P < 0.05$, **$P < 0.01$, *** $P< 0.001$).

A

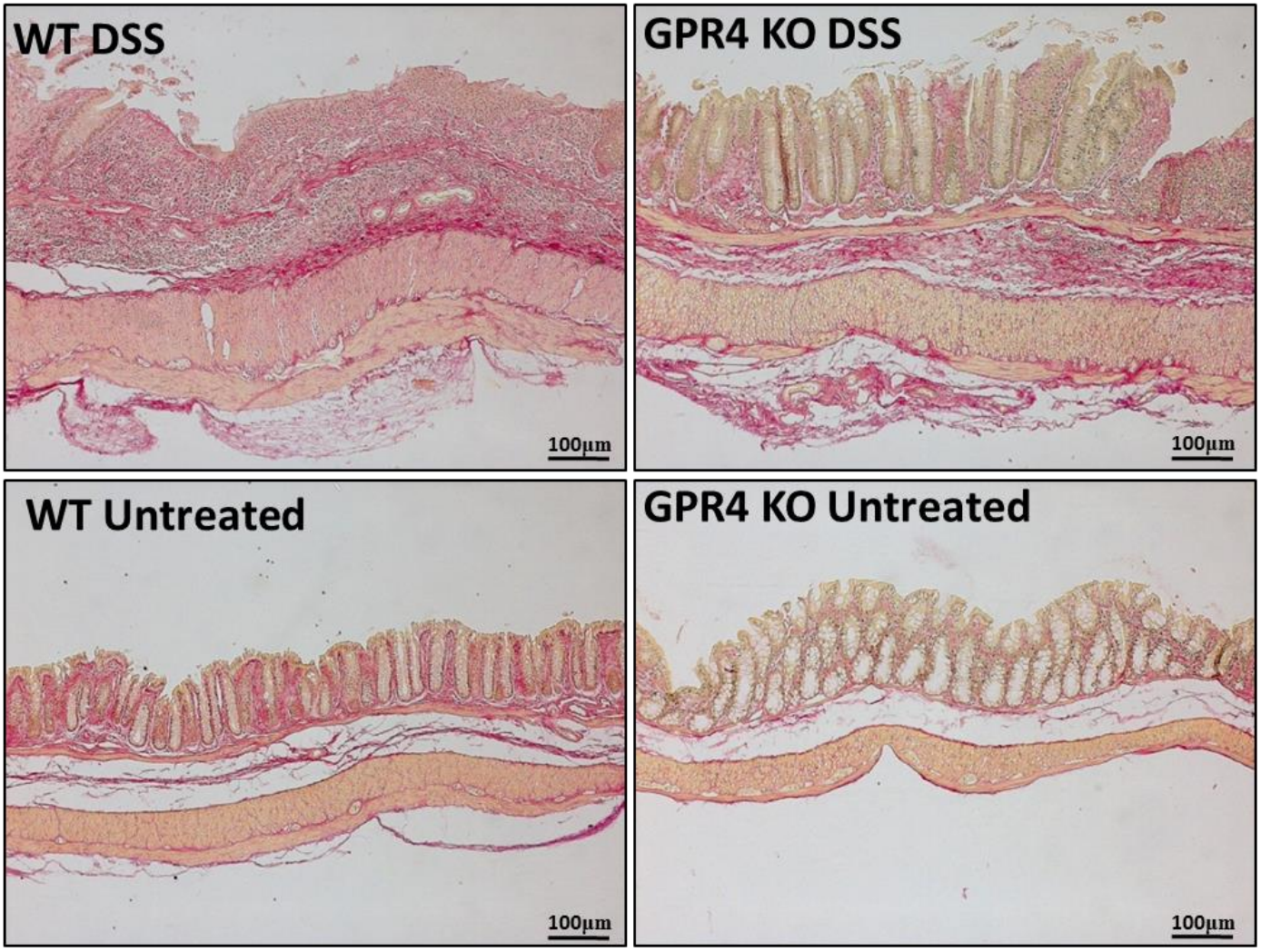
WT DSS
100µm
GPR4 KO DSS
100µm
WT Untreated
100µm
GPR4 KO Untreated
100µm

B

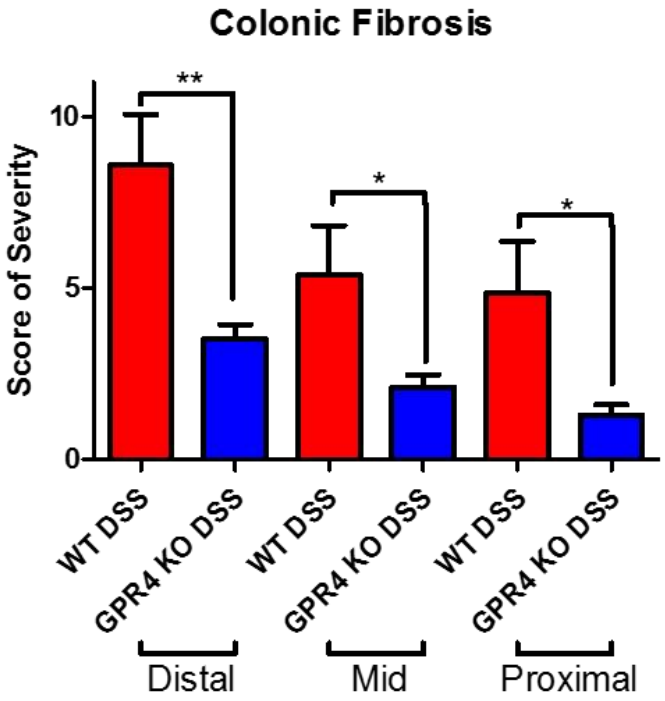
Colonic Fibrosis
Score of Severity
10
5
0
**
*
*
WT DSS
GPR4 KO DSS
WT DSS
GPR4 KO DSS
WT DSS
GPR4 KO DSS
Distal
Mid
Proximal

Figure 3.24: Pathological fibrosis analysis in colon. GPR4 knockout-DSS mice have reduced score for fibrosis development when compared to WT-DSS mice. (A) Representative images and (B) graphical representation of fibrotic development in colon of WT and GPR4 KO DSS-induced mice. WT-untreated (n=14), WT-DSS (n=18), GPR4 KO-untreated (n=14), and GPR4 KO-DSS (n=18). Data are presented as mean ± SEM and was analyzed for statistical significance using the unpaired t-test between WT-DSS mice and GPR4 KO-DSS mice or as indicated within the graph. (*P < 0.05, **P < 0.01, *** P< 0.001).

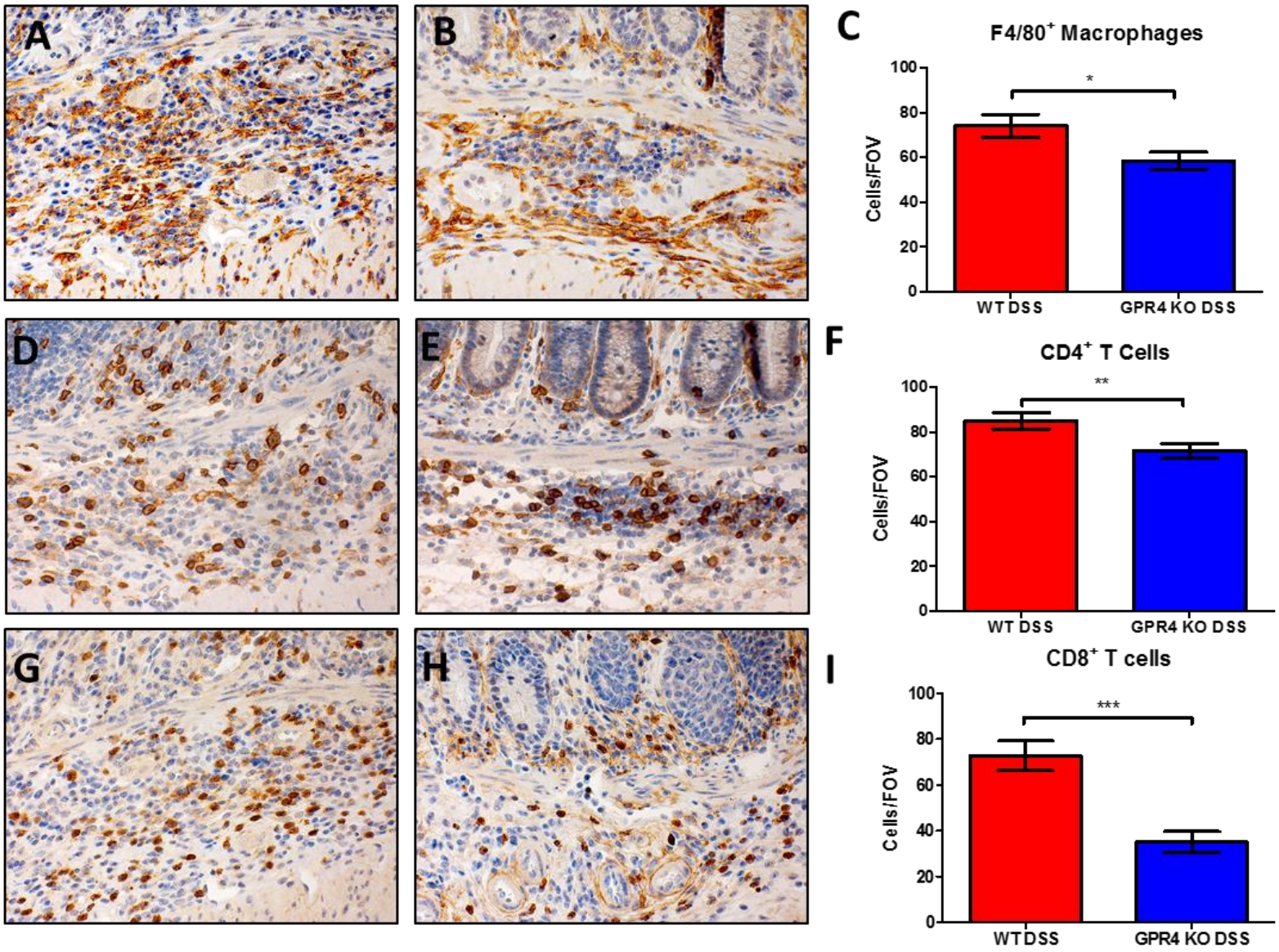
WT DSS
GPR4 KO DSS
A
B
C
F4/80+ Macrophages
Cells/FOV
WT DSS
GPR4 KO DSS
D
E
F
CD4+ T Cells
G
H
I
CD8+ T cells

Figure 3.25: **Immune cell infiltrate quantification**. GPR4 deletion results in fewer immune cell infiltrates such as (A-C) F4/80+ macrophages, (D-F) CD4+ T cells, and (G-I) CD8+ T cells into the inflamed intestine. WT-DSS (n=5-6) and GPR4 KO-DSS (n=5-6). Data are presented as mean ± SEM and was analyzed for statistical significance using the unpaired *t*-test between WT-DSS mice and GPR4 KO-DSS mice or as indicated within graph. (*$P < 0.05$, **$P < 0.01$, *** $P < 0.001$)

C.3 Pharmacological inhibition of GPR4 reduces intestinal inflammation in the acute DSS-induced experimental colitis mouse model.

Wild-type C57BL/6 mice were initiated on the acute DSS model and given vehicle or 30mg/kg of GPR4 antagonist 13 BID by oral gavage (Figure 3.26, Figure 3.27A). During each day of the experimental course mouse body weight in conjunction with fecal blood and diarrhea scores were evaluated to provide clinical assessment of disease severity between vehicle and GPR4 antagonist 13 groups. GPR4 antagonist 13 treated mice were protected from body weight loss commencing from day five through seven (Figure 3.27B). Mice given vehicle lost 11-14% body weight by day seven while mice provided GPR4 antagonist 13 lost between 3-6% body weight. Fecal blood and diarrhea scores provided further indication GPR4 antagonist 13 protects against intestinal inflammation as mouse fecal scores were reduced in GPR4 antagonist 13 treated mice compared to vehicle (Figure 3.27C). Fecal blood and diarrhea could be observed in mice with progressive severity from day one through seven. Vehicle mice developed heighted fecal scores earlier than GPR4 antagonist 13 treated mice and maintained more severe scores throughout the seven-day DSS experiment. These results collectively provide evidence GPR4 antagonist 13 can blunt clinical severity of DSS-induced intestinal inflammation.

Upon completion of the seven-day DSS-induced experimental colitis, mice were dissected for assessment of macroscopic disease indicators such as colon shortening, mesenteric lymph node expansion, and splenic expansion. We observed mice treated with GPR4 antagonist 13 had reduced colon shortening when compared to vehicle (colon length ~7.3cm versus ~6.1cm, respectively) (Figure 3.27D-E). Mesenteric lymph nodes (MLNs) were also collected, and the volume was measured in vehicle and GPR4 antagonist 13 treated mice. Vehicle MLN volume was expanded by more than 2-fold when compared to GPR4 antagonist 13 mice (Figure 3.27F).

These results indicate GPR4 antagonist 13 reduces colonic inflammation and associated expansion of MLNs when compared to vehicle. Finally, the spleen to body weight ratio was assessed in vehicle and GPR4 antagonist 13 DSS-treated mice. We observed reduced splenic expansion in mice treated with GPR4 antagonist 13 when compared to vehicle suggesting reduced disease severity due to GPR4 inhibition (Figure 3.27G).

To assess the effects of GPR4 inhibition at the histological level, distinct pathological cellular features of colitis were assessed in the distal, middle, and proximal colon segments. Some such features assessed in the colon were leukocyte infiltration, epithelium erosion, crypt distortion, and mucosal ulceration. In both vehicle and GPR4 antagonist 13 DSS-treated mice, the highest degree of histopathology can be observed in the distal colon segments followed by the middle and proximal, respectively. The observation that intestinal inflammation is most severe in the distal colon within the DSS model are consistent with literature [119, 122, 123]. When comparing vehicle and GPR4 antagonist 13 mouse groups, the degree of histopathology was significantly reduced by GPR4 antagonist 13 when compared to vehicle (Figure 3.28A-G). This GPR4 antagonist 13-mediated reduction in histopathology occurred in both the distal and middle colon segments with a trend in reduction at the proximal segment, though not statically significant. Interestingly, the degree of leukocyte infiltration was also reduced by GPR4 antagonist 13 when compared to vehicle (Figure 3.28H).

Previous studies have demonstrated GPR4 activation in endothelial cells (ECs) induces vascular cell adhesion molecule-1 (VCAM-1) and E-selectin expression [113, 114]. Additionally, reports have shown GPR4 genetic deletion can reduce VCAM-1 and E-selectin expression in the vascular endothelium [128]. Here we assessed the protein expression signal intensity of VCAM-1 and E-selectin in vascular endothelial cells in the distal, middle, and

proximal colon mucosa segments of vehicle and GPR4 antagonist 13 DSS-treated mice. The intensity scoring of VCAM-1 and E-selectin expression revealed highest signal within the distal intestinal endothelia with progressive intensity reduction in the middle and proximal colon, respectively. These data are consistent with the previous observation of reduced leukocyte infiltration in the middle and proximal colon segments compared to the distal segment. Interestingly, VCAM-1 and E-selectin signal intensity in intestinal microvascular ECs was reduced in GPR4 antagonist 13 DSS-treated mice when compared to vehicle in the distal colon (Figures 3.29-30). Collectively, these data provide evidence GPR4 antagonist 13 reduces EC activation and subsequently leukocyte infiltration into the inflamed intestinal mucosa.

Immunohistochemical analysis also revealed expression of VCAM-1 and E-selectin on cell types not regulated by GPR4. VCAM-1 expression could be strongly observed in activated fibroblasts and other mononuclear cells within the intestinal mucosa (Figure 4A-D). Previous reports have observed expression of VCAM-1 in skeletal muscle, fibroblast, and some leukocyte populations [158, 159]. E-selectin expression could be observed in some mononuclear cells within the intestinal mucosa (Figure 3.29A-B). Additionally, E-selectin expression could be detected within the colon epithelium (Data not shown). These results are consistent with previous studies showing E-selectin can be expressed in the colon epithelium and in mononuclear cells in the intestinal mucosa during active colitis [157]. Furthermore, additional studies have shown E-selectin is expressed in T cells and can be upregulated by pro-inflammatory mediators [160, 161]. We observed similar levels of signal intensity of VCAM-1 and E-selectin in cell types other than intestinal microvascular endothelial cells between vehicle and GPR4 antagonist 13 groups.

In addition to VCAM-1 and E-selectin expression analysis, we assessed the expression intensity and distribution of mucosal vascular addressin cell adhesion molecule-1 (MAdCAM-1) in colon tissues. We observed prominent MAdCAM-1 expression in intestinal microvasculature with high expression density in the lamina propria. No MAdCAM-1 expression could be observed in arteries and extramural blood vessels and minimal expression could be detected in lymphatic endothelial cells. MAdCAM-1 expression signal intensity in the intestinal microvasculature were similar between vehicle and GPR4 antagonist 13 DSS-treated mouse groups (Figure 3.31). Total number of vessels positive for MAdCAM-1, however, were markedly reduced in GPR4 antagonist 13 mice compared to vehicle control mice (Figure 3.31). Total MAdCAM-1 positive vessels were counted per centimeter (cm) of colon length and vehicle mice had ~60 MAdCAM-1 positive vessels/cm compared to ~35 MAdCAM-1 positive vessels/cm in GPR4 antagonist 13 mice (Figure 3.31).

Following the assessment of histopathology and EC-specific inflammatory protein expression, we assessed inflammatory gene expression at the whole tissue level to discern the anti-inflammatory effects of GPR4 antagonist 13. Inflammatory genes were measured from the distal colon segment of vehicle and GPR4 antagonist 13 DSS-treated mice. Additionally, distal colon segments of wild-type mice not treated with DSS were collected and assessed to serve as a baseline gene expression reference. Inflammatory mediators such as TNF-α, IL-1β, IL-6, IL-10, and COX-2 were measured between vehicle and GPR4 antagonist 13 groups. A statistically significant reduction of TNF-α and IL-10 gene expression could be appreciated in the GPR4 antagonist 13 group compared to vehicle. Reduction of TNF-α is correlated with reduced inflammation in the mouse distal colon of the GPR4 antagonist 13 group. IL-10 can inhibit the function of macrophages and other inflammatory cells which are required for optimal pathogen

clearance and subsequent inflammatory resolution. As such, reduced levels of IL-10 mRNA in the tissues of GPR4 antagonist 13 treated mice could potentially enhance pathogen clearance during the acute inflammatory phase. Furthermore, vehicle administered mice also had a trend in heighted expression of the inflammatory genes IL-1β, IL-6, and COX-2 when compared to the GPR4 antagonist 13 treated group. In addition to inflammatory cytokines, adhesion molecule gene expression including E-selectin, MAdCAM-1, and VCAM-1 were assessed. A statistically significant reduction of MAdCAM-1 expression could be discerned in the GPR4 antagonist 13 treated mice compared to vehicle. VCAM-1 gene expression was modestly reduced in the GPR4 antagonist 13 group compared to vehicle and no trend in reduction could be discerned for E-selectin at the whole tissue level. As VCAM-1 and E-selectin are expressed in cells that are not regulated by GPR4, whole tissue gene expression analysis presents complications for assessing VCAM-1 and E-selectin expression specific to GPR4 regulated vascular endothelial cells. To overcome this complication, we assessed VCAM-1 and E-selectin protein expression specific to vascular endothelial cells as described above (Figures 3.29-30).

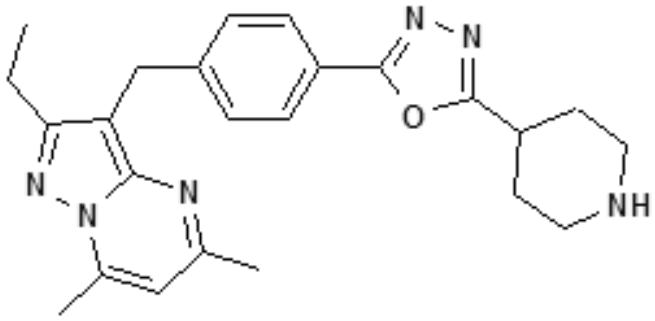

GPR4 antagonist 13 (NE 52-QQ57)

Figure 3.26: The chemical structure of GPR4 antagonist 13 (NE 52-QQ57) developed by Novartis Pharmaceuticals.

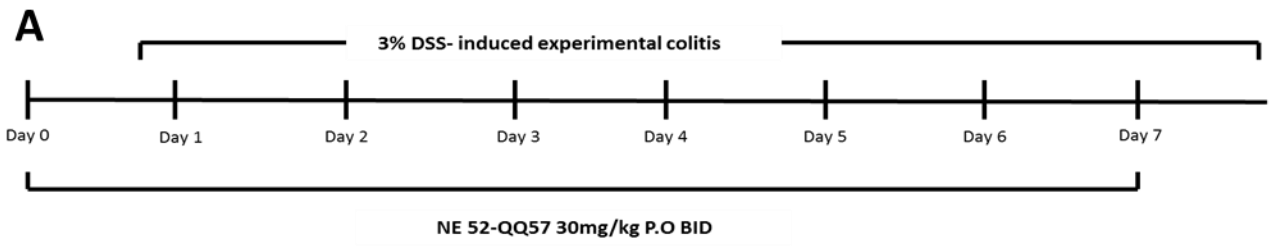
A
3% DSS- induced experimental colitis
Day 0
Day 1
Day 2
Day 3
Day 4
Day 5
Day 6
Day 7
NE 52-QQ57 30mg/kg P.O BID

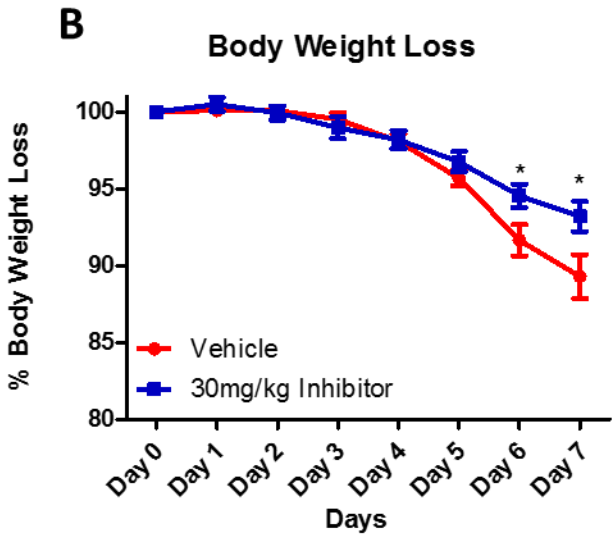
B
Body Weight Loss
% Body Weight Loss
100
95
90
85
80
Vehicle
30mg/kg Inhibitor
Day 0
Day 1
Day 2
Day 3
Day 4
Day 5
Day 6
Day 7
Days

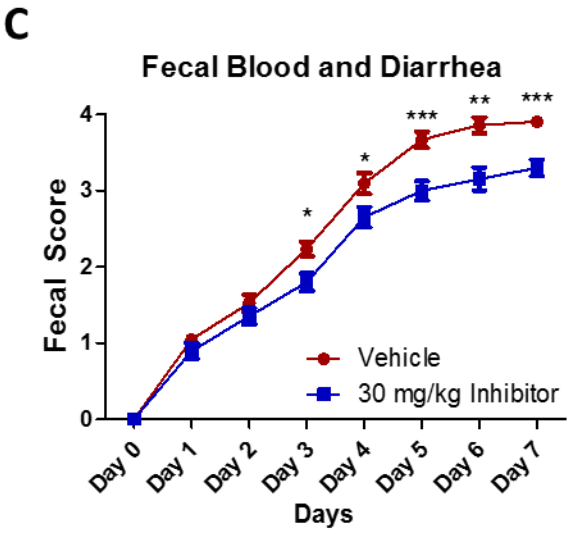
C
Fecal Blood and Diarrhea
Fecal Score
4
3
2
1
0
Vehicle
30 mg/kg Inhibitor
Day 0
Day 1
Day 2
Day 3
Day 4
Day 5
Day 6
Day 7
Days

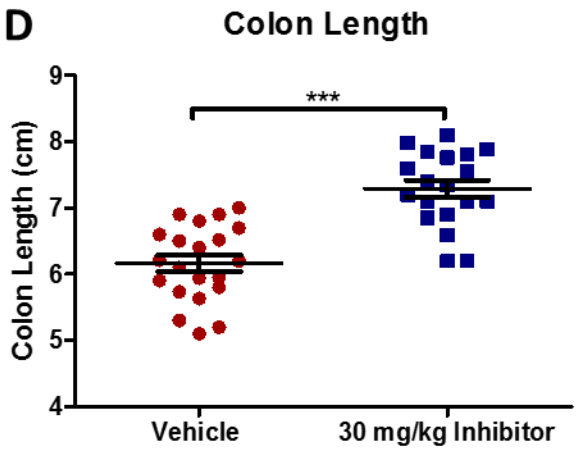
D
Colon Length
Colon Length (cm)
9
8
7
6
5
4
***
Vehicle
30 mg/kg Inhibitor


E
Vehicle
GPR4 Inhibitor

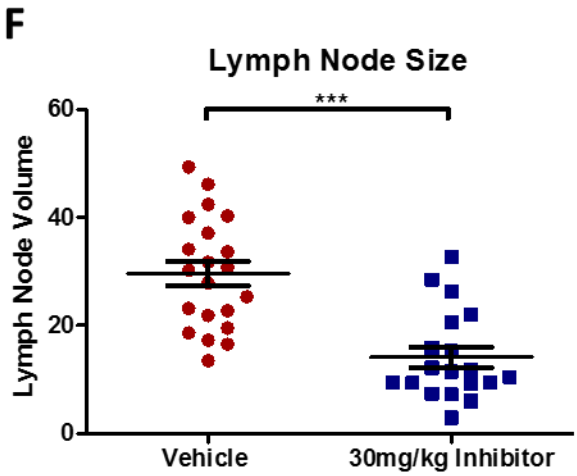
F
Lymph Node Size
Lymph Node Volume
60
40
20
0
***
Vehicle
30mg/kg Inhibitor

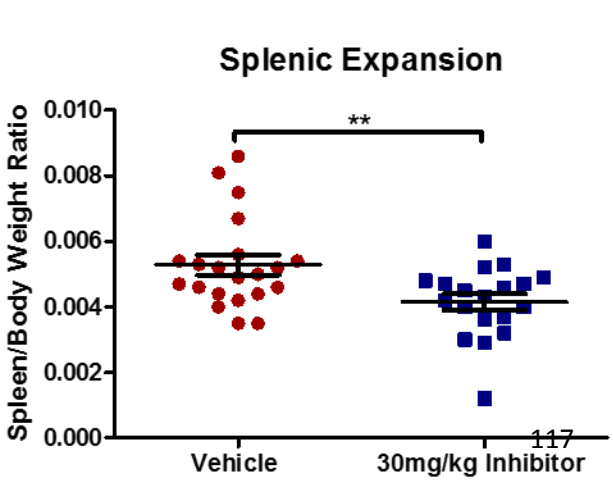
G
Splenic Expansion
Spleen/Body Weight Ratio
0.010
0.008
0.006
0.004
0.002
0.000
**
Vehicle
30mg/kg Inhibitor

Figure 3.27: GPR4 antagonist 13 reduces clinical severity and macroscopic disease indicators of intestinal inflammation in mice. Mice were provided GPR4 antagonist 13 P.O. b.i.d. during experimental time course (A) and mouse body weight loss (B) and fecal blood and diarrhea scores (C) were daily measured. Mouse colon length (D-E), mesenteric lymph node expansion, and splenic enlargement were also assessed. Vehicle: N=21 (10 male/11 female) and GPR4 antagonist 13: N=19 (10male/9 female). Data are presented as mean ± SEM and was analyzed for statistical significance using the *t*-test between vehicle and GPR4 antagonist 13 groups. (*P < 0.05, **P < 0.01, *** P < 0.001). 10x objective. Scale bar = 100mm.

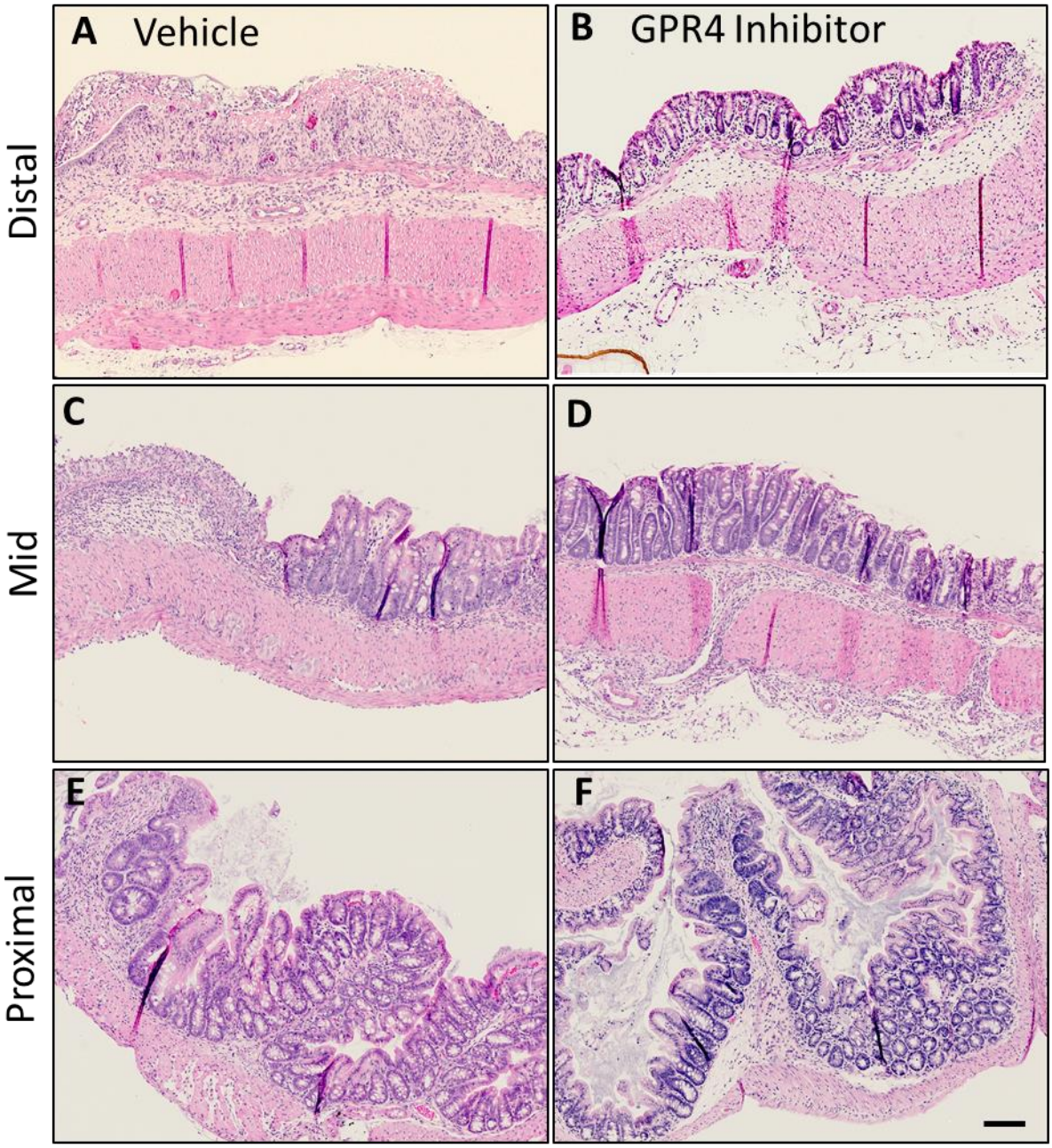
A Vehicle
B GPR4 Inhibitor
C
D
E
F
Distal
Mid
Proximal

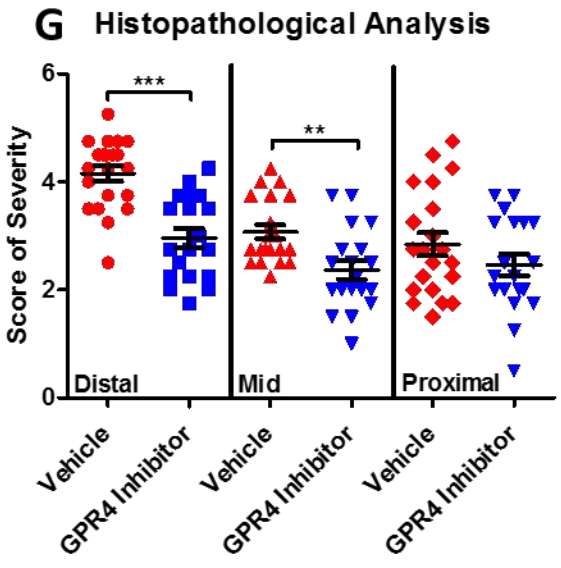
G Histopathological Analysis
Score of Severity
***
**
Distal
Mid
Proximal
Vehicle
GPR4 Inhibitor

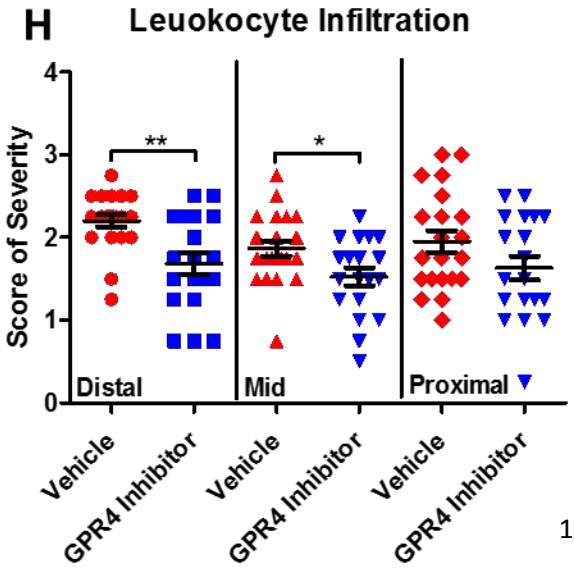
H Leuokocyte Infiltration
Score of Severity
**
*
Distal
Mid
Proximal
Vehicle
GPR4 Inhibitor

Figure 3.28: GPR4 antagonist 13 reduces histopathological parameters of intestinal inflammation in the inflamed mouse colon. Distinct histopathological features of intestinal inflammation were assessed and scored for degree of severity**.** Representative pictures of vehicle distal (A), Middle (C), and proximal (E) colon segments compared to GPR4 antagonist 13 distal (B), middle (D), and proximal (F) colon segments. Graphical representation of total histopathological parameters (G) and leukocyte infiltration score (H). Vehicle: N=21 (10 male/11 female) and GPR4 antagonist 13: N=19 (10male/9 female). Data are presented as mean ± SEM and was analyzed for statistical significance using the *t*-test between vehicle and GPR4 antagonist 13 groups between each colon segment. (*P < 0.05, **P < 0.01, *** P < 0.001). 10x objective. Scale bar = 100μm.

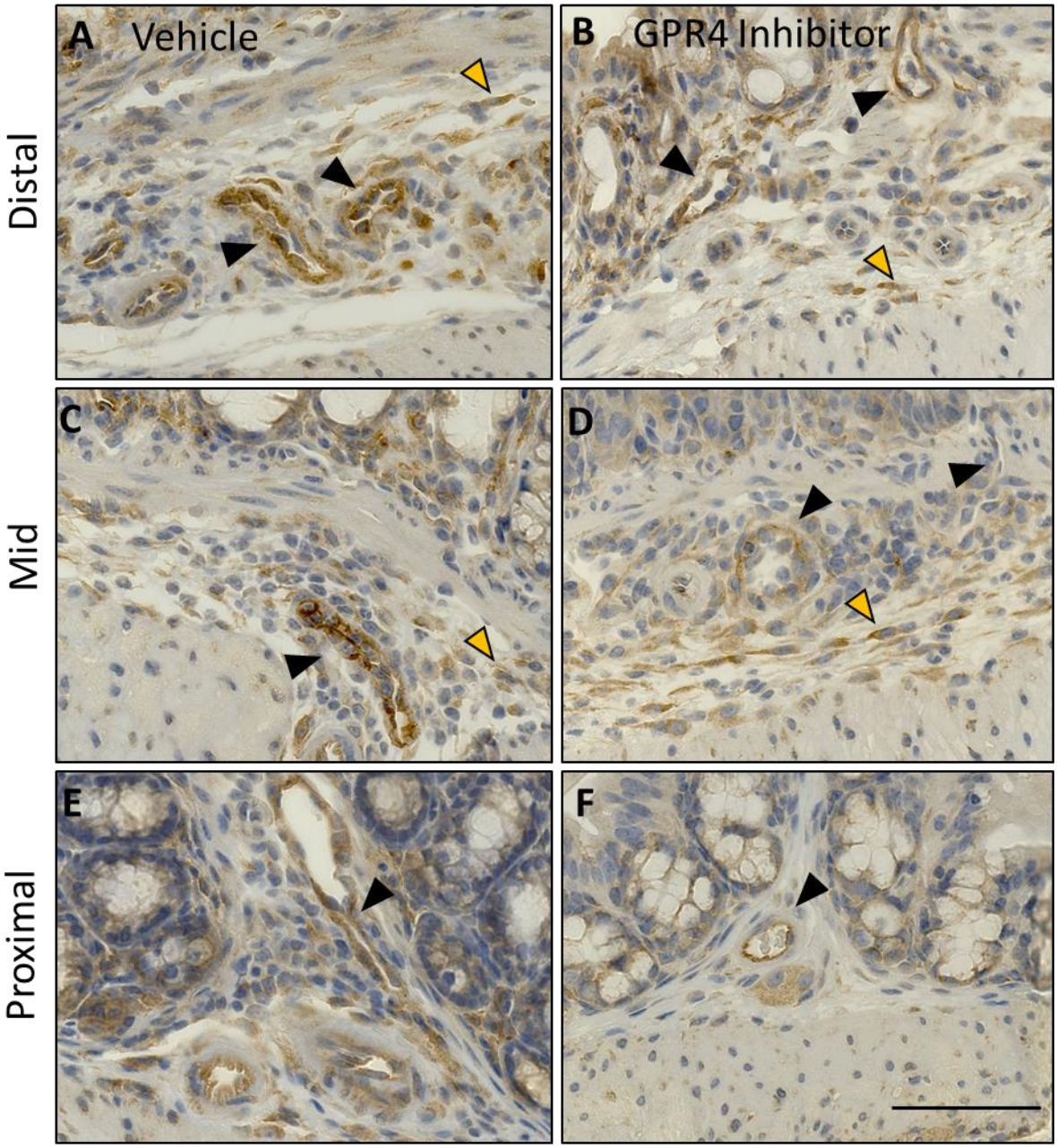
A Vehicle
B GPR4 Inhibitor
C
D
E
F
Distal
Mid
Proximal

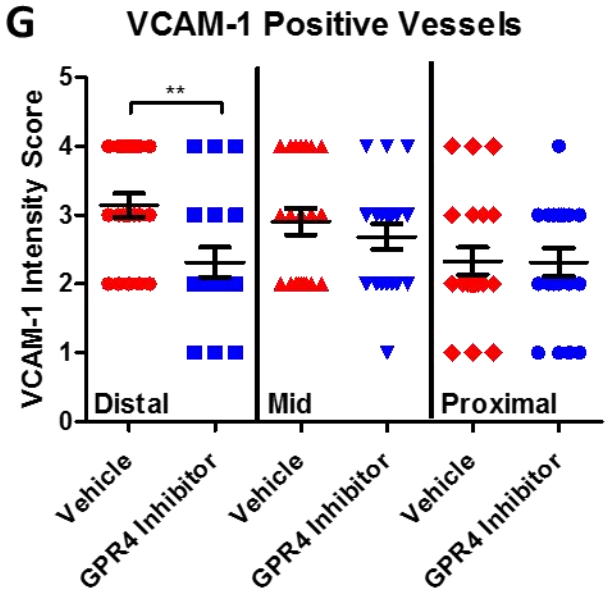
G
VCAM-1 Positive Vessels
VCAM-1 Intensity Score
0
1
2
3
4
5
**
Distal
Mid
Proximal
Vehicle
GPR4 Inhibitor
Vehicle
GPR4 Inhibitor
Vehicle
GPR4 Inhibitor

Figure 3.29: GPR4 antagonist 13 reduces VCAM-1 protein expression in colon microvascular endothelial cells. VCAM-1 protein expression intensity was assessed in colon microvascular endothelial cells**.** Representative pictures of vehicle distal (A), Middle (C), and proximal (E) colon segments compared to GPR4 antagonist 13 distal (B), middle (D), and proximal (F) colon segments followed by graphical representation of VCAM-1 intensity score (G). Vehicle: N=21 (10 male/11 female) and GPR4 antagonist 13: N=19 (10male/9 female). Data are presented as mean ± SEM and was analyzed for statistical significance using the *t*-test between vehicle and GPR4 antagonist 13 groups between each colon segment. (**P < 0.01). 40x objective. Scale bar = 100µm. Black arrow heads indicate blood vessel; yellow arrow indicates non-endothelial cell.

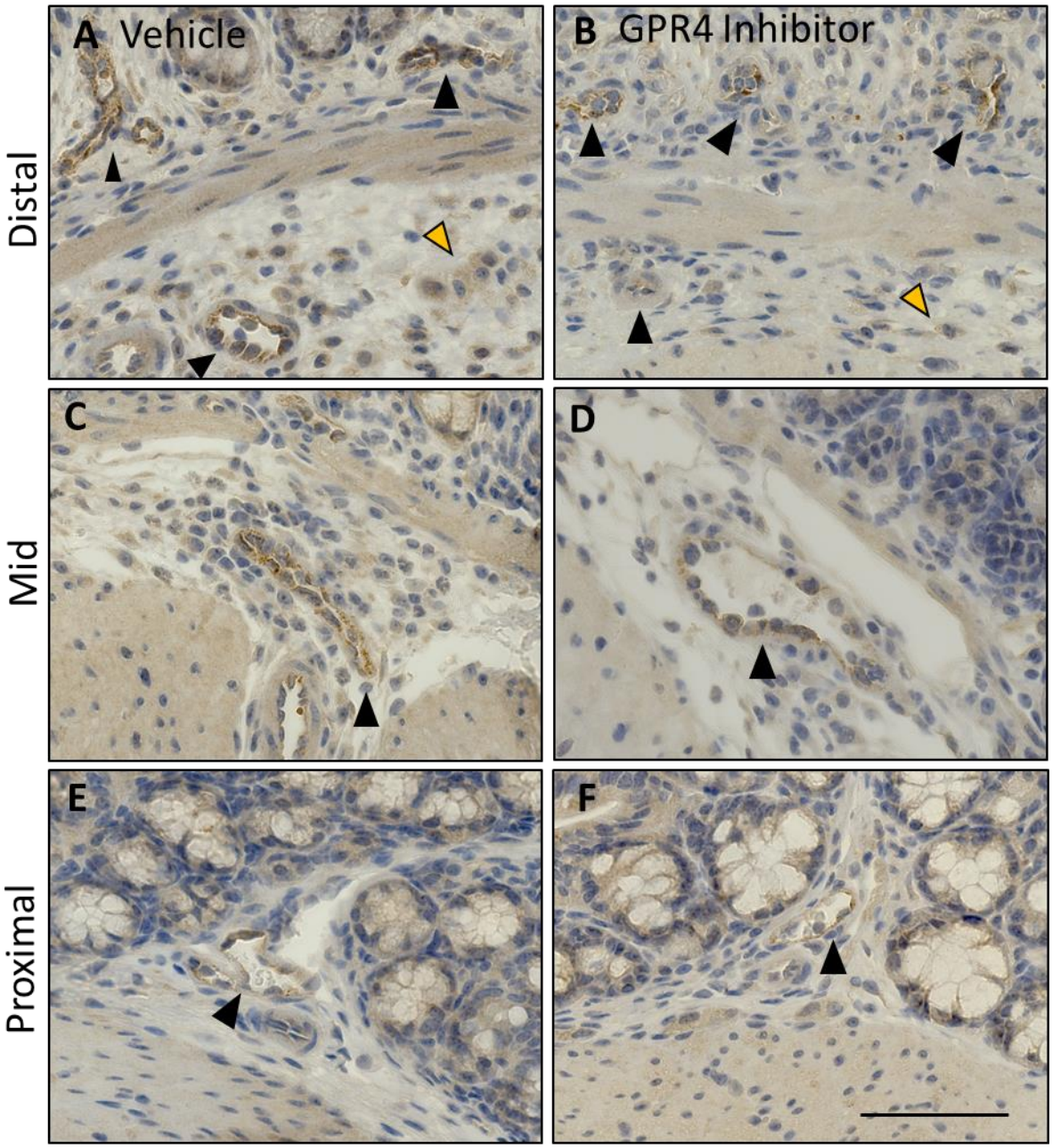
A Vehicle
B GPR4 Inhibitor
C
D
E
F
Distal
Mid
Proximal

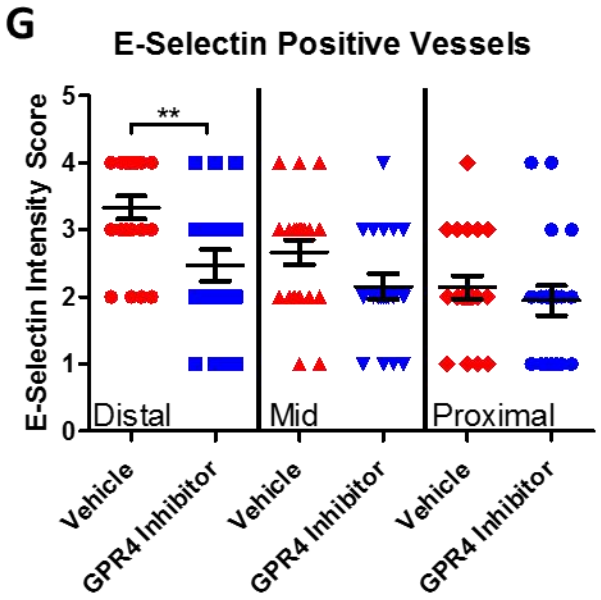
G
E-Selectin Positive Vessels
E-Selectin Intensity Score
0
1
2
3
4
5
**
Distal
Mid
Proximal
Vehicle
GPR4 Inhibitor
Vehicle
GPR4 Inhibitor
Vehicle
GPR4 Inhibitor

Figure 3.30: GPR4 antagonist 13 reduces E-selectin protein expression in colon microvascular endothelial cells. E-selectin protein expression intensity was assessed in colon microvascular endothelial cells**.** Representative pictures of vehicle distal (A), Middle (C), and proximal (E) colon segments compared to GPR4 antagonist 13 distal (B), middle (D), and proximal (F) colon segments followed by graphical representation of E-selectin intensity score (G). Vehicle: N=21 (10 male/11 female) and GPR4 antagonist 13: N=19 (10male/9 female). Data are presented as mean ± SEM and was analyzed for statistical significance using the *t*-test between vehicle and GPR4 antagonist 13 groups between each colon segment. (**P < 0.01). 40x objective. Scale bar = 100µm. Black arrow heads indicate blood vessel; yellow arrow indicates non-endothelial cell.

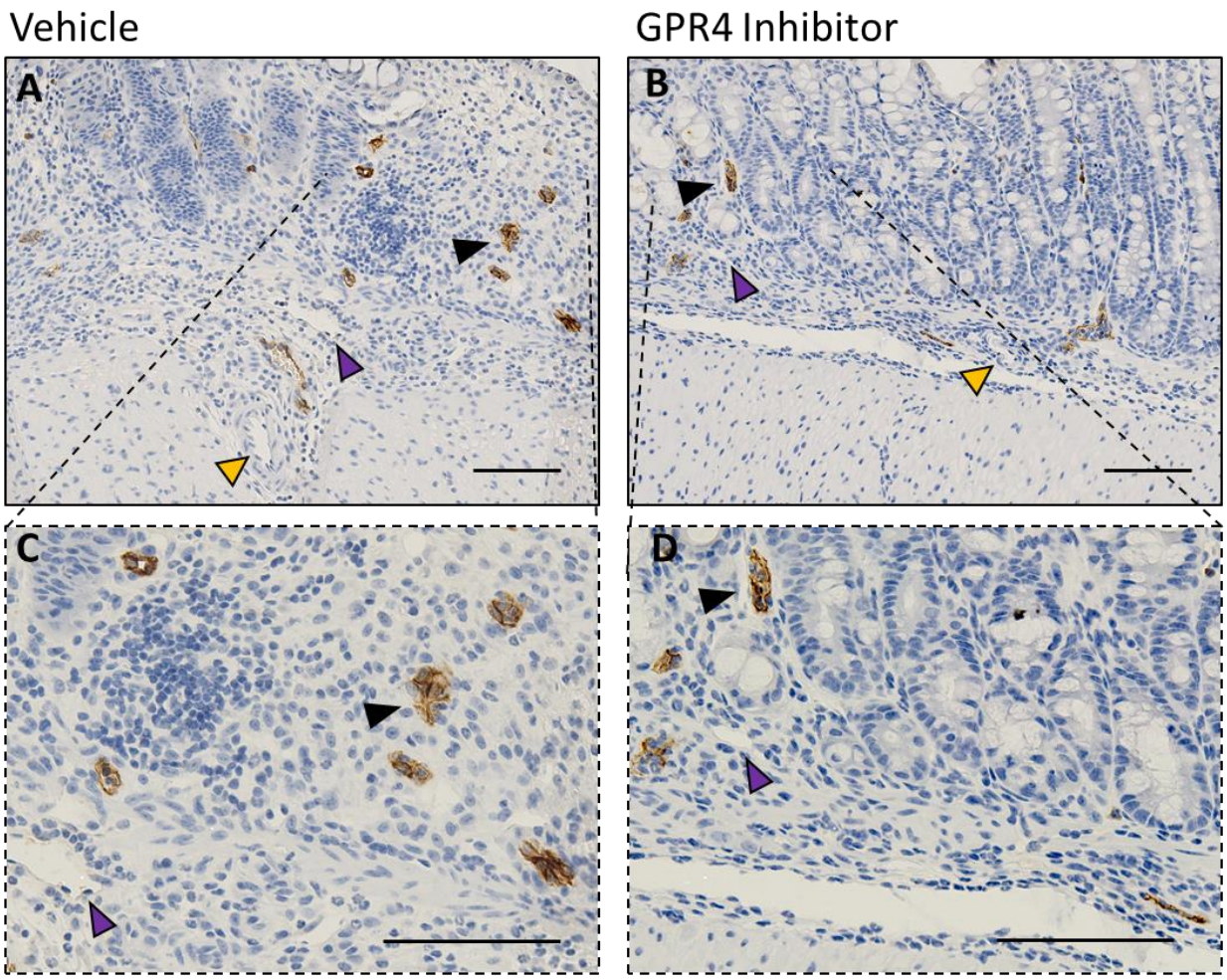
Vehicle
GPR4 Inhibitor
A
B
C
D

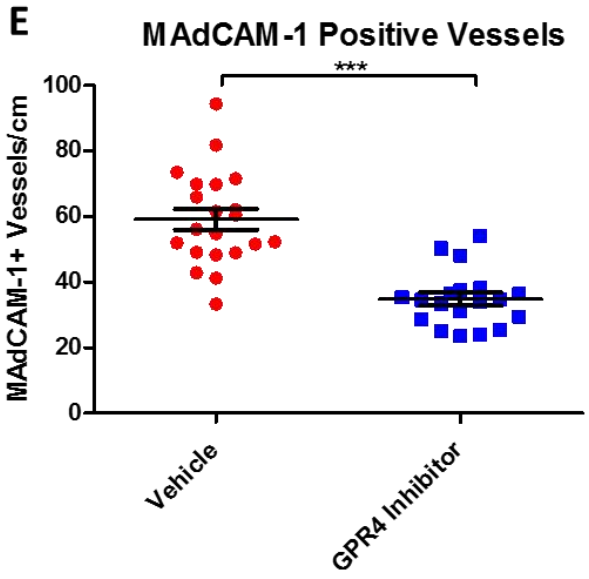
E
MAdCAM-1 Positive Vessels
***
MAdCAM-1+ Vessels/cm
100
80
60
40
20
0
Vehicle
GPR4 Inhibitor

Figure 3.31 GPR4 antagonist 13 reduces MAdCAM-1 positive vessels in the mouse colon. No difference in MAdCAM-1 protein expression intensity was observed between vehicle and GPR4 antagonist 13 colon microvascular endothelial cells, however, differences in total number of MAdCAM-1 positive vessels were observed between the two treatment groups. Representative pictures of vehicle distal (A, C) compared to GPR4 antagonist 13 (B, D). Graphical representation of MAdCAM-1+ blood vessels per colon centimeter are depicted (E). Vehicle: N=21 (10 male/11 female) and GPR4 antagonist 13: N=19 (10male/9 female). Data are presented as mean ± SEM and was analyzed for statistical significance using the *t*-test between vehicle and GPR4 antagonist 13 groups. (*** $P < 0.001$). 20x and 40x objective. Black arrow indicates microvasculature, purple arrow indicates lymphatic endothelial cell, yellow arrow indicates artery. Scale bar = 100μm.

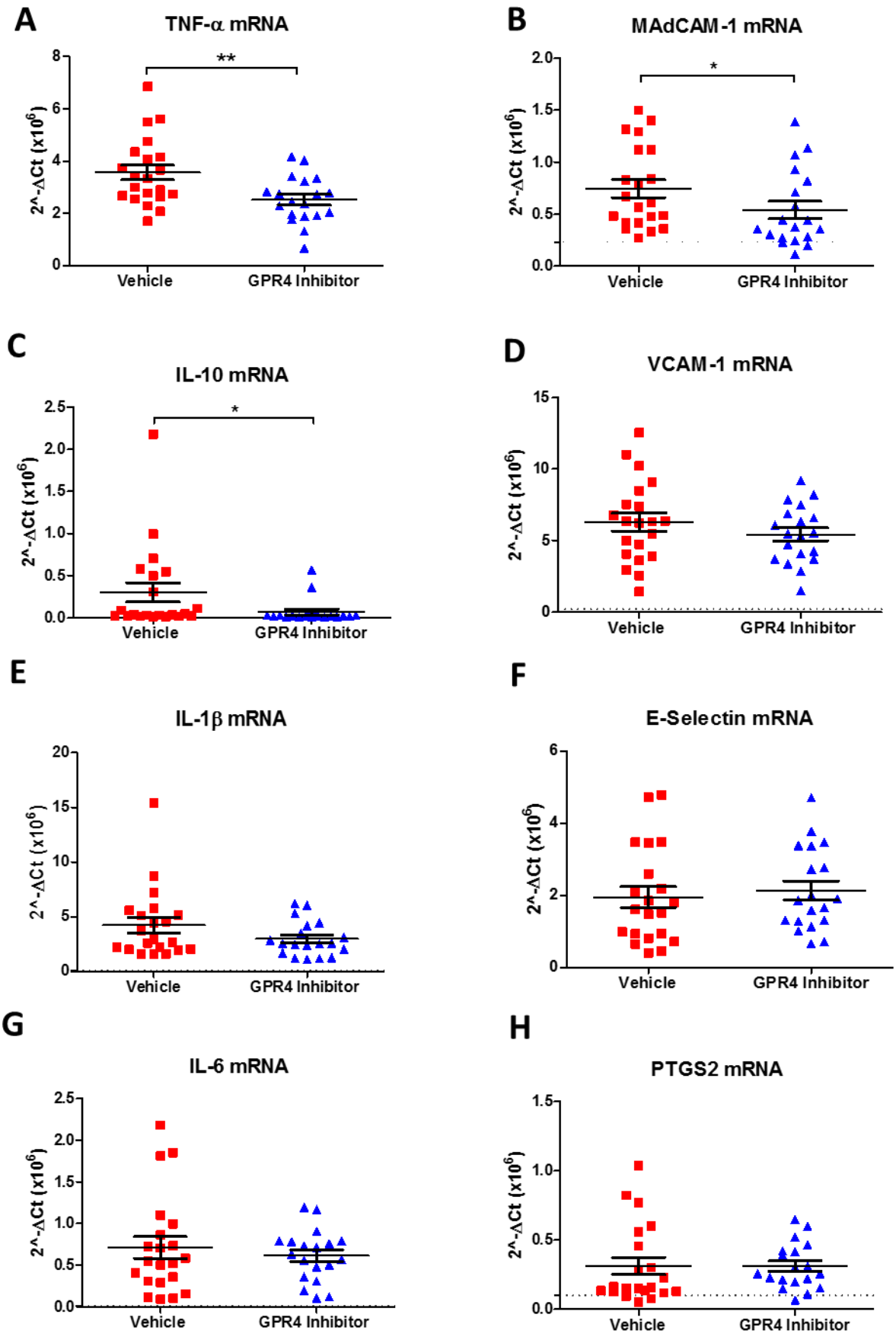
A
TNF-α mRNA
**
2^-ΔCt (x10^6)
Vehicle
GPR4 Inhibitor
B
MAdCAM-1 mRNA
*
C
IL-10 mRNA
*
D
VCAM-1 mRNA
E
IL-1β mRNA
F
E-Selectin mRNA
G
IL-6 mRNA
H
PTGS2 mRNA

Figure 3.32: GPR4 antagonist 13 reduces inflammatory gene expression in the distal colon. Tissue level gene expression of cytokines, adhesion molecules, and an inflammatory enzyme were assessed in the distal colon segment of DSS-treated mice given vehicle or GPR4 antagonist 13. Graphical representation of TNF-α (A), MAdCAM-1 (B), IL-10 (C), VCAM-1 (D), IL-1β (E), E-selectin (F), IL-6 (G), and PTGS2 (H) gene expression. Vehicle: N=21 (10 male / 11 female) and GPR4 antagonist 13: N=19 (10male / 9 female). Data are presented as mean ± SEM and was analyzed for statistical significance using the Mann-Whitney test between vehicle and GPR4 antagonist 13 groups between each colon segment. (*P < 0.05, **P < 0.01, *** P < 0.001).

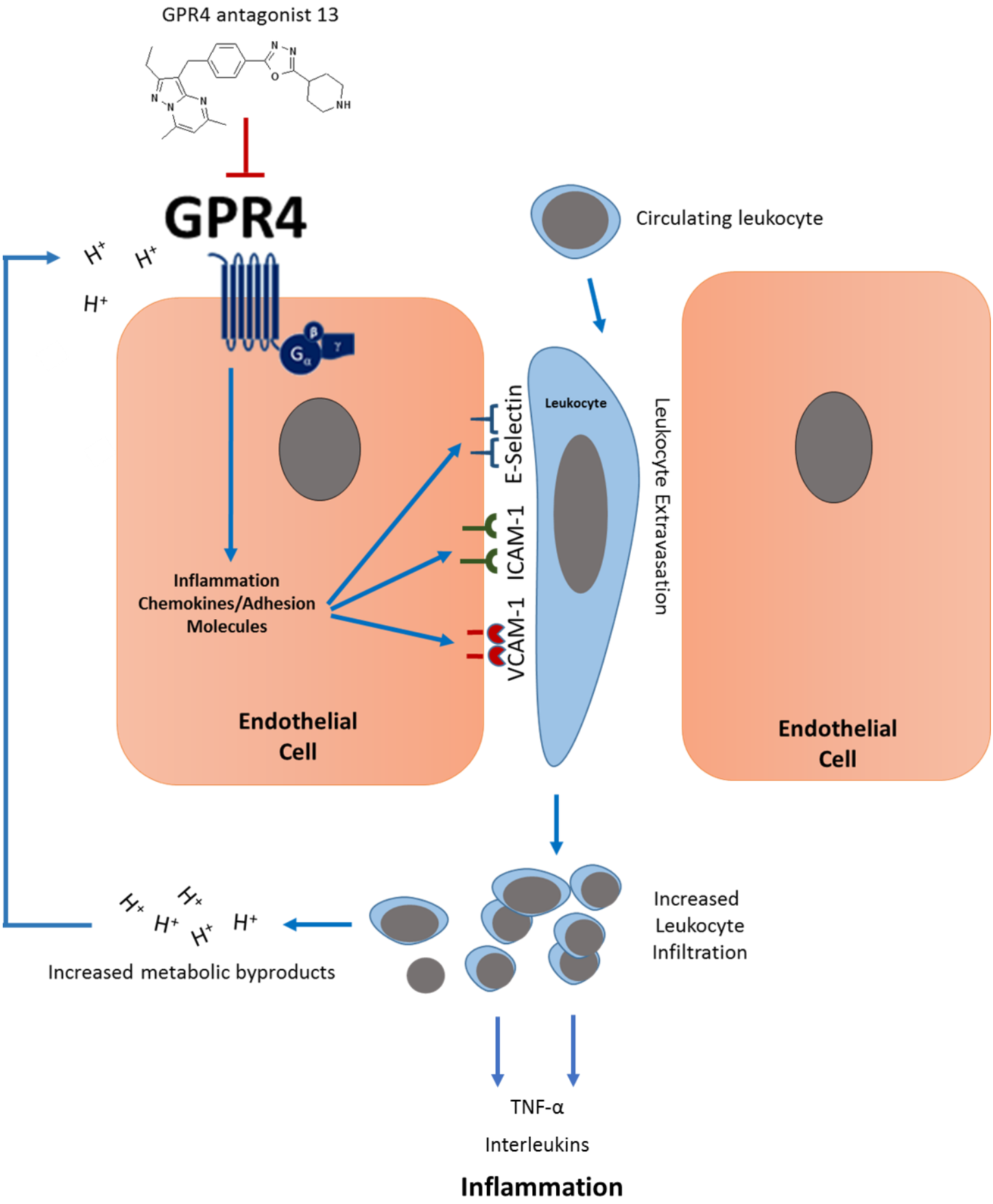
GPR4 antagonist 13
GPR4
Circulating leukocyte
H+
Gα
β
γ
Inflammation
Chemokines/Adhesion
Molecules
E-Selectin
ICAM-1
VCAM-1
Leukocyte
Leukocyte Extravasation
Endothelial
Cell
Endothelial
Cell
Increased metabolic byproducts
Increased
Leukocyte
Infiltration
TNF-α
Interleukins
Inflammation

Figure 3.33: Model of proposed mechanism of the anti-inflammatory action of GPR4 inhibitor GPR4 antagonist 13. GPR4 activation by protons in the extracellular milieu mediates the activation of vascular endothelial cells, the recruitment of immune cells and subsequent leukocyte extravasation into the inflamed tissue. Heavy immune cell infiltration into the inflammatory loci will result in further production of protons, as well as pro-inflammatory mediators, and subsequently maintain tissue inflammation and GPR4 activation. Inhibition of GPR4 activity by small molecules may present a novel approach to reduce inflammation by inhibiting vascular endothelial cell activation and leukocyte infiltration into inflamed tissues.

D. Discussion

This work demonstrates that GPR4 deficiency and pharmacological inhibition alleviates intestinal inflammation in the DSS-induced acute and chronic experimental colitis mouse model, suggesting that GPR4 is a pro-inflammatory mediator in IBD. These results corroborate previous studies showing GPR4 contributes to the inflammatory response in endothelial cells by isocapnic and hypercapnic acidotic stress *in vitro* [113, 114, 162]. GPR4 significantly increased endothelial cell and leukocyte interaction through the up-regulation of cytokines, chemokines, and adhesion molecule gene expression. Our *in vivo* data described in this study provide novel insights into the vascular inflammatory response in intestinal inflammation. In keeping with previous results describing the role of GPR4 in various endothelial cell types, our results suggest that GPR4 increases the expression of cytokines, chemokines, and adhesion molecules in intestinal endothelial cells and potentiates intestinal inflammation by increasing leukocyte recruitment to the gut and extravasation from blood to intestinal mucosa in response to acidic tissue microenvironments.

Acid sensing is critical for cells in the maintenance of proper cellular functions. When improper pH homeostasis occurs, various pathological conditions can arise. Extracellular tissue pH is tightly regulated around 7.4, while intracellular pH is slightly more acidic (pH 7.2). If cells are unable to maintain this narrow pH range, cell death will occur[163-165]. Cells must be able to sense and modulate their processes in response to an altered extracellular pH gradient. pH sensing can occur through acid sensing ion channels (ASICs), transient receptor potential (TRP) channels, and the GPR4 family of proton-sensing GPCRs [78, 82]. Recently, GPR4 has been implicated in regulating systemic pH through the renal system [166]. GPR4 is expressed in the kidney and involved in the pH sensing function of kidney collecting duct cells and regulating

renal acid secretion in response to systemic acidotic challenges. In addition to the renal system, GPR4 expression in retrotrapezoid nucleus (RTN) neurons mediate the central respiratory chemoreflexes to altered systemic CO_2/pH homeostasis [167]. This study showed GPR4 is required for RTN neurons to respond to elevated brain pCO_2. GPR4 is also involved in local pH responses where tissue becomes acidic due to pathological conditions such as ischemia, hypoxia, and inflammation. Indeed, tissue acidosis is a hallmark of inflammation [82, 102, 136].

Numerous studies have demonstrated that acute and chronically inflamed tissues are characterized by acidosis and can modulate the function of both immune cells and stromal cells [62, 63]. The reduced tissue pH is owing to multiple factors in the context of inflammation. Increased leukocyte infiltrates quickly deplete available O_2 and cells in the hypoxic tissue switch from aerobic to anaerobic glycolysis generating lactic acid. Neutrophils are typically the first responders to an inflammatory stimulus which is often due to bacterial infiltration. These bacteria can acidify the inflammatory microenvironment owing to accumulation of short chain fatty acids as microbial metabolic by-products. Neutrophils and macrophages can attempt to eliminate these harmful bacteria through respiratory bursts, which can further acidify the microenvironment. Interestingly, reports find that the colonic lumen of patients with active UC is more acidic than the normal colon [72, 74]. There are some varying reports regarding intraluminal colonic pH, however, the consensus seems to hold the lumen of active UC patients are more acidic than control patients [71, 77].

To confirm the expression profile of GPR4 in the intestinal tissues, we used GFP knock-in as a surrogate marker for GPR4 expression in GPR4 KO intestinal tissues. We were able to observe GFP expression on ECs of blood vessels in the muscularis externa, mucosa, and transverse folds (Figures 3.6-7, and Figures 3.15-18). Interestingly, however, no appreciable

expression of GFP was visible in lymphatic ECs. Increased density of GFP-positive blood vessels could clearly be observed in the context of inflamed intestinal lesions of GPR4 KO-DSS mice where tissue acidosis is co-existent with inflammation. It is possible that the increased GPR4 expression could be correlated with increased blood vessel density in the inflamed tissues. Increased angiogenesis is common in the mucosa of IBD patients and these blood vessels grow into inflamed, acidic tissues. With previous reports showing GPR4 expression is increased by TNF-α and H_2O_2, of which is commonly expressed in the milieu of the inflamed gut mucosa [140], GPR4 expression could be upregulated in vascular endothelial cells and potentiate inflammation in response to the acidic microenvironment. Consistently, the increased mRNA expression of GPR4 by nearly 2.7 fold was observed in WT-DSS mice and 4.7 fold in human intestinal IBD lesions (Figure 3.5). Due to the lack of a reliable GPR4 antibody, we cannot directly examine the expression of GPR4 protein. Using IHC methods for detecting the knock-in GFP expression can serve as a surrogate marker to localize GPR4 expression in intestinal tissues (Figures 3.6-7, and Figures 3.15-18), but does not necessarily correlate to the level of GPR4 protein and cannot be used to quantitatively measure GPR4 protein expression between non-inflamed and inflamed ECs. Nonetheless, increased GPR4 expression correlates with the observed IBD pathology and can contribute to the pathogenesis of the disease.

High endothelial venules (HEVs) are specialized ECs for lymphoid tissues. In addition to visualizing GFP expression in mucosal vasculature, we were also able to observe GFP expression in HEVs of mesenteric lymph nodes and microvessels of ILFs (Figures 3.6-7). GPR4 could play a substantial role in the expansion of secondary and tertiary lymphoid tissue. Based on macroscopic disease indicators, we observed the average volume of mesenteric lymph nodes from GPR4 KO-DSS mice were similar in size to WT control mice and ~40% reduced when

compared to WT-DSS mice in the acute DSS model (Figure 3.1). Additionally, a significant reduction can be observed in isolated lymphoid follicle numbers between WT-DSS and GPR4 KO-DSS (Figure 3.4). GPR4 could play a novel role in regulating the passage of leukocytes, such as lymphocytes and antigen presenting cells into lymph tissue and thereby regulate the adaptive immune response.

As immunologic, environmental, and genetic factors have been clearly shown to contribute to the development and progression of IBD, so too are these pH-sensing GPCRs implicated in the regulation of IBD within these categories. Ovarian cancer G protein-coupled receptor 1 (OGR1) has recently been implicated as a regulator of intestinal inflammation through the control of macrophage inflammatory responses [116]. Using IL-$10^{-/-}$ (knockout) mice for the development of chronic spontaneous intestinal inflammation, OGR1 deficiency alleviated mucosal inflammation when compared to control mice. This group demonstrates OGR1 expression, among other pH-sensors, is exclusively upregulated by TNF-α, PMA, and LPS in macrophages and potentiates intestinal inflammation. Interestingly, using IHC analysis, we observed GFP (a surrogate marker for GPR4) expression in mouse macrophages in both the lymph node sinus region and inflamed mucosal lesions of GPR4-KO mice (Figure 3.6-7). This observation is consistent with previous results showing that GPR4 is expressed in purified monocytes and macrophages [98, 103, 114, 156]. However, the role of GPR4 in macrophages is unknown and further studies must be done to characterize the functional role of GPR4 in macrophages. This endeavor may be confounded by genetic redundancy as the whole family of proton sensing GPCRs are expressed in macrophages. Additionally, in keeping with these observations that GPR4 KO and OGR1 KO mice have a similar phenotype under intestinal inflammation, it is possible GPR4 and OGR1 may have redundant roles. Additional studies using

OGR1 and GPR4 double knockouts will need to be done to reveal further biological functions of these receptors. Finally, T cell death associated gene 8 (TDAG8) has recently been presented as an IBD susceptibility candidate gene. Polymorphisms in the *TDAG8* (*GPR65*) gene have been linked with increased risk of developing IBD based on several genome-wide association study (GWAS) efforts [168]. A recent study showed that TDAG8 (GPR65) deficient mice have increased susceptibility to bacteria-induced colitis [169]. Collectively, the GPR4 family of receptors are emerging as regulators of intestinal inflammation.

Here we propose a mechanism of how GPR4 specifically contributes to intestinal inflammation (Figure 3.11). As mentioned earlier, we have previously reported that GPR4 can stimulate the expression of adhesion molecules, chemokines, and other inflammatory genes in a variety of endothelial cells in response to isocapnic and hypercapnic acidosis [113, 114]. Notably, some of these inflammatory molecules are E-selectin, VCAM-1, and ICAM-1. These adhesion molecules are involved in the tethering and firm adhesion of leukocytes to endothelial cells and are regulated by GPR4. To confirm a functional role for the GPR4-dependent expression of adhesion molecules, we performed adhesion assays under static and flow conditions. We observed an increase in leukocyte adhesion to endothelial cells in a GPR4 dependent manner [113, 114]. The leukocyte adhesion was reduced when treated with a GPR4 inhibitor in a dose dependent manner or by GPR4 shRNA knockdown in ECs.

Consistent with our previous publications on the role of GPR4 in cellular adhesion, we observed GPR4 increased pro-inflammatory molecule mRNA expression in WT mice (Figure 3.8). Even though whole colon tissue is not ideal for the examination of EC specific gene expression, we were able to observe a trend of reduction in E-selectin, VCAM-1, ICAM-1, MAdCAM-1, and COX-2 mRNA in GPR4 KO-DSS mice compared to WT-DSS mice.

Furthermore, inflammatory gene expression positively correlated with GPR4 mRNA gene expression in WT-DSS colon tissues (Figure 3.8), which could suggest the inflammatory genes are co-regulated by GPR4. Using immunohistochemistry, we were able to observe the reduction in E-selectin and VCAM-1 specifically in the blood vessels of GPR4 KO-DSS mice compared to WT-DSS mice (Figure 3.9-10). These observations are consistent with our previous reports showing GPR4 increases the expression of adhesion molecules, chemokines and other inflammatory genes. Additionally, histopathological analysis confirmed a reduction of total leukocyte infiltration into the mucosa of GPR4-KO-DSS mice compared to WT-DSS mice (Figure 3.2-3), suggesting GPR4 deficiency can reduce leukocyte infiltration into inflamed tissue through the regulation of adhesion molecules in ECs *in vivo*. Reduced inflammatory cell infiltration can be associated with less intestinal epithelial defects and crypt damage observed in GPR4 KO-DSS mice. These results were further corroborated through analyzing specific immune cell infiltrates such as neutrophils, macrophages, and T cells. All immune cell numbers were reduced in GPR4 KO-DSS colon tissues compared to WT-DSS colon tissues in both the acute and chronic DSS-induced colitis models (Figures 3.3, 3.25). We propose the reduced inflammation associated clinical severity, pro-inflammatory molecule expression, and isolated lymphoid follicle development in GPR4-KO-DSS mice is owing to the GPR4 dependent effects on pro-inflammatory molecule expression, leukocyte trafficking, and extravasation into inflamed mucosal tissue in the gut (Figure 3.11). While focused on intestinal inflammation in this study, a similar GPR4 regulating mechanism can potentially be extrapolated to many other inflammatory disorders.

Inhibition of leukocyte-endothelial cell interactions are an attractive approach to treat inflammatory diseases as the inhibition of leukocyte adhesion would reduce the influx of

inflammatory cells into inflamed tissue. Currently, FDA approved therapeutics targeting EC-leukocyte interaction, such as vedolizumab and natalizumab, are used for IBD treatment [146, 147]. Even though these drugs have been shown to reduce aberrant inflammatory responses, the efficacy of targeting specific inflammatory mediators can be reduced over time through host immune compensatory mechanisms. Examples can be observed in the recently failed efforts to attenuate intestinal inflammation by supplementing interleukin-10 in IBD patients [170]. GPR4 is a strong potential candidate for targeted therapy, as it is upstream of the predominate EC-leukocyte targets currently used in IBD therapy and can up-regulate adhesion molecules and chemokines involved in both tethering and firm adhesion of leukocytes to the endothelium as well as leukocyte activation. Use of GPR4 inhibitors could prove as a valuable tool to inhibit inflammation by reducing leukocyte recruitment and adhesion to inflamed tissues. Recently, our group and others have demonstrated the effectiveness of the GPR4 inhibitors in the selective targeting of GPR4 and inhibition of GPR4 target gene expression. Additionally, GPR4 antagonists have been used *in vivo* and no obvious toxicities have been reported. A recent study showed that GPR4 antagonists provided therapeutic benefits in a myocardial infarction mouse model [171].

For this reason, we sought to investigate the function and efficacy of GPR4 antagonist 13, a novel GPR4 inhibitor, within the dextran sulfate sodium (DSS)-induced acute experimental colitis mouse model as a potential therapeutic for the alleviation of intestinal inflammation. GPR4 antagonist 13 was recently developed and characterized by Novartis Pharmaceuticals and shown effective following oral administration. GPR4 antagonist 13 was capable of reducing inflammation in the rat antigen induced arthritis model, angiogenesis in the mouse chamber implant model, and inflammation-associated nociception in the rat complete Freund's adjuvant

model [172]. Furthermore, oral pharmacokinetics, GPR4 selectivity, and potency was thoroughly evaluated and GPR4 antagonist 13 proved promising for further evaluation. Another study evaluated GPR4 antagonist 13 in mouse ventilatory responses and observed no obvious toxicities [173]. Upon initiation of DSS-induced colitis, mice provided 30mg/kg of GPR4 antagonist 13 BID during the seven-day colitis insult were protected from body weight loss, fecal blood and diarrhea, colon shortening, mesenteric lymph node expansion, and splenic enlargement. Upon evaluation of distinct histopathological features of intestinal inflammation, reduced epithelium erosion, crypt loss, and ulceration was observed in the colon of mice given the GPR4 antagonist compared to vehicle. The degree of leukocyte infiltration was also assessed, and mice provided the GPR4 antagonist had reduced leukocyte infiltration compared to vehicle. Following the observation of reduced leukocyte infiltration in mice, coupled with previous reports showing that GPR4 can reduce vascular adhesion molecule expression *in vitro* and *in vivo*, we performed immunohistochemistry to evaluate the protein expression of VCAM-1, E-selectin, and MAdCAM-1 specific to the cell type regulated by GPR4, namely, vascular endothelial cells within the intestinal microvasculature. We were able to observe a notable reduction of VCAM-1 and E-selectin in vascular endothelial cells within the distal colon segments of mice given the GPR4 antagonist compared to vehicle. These observations may provide a potential explanation as to why reduced leukocyte infiltration was observed in mice given the GPR4 antagonist. Upon immunohistochemical evaluation of VCAM-1 and E-selectin within the colon, notable expression could be detected in cell types not known to be regulated by GPR4. VCAM-1 could be observed on fibroblasts, macrophages, and other mononuclear cells within the intestinal mucosa and muscularis externa. Furthermore, VCAM-1 was highly expressed on distinct cellular populations within colonic isolated lymphoid follicles. These observations are supported by

several other studies describing basal and inflammation-associated VCAM-1 upregulation on activated fibroblasts and inflammatory cells [158, 159]. Studies have also observed E-selectin expression is not restricted to the vascular endothelium. These studies reported E-selectin can be expressed by colonic epithelial cells and mononuclear cells within the inflamed colon tissue of patients with active ulcerative colitis [144]. Furthermore, other studies have described the expression of E-selectin on T cells and other inflammatory cells [160, 161]. Our results were consistent with these reports as E-selectin could be detected in colonic epithelial cells and mononuclear cell populations within the inflamed mucosa. MAdCAM-1 protein expression was also assessed in intestinal microvasculature between vehicle and GPR4 antagonist 13 DSS-treated groups. There was no observable differences in signal intensity between vehicle and GPR4 antagonist 13 groups, however, the total number of MAdCAM-1 positive vessels were markedly reduced in the GPR4 antagonist 13 when compared to vehicle. A possible explanation of the reduced MAdCAM-1 positive vessels could be owing to a reduction of local inflammation-associated angiogenesis in the intestinal tissues caused by GPR4 antagonist 13. Heightened angiogenesis is a hallmark of IBD and is a major contributor to vascular associated pathology [45, 174, 175]. As such, increased density of CD31+ blood vessels can be observed in inflamed mucosal lesions in IBD tissues when compared to non-inflamed intestinal tissues.

We next assessed a panel of inflammatory genes including cytokines, an enzyme, and adhesion molecules within the whole distal colon tissue. We observed a statistically significant reduction of TNF-α, IL-10, and MAdCAM-1 gene expression in mice given the GPR4 antagonist when compared to vehicle consistent with reduced leukocyte infiltrates and MAdCAM-1 positive vessels, respectively. TNF-α and IL-10 mRNA reduction at the whole tissue level is most likely due to the subsequent reduction of inflammatory cells into the colon

observed in the GPR4 antagonist treated mice compared to vehicle. IL-10 has been reported to inhibit the anti-microbial functions of macrophages and other inflammatory cells which are required for optimal pathogen clearance and subsequent inflammatory resolution. As such, reduced levels of IL-10 mRNA in the tissues of GPR4 antagonist 13 treated mice could enhance pathogen clearance during the acute inflammatory phase. A modest reduction of IL-1β, IL-6, and PTGS2 could be observed in mice treated with the GPR4 antagonist. As for adhesion molecules, a moderate to no alteration of gene expression could be observed with VCAM-1 and E-selectin, respectively. These results are most likely due to cell types in the colon tissue that are not regulated by GPR4 of which highly express VCAM-1 and E-selectin.

Collectively, these results implicate GPR4 as a regulator of intestinal inflammation as the genetic deletion in both acute and chronic DSS-induced colitis resulted in reduced disease severity. Similarly, GPR4 pharmacological inhibition resulted in reduced intestinal inflammation in the acute DSS colitis mouse model and presents GPR4 as a potential therapeutic target in IBD.

Chapter IV: The Role of GPR65 in the Regulation of Intestinal Inflammation

A. Summary

T cell death-associated gene 8 (TDAG8, also known as GPR65) is a proton-sensing G protein-coupled receptor (GPCR) predominantly expressed in immune cells. Genome-wide association studies identify TDAG8 as a susceptibility candidate gene linked to several human inflammatory diseases including inflammatory bowel disease (IBD), asthma, spondyloarthritis, and multiple sclerosis. In this study, our results demonstrated that mice deficient of TDAG8 exhibited more severe inflammatory phenotypes than wild-type mice in a chronic dextran sulfate sodium (DSS)-induced colitis mouse model. Several disease parameters, such as diarrhea, colon shortening, fibrosis, histopathological score, and mesenteric lymph node enlargement were aggravated in TDAG8-null mice in comparison to wild-type mice treated with DSS. Increased leukocyte infiltration and myofibroblast expansion were observed in colonic tissues of DSS-treated TDAG8-null mice. These changes may represent a cellular basis of the observed exacerbation of intestinal inflammation and fibrosis in these mice. In line with high expression of TDAG8 in infiltrated leukocytes, real-time RT-PCR revealed that TDAG8 mRNA expression was increased in inflamed intestinal tissue samples of IBD patients when compared to normal intestinal tissues. To investigate the role of GPR65 in immune cell function, mouse thymocytes, bone marrow derived macrophages, and bone marrow derived dendritic cells were used. GPR65 is expressed and signals through Gαs in each cell type. Furthermore, GPR65 reduces anti-inflammatory functions in acidosis-induced macrophage inflammatory responses. Altogether, our data demonstrate that GPR65 suppresses intestinal inflammation and fibrosis in the chronic DSS-induced colitis mouse model, suggesting potentiation of TDAG8 with agonists may have anti-inflammatory therapeutic effects in IBD.

B. Introduction

Genome-wide association studies (GWAS) have identified numerous genetic risk loci for chronic inflammatory diseases. Large-scale GWAS studies have identified T cell death-associated gene 8 (TDAG8, also known as GPR65) as a susceptibility candidate gene for several human chronic inflammatory diseases such as multiple sclerosis, asthma, spondyloarthritis, and inflammatory bowel disease (IBD) [168, 176]. A recent study demonstrates that TDAG8-deficient mice are more susceptible to bacteria-induced colitis and an IBD-associated TDAG8 genetic variant (I231L) confers reduced TDAG8 signaling activity as well as impaired lysosomal function [169]. These data suggest TDAG8 could negatively regulate inflammation in certain diseases such as IBD.

TDAG8 was initially discovered as a gene up-regulated during T cell activation and apoptosis [100]. TDAG8 is highly expressed on leukocytes and leukocyte-rich tissues such as the spleen, lymph nodes, and thymus. Biochemically, TDAG8 can be activated by acidic extracellular pH through the protonation of several histidine residues on the receptor extracellular domains and transduce downstream signals through the G_s/cAMP and $G_{12/13}$/Rho pathways [82, 177].

It has long been observed that the inflammatory loci can be more acidic than non-inflamed tissues and that acidic pH can alter the function of inflammatory cells, vascular cells, and other stromal cells. The ways in which immune cells sense extracellular pH within inflamed microenvironments and subsequently alter their phenotypes have only recently been investigated. The role of TDAG8 activation by inflammation-associated acidosis has been investigated both *in vitro* and *in vivo*. Functionally, both pro- and anti-inflammatory effects of TDAG8 have been described [82, 178]. TDAG8 has been reported to impede pro-inflammatory profiles of primary murine macrophages, T cells, and microglia [82]. Investigation of TDAG8 in animal models of

acute lung injury, arthritis, myocardial infarction, experimental autoimmune encephalomyelitis, and bacteria-induced colitis have indicated TDAG8 functions to inhibit inflammation in a variety of inflammatory diseases [107, 109, 169, 179].

As aberrant TDAG8 function is associated with IBD development and progression, we sought to further characterize the role of TDAG8 in IBD. IBD is a broad term covering both Crohn's disease (CrD) and ulcerative colitis (UC). IBD is characterized by recurrent, aberrant inflammation within the intestinal tissue [25, 32]. These two disease forms are distinct, yet have overlapping clinical and histopathological features. The exact etiology is unknown, however, a complex interaction between immunologic, environmental, and genetic constituents is believed to contribute to the disease onset and progression. We utilized the acute and chronic dextran sulfate sodium (DSS)-induced colitis mouse model to investigate the role of TDAG8 in colitis. We observed that TDAG8 is protective against colonic inflammation and IBD associated complications in the chronic DSS-induced colitis model, but not in the acute DSS model. TDAG8 knockout (KO) mice treated with DSS had more severe clinical phenotypes such as body weight loss, fecal score, colon shortening, and mesenteric lymph node enlargement when compared to DSS-treated wild type (WT) mice. Histopathological analysis revealed that TDAG8 KO mice also had more severe histopathological features, intestinal inflammation, leukocyte infiltration, intestinal fibrosis, and isolated lymphoid follicles than WT mice. We also investigated the pH-sensing GPCR expression profiles, G-protein activation status, and inflammatory programs in mouse bone marrow derived macrophage. Furthermore, we assessed the expression and G-protein activation status in other immune cell populations such as thymocytes and bone marrow derived dendritic cells. Our results show that GPR65 is highly expressed in T-cells and macrophages but is moderately expressed in dendritic cells. GPR65 also

couples to Gαs and is responsible for acidosis-induced Gαs/cAMP/CREB-ATF-1 pathway signaling in T-cells, macrophages, and dendritic cells. Finally, GPR65 suppresses TNF-α expression in mouse bone marrow derived macrophages and might be involved in the M1-M2 macrophage polarization paradigm.

C. Results

C.1 GPR65 moderately modulates the clinical severity of intestinal inflammation in the acute DSS- induced chemical colitis mouse model.

GPR65 KO mice were used to assess the role of GPR65 in acute chemical colitis. WT and GPR65 KO mice were given 3% DSS into normal drinking water for seven days. During the course experimentation mouse body weight and fecal blood scores were measured. No body significant weight loss differences between WT and GPR65 KO mice could be appreciated until day six where WT-DSS mice were less severe than GPR65 KO mice. Following day six, GPR65 KO-DSS mouse weight loss was comparable to WT-DSS mice (Figure 4.1A). WT and GPR65 KO DSS-induced fecal scores were similar in severity through days six, where day seven revealed a moderate heightened severity of WT-DSS mice when compared to GPR65 KO-DSS (Figure 4.1B). Mesenteric lymph node (MLN) expansion was heightened in DSS-treated groups with a trend in higher MLN volume in GPR65 KO groups compared to WT-DSS, though not statistically significant (Figure 4.1C). Colon length assessment revealed reduced colon shortening of GPR65 KO-DSS mice compared to WT-DSS (Figure 4.1D). Collectively, these results provide a moderate role of GPR65 in acute DSS-induced colitis.

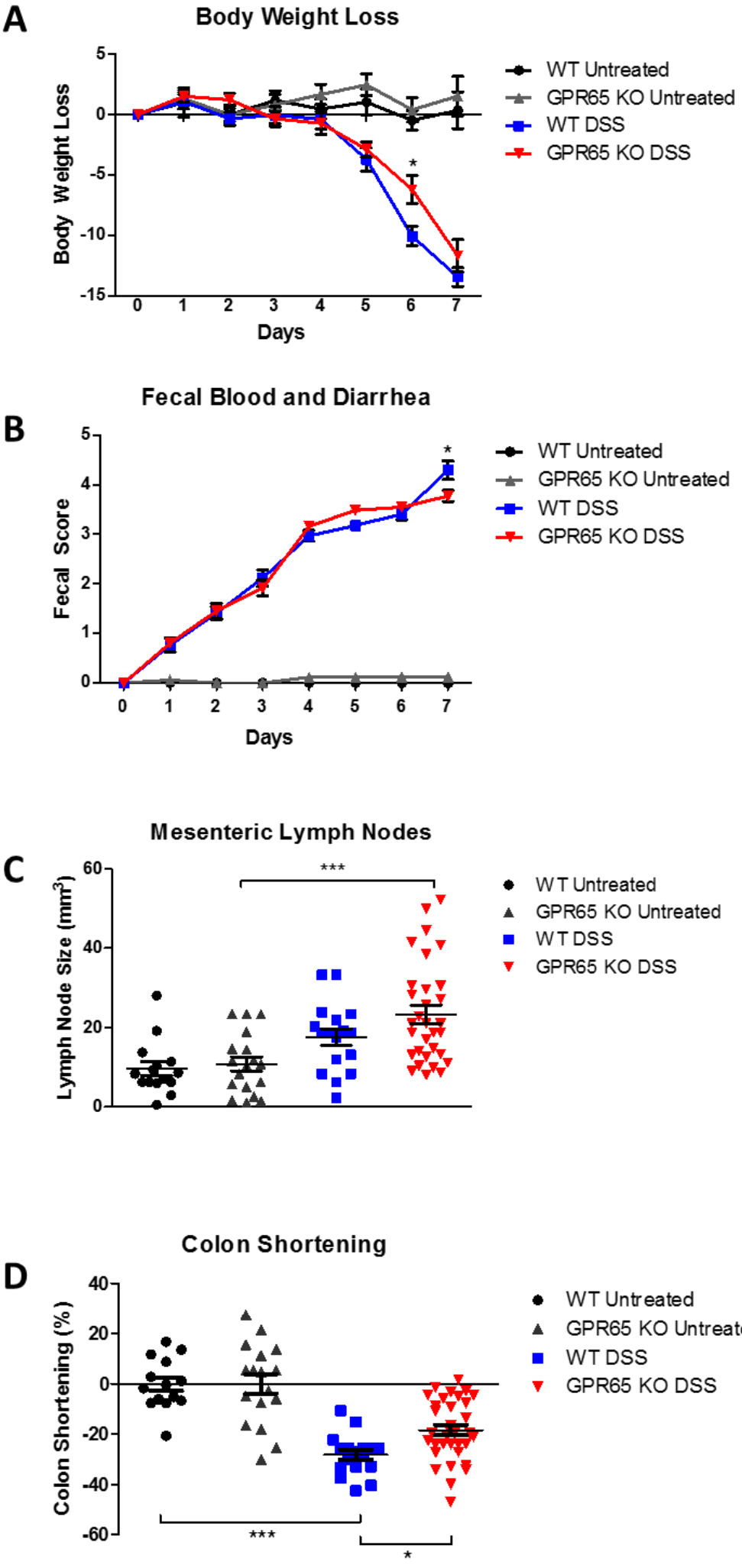
A
Body Weight Loss
Body Weight Loss
Days
WT Untreated
GPR65 KO Untreated
WT DSS
GPR65 KO DSS
B
Fecal Blood and Diarrhea
Fecal Score
Days
C
Mesenteric Lymph Nodes
Lymph Node Size (mm3)
D
Colon Shortening
Colon Shortening (%)

Figure 4.1: **Clinical parameters and macroscopic disease indicators**. The effects of GPR65 deletion was assessed in the acute DSS-induced colitis mouse model. GPR65 deletion had moderate effects on (A) body weight loss, (B) fecal score, (C) mesenteric lymph node enlargement, and (D) colon shortening. WT-control (n=15), WT-DSS (n=17), GPR65 KO-control (n=18), and GPR65 KO-DSS (n=31) mice. A portion of WT control mice used for analysis in this experiment were randomly selected from WT control grouping used for analysis with GPR4 KO acute DSS experiments. Each dot represents the data from an individual mouse. Data are presented as mean ± SEM and was analyzed for statistical significance using the two-way ANOVA followed by Bonferroni post hoc for body weight loss and fecal score assessment. One-way ANOVA was performed for mesenteric lymph node enlargement and colon shortening followed by Bonferroni post hoc. (**$P < 0.01$, *** $P< 0.001$).

C.2 GPR65 reduces the severity of intestinal inflammation in the DSS-induced chronic colitis mouse model.

To characterize the role of TDAG8 in chronic colitis, we utilized the chronic DSS-induced mouse model for the reliable induction of chronic intestinal inflammation. During the experiment, clinical parameters were assessed such as body weight loss and fecal blood and diarrhea score. Both wild-type (WT)-DSS and TDAG8 knockout (KO)-DSS mice body weight loss was normalized to WT and TDAG8 untreated control mice. No body weight loss difference was observed between WT-DSS and TDAG8 KO-DSS during the first cycle, however, TDAG8 KO-DSS mice trended more body weight loss with most significant weight loss occurring at the end of cycle two and cycle three compared to WT-DSS mice (Figure 4.2A). Fecal scores also indicated heightened severity of TDAG8 KO-DSS mice compared to WT-DSS mice (Figure 4.2B). Both WT-DSS and TDAG8 KO-DSS mice reached an average fecal score of 3 by the end of the first cycle, however, TDAG8 KO-DSS mice maintained a more severe score during cycle two and cycle three compared to WT-DSS mice. Interestingly, during cycle four the TDAG8 KO-DSS mice partially recovered compared to WT-DSS. Upon the terminal point of the experiment, macroscopic disease indicators were evaluated such as mesenteric lymph node expansion and colon length shortening. Expansion of mesenteric lymph nodes (MLN) is a common parameter for colonic inflammation in the DSS-induced colitis model. Untreated control mice had MLN volumes approximately 5-6mm^3 for WT and TDAG8 KO mice. MLN volume was significantly increased in DSS-treated mice as WT-DSS mice had an average volume of ~20mm^3. Interestingly, TDAG8 KO-DSS MLN expansion was almost 2-fold higher than WT-DSS, indicating the inflammation of TDAG8 KO-DSS was more severe than WT-DSS. Finally, colon length was measured to assess the degree of shortening, which corresponds to

heightened DSS-induced inflammation. WT-DSS mice had ~7% shortening compared to WT-untreated mice. TDAG8 KO-DSS mice, however, had more than 13% colon shortening. These data are not yet statistically significant given the current sample size.

To further assess the role of TDAG8 in intestinal inflammation, histopathological analysis was performed to quantify the degree of histological features of colitis between WT and TDAG8 KO mice. Distal, middle, and proximal segments of the colon were examined for common histopathological features of colitis, such as edema, crypt damage, architectural distortion, leukocyte infiltration, fibrosis, and inflammation. Untreated control mice had no colitis histopathological features (data not shown). We observed that the TDAG8 KO-DSS mice were more severe than WT-DSS mice in terms of total histopathology Figure 4.3B A-D, I). Greatest histopathology was observed in the distal colon and is consistent with previous studies showing DSS model affects distal colon most severely.

Isolated lymphoid follicles (ILFs) are tertiary lymphoid tissues which can be induced within inflamed murine intestinal tissues. We have previously reported that ILFs are increased in intestinal tissues of mice in the DSS-induced acute colitis model when compared to untreated control mice. Here we demonstrate that ILF numbers are increased in areas of heightened colonic inflammation and are further increased in mice deficient of TDAG8 (Figure 4.4). ILF numbers were counted in distal, middle, and proximal colon segments in untreated and DSS-treated WT and TDAG8 KO mice. ILFs were less prevalent in proximal segment when compared to middle and distal inflamed colon segments in both WT-DSS and TDAG8 KO-DSS mice (Figure 4.4). TDAG8 KO-DSS mice had increased ILFs/centimeter within each colon segment and subsequently full-length colon when compared to WT-DSS (Figure 4.4E-F). These data suggest TDAG8 prevents inflammation-associated ILF development.

Fibrosis is another common pathological feature of IBD and can lead to life-threatening complications. We stained colon segments with picrosirius red and Masson's trichrome for the assessment of colonic fibrosis after chronic intestinal inflammation (Figure 4.3E-H). Distal, middle, and proximal colon segments were assessed for fibrotic development and scored accordingly for severity. Pathological fibrosis was assessed as the degree of increase compared to untreated controls. The greatest degree of fibrosis was found in both WT-DSS and TDAG8 KO-DSS distal colons with a gradual decrease in fibrosis towards proximal colon (Figure 4.3J). We observed an almost 2-fold increase in fibrosis within distal colon of TDAG8 KO-DSS mice compared to WT-DSS mice. Severely fibrotic areas of the colon were characterized by increased collagen deposition within the lamina propria, muscularis mucosa, muscularis externa, and serosa when compared to control tissues (Figure 4.3E-H, Figure 4.9).

To further investigate why TDAG8 KO-DSS mice had heightened fibrosis compared to WT-DSS mice, we examined the number of myofibroblasts within the inflamed and fibrotic distal colon mucosa. Myofibroblasts are one of several cellular constituents which can contribute to intestinal fibrosis. Normal intestinal myofibroblasts exist subjacent to the epithelium and regulate tissue repair, fibrosis, glandular secretion, and mucosal regeneration. α-SMA^{+} myofibroblasts numbers within noninflamed distal colon segments were quantified and compared to DSS-treated mouse colon segments (Figure 4.5). There was a discernable increase in sub-epithelial mucosal myofibroblasts between WT-untreated and WT-DSS mice (~14/FOV vs. ~25/FOV) (Figure 4.5G). Interestingly, TDAG8 KO mice had a further increase when TDAG8 KO untreated mice were compared to TDAG8 KO-DSS mice (~15/FOV vs. ~31/FOV). Very few myofibroblasts were observed within the submucosa (data not shown). Increased myofibroblast numbers could be detected within ulcerated areas of the colon when compared to

non-ulcerated colon areas. Furthermore, during epithelial cell loss within ulcerated regions of the colon, myofibroblasts could be observed interspersing within disrupted epithelium for mucosal repair (Figure 4.5C-D).

To further characterize colonic inflammation differences between WT-DSS and TDAG8 KO-DSS mice, we examined the populations of inflammatory cell infiltrates. The numbers of neutrophils, macrophages, and T cells within the distal colon were assessed. There was a significant increase in polymorphonuclear neutrophil, $F4/80^+$ macrophage, and $CD3^+$ T cell numbers between untreated and DSS-treated mice. We observed a 20-30% increase in leukocyte infiltrates within TDAG8 KO-DSS tissues when compared to WT-DSS colon tissues (Figure 4.6).

TDAG8 has been reported to be highly expressed in immune cells and leukocyte rich tissues such as the spleen, lymph nodes, and thymus. Increased TDAG8 expression can also be observed in tissues with higher baseline levels of resident leukocytes such as the lung and intestinal tissues. TDAG8 localization has not yet been investigated within the colon and mesenteric lymph nodes (MLN), most likely due to the lack of a reliable antibody. To investigate TDAG8 expression within the colon and MLN, we performed immunohistochemistry for green fluorescence protein (GFP) which functions as a surrogate marker for TDAG8 gene expression within TDAG8 KO mice. TDAG8 KO mice were generated by replacing the TDAG8 coding region with a promoterless internal ribosomal entry site-GFP cassette. Therefore, GFP expression is under the control of the endogenous TDAG8 promoter. GFP was detected in interstitial leukocytes within colon mucosa, transverse folds, and intestinal isolated lymphoid follicles (Figure 4.7). Additionally, high GFP expression could be observed in MLN of untreated TDAG8 KO mice. Based on cellular morphology and localization, GFP expression within these

colon leukocytes appears to be predominately macrophages, neutrophils, and lymphocytes. Within the MLN, high GFP expression was detected in histocytes and lymphocytes within the sinus regions, B cell follicles/germinal centers, and paracortical/interfollicular T cell zone. GFP expression was also assessed in DSS-treated TDAG8 KO mouse colon and MLN. A discernable increase of GFP positive leukocytes could be detected within the inflamed colon mucosa and transverse folds when compared to non-inflamed colon tissues. GFP could also be highly detected in ILFs and MLNs as observed in untreated mice. GFP expression is negative in both untreated and DSS-treated TDAG8 KO mouse epithelial cells and mesenchymal cells such as fibroblasts and smooth muscle cells. Additionally, endothelial cells are negative for GFP expression. There was also no GFP signal detected in any WT mouse tissues (Figure 4.10).

TDAG8 gene expression was assessed in intestinal tissues from patients with ulcerative colitis (UC) and Crohn's disease (CrD) in comparison to normal intestinal tissues. A cDNA array including 7 non-inflamed intestinal tissue samples, 14 CrD tissue samples, and 26 UC tissue samples was utilized. We observed a ~4-fold increase of TDAG8 gene expression in UC samples and a ~6-fold increase in CrD samples compared to normal intestinal samples (Figure 4.8).

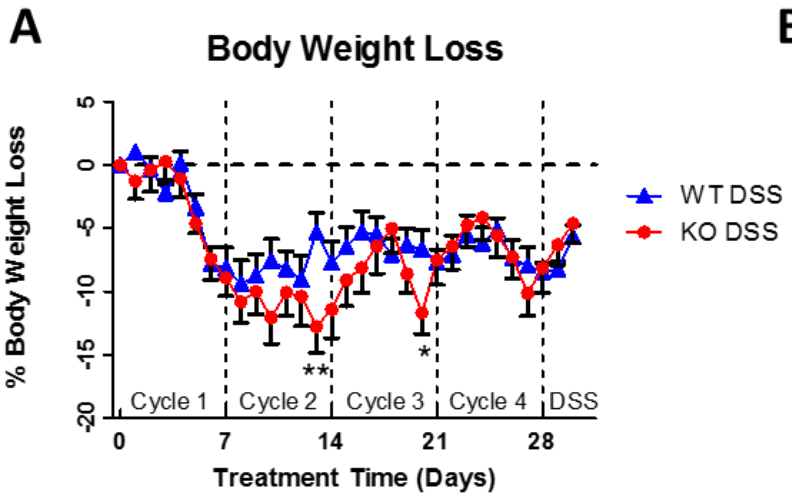
A
Body Weight Loss
% Body Weight Loss
5
0
-5
-10
-15
-20
Cycle 1
Cycle 2
Cycle 3
Cycle 4
DSS
**
*
0
7
14
21
28
Treatment Time (Days)
WT DSS
KO DSS

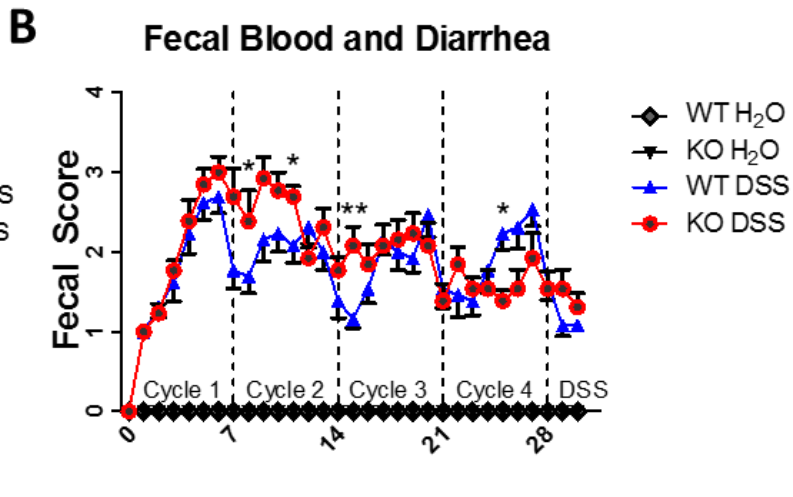
B
Fecal Blood and Diarrhea
Fecal Score
4
3
2
1
0
Cycle 1
Cycle 2
Cycle 3
Cycle 4
DSS
*
*
**
*
0
7
14
21
28
WT H2O
KO H2O
WT DSS
KO DSS

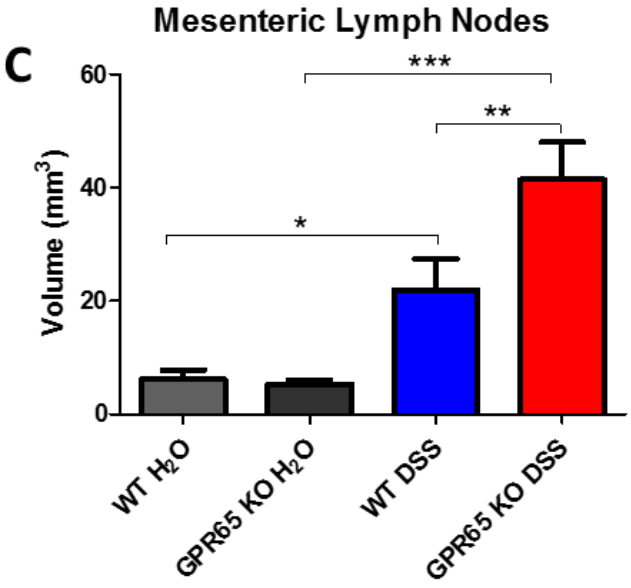
C
Mesenteric Lymph Nodes
Volume (mm3)
60
40
20
0
***
**
*
WT H2O
GPR65 KO H2O
WT DSS
GPR65 KO DSS

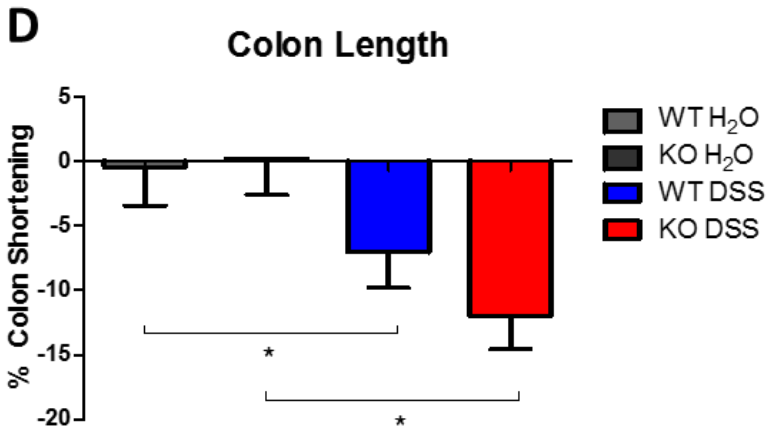
D
Colon Length
% Colon Shortening
5
0
-5
-10
-15
-20
*
*
WT H2O
KO H2O
WT DSS
KO DSS

Figure 4.2. Disease indicators of chronic colitis induction in wild-type (WT) and GPR65 knockout (KO) mice. GPR65 KO-DSS mice have elevated disease parameters when compared to WT-DSS mice. The extent of DSS-induced inflammation was assessed in WT-DSS and GPR65 KO-DSS mice compared to WT and GPR658 KO control mice. GPR65 KO-DSS mice presented elevated disease parameters compared to WT-DSS mice. Clinical phenotypes of intestinal inflammation such as (A) body weight loss and (B) fecal blood and diarrhea were assessed. Macroscopic disease indicators such as (C) mesenteric lymph node expansion and (D) colon shortening were also recorded. Data are presented as the mean ± SEM and statistical significance was determined using the unpaired *t*-test between WT-DSS and GPR65 KO-DSS groups. WT control (N=10), WT-DSS (N=13), GPR65 KO control (N=11), and GPR65 KO-DSS (N=13) mice were used for experiments. Data are representative of four independent experiments with 4-8 mice in each group (*P < 0.05, **P < 0.01).

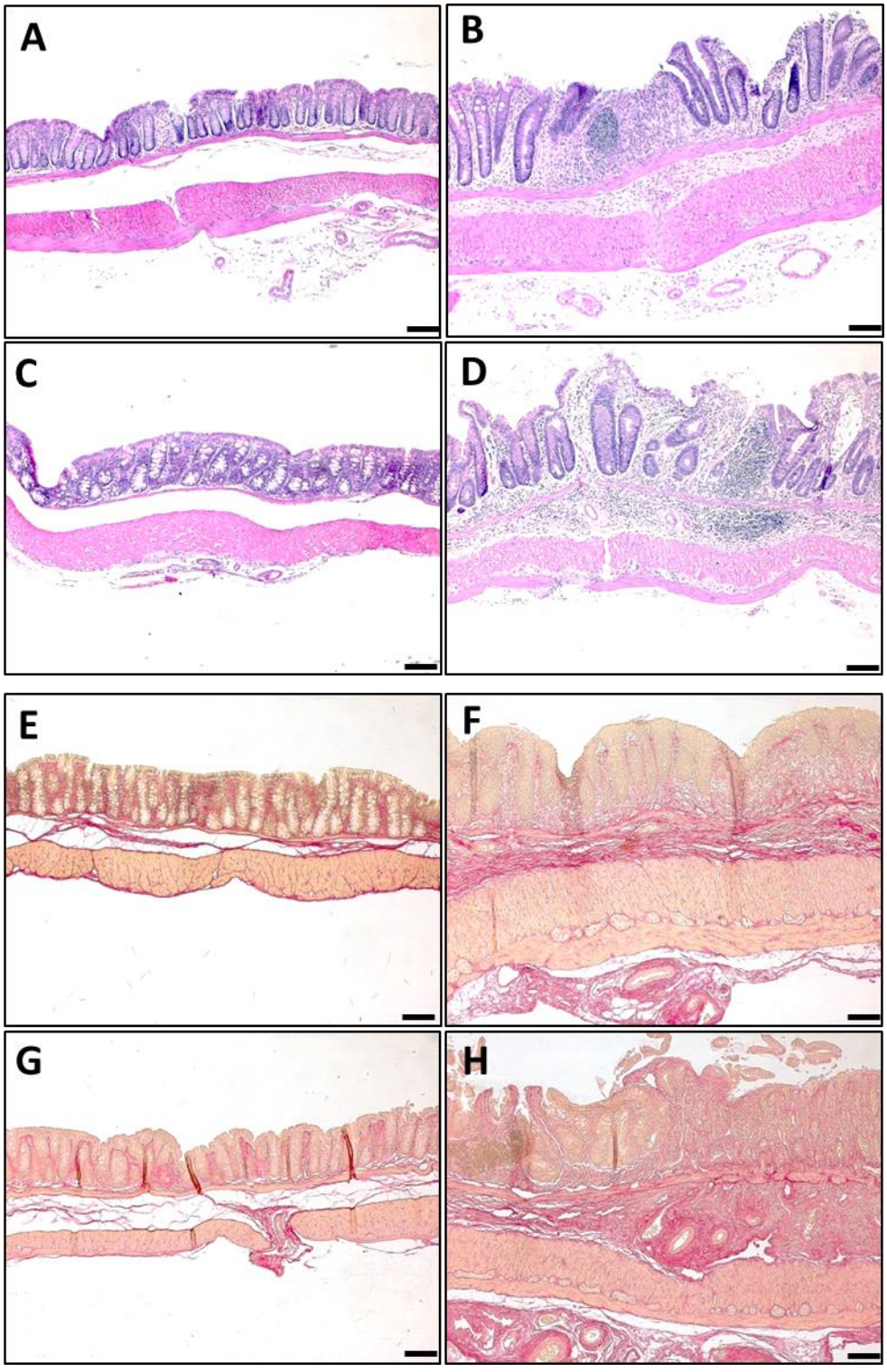
A
B
C
D
E
F
G
H

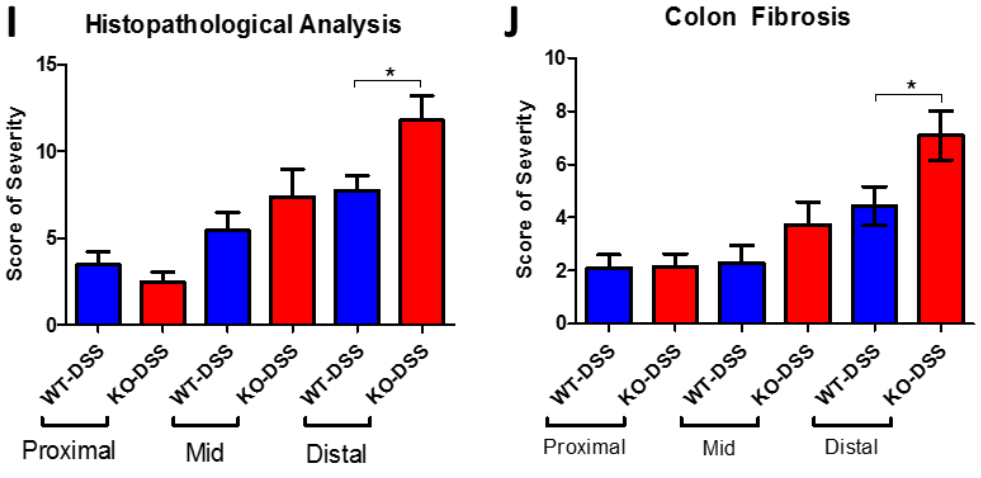
I
Histopathological Analysis
Score of Severity
15
10
5
0
*
WT-DSS
KO-DSS
WT-DSS
KO-DSS
WT-DSS
KO-DSS
Proximal
Mid
Distal
J
Colon Fibrosis
Score of Severity
10
8
6
4
2
0
*
WT-DSS
KO-DSS
WT-DSS
KO-DSS
WT-DSS
KO-DSS
Proximal
Mid
Distal

Figure 4.3. Histopathological analysis of proximal, middle, and distal colon of WT and GPR65 KO mice. Characteristic histopathological features of colitis were assessed to further characterize the degree of intestinal inflammation. GPR65 KO-DSS mice presented elevated disease parameters compared to WT-DSS mice. Representative H&E pictures were taken for (A) WT-control, (B) WT-DSS, (C) GPR65 KO control, and (D) GPR65 KO-DSS mice. Representative pictures of Picrosirius red stained tissue sections for fibrosis assessment were taken of (E) WT control, (F) WT-DSS, (G) GPR65 KO control, and (H) GPR65 KO-DSS mice. Graphical representation of (I) total histopathological parameters and (J) colonic fibrosis are presented. WT control (N=10), WT-DSS (N=13), GPR65 KO control (N=11), and GPR65 KO-DSS (N=13) mouse tissues were used for histopathological analysis. Scale bar is 100μm. Data are presented as the mean ± SEM and statistical significance was determined using the unpaired *t*-test between WT-DSS and GPR65 KO-DSS groups. Data are representative of four independent experiments with 4-8 mice in each group (*$P < 0.05$).

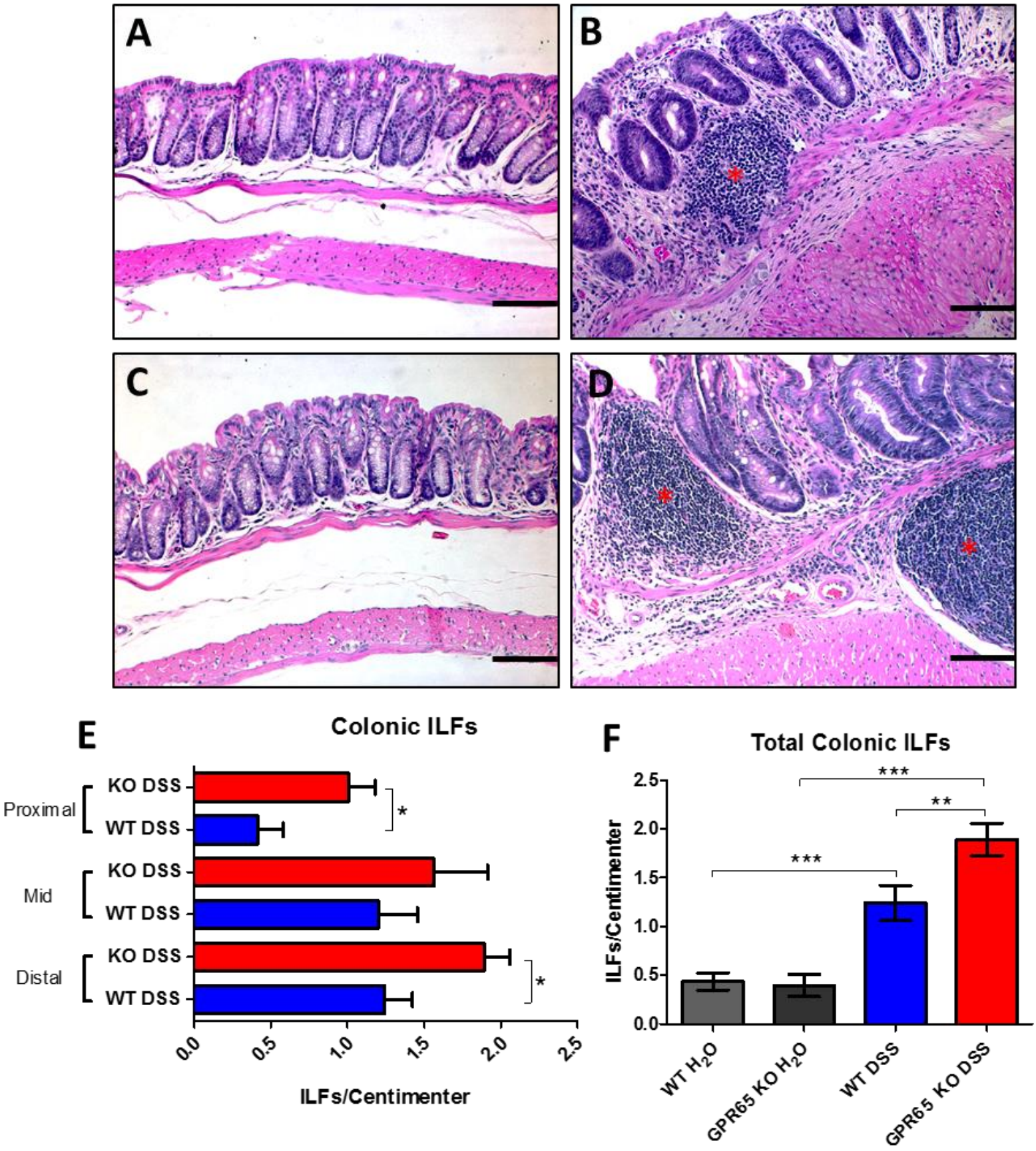
A
B
C
D
E
Colonic ILFs
Proximal
Mid
Distal
KO DSS
WT DSS
KO DSS
WT DSS
KO DSS
WT DSS
*
*
0.0
0.5
1.0
1.5
2.0
2.5
ILFs/Centimenter
F
Total Colonic ILFs
ILFs/Centimenter
2.5
2.0
1.5
1.0
0.5
0.0
***
**
***
WT H2O
GPR65 KO H2O
WT DSS
GPR65 KO DSS

Figure 4.4. Isolated lymphoid follicle (ILF) quantification in proximal, middle, and distal colon segments of WT and GPR65 KO mice. ILF numbers were assessed as an indicator of intestinal inflammation. ILF numbers were highest in distal colon with reduced numbers of ILFs in the proximal colon in DSS-treated mice. GPR65 KO-DSS mice had a further increase in ILF numbers compared to WT-DSS mice. Representative pictures of ILFs in (A) WT-control, (B) WT-DSS, (C) GPR65 KO-control, and (D) GPR65 KO-DSS distal colon segments. Graphical representation of (E) ILF numbers in each segment of the colon and (F) combined full length colon. WT control (N=10), WT-DSS (N=13), GPR65 KO control (N=11), and GPR65 KO-DSS (N=13) mouse tissues were used for ILF quantification. Scale bar is 100µm. Data are presented as the mean ± SEM and statistical significance was determined using the unpaired *t*-test between WT-DSS and GPR65 KO-DSS groups. (*$P < 0.05$).

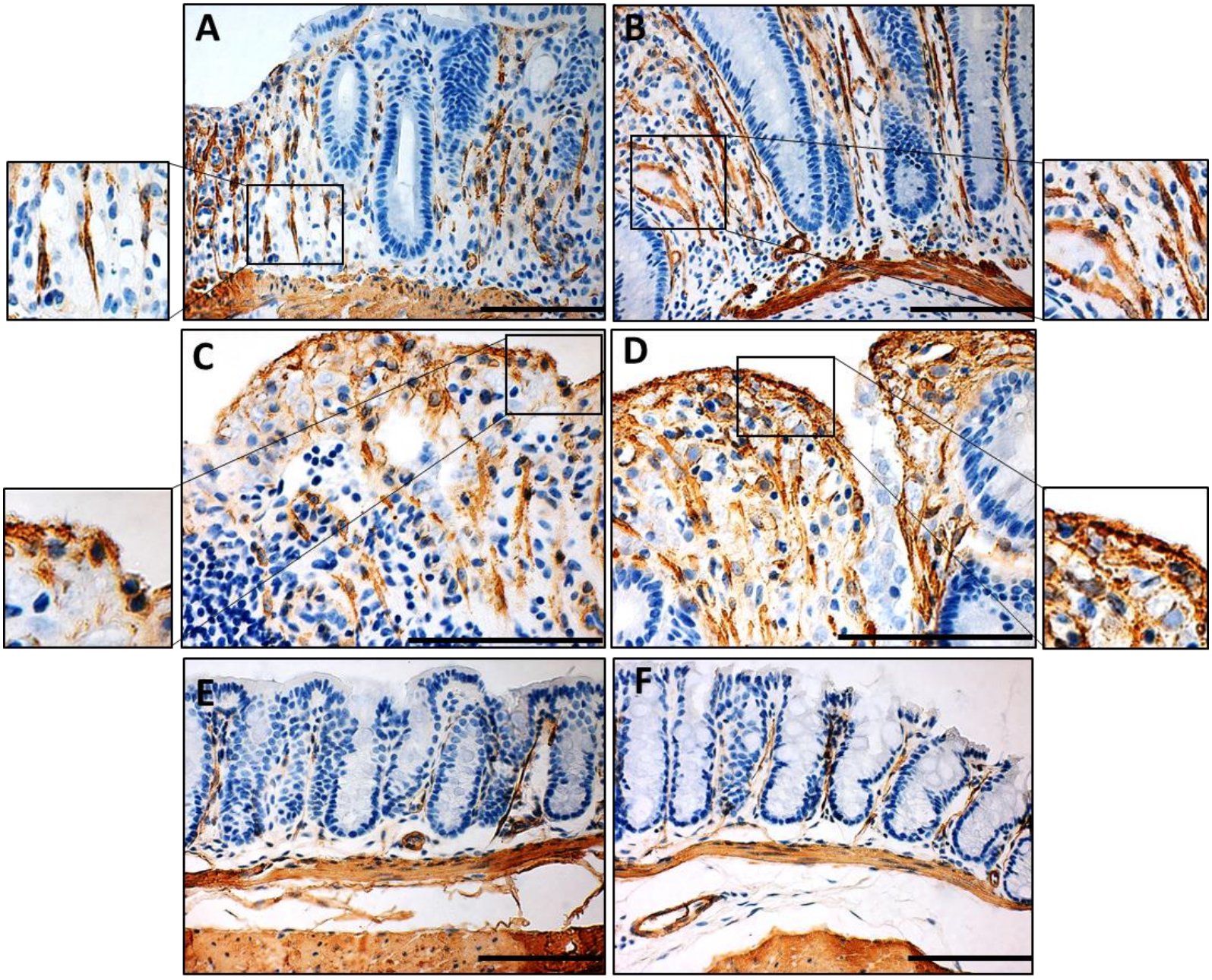
A
B
C
D
E
F

G

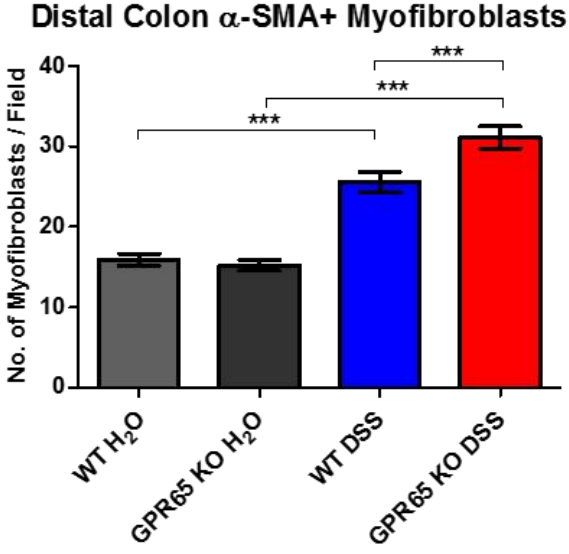
Distal Colon α-SMA+ Myofibroblasts
No. of Myofibroblasts / Field
40
30
20
10
0
***
***
***
WT H2O
GPR65 KO H2O
WT DSS
GPR65 KO DSS

Figure 4.5. Myofibroblast expansion in distal colon mucosa of WT and GPR65 KO mice. SMA^+ myofibroblasts were quantified in distal colon as a cellular basis for increased colonic fibrosis. GPR65 KO-DSS mice had increased myofibroblast numbers in distal colon compared to WT-DSS mice. Representative pictures of (A,C) WT-DSS, (B,D) GPR65 KO-DSS, and (E) WT-control, and (F) GPR65 KO-control. (G) Graphical representation of myofibroblast numbers in distal colon. WT-control (N=3), WT-DSS (N=6), GPR65 KO-control (N=3), and GPR65 KO-DSS (N=6). Scale bar is 100μm. Data are presented as the mean ± SEM and statistical significance was determined using the unpaired *t*-test between WT and TDAG8 KO groups. (**P < 0.01, ***$P < 0.001$).

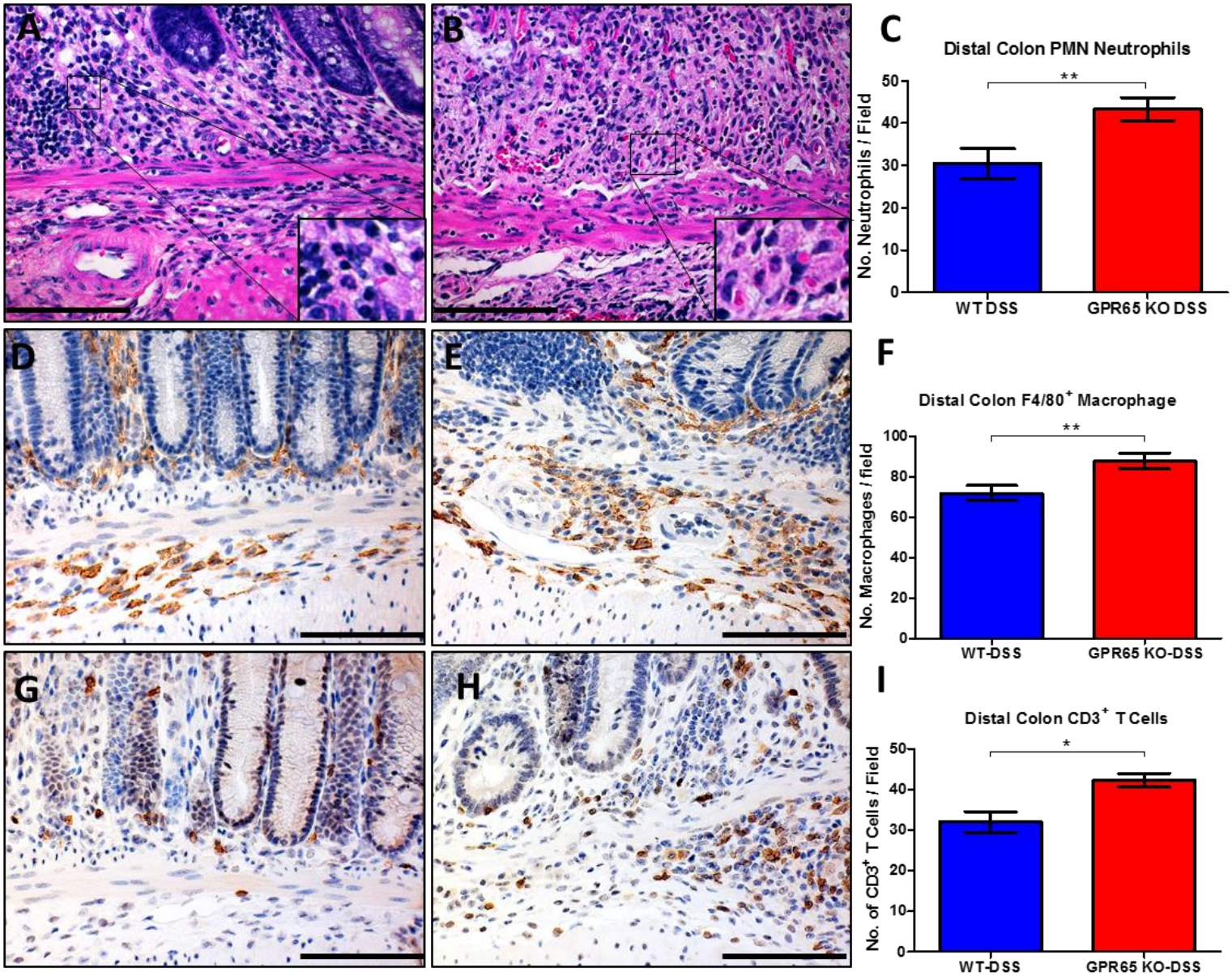
A
B
C
Distal Colon PMN Neutrophils
No. Neutrophils / Field
WT DSS
GPR65 KO DSS
D
E
F
Distal Colon F4/80+ Macrophage
No. Macrophages / field
WT-DSS
GPR65 KO-DSS
G
H
I
Distal Colon CD3+ T Cells
No. of CD3+ T Cells / Field
WT-DSS
GPR65 KO-DSS

Figure 4.6. Leukocyte infiltrates in distal colon of WT and GPR65 KO mice.

Polymorphonuclear (PMN) neutrophils, F4/80^{+} macrophages, and CD3^{+} T cells were counted in the distal colon. GPR65 (TDAG8) KO-DSS mice had increased neutrophils, macrophages, and T cells in distal colon when compared to WT-DSS mice. (A) Representative pictures of WT-DSS and GPR65 KO-DSS mouse (A-B) neutrophils, (D-E) macrophages, and (G-H) T cells, respectively. Graphical representation of (C) neutrophils, (F) macrophages, (I) and T cells. Scale bar is 100μm. Data are presented as the mean ± SEM and statistical significance was determined using the unpaired *t*-test between WT-DSS and GPR65 KO-DSS groups. (*P < 0.05, **P <0.01).

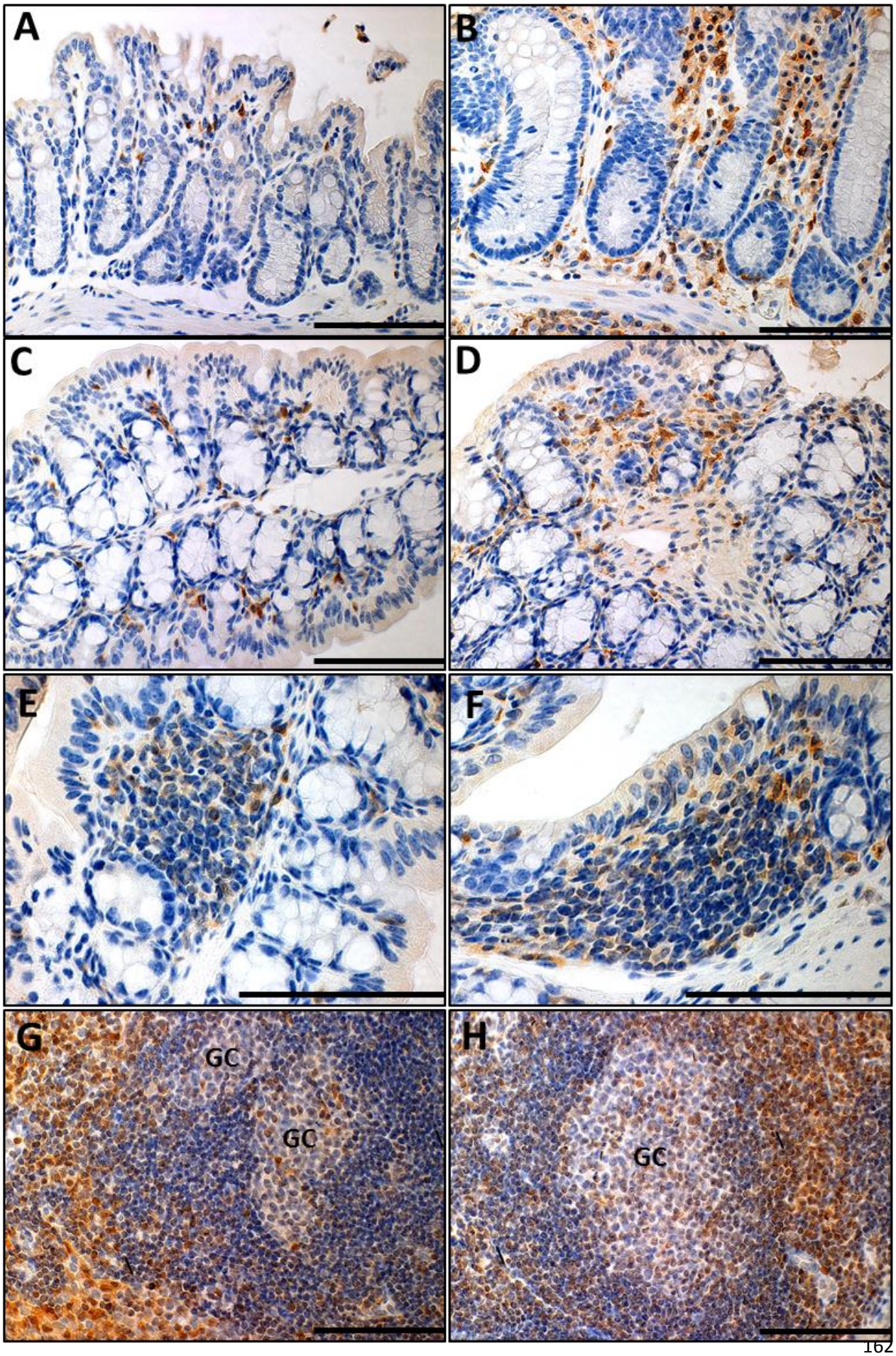
A
B
C
D
E
F
G
GC
GC
H
GC

Figure 4.7 GFP signal in the intestine and intestinal associated lymphoid tissues. GFP knock-in signal serves as a surrogate marker for endogenous GPR65 expression in GPR65 KO mice. GFP signal could be detected in GPR65 KO control (A) distal colon mucosa, (C) proximal colon transverse folds, (E) isolated lymphoid follicles (ILFs), and (G) mesenteric lymph nodes (MLNs). GFP signal could be detected in DSS-treated GPR65 KO (B) intestinal mucosa, (D) transverse folds, (F) ILFs, and (H) MLNs. Based on cellular morphology and compartmental localization, GFP signal was observed in intestinal resident macrophages, lymphocytes, and neutrophils. GC: germinal center. Scale bar is 100μm.

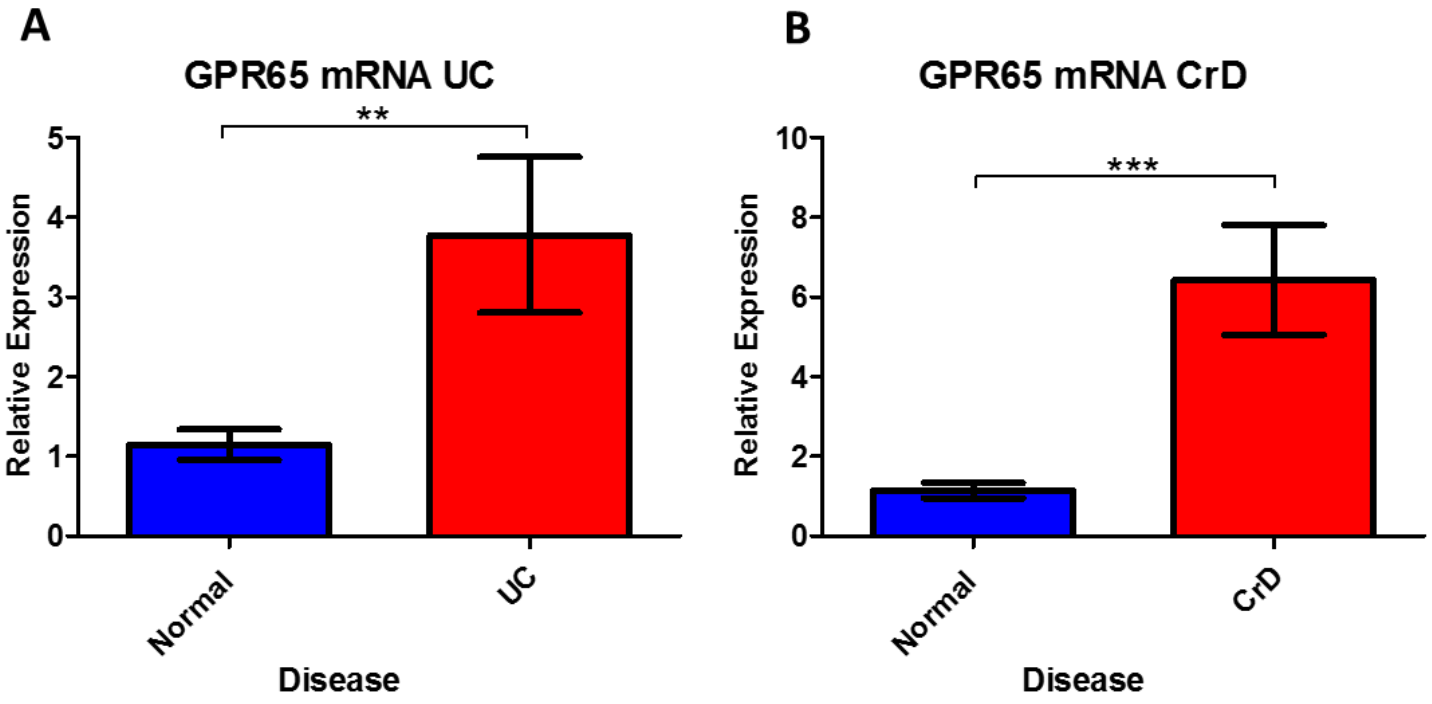
A
GPR65 mRNA UC
**
Relative Expression
5
4
3
2
1
0
Normal
UC
Disease
B
GPR65 mRNA CrD
***
Relative Expression
10
8
6
4
2
0
Normal
CrD
Disease

Figure 4.8. GPR65 gene expression in human ulcerative colitis and Crohn's disease. GPR65 mRNA is increased in ulcerative colitis and Crohn's disease intestinal tissues compared to non-inflamed intestinal tissues. (A) GPR65 gene expression in ulcerative colitis and (B) Crohn's disease. Data are presented as the mean ± SEM and statistical significance was determined using the unpaired *t*-test between control and diseased intestinal tissues. (**P < 0.01, ***P < 0.001).

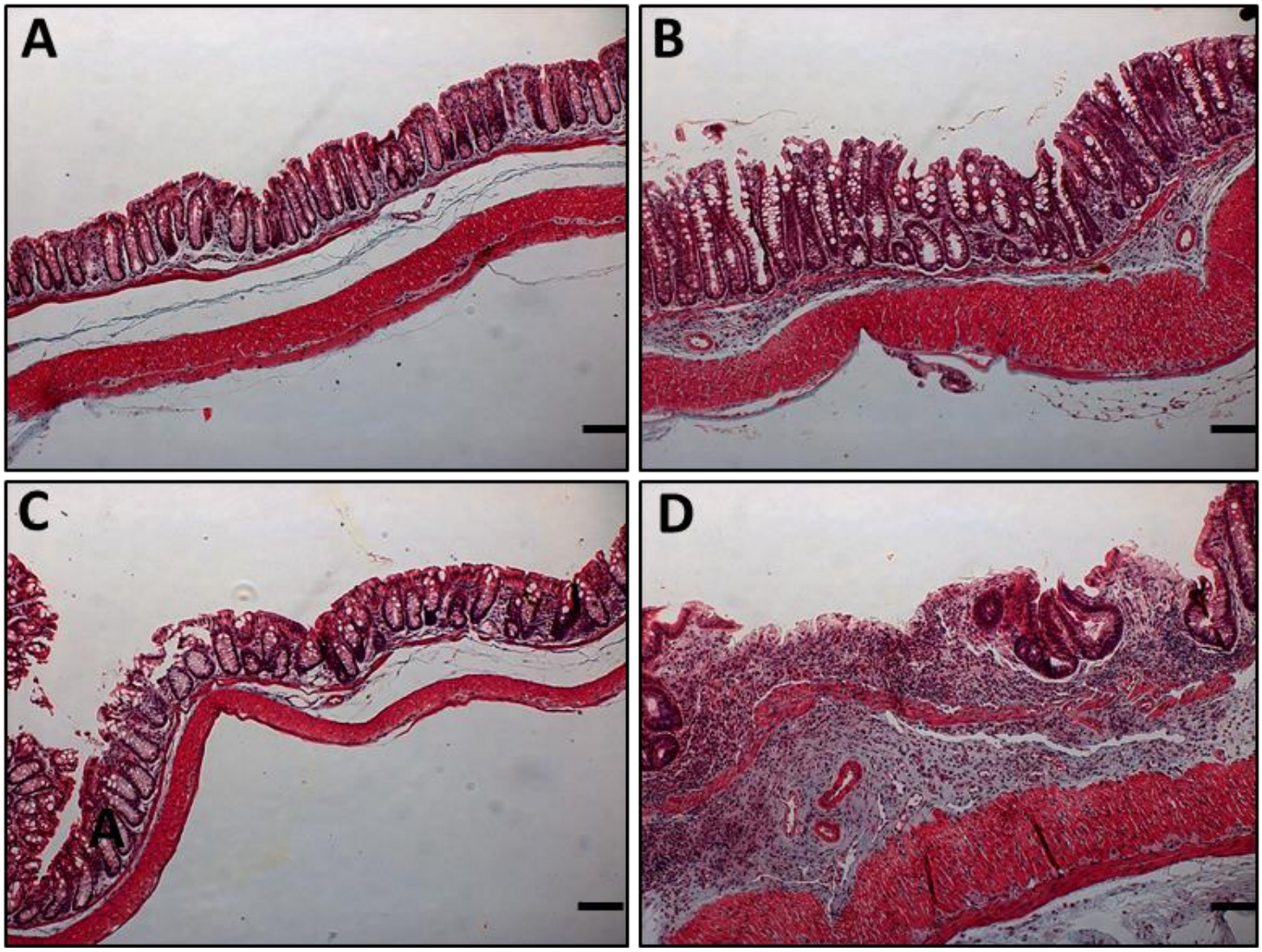
A
B
C
A
D

Figure 4.9. Representative pictures of distal colonic fibrosis in WT and GPR65 KO mice. Masson's trichrome stain indicates DSS-treated GPR65 KO mice have increased pathological fibrosis compared to WT-DSS mice. (A) WT untreated, (B) WT-DSS, (C) GPR65 KO untreated, and (D) GPR65 KO-DSS. Scale bar is 100μm.

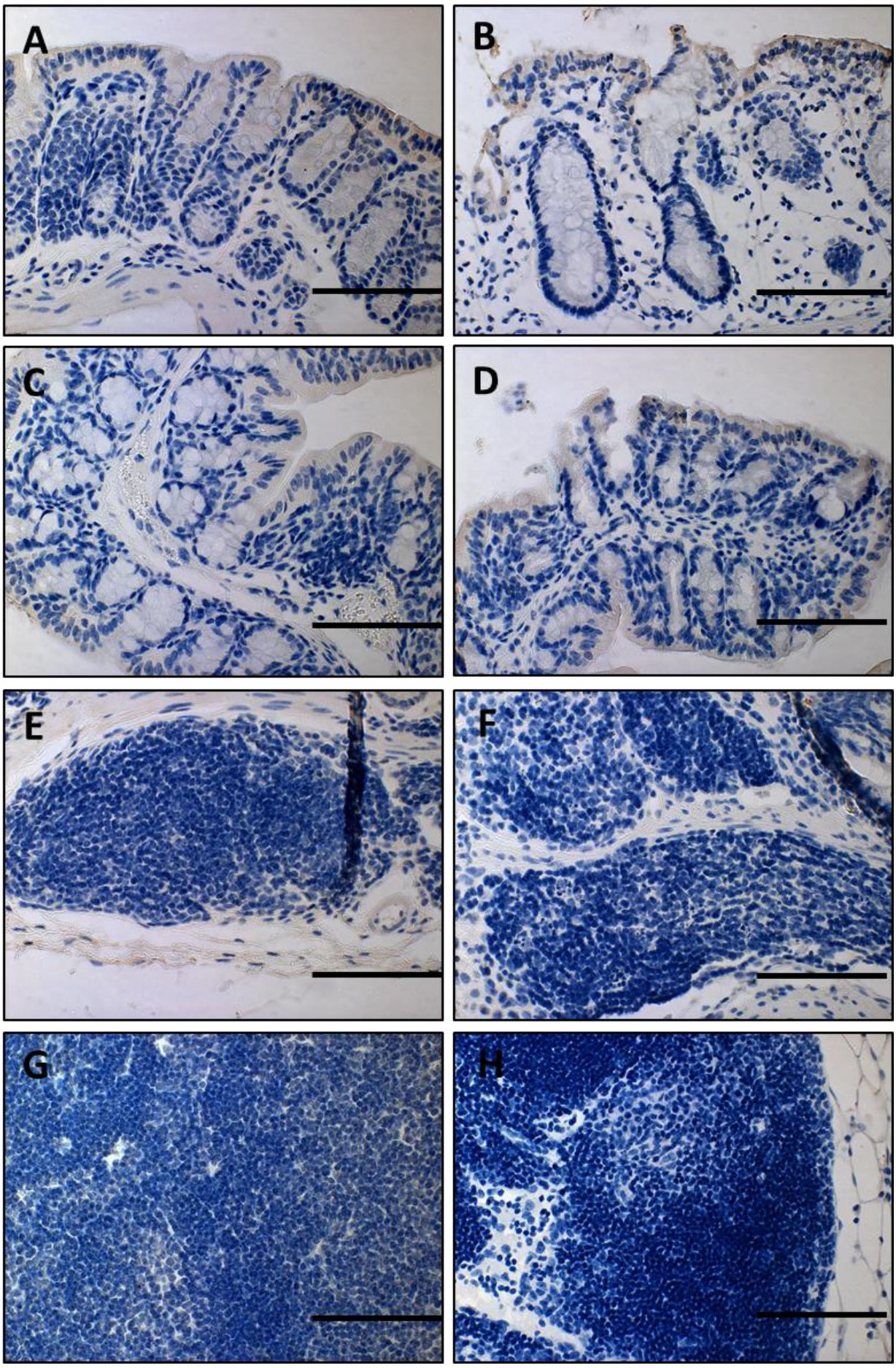
A
B
C
D
E
F
G
H

Figure 4.10. WT negative control for GFP signal in the intestine and intestinal associated lymphoid tissues. No GFP signal could be detected in WT tissues. GFP signal could not be observed in WT-control (A) distal colon mucosa, (C) proximal colon transverse folds, (E) isolated lymphoid follicles (ILFs), and (G) mesenteric lymph nodes (MLNs). GFP signal also could not be detected in WT-DSS (B) intestinal mucosa, (D) transverse folds, (F) ILFs, and (H) MLNs. Minor non-specific staining could be seen on intestinal epithelium and ex-mural connective tissues. Scale bar is 100μm.

C.3 GPR65 modulates immune cell function in response to acidic pH *in vitro*

The role of GPR65 was next assessed in immune cell function. Mouse thymocytes, macrophages, and dendritic cells were investigated. Thymocytes were isolated from the thymus gland of wild-type (WT) and GPR65 knockout (KO) mice while both macrophages and dendritic cells were differentiated from WT or GPR65 KO mouse bone marrow progenitor cells using macrophage colony-stimulating factor (M-CSF) in the L-929 conditioned medium or granulocyte-macrophage colony-stimulating factor (GM-CSF), respectively (Figure 4.11-12).

We first assessed the G-protein activation status of WT and GPR65 KO thymocytes, bone marrow derived macrophages (BMDMs), and bone marrow derived dendritic cells (BMDCs) in response to physiological and acidic pH. Cells were treated at pH 7.4 or pH 6.4 for 30 minutes and protein lysate was collected for CREB and ATF1 phosphorylation assessment as a downstream indicator of the Gαs/cAMP/CREB-ATF-1 pathway. Acidic pH increased the phosphorylation of CREB and ATF1 in mouse thymocytes, BMDMs, and BMDCs when compared to physiological pH by ~2-fold. However, when GPR65 KO mouse thymocytes, BMDMs, and BMDCs were stimulated with acidic pH there was minimal CREB and ATF1 phosphorylation when compared to WT pH 6.4 (Figures 4.13-15). These results, along with previous publications, indicate GPR65 is pH sensitive and couples to Gαs and subsequently signals through the cAMP/CREB-ATF-1 pathway. As previous literatures have associated Gαs with anti-inflammatory programs in immune cells, it is possible GPR65 displays an anti-inflammatory role in the inflammatory response.

We next assessed the proton-sensing GPCR family member expression levels in the thymocyte, BMDM, and BMDC populations under physiological and acidic pH conditions.

These experiments were done to determine the role of acidic pH on the expression of the family of proton-sensing GPCRs and to determine if another proton-sensing GPCR family member compensates for the loss of GPR65 in thymocyte, BMDM, and BMDC populations. At physiological pH, GPR65 was the highest expressed proton-sensing GPCR in BMDMs while GPR68 was highest expressed in BMDCs. All the proton-sensing GPCR family members were equally expressed in thymocytes (Figures 4.16-18). In response to acidic pH, thymocytes and BMDCs GPR65 mRNA levels were not significantly modulated. However, GPR65 mRNA was more than 50% reduced in BMDMs treated with acidic pH (Figure 4.18). When BMDMs were classically activated (M1) or alternatively activated (M2) GPR65 mRNA levels were also reduced in acidic pH compared to physiological pH (Figure 4.18). No expression of GPR65 could be detected in GPR65 KO thymocytes, BMDMs, or BMDCs. Proton-sensors GPR4 and GPR68 were also assessed in GPR65 KO thymocytes, BMDM, and BMDCs. No significant compensation could be observed in GPR65 KO thymocytes or BMDCs. However, GPR68 was more than 80% downregulated in GPR65 KO BMDMs compared to WT BMDMs at physiological and acidic pH conditions (Figure 4.18).

Provided GPR65 was the highest expressed amongst the proton-sensing GPCRs in BMDMs, we sought to investigate the role of GPR65 in macrophage inflammatory programs. The functional effects of acidosis-induced GPR65 activity was assessed in naïve BMDM migration and proliferation, respectively. Acidosis reduced BMDM directional migration toward chemoattractant C5a (Figure 4.19). In the absence of GPR65, BMDM migration was partially recovered toward C5a when compared to physiological pH. These results indicate GPR65 reduces macrophage directional migration toward the inflammatory stimulus C5a in the transwell migration assay. We next assessed the role of GPR65 in BMDM proliferation. In WT BMDMs,

acidic pH reduced proliferation when compared to physiological pH (Figure 4.20). However, GPR65 KO BMDM proliferation was partially recovered in the presence of acidic pH when compared to physiological pH (Figure 4.20).

We next assessed the role of GPR65 when macrophages are classically activated (M1 phenotype) and alternatively activated (M2 phenotype). BMDMs were polarized to M1 or M2 for 24hrs and then treated with physiological pH or acidic pH for 5hrs. In the case of M1 polarization, pH stimulation occurred in the presence or absence of 100ng/mL LPS. For M1 polarization, GPR65 KO BMDMs exhibited increased TNF-α mRNA levels than WT BMDMs at acidic pH conditions (Figure 4.21). However, no such trend could be observed in IL-1β mRNA levels. Interestingly, however, acidosis alone was capable of increasing IL-1β in WT and GPR65 KO BMDMs (Figure 4.21). Taken together, GPR65 seems to have differential effects on M1-associated pro-inflammatory gene expression as GPR65-null macrophages display heightened TNF-α mRNA levels but not IL-1β. However, we have not investigated the functional role of GPR65 in chemotaxis or phagocytosis in M1 macrophages. We then investigated the role of GPR65 in the M2 phenotype. Alternatively activated BMDMs were assessed for Arginase 1, FIZZ1, and IL-10 gene expression. GPR65 KO M2 BMDMs displayed a heightened expression of arginase 1 and FIZZ1 genes when compared to WT BMDMs under acidic pH conditions (Figure 4.22). These results suggest GPR65 may be involved in suppressing M2-associated activity through the downregulation of arginase 1 and FIZZ1 gene expression. Interestingly, GPR65-null M2-polarized macrophages had reduced IL-10 mRNA levels at physiological pH when compared to WT M2 macrophages. These results suggest GPR65 mediates IL-10 mRNA production in M2 macrophages within physiological pH conditions. When alternatively activated

BMDMs were treated with acidic pH, IL-10 mRNA was reduced by more than 50%. However, there was no further reduction of IL-10 mRNA in GPR65-null M2 BMDMs (Figure 4.22).

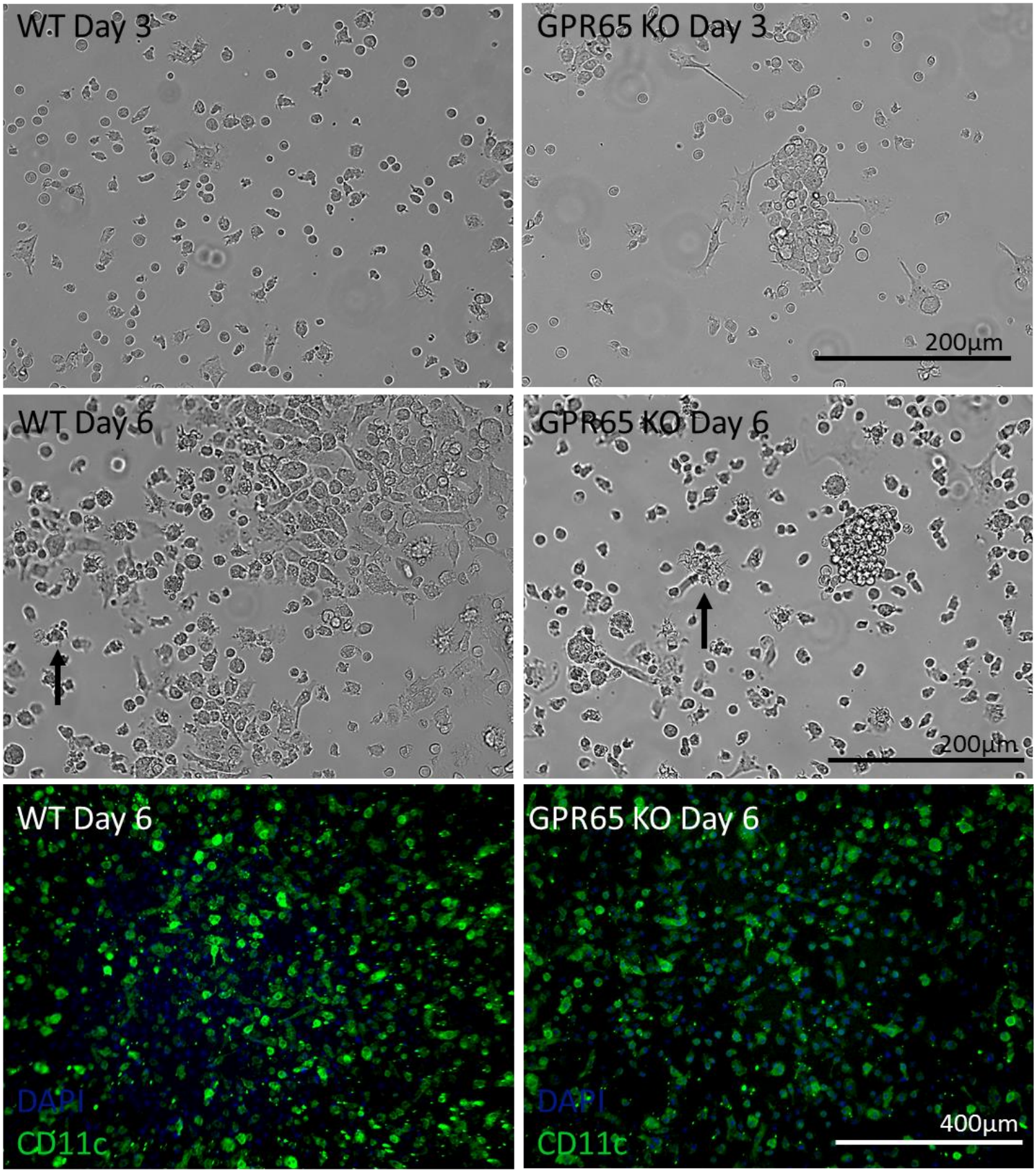
WT Day 3
GPR65 KO Day 3
200µm
WT Day 6
GPR65 KO Day 6
200µm
WT Day 6
DAPI
CD11c
GPR65 KO Day 6
DAPI
CD11c
400µm

Figure 4.11: **Bone marrow derived dendritic cell differentiation from bone marrow progenitor cells**. WT and GPR65 KO bone marrow progenitor cells were differentiated to BMDCs for 6 days by 20ng/mL mrGM-CSF. WT and GPR65 KO BMDC differentiation resulted in more than 90% purity based on CD11c staining. Black arrows indicate BMDC with visible dendritic processes. Scale bar length is indicated on individual representative picture.

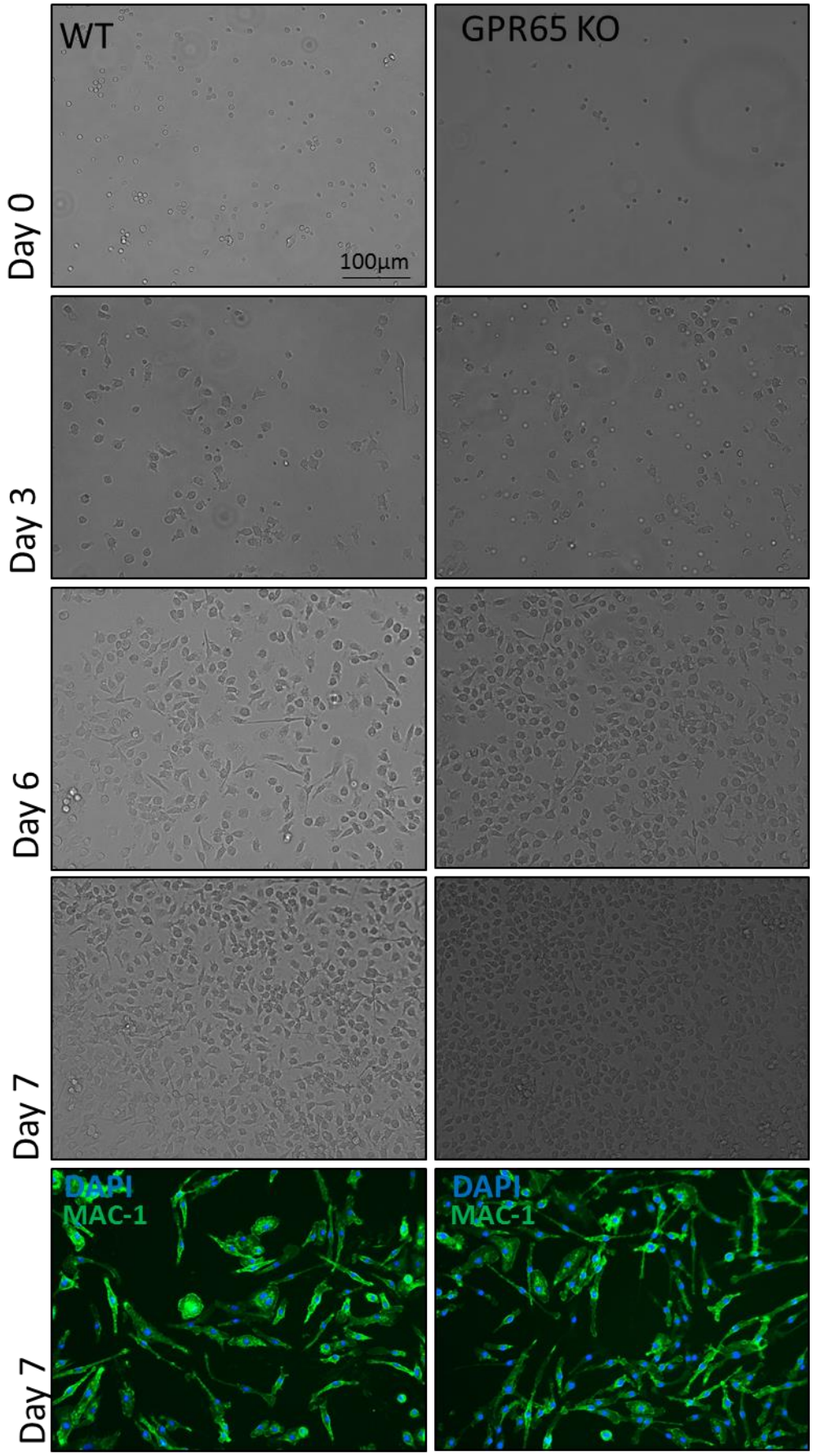
WT
GPR65 KO
100µm
Day 0
Day 3
Day 6
Day 7
DAPI
MAC-1
DAPI
MAC-1
Day 7

Figure 4.12: **Bone marrow derived macrophage (BMDM) differentiation from bone marrow progenitor cells**. WT and GPR65 KO bone marrow progenitor cells were differentiated to BMDMs for 7 days by 15% L929 conditioned medium. WT and GPR65 KO BMDM differentiation resulted in more than 97% purity based on CD11b (MAC-1) staining. Scale bar =100µm

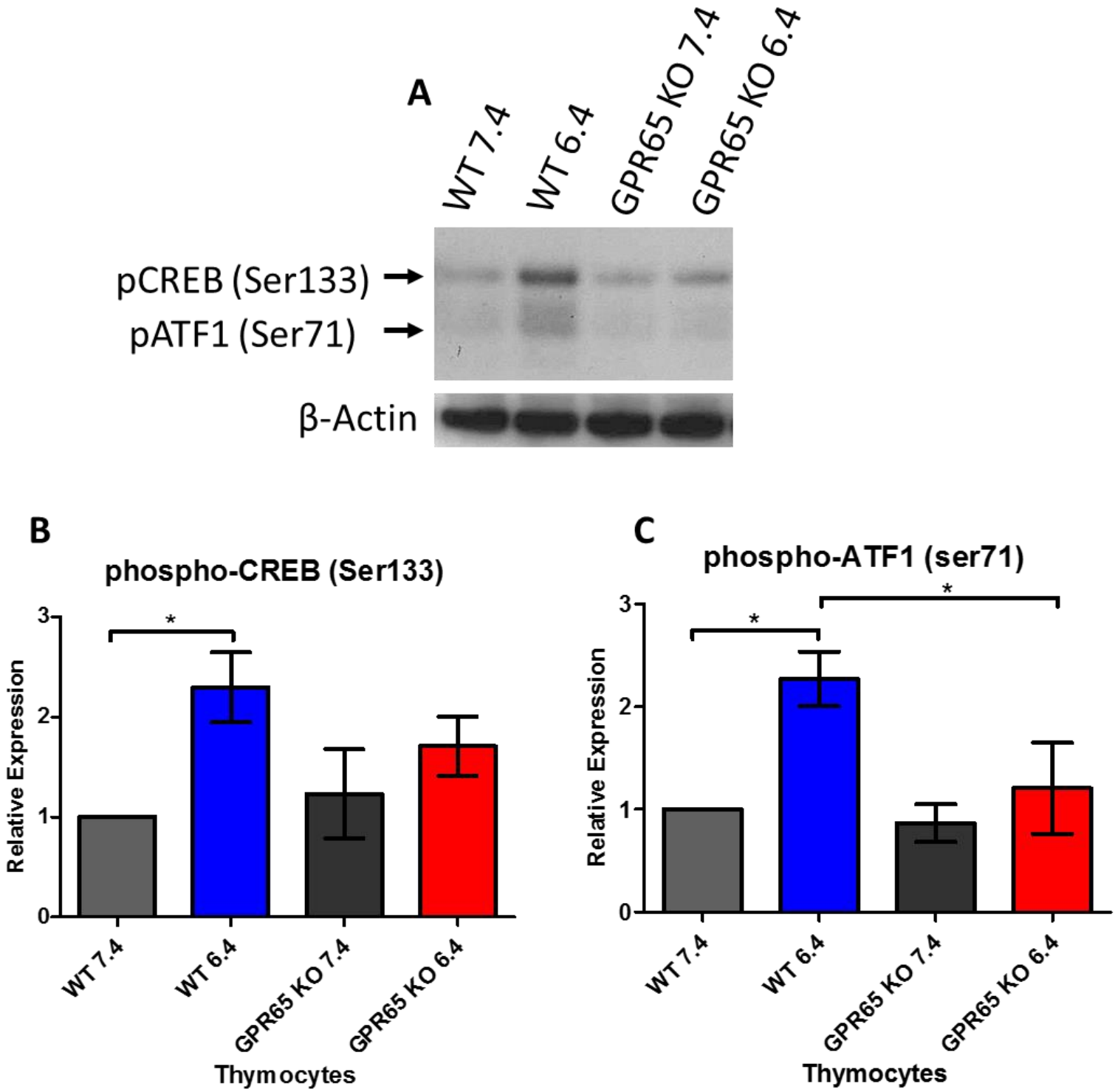
A
WT 7.4
WT 6.4
GPR65 KO 7.4
GPR65 KO 6.4
pCREB (Ser133)
pATF1 (Ser71)
β-Actin
B
phospho-CREB (Ser133)
Relative Expression
0
1
2
3
*
WT 7.4
WT 6.4
GPR65 KO 7.4
GPR65 KO 6.4
Thymocytes
C
phospho-ATF1 (ser71)
Relative Expression
0
1
2
3
*
*
WT 7.4
WT 6.4
GPR65 KO 7.4
GPR65 KO 6.4
Thymocytes

Figure 4.13: **Acidosis-induced phosphorylation of CREB and ATF1 in WT and GPR65 KO thymocytes**. GPR65 KO thymocytes display reduced CREB and ATF1 phosphorylation at acidic pH when compared to WT. WT and GPR65 KO mouse thymocytes were treated with pH 7.4 and pH 6.4 for 30min. (A) Representative images of pCREB (Ser133) and pATF1 (Ser71) western blot results, graphical representation of (B) pCREB, and (C) pATF1. WT 7.4 (n=3), WT 6.4 (n=3), GPR65 KO 7.4 (n=3), and GPR65 KO 6.4 (n=3). One-way ANOVA followed by Bonferroni post-hoc was performed for statistical analysis. Data representative of three independent experiments. (*$P < 0.05$)

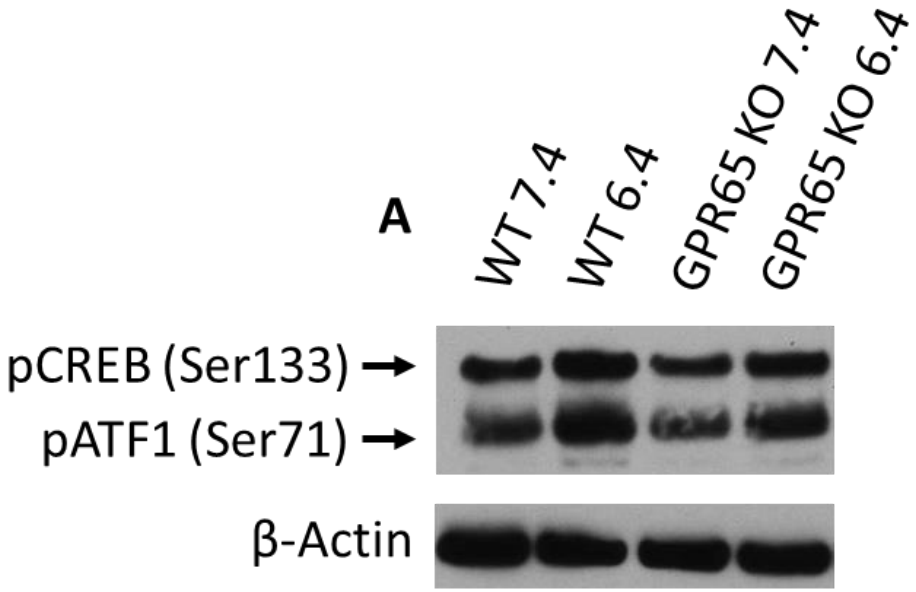
A
WT 7.4
WT 6.4
GPR65 KO 7.4
GPR65 KO 6.4
pCREB (Ser133)
pATF1 (Ser71)
β-Actin

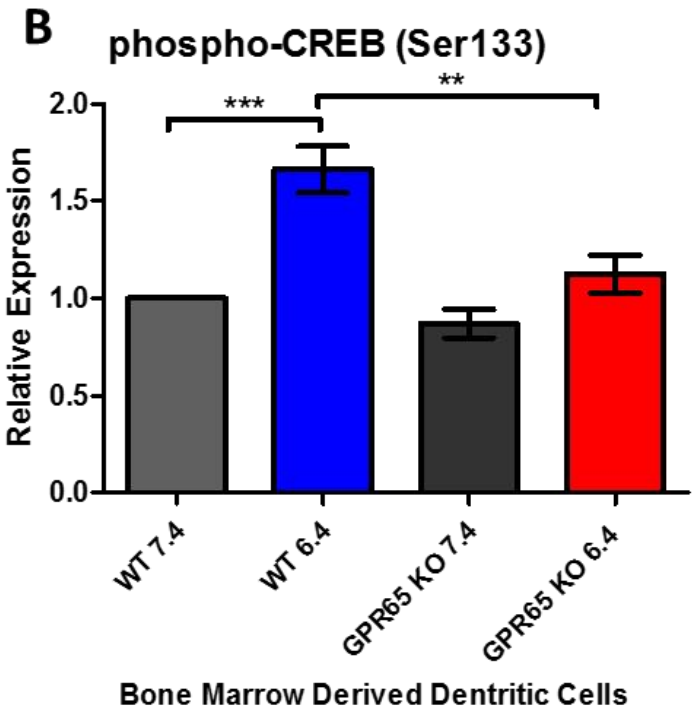
B
phospho-CREB (Ser133)
***
**
Relative Expression
2.0
1.5
1.0
0.5
0.0
WT 7.4
WT 6.4
GPR65 KO 7.4
GPR65 KO 6.4
Bone Marrow Derived Dentritic Cells

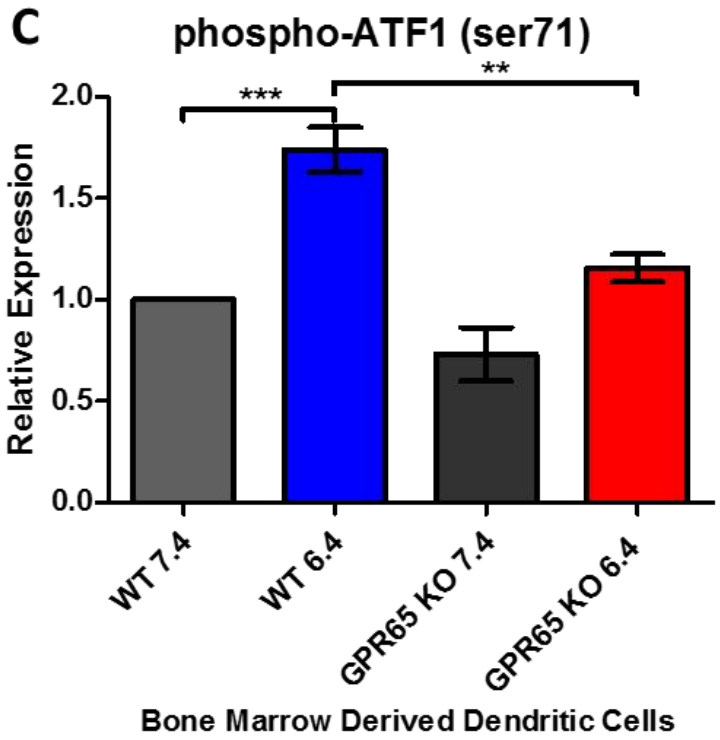
C
phospho-ATF1 (ser71)
***
**
Relative Expression
2.0
1.5
1.0
0.5
0.0
WT 7.4
WT 6.4
GPR65 KO 7.4
GPR65 KO 6.4
Bone Marrow Derived Dendritic Cells

Figure 4.14: **Acidosis-induced phosphorylation of CREB and ATF1 in mouse bone marrow derived dendritic cells**. GPR65 KO BM-DCs display reduced CREB and ATF1 phosphorylation at acidic pH when compared to WT. WT and GPR65 KO mouse bone marrow derived dendritic cells were treated with pH 7.4 and pH 6.4 for 30min. (A) Representative images of pCREB (Ser133) and pATF1 (Ser71) western blot results, graphical representation of (B) pCREB, and (C) pATF1. One-way ANOVA followed by Bonferroni post-hoc was performed for statistical analysis. WT 7.4 (n=3), WT 6.4 (n=3), GPR65 KO 7.4 (n=3), and GPR65 KO 6.4 (n=3). Data representative of three independent experiments. (**$P < 0.01$, *** $P< 0.001$)

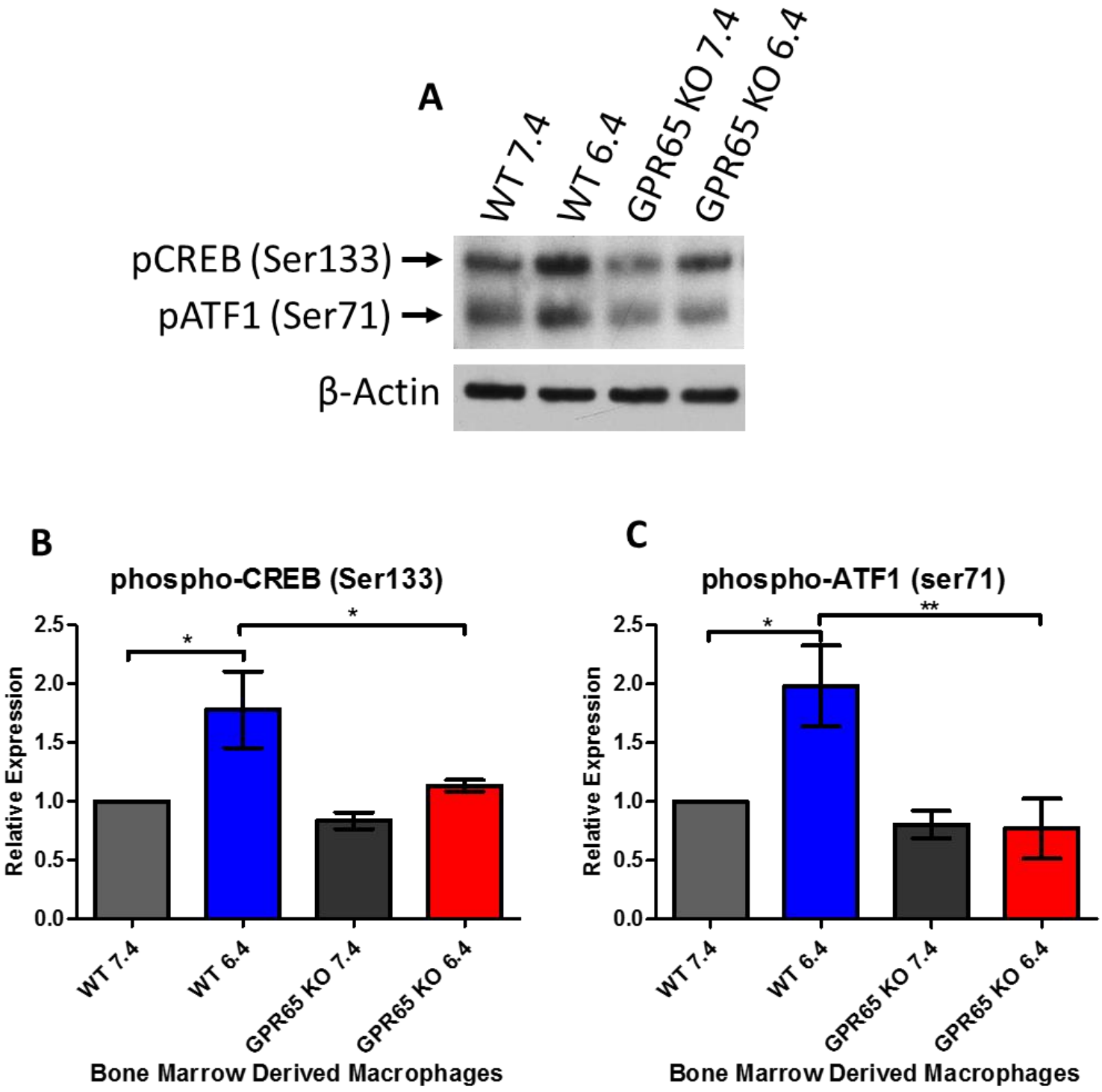
A
WT 7.4
WT 6.4
GPR65 KO 7.4
GPR65 KO 6.4
pCREB (Ser133)
pATF1 (Ser71)
β-Actin
B
phospho-CREB (Ser133)
Relative Expression
2.5
2.0
1.5
1.0
0.5
0.0
*
*
WT 7.4
WT 6.4
GPR65 KO 7.4
GPR65 KO 6.4
Bone Marrow Derived Macrophages
C
phospho-ATF1 (ser71)
Relative Expression
2.5
2.0
1.5
1.0
0.5
0.0
*
**
WT 7.4
WT 6.4
GPR65 KO 7.4
GPR65 KO 6.4
Bone Marrow Derived Macrophages

Figure 4.15: Acidosis-induced phosphorylation of CREB and ATF1 in mouse bone marrow derived macrophages. GPR65 KO BMDMs display reduced CREB and ATF1 phosphorylation at acidic pH when compared to WT. WT and GPR65 KO mouse bone marrow derived macrophages were treated with pH 7.4 and pH 6.4 for 30min. (A) Representative images of pCREB (Ser133) and pATF1 (Ser71) western blot results, graphical representation of (B) pCREB, and (C) pATF1. One-way ANOVA followed by Bonferroni post-hoc was performed for statistical analysis. WT 7.4 (n=3), WT 6.4 (n=3), GPR65 KO 7.4 (n=3), and GPR65 KO 6.4 (n=3). Data representative of three independent experiments. (*$P < 0.05$, **$P < 0.01$)

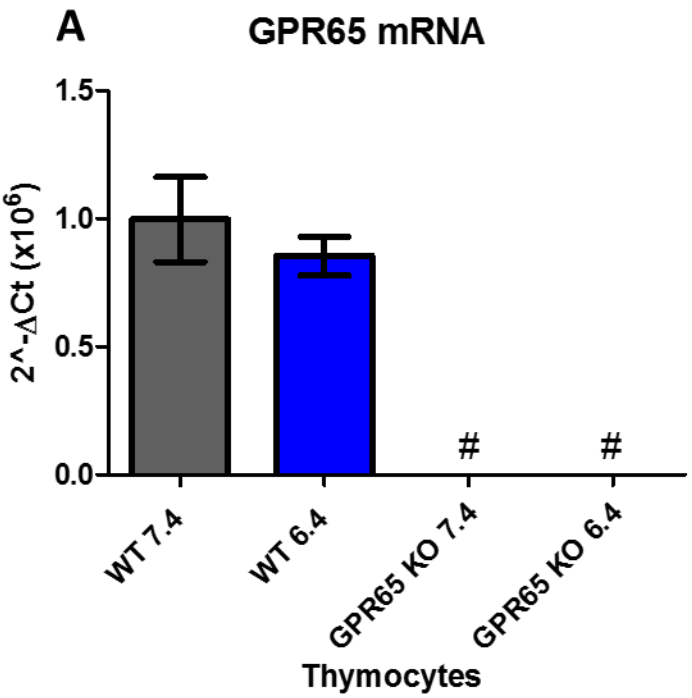
A
GPR65 mRNA
2^-ΔCt (x10^6)
1.5
1.0
0.5
0.0
#
#
WT 7.4
WT 6.4
GPR65 KO 7.4
GPR65 KO 6.4
Thymocytes

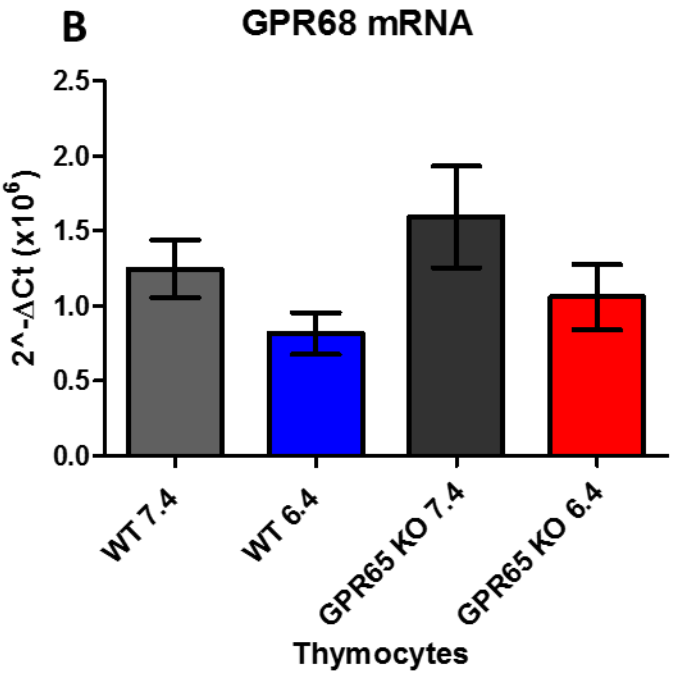
B
GPR68 mRNA
2^-ΔCt (x10^6)
2.5
2.0
1.5
1.0
0.5
0.0
WT 7.4
WT 6.4
GPR65 KO 7.4
GPR65 KO 6.4
Thymocytes

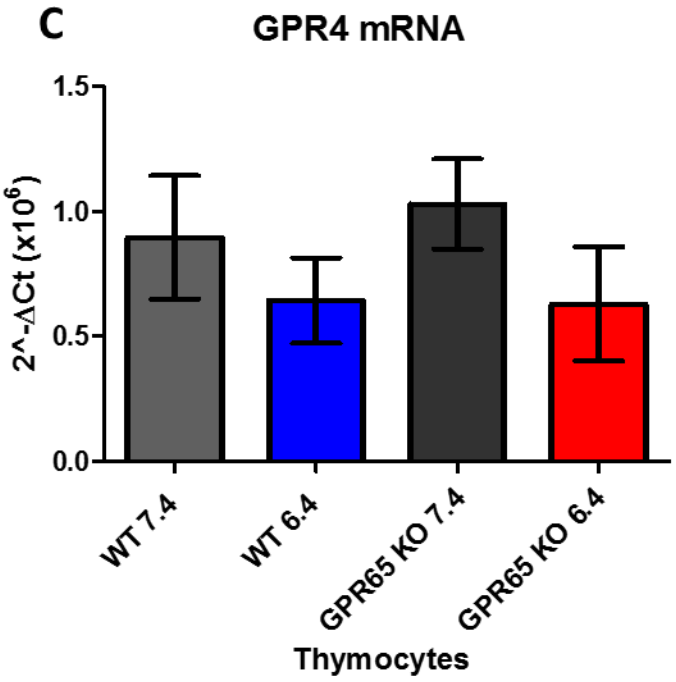
C
GPR4 mRNA
2^-ΔCt (x10^6)
1.5
1.0
0.5
0.0
WT 7.4
WT 6.4
GPR65 KO 7.4
GPR65 KO 6.4
Thymocytes

Figure 4.16: Proton-sensing GPCR family member mRNA expression in mouse thymocytes. GPR68 and GPR4 have similar expression levels and do not compensate for the loss of GPR65 in the knockout thymocytes. WT and GPR65 KO mouse thymocytes were treated with pH 7.4 and pH 6.4 for 3hrs. (A) GPR65, (B) GPR68, and (C) GPR4 mRNA levels were assessed using qPCR. One-way ANOVA followed by Bonferroni post-hoc was performed for statistical analysis. WT 7.4 (n=4), WT 6.4 (n=4), GPR65 KO 7.4 (n=4), and GPR65 KO 6.4 (n=4). Data representative of two independent experiments. #= no detectable signal.

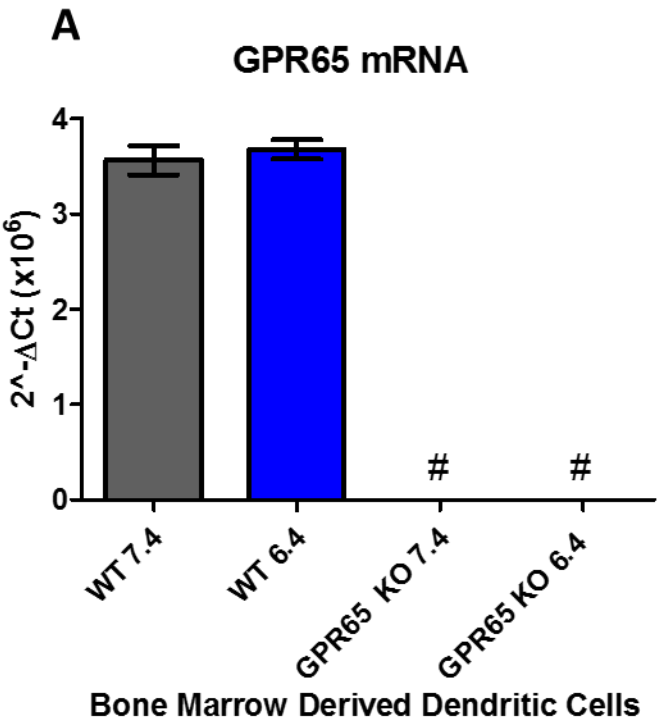
A
GPR65 mRNA
2^-ΔCt (x10^6)
4
3
2
1
0
#
#
WT 7.4
WT 6.4
GPR65 KO 7.4
GPR65 KO 6.4
Bone Marrow Derived Dendritic Cells

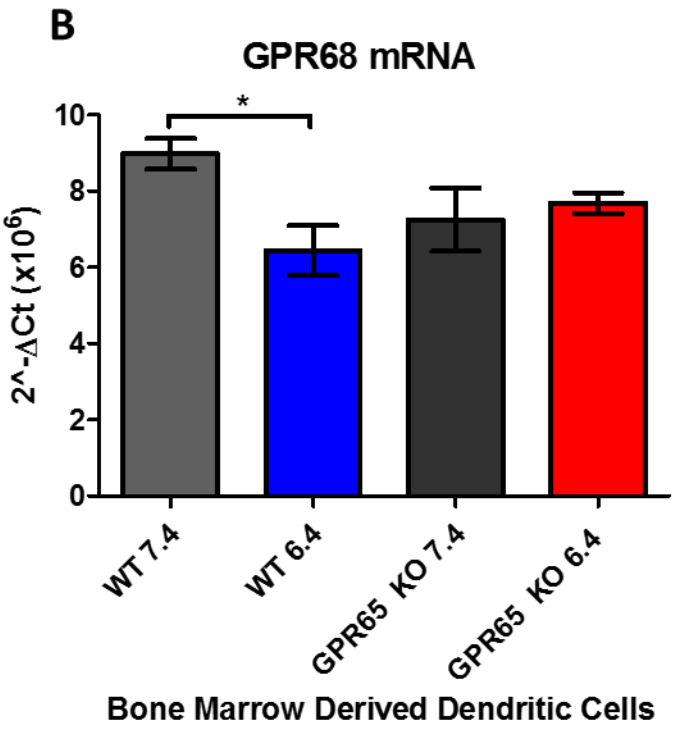
B
GPR68 mRNA
2^-ΔCt (x10^6)
10
8
6
4
2
0
*
WT 7.4
WT 6.4
GPR65 KO 7.4
GPR65 KO 6.4
Bone Marrow Derived Dendritic Cells

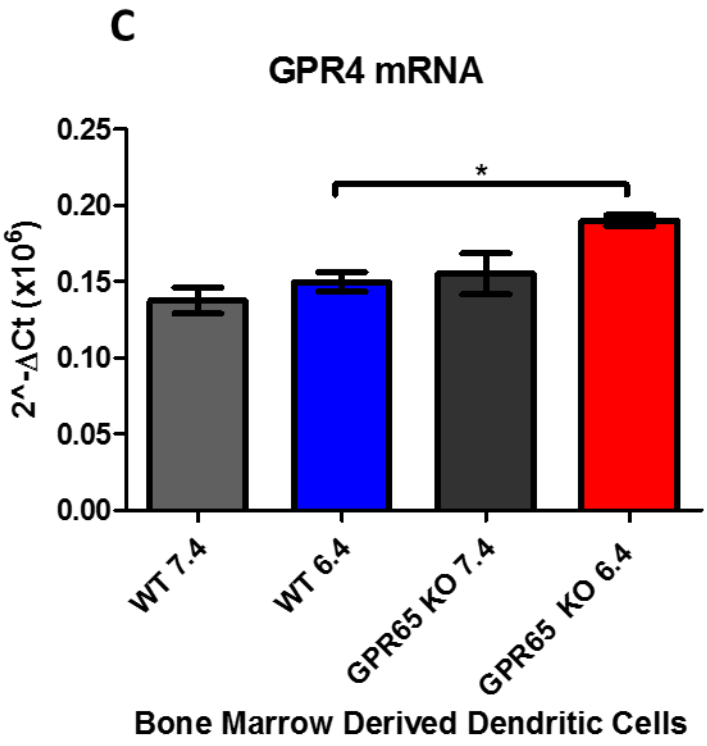
C
GPR4 mRNA
2^-ΔCt (x10^6)
0.25
0.20
0.15
0.10
0.05
0.00
*
WT 7.4
WT 6.4
GPR65 KO 7.4
GPR65 KO 6.4
Bone Marrow Derived Dendritic Cells

Figure 4.17: Proton-sensing GPCR family member mRNA expression in bone marrow derived dendritic cells. GPR65 mRNA expression is not altered by changes in pH and GPR68 is the highest expressed pH-sensing GPCR in BMDMs and is reduced at acidic pH. WT and GPR65 KO mouse bone marrow derived dendritic cells were treated with pH 7.4 and pH 6.4 for 3hrs. (A) GPR65, (B) GPR68, and (C) GPR4 mRNA levels were assessed using qPCR. One-way ANOVA followed by Bonferroni post-hoc was performed for statistical analysis. WT 7.4 (n=3), WT 6.4 (n=3), GPR65 KO 7.4 (n=3), and GPR65 KO 6.4 (n=3). Data from one experiment. (*$P < 0.05$) #= no detectable signal.

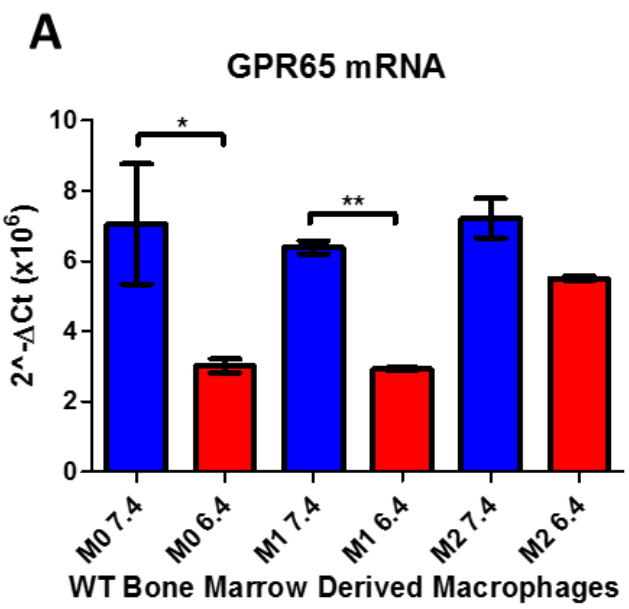
A
GPR65 mRNA
2^-ΔCt (x10^6)
10
8
6
4
2
0
*
**
M0 7.4
M0 6.4
M1 7.4
M1 6.4
M2 7.4
M2 6.4
WT Bone Marrow Derived Macrophages

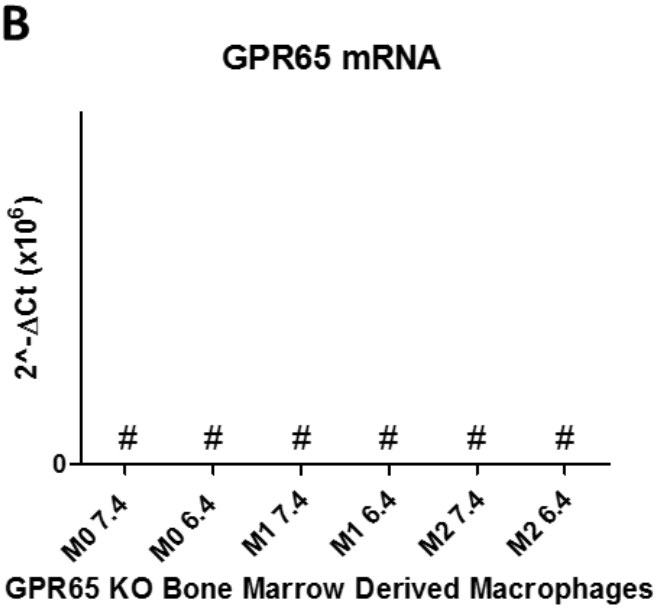
B
GPR65 mRNA
2^-ΔCt (x10^6)
0
#
#
#
#
#
#
M0 7.4
M0 6.4
M1 7.4
M1 6.4
M2 7.4
M2 6.4
GPR65 KO Bone Marrow Derived Macrophages

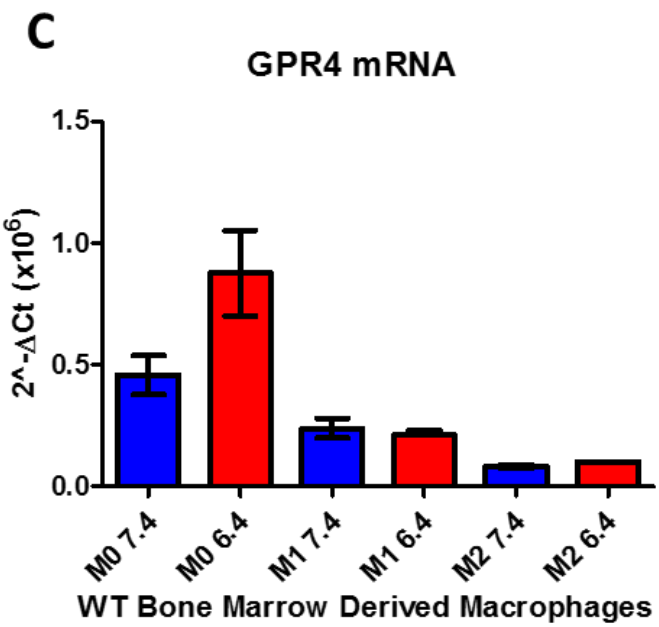
C
GPR4 mRNA
2^-ΔCt (x10^6)
1.5
1.0
0.5
0.0
M0 7.4
M0 6.4
M1 7.4
M1 6.4
M2 7.4
M2 6.4
WT Bone Marrow Derived Macrophages

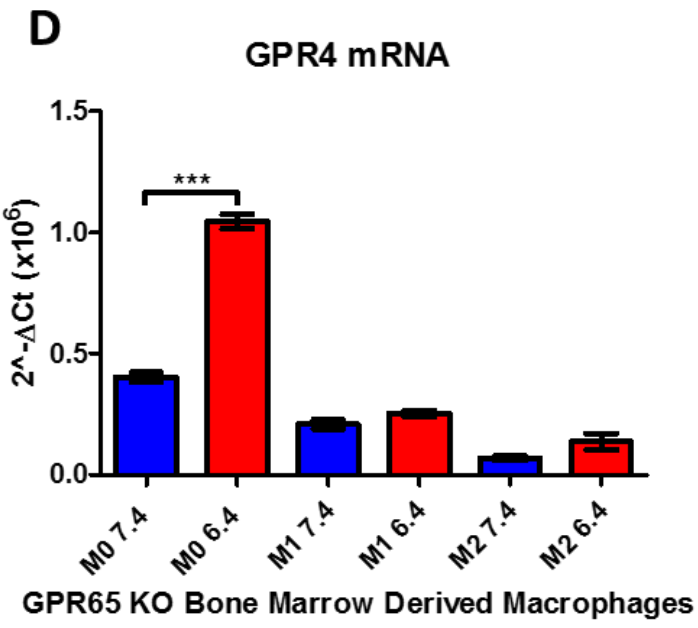
D
GPR4 mRNA
2^-ΔCt (x10^6)
1.5
1.0
0.5
0.0
***
M0 7.4
M0 6.4
M1 7.4
M1 6.4
M2 7.4
M2 6.4
GPR65 KO Bone Marrow Derived Macrophages

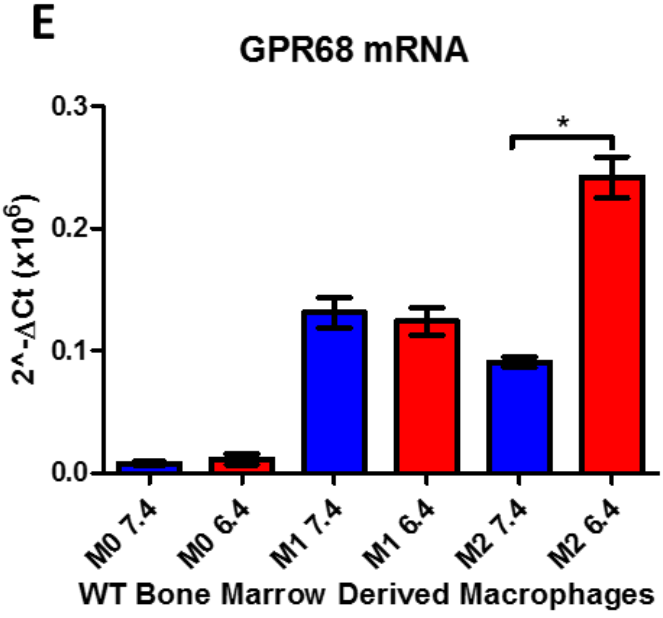
E
GPR68 mRNA
2^-ΔCt (x10^6)
0.3
0.2
0.1
0.0
*
M0 7.4
M0 6.4
M1 7.4
M1 6.4
M2 7.4
M2 6.4
WT Bone Marrow Derived Macrophages

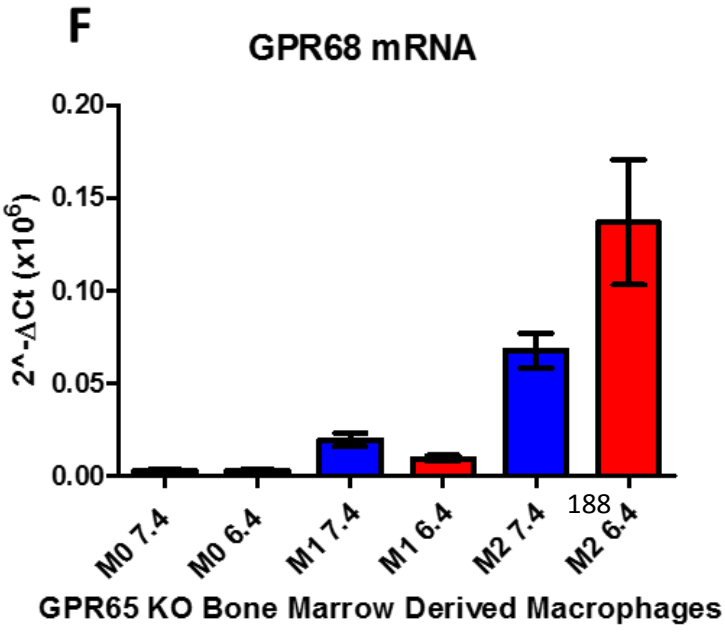
F
GPR68 mRNA
2^-ΔCt (x10^6)
0.20
0.15
0.10
0.05
0.00
M0 7.4
M0 6.4
M1 7.4
M1 6.4
M2 7.4
M2 6.4
GPR65 KO Bone Marrow Derived Macrophages

Figure 4.18: Proton-sensing GPCR family member mRNA expression in bone marrow derived macrophages. GPR65 (TDAG8) mRNA expression is altered by acidic pH in BMDMs. WT and GPR65 KO bone marrow derived macrophages (BMDMs) were polarized to M1 and M2 phenotypes. Naïve BMDMs are indicated as M0. BMDMs were treated with pH 7.4 and pH 6.4 for 5hrs. (A, C, D) representative gene expression changes from WT BMDMs and (B, D, F) for GPR65 KO BMDMs. (A-B) GPR65, (C-D) GPR4, and (E-F) GPR68 mRNA levels were assessed using qPCR. Student's *t*-test was performed between pH 7.4 vs. pH 6.4 groups within each BMDM phenotype. WT 7.4 (n=2-4), WT 6.4 (n=2-4), GPR65 KO 7.4 (n=2-4), and GPR65 KO 6.4 (n=2-4). Data representative of two to four phenotypically similar, biologically independent experiments. (*$P < 0.05$, **$P < 0.01$, *** $P< 0.001$) #= no detectable signal.

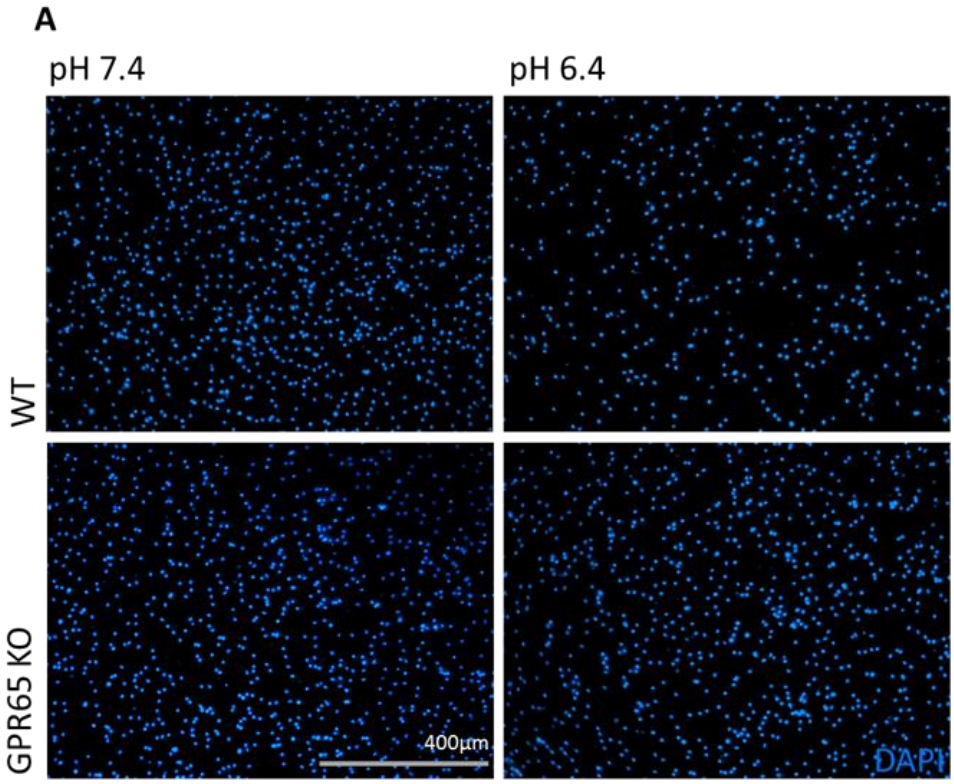
A
pH 7.4
pH 6.4
WT
GPR65 KO
400µm
DAPI

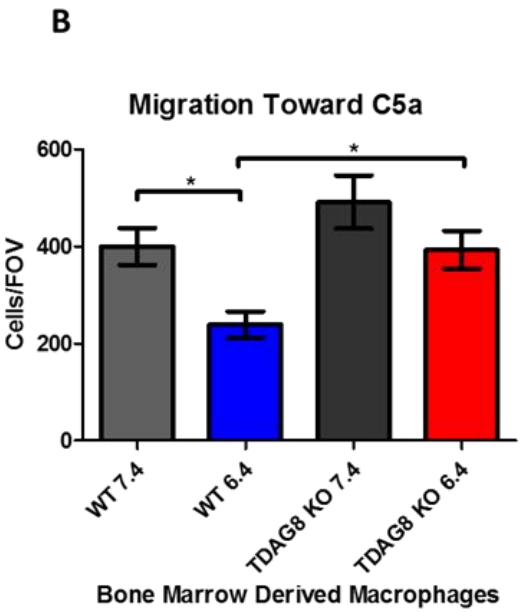
B
Migration Toward C5a
Cells/FOV
600
400
200
0
*
*
WT 7.4
WT 6.4
TDAG8 KO 7.4
TDAG8 KO 6.4
Bone Marrow Derived Macrophages

Figure 4.19: BMDM migration toward C5a chemoattractant in response to acidic pH. GPR65 (TDAG8) reduces the directional migration of BMDMs toward C5a in response to acidic pH. WT and GPR65 KO BMDMs were resuspended in pH 7.4 or 6.4 migration media and added to the upper chamber of the transwell insert. 5ng/mL of C5a was added to the lower chamber and cells were incubated for 3hrs. Cellular migration was (A) visualized and (B) counted following staining migrated cells with DAPI. One-way ANOVA followed by Tukey post-hoc was performed for statistical analysis. WT 7.4 (n=6), WT 6.4 (n=6), GPR65 KO 7.4 (n=6), and GPR65 KO 6.4 (n=6). Data from three independent experiments. Scale bar = 400μm. (*$P < 0.05$)

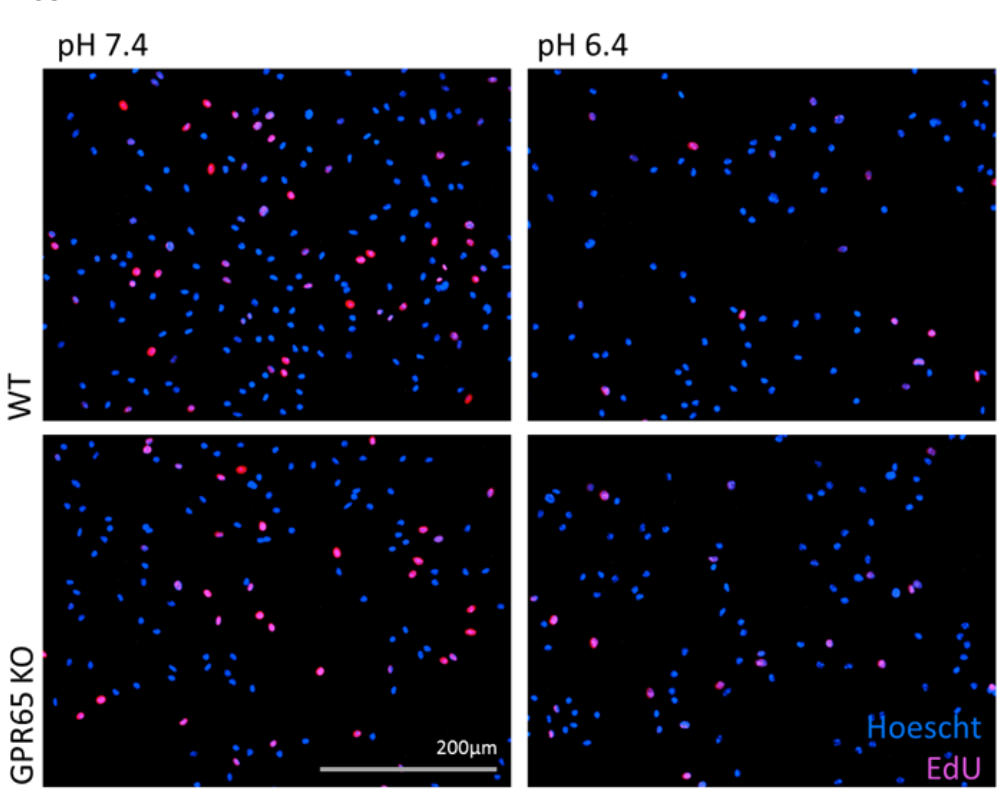
pH 7.4
pH 6.4
WT
GPR65 KO
200µm
Hoescht
EdU

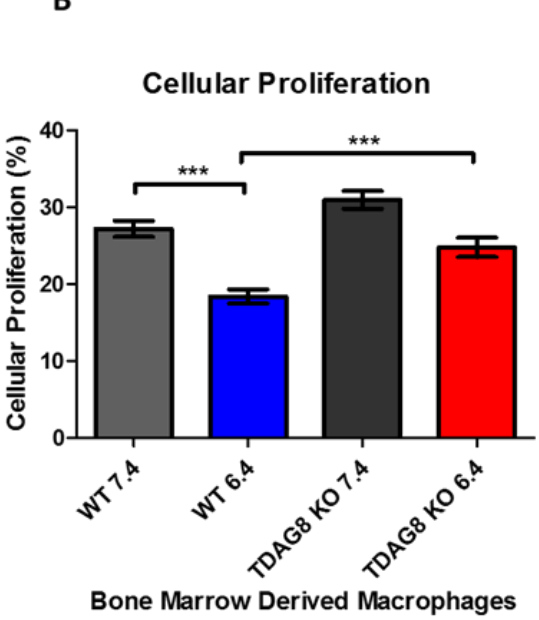
B
Cellular Proliferation
Cellular Proliferation (%)
40
30
20
10
0
***
***
WT 7.4
WT 6.4
TDAG8 KO 7.4
TDAG8 KO 6.4
Bone Marrow Derived Macrophages

Figure 4.20: BMDM proliferation in response to acidic pH. GPR65 reduced BMDM proliferation in response to acidic pH when compared to WT. (A) WT and GPR65 KO BMDMs were treated with pH stimulation media for 18hrs followed by EdU incorporation and visualization. (B) The percent of EdU positive cells were calculated. One-way ANOVA followed by Tukey post-hoc was performed for statistical analysis. WT 7.4 (n=6), WT 6.4 (n=6), GPR65 KO 7.4 (n=6), and GPR65 KO 6.4 (n=6). Data are representative from three independent experiments. Blue staining indicates nuclear staining using Hoechst dye and red signal indicates EdU signal. Scale bar = 200µm. (*** $P< 0.001$)

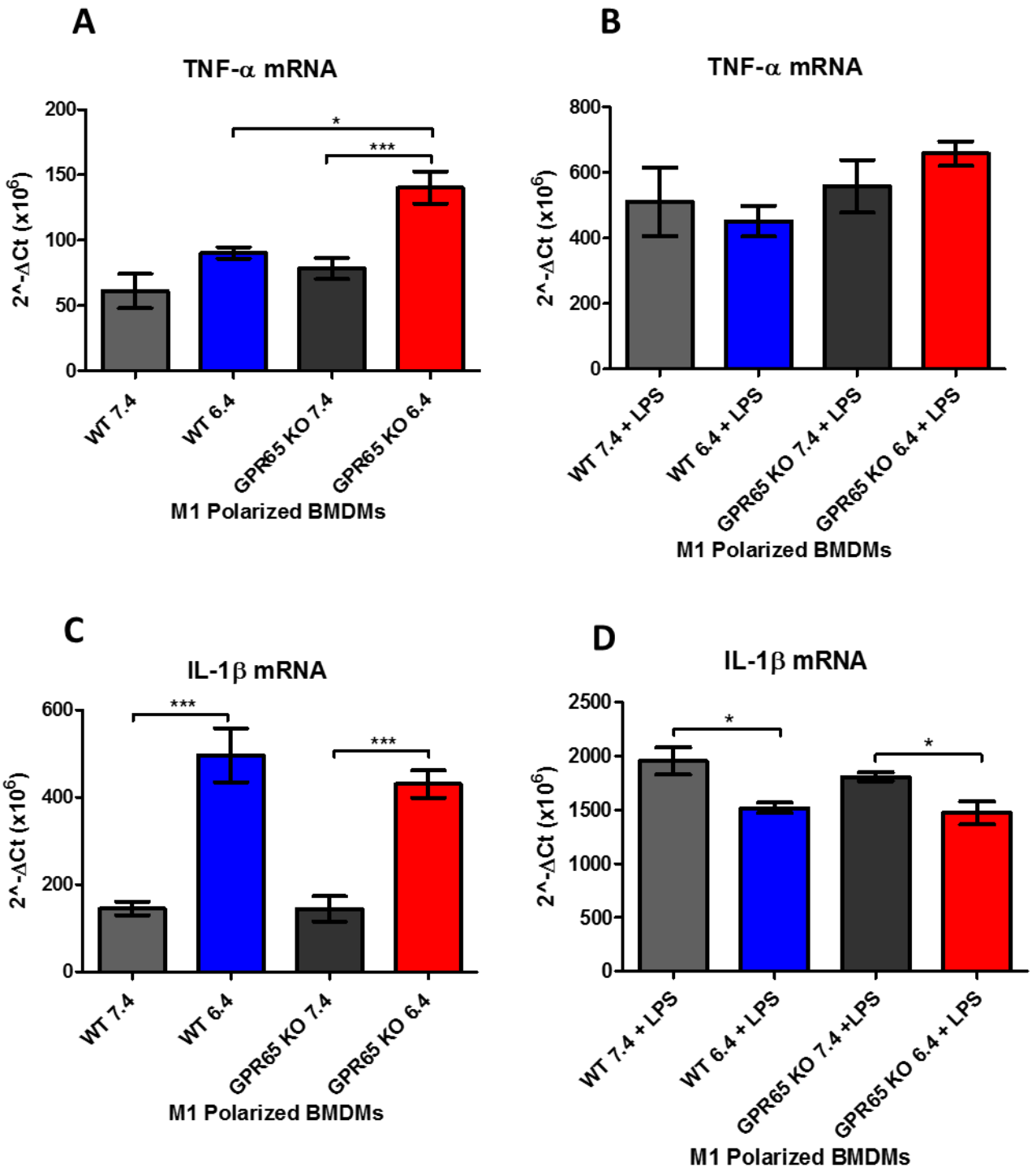
A
TNF-α mRNA
2^-ΔCt (x10^6)
200
150
100
50
0
*
***
WT 7.4
WT 6.4
GPR65 KO 7.4
GPR65 KO 6.4
M1 Polarized BMDMs
B
TNF-α mRNA
2^-ΔCt (x10^6)
800
600
400
200
0
WT 7.4 + LPS
WT 6.4 + LPS
GPR65 KO 7.4 + LPS
GPR65 KO 6.4 + LPS
M1 Polarized BMDMs
C
IL-1β mRNA
2^-ΔCt (x10^6)
600
400
200
0
***
***
WT 7.4
WT 6.4
GPR65 KO 7.4
GPR65 KO 6.4
M1 Polarized BMDMs
D
IL-1β mRNA
2^-ΔCt (x10^6)
2500
2000
1500
1000
500
0
*
*
WT 7.4 + LPS
WT 6.4 + LPS
GPR65 KO 7.4 +LPS
GPR65 KO 6.4 + LPS
M1 Polarized BMDMs

Figure 4.21: BMDM gene expression indicators of the M1 phenotype in response to acidic pH. GPR65 has moderate effects in M1 BMDMs in response to acidic pH. WT and GPR65 KO BMDMs were treated with 100ng/mL LPS and 150ng/mL mrIFNγ for 24hrs. Polarization medium was removed and pH stimulation media was added for 5hrs with and without 100ng/mL LPS. (A, B) TNF-α and IL-1β mRNA from pH stimulation only and (C, D) pH stimulation media with 100ng/mL LPS, respectively. WT 7.4 (n=4), WT 6.4 (n=4), GPR65 KO 7.4 (n=4), and GPR65 KO 6.4 (n=4). One-way ANOVA followed by Bonferroni post-hoc was performed for statistical analysis. Data representative of two biologically independent experiments. (*P < 0.05, **P < 0.01, *** P< 0.001)

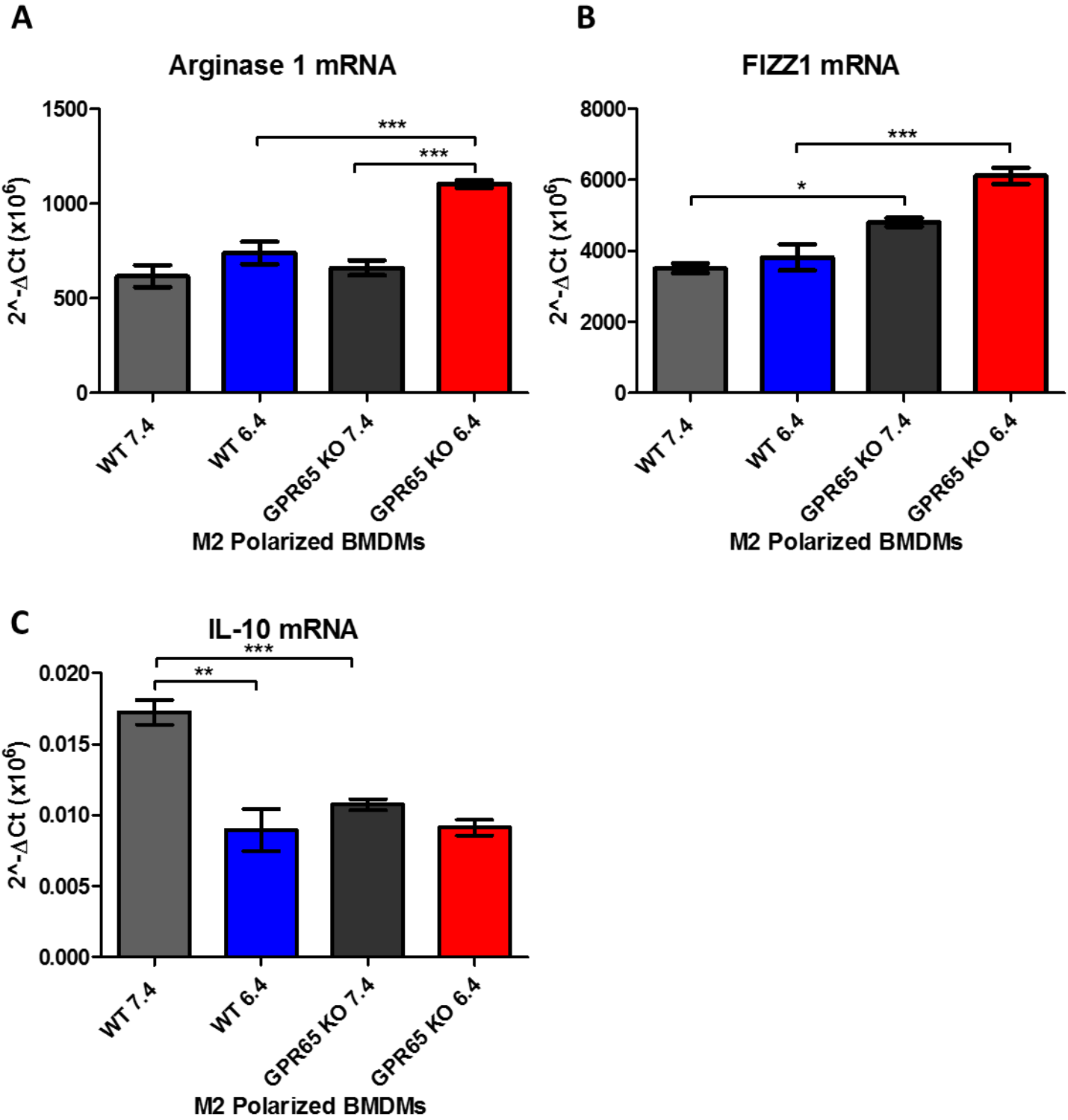
A
Arginase 1 mRNA
2^-ΔCt (x10^6)
1500
1000
500
0
***
***
WT 7.4
WT 6.4
GPR65 KO 7.4
GPR65 KO 6.4
M2 Polarized BMDMs
B
FIZZ1 mRNA
2^-ΔCt (x10^6)
8000
6000
4000
2000
0
*
***
WT 7.4
WT 6.4
GPR65 KO 7.4
GPR65 KO 6.4
M2 Polarized BMDMs
C
IL-10 mRNA
2^-ΔCt (x10^6)
0.020
0.015
0.010
0.005
0.000
**
***
WT 7.4
WT 6.4
GPR65 KO 7.4
GPR65 KO 6.4
M2 Polarized BMDMs

Figure 4.22: BMDM gene expression indicators of the M2 phenotype in response to acidic pH. GPR65 modulates M2 BMDM gene expression in response to acidic pH when compared to WT. WT and GPR65 KO BMDMs were treated with mrIL-4 at 10ng/mL for 24hrs. Polarization medium was removed and pH stimulation media was added for 5hrs. (A) arginase 1, (B) FIZZ1, and (C) IL-10 mRNA were assessed by qPCR analysis. One-way ANOVA followed by Bonferroni post-hoc was performed for statistical analysis. WT 7.4 (n=3), WT 6.4 (n=3), GPR65 KO 7.4 (n=3), and GPR65 KO 6.4 (n=3). Data representative of two biologically independent experiments. (*$P < 0.05$, **$P < 0.01$, *** $P< 0.001$)

D. Discussion

In our study, we investigated the functional role of TDAG8 in a mouse model of acute and chronic DSS-induced experimental colitis. Our results indicated that TDAG8 provides a protective role in chronic intestinal inflammation and reduces disease severity in the DSS-induced chronic colitis mouse model. TDAG8 deficiency in mice aggravated body weight loss, fecal scores, mesenteric lymph node expansion, and colon shortening in comparison to WT mice. Additionally, TDAG8 absence resulted in exacerbated histopathological features of IBD such as inflammation, edema, leukocyte infiltration, and fibrosis. Isolated lymphoid follicles (ILFs) were also expanded in TDAG8 KO colon tissues compared to WT. TDAG8 was also shown to be expressed in the colon infiltrated leukocytes and likely impedes inflammation through inhibition of immune cell inflammatory programs once activated by acidic pH in the inflamed intestinal loci. These results are supportive of previous studies demonstrating an anti-inflammatory role of TDAG8 in a diverse set of diseases, including chronic intestinal inflammation and provide new insights into the role of TDAG8 in colitis [82, 107, 109, 169, 179].

As previously described, the inflammatory loci and colonic luminal pH can be reduced during intestinal inflammation. Mesenchymal cells and leukocytes will function within these acidic, inflamed microenvironments and either potentiate or inhibit local inflammation. Wound-healing mechanisms will also occur within acidic and inflamed intestinal lesions [180]. pH-sensing is critical for cells to sense alterations in environmental proton gradients to maintain proper cellular functions. These microenvironmental conditions within inflamed tissues present a role for the pH-sensing GPCR TDAG8. TDAG8 can sense alterations in local pH by leukocytes and subsequently alter immune cell functions [108]. In our current study, we provide evidence that genetic deletion of TDAG8 exacerbates intestinal inflammation in a chemically induced colitis mouse model. Further studies are warranted to assess alterations in local interstitial pH

within inflamed lesions of the gut as well as the effects of tissue associated acidosis on both TDAG8 expression and function of immune cells within the inflamed intestinal loci.

Previous studies have characterized TDAG8 as a functional pH-sensor expressed predominately within leukocytes and can negatively regulate the inflammatory response of immune cells [82]. Furthermore, downstream effectors of the TDAG8-coupled $G\alpha_s$/cAMP have demonstrated anti-inflammatory roles in a diverse set of processes. $G\alpha_s$/cAMP/PKA/CREB pathway has been shown to reduce granulocyte, macrophage, and monocyte inflammatory programs [181]. Additionally, cAMP can reduce dendritic cell function in lymph nodes, T cell activation, and can increase T regulatory cell activity [181]. These data are consistent with reports that TDAG8 activation can inhibit inflammatory profiles in macrophages, microglia, neutrophils, and T cells. Additionally, the role of TDAG8 was investigated in immune-mediated murine disease models such as arthritis, lipopolysaccharide (LPS)-induced acute lung injury, myocardial infraction, ischemic stroke, and bacterial-induced colitis [82, 107, 109, 169, 179]. However, there are also some studies suggesting TDAG8 expression in eosinophils promotes inflammation through increasing eosinophil viability in an asthma mouse model [110]. Furthermore, recent studies found TDAG8 is a regulator for Th17 pathogenicity and increases the severity in the experimental autoimmune encephalomyelitis (EAE) mouse model as well as increases GM-CSF production in $CD4^+$ T cells [111]. Pertaining to Th17 cell pathogenicity, reports have provided evidence for both protective and pathogenic roles in the context of intestinal inflammation [6, 8, 9, 182]. In addition to these *in vitro* and *in vivo* animal studies, recent genome wide association studies (GWAS) have identified small nucleotide polymorphisms (SNPs) of TDAG8 associated with several human inflammatory-mediated disease states such as multiple sclerosis, asthma, heparin-induced thrombocytopenia,

spondyloarthritis, and IBD [168, 176]. As previously mentioned, a recent study investigated an IBD-associated TDAG8 genetic variant (I231L) within a bacteria-induced colitis mouse model and found that this TDAG8 gene variant confers reduced TDAG8 activity as well as impaired lysosomal function [169]. Our study focuses on the functional role of TDAG8 in the regulation of inflammation in a chemically induced chronic colitis mouse model and provides further evidence TDAG8 functions to inhibit inflammation in colitis. We demonstrated that TDAG8 is expressed in infiltrated leukocytes within the colon of inflamed intestinal tissues using GFP as a surrogate marker in TDAG8 KO mice. GFP-positive leukocytes were predominately macrophages, neutrophils, and lymphocytes based on cellular morphology in comparison to F4/80 and CD3 immunostaining. There is a discernable increase in GFP positive leukocytes in the DSS treated mouse colon tissues compared to the untreated tissues indicating TDAG8 expression is increased in inflamed tissues compared to non-inflamed intestinal tissues. We then assessed TDAG8 gene expression in human colitis and Crohn's intestinal lesions compared to non-inflamed intestinal tissues. We observed that TDAG8 is increased by more than 4-fold in inflamed intestinal tissues compared to control. It is likely the increased expression of TDAG8 in IBD intestinal samples is due to the increase of infiltrated leukocytes, which have high endogenous TDAG8 expression.

We also found that pathological fibrosis was increased in TDAG8 KO-DSS mice compared to WT-DSS mice. Fibrosis is a serious consequence of recurrent intestinal inflammation and can lead to complications such as intestinal strictures and obstruction [29, 183, 184]. Collagen can be produced by several cellular constituents within the intestinal tissues. Some such cells include fibroblasts, sub-epithelial myofibroblasts, smooth muscle cells, and pericytes. Additionally, fibroblasts, smooth muscle cells, fibrocytes, endothelial cells, pericytes

can undergo epithelial/endothelial- mesenchymal transition into myofibroblasts for wound healing functions [185]. Myofibroblasts are described as a major contributor of pathological extracellular matrix deposition within the inflamed intestine [186]. As such, we quantified the number of SMA^+ myofibroblasts in the mucosa and observed TDAG8 KO mice had more myofibroblasts than WT mice, supporting the observed increased fibrotic deposition in the DSS-treated TDAG8 KO colon. It remains to be determined how TDAG8 regulates fibrosis in the chronic colitis model. Interestingly, however, a recent study demonstrates that TDAG8 regulates macrophage CCL20 expression, γδT cell infiltration, and fibrosis in a myocardial infarction mouse model [107].

We next investigated the pH-sensing GPCR expression profiles, G-protein activation status, and inflammatory programs in mouse bone marrow derived macrophage. Furthermore, we assessed the expression and G-protein activation status in immune cell populations involved in intestinal inflammation such as T cells, dendritic cells, and macrophages. Gαs signaling has been associated with impeded inflammatory programs in a diverse range of immune cell populations of which GPR65 is highly expressed. Our results show that GPR65 is highly expressed in mouse thymocytes and bone marrow derived macrophages but is moderately expressed in bone marrow derived dendritic cells. As mentioned above, cAMP has been shown to negatively regulate macrophage, dendritic cell, and T cell activation. Furthermore, inhibition of cAMP degradation is a current therapeutic explorative avenue in IBD [187]. We showed that GPR65 couples to Gαs and is responsible for acidosis-induced Gαs/cAMP/CREB-ATF-1 pathway signaling in T-cells, macrophages, and dendritic cells through the assessment of CREB/ATF1 phosphorylation. Genetic deletion of GPR65 blunted the acidosis-induced phosphorylation of CREB and ATF1. These results suggest GPR65 could exert anti-inflammatory functions in these immune cell types

in response to acidic pH. Finally, GPR65 activation moderately reduced TNF-α expression in classically activated mouse bone marrow derived macrophages, but not IL-1β. Furthermore, GPR65 increased M2 activation markers such as Arginase 1 and FIZZ1 in alternatively activated macrophages. As heightened numbers of F4/80+ macrophages were observed in the colon of GPR65 KO-DSS mice when compared to WT-DSS mice, the phenotypes of these macrophages have yet to be explored in the regulation of intestinal inflammation.

Altogether, our results provide further support for an anti-inflammatory role of TDAG8 in colitis and present TDAG8 as a potential target for therapeutic intervention. Currently, IBD treatment options are limited and predominately consist of steroids, anti-TNFα monoclonal antibodies, and anti-integrin monoclonal antibodies. The TDAG8 agonist BTB09089 has been developed and recently investigated for anti-inflammatory properties. BTB09089 was shown to activate TDAG8 *in vitro* but provided weak activity *in vivo* according to one study [105]. An additional study has shown *in vivo* efficacy of BTB09089 using an ischemic stroke murine disease model [188]. Further studies must be done to develop highly efficacious TDAG8 agonists for potential use as IBD therapeutics.

Chapter V: The role of GPR132 in DSS-induced mouse colitis

A. Summary

GPR132, also known as G2 accumulation (G2A) is highly and broadly expressed on immune cells such as macrophages, T cells, B cells, and neutrophils. Numerous studies provide pro- and anti-inflammatory roles for GPR132 in immune cell inflammatory programs suggesting cell type and biological context a key determinate in GPR132 function. GPR132 is a controversial member of the proton-sensing GPCR family of receptors owing to GPR132 receptor promiscuity. GPR132 has been shown to be activated by protonation in an acidic environment, however, in addition to protons, GPR132 can also be activated by lactate and several bioactive molecules such as lysophosphatidylcholine (LPC), 9-hydroxyoctadecadienoic acid (9-HODE), and recently N-acyl-3-hydroxy-palmitoyl glycine (commendamide) [83, 86, 88-90, 92, 189, 190]. These proposed endogenous ligands are readily available in the mucosa of intestinal tissues and some bioactive molecules have been implicated in the pathology of unresolved intestinal inflammation. Therefore, we investigated the functional role of GPR132 in acute and chronic intestinal inflammation using the DSS-induced colitis mouse model. We present a proposed anti-inflammatory role of GPR132 in DSS-induced colitis mouse model. GPR132 KO mice backcrossed twelve generations (GPR132 KO N12) and GPR132 KO mice backcrossed fourteen generations (GPR132 N14 KO) into the C57BL/6 background were compared to wild-type (WT) mice during chronic intestinal inflammation. GPR132 N12 KO DSS-treated mice displayed marked sensitivity to the DSS chemical insult where clinical phenotypes, macroscopic disease indicators, and histopathology were more severe when compared to WT DSS-treated mice. The GPR132 N14 KO mice, however, showed only a mild

increase in clinical severity when compared to WT DSS-treated mice. These results indicate GPR132 reduces intestinal inflammation, however, these data necessitate further experimentation to elucidate the functional role of GPR132 in intestinal inflammation.

B. Introduction

Ulcerative colitis and Crohn's disease is a mucosal disease associated with an uncontrolled and recurring inflammatory response in the mucosal tissues of the intestine [25, 32]. Normal intestinal homeostasis is orchastrated through intricate interations between the immune system, intestinal flora, and the intestinal epithelium. Numerous studies have suggested that a damaged epithelium is either the cause or consequence of intestinal inflammation [21, 26, 191, 192]. Lyso-phospholipids and linoleic acid metabolites such as lysophosphatidylcholine (LPC) and 9-hydroxyoctadecadienoic acid (9-HODE) have been implicated in the regulation of intestinal epithelial homeostasis. LPC levels have shown to increase in IBD by release of injured intestinal epithelium and apoptotic cells. LPC has been proposed to function as a "find me" signal for the clearance of apoptotic cells by phagocytes for the subsequent resolution of inflammation in the inflammatory loci [98]. Further studies have shown that the inflammatory loci are characteristically acidic owing, in part, to the metabolic production of protons by leukocyte infiltrates [63]. As described above, LPC, 9-HODE, and protons have been proposed as ligands for GPR132 and have modulated immune cell functions. Additionally, lactate and N-acyl-3-hydroxy-palmitoyl glycine (commendamide) have been proposed to work through GPR132 and are both present in gastrointestinal tissues [89].

GPR132 was orginally discovered as a target gene of BCR-ABL tyrosine kinase in murine B Lymphoid progenitor cells [84]. This receptor is highly expressed in leukocytes (macrophages, dendritic cells, neutrophils, T cells, B cells, and mast cells) and was originally

discovered as a GPCR induced from cell stress or DNA damage in B and T lymphocytes [84]. Several studies have characterized the activation of GPR132 and G protein signalling. The initial studies of GPR132 supported GPR132 as a tumor supressor through the reduction of cell cycle progression in myelogenous leukemia and acute lymphocytic leukemia. Overexpression of GPR132 in BCR-ABL cells reduced B lymphoid cell expansion *in vitro* by cell accumulating in the G2/M phase [84]. With GPR132 having high expression in immature T and B lymphocyte progenitors and thymocytes in all stages of intrathymic maturation, it seems likely that GPR132 would have central roles in immunity and inflammation. Indeed, further studies using GPR132 knockout mice demonstrated GPR132-genetic deletion resulted in late onset autoimmune disease characterized by hyperproliferation of immune cells [85]. Additional studies demonstrated GPR132 was involved in reduced suseptability to atherosclerosis in mice [95].

Provided the endogenous ligands of GPR132 exist in the mucosa of the intestine and are implicated in the pathological consequence of unresolved intestinal inflammation, we sought to investigate the functional role of GPR132 in acute and chronic intestinal inflammation. We utilized the dextran sulfate sodium (DSS)- induced colitis mouse model where WT and GPR132 N12 knockout (KO) mice were provided 3% DSS for acute or chronic time points. No significant difference was observed between WT and GPR132 N12 KO mice during the acute DSS-induced colitis model. However, during the chronic DSS-induced colitis model, GPR132 N12 KO mice provided 3% DSS were highly sensitive to the DSS chemical insult and resulted in more than 70% of mice reaching the humane endpoint before the final day of the experimental time course. Mouse body weight loss and fecal blood and diarrhea scores were measured and GPR132 N12 KO DSS-treated mice displayed higher clinical severity scores then the WT DSS-treated mice. Histopathological analysis of the mice following the DSS experimental time course revealed

elevated scores of severity for GPR132 N12 KO DSS-treated mice when compared to WT DSS-treated mice. These results suggested GPR132 functioned as a regulator of intestinal inflammation.

GPR132 N12 KO mice were backcrossed two additional generations to develop GPR132 N14 KO mice. Interestingly, when GPR132 N14 KO mice were initiated on the chronic DSS-induced colitis mouse model, the severity observed from GPR132 N12 KO mice were markedly reduced. GPR132 N14 KO DSS-treated mice body weight loss was assessed and was similar as WT DSS-treated mice. However, fecal blood and diarrhea scores were still elevated when compared to WT-DSS mice. These results suggest differences in the genetic background between GPR132 N12 KO and GPR132 N14 KO mice may contribute to the observed phenotype in either mouse generation and further experimentation is needed to elucidate the functional role and mechanism of GPR132 in intestinal inflammation.

C. Results

C.1 The role of GPR132 in acute DSS-induced chemical colitis.

We assessed the role of GPR132 in the acute DSS-induced chemical colitis mouse model. WT and GPR132 KO N12 mice were administered 3% DSS into the drinking water for the development of acute intestinal inflammation for seven days. To assess the disease severity of mice, clinical and macroscopic disease indicators were measured. Mouse body weight loss was measured from day of initial DSS administration until the completion of the experimental time course. In addition, fecal blood and diarrhea scores were assessed. There were no discernable differences between WT and GPR132 KO N12 DSS-induced mice in terms of body weight loss and fecal scores (Figure 5.1). Upon completion of the seven days of DSS administration the

mesenteric lymph node volume was measured, and the colon length was assessed. DSS-induced mice displayed expanded mesenteric lymph nodes when compared to untreated mice (~20 mm^3 vs. ~8 mm^3), respectively (Figure 5.1). Additionally, colon length was shortened in mice provided DSS when compared to untreated mice (~4.5cm vs. ~7cm), respectively (Figure 5.1). However, there was no significant differences between WT-DSS and GPR132 KO N12-DSS groups for both mesenteric lymph node volume and colon length (Figure 5.1).

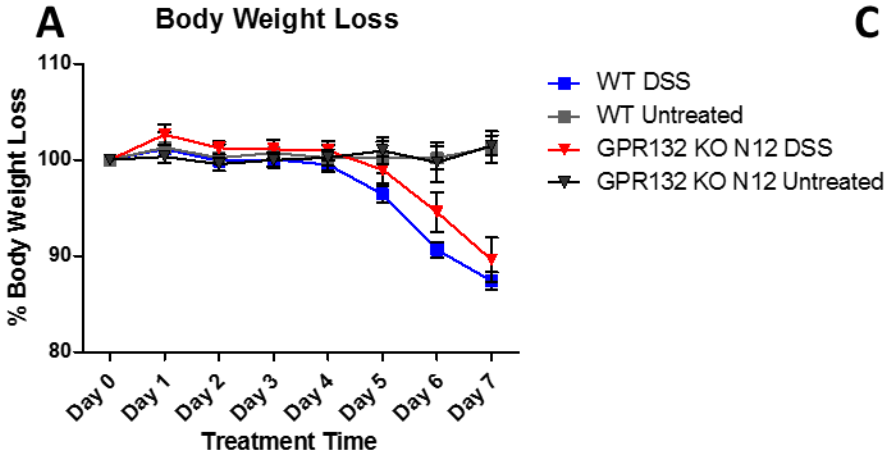
A
Body Weight Loss
% Body Weight Loss
110
100
90
80
Day 0
Day 1
Day 2
Day 3
Day 4
Day 5
Day 6
Day 7
Treatment Time
WT DSS
WT Untreated
GPR132 KO N12 DSS
GPR132 KO N12 Untreated

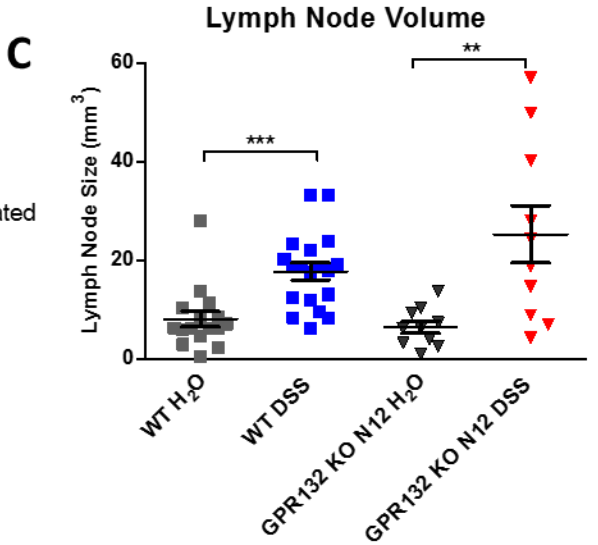
C
Lymph Node Volume
Lymph Node Size (mm3)
60
40
20
0
***
**
WT H2O
WT DSS
GPR132 KO N12 H2O
GPR132 KO N12 DSS

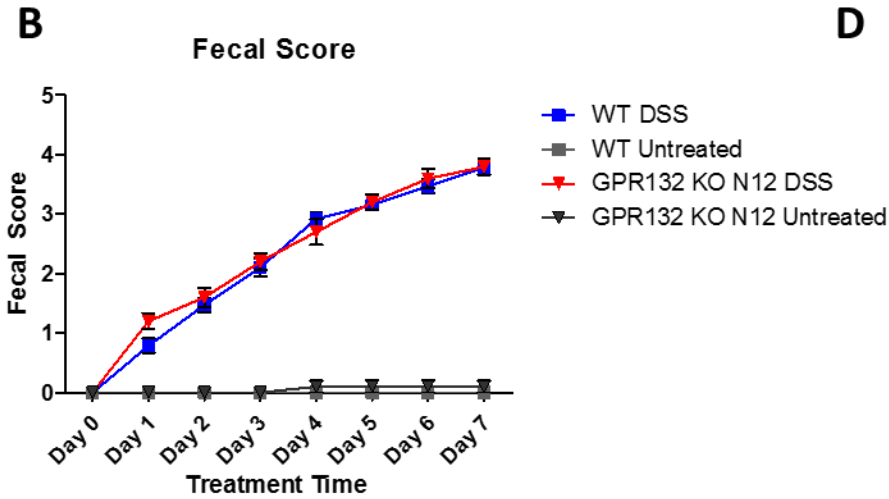
B
Fecal Score
Fecal Score
5
4
3
2
1
0
Day 0
Day 1
Day 2
Day 3
Day 4
Day 5
Day 6
Day 7
Treatment Time
WT DSS
WT Untreated
GPR132 KO N12 DSS
GPR132 KO N12 Untreated

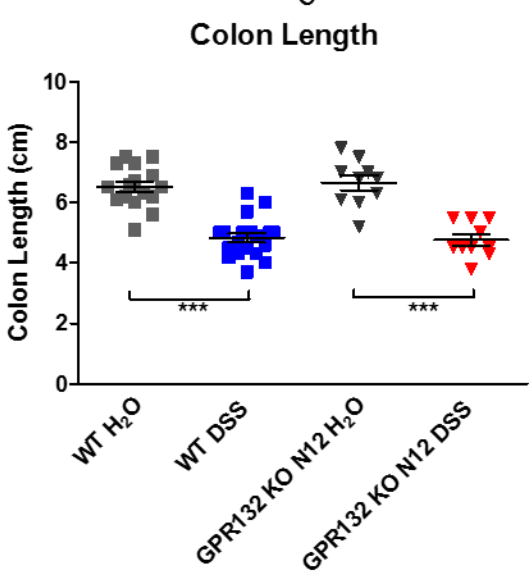
D
Colon Length
Colon Length (cm)
10
8
6
4
2
0
***
***
WT H2O
WT DSS
GPR132 KO N12 H2O
GPR132 KO N12 DSS

Figure 5.1: Clinical parameters and macroscopic disease indicators. The effects of GPR132 deletion was assessed in the acute DSS-induced colitis mouse model. GPR132 deletion had no effects on (A) body weight loss, (B) fecal score, (C) colon shortening, and (D) mesenteric lymph node enlargement. WT-control (n=16), WT-DSS (n=19), GPR132 KO N12-control (n=10), and GPR132 KO N12-DSS (n=10) mice. WT mice used in this analysis were randomly assigned for comparison with G2A KO N12 mice and were duplicated from analysis used for GPR4 KO and GPR65 KO acute DSS experiment groups. Each dot represents the data from an individual mouse. Data are presented as mean ± SEM and was analyzed for statistical significance using the one-way ANOVA followed by Bonferroni post hoc. (**$P < 0.01$, *** $P< 0.001$).

C.2 The role of GPR132 in chronic DSS-induced intestinal inflammation

In addition to investigating the role of GPR132 in acute intestinal inflammation, GPR132 deficiency was investigated in the chronic DSS-induced colitis mouse model. During the chronic DSS-induced colitis experimental time course the body condition score was measured for WT and GPR132 KO mice. More than 70% of GPR132 KO N12 mice reached human endpoint parameters when compared to 10% WT mice and were humanely euthanized for macroscopic disease parameter assessment (Figure 5.2). Body weight loss and fecal scores were also measured daily. GPR132 KO N12 DSS-induced mice displayed heightened body weight loss and fecal blood scores compared to WT-DSS mice. Furthermore, macroscopic disease indicators were measured such as mesenteric lymph node volume and colon length. Interestingly, there were no differences in mesenteric lymph node volume between WT-DSS and GPR132 KO N12 DSS groups (Figure 5.3). The colon length, however, was significantly reduced in GPR132 KO N12 DSS mice compared to WT DSS mice (Figure 5.3).

Histopathological parameters such as leukocyte infiltration, edema, crypt damage, architectural distortion, and total area of inflammation were assessed between WT and GPR132 KO N12 mice. Histopathological scores were most severe in the distal colon followed by the middle colon and proximal colon segments, respectively. When GPR132 KO N12-DSS mice were assessed the score of severity were significantly higher in each colon segment compared to WT-DSS mice (Figure 5.4). Pathological fibrosis has been described in chronic DSS-induced colitis mouse models. We investigated the degree of fibrosis in the colon of WT and GPR132 KO N12 mice. WT untreated mice were used as a baseline for scoring. The distal colon revealed the highest degree of fibrosis followed by the middle and proximal segments. GPR132 KO N12-

DSS obtained higher scores of severity then WT DSS mice in the distal and middle colon segments (Figure 5.5).

GPR132 KO N12 mice were backcrossed with C57Bl/6J mice two additional generations resulting in GPR132 KO N14 mice. The GPR132 KO N14 mice were initiated on the chronic DSS-induced colitis mouse model to corroborate previous experiments with the GPR132 KO N12 generation. GPR132 KO N14 DSS-induced colitis mouse body weight loss and fecal blood score were measured daily. The GPR132 KO N14 chronic DSS-induced colitis results indicate a mild phenotype when compared to previous GPR132 KO N12-dependent phenotypic sensitivity to the DSS chemical insult. GPR132 KO N14 DSS-induced mice showed no significant differences in body weight loss when compared to WT-DSS mice. However, fecal blood and diarrhea scores were more severe in GPR132 KO N14 mice when compared to WT-DSS mice. No significant differences could be observed between WT-DSS and GPR132 KO N14-DSS mice with respect to mesenteric lymph node enlargement or colon shortening. These results suggest the genetic background between the N12 and N14 generation contributes to differing degrees of sensitivity to the DSS chemical insult.

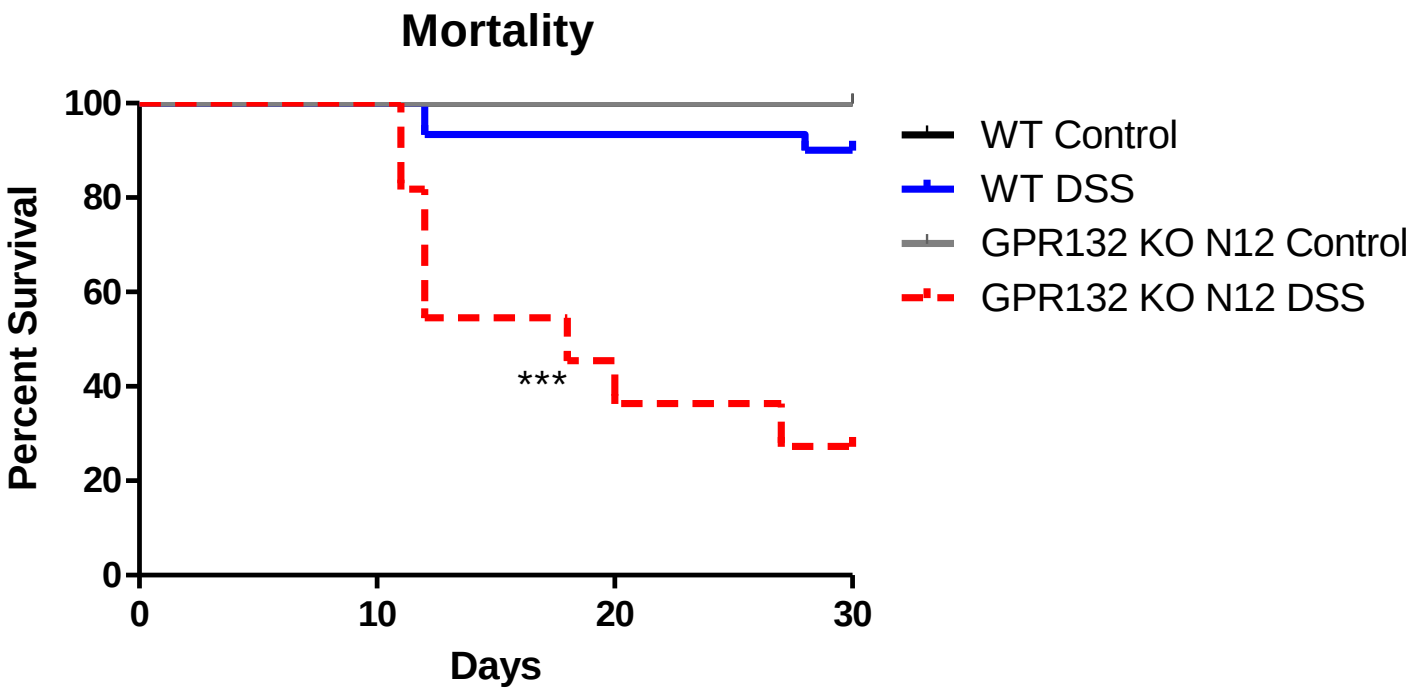
Mortality
Percent Survival
100
80
60
40
20
0
0
10
20
30
Days
***
WT Control
WT DSS
GPR132 KO N12 Control
GPR132 KO N12 DSS

Figure 5.2: Mortality events in the chronic DSS-induced mouse colitis model. GPR132 KO N12 DSS-induced mice displayed ~30% survival compared to ~90% survival of WT DSS-induced mice. Data are presented as mean ± SEM. WT-Control (n=20), WT-DSS (n=30), GPR132 KO N12 control (n=11), and GPR132 KO N12 DSS (n=11) tissues were used for analysis. WT mice used in this analysis are the sum of all mice included for comparison with GPR4 KO and GPR65 KO chronic DSS experimental groups. Statistical analysis was performed using the two-way ANOVA followed by Bonferroni post hoc. (*** $P< 0.001$)

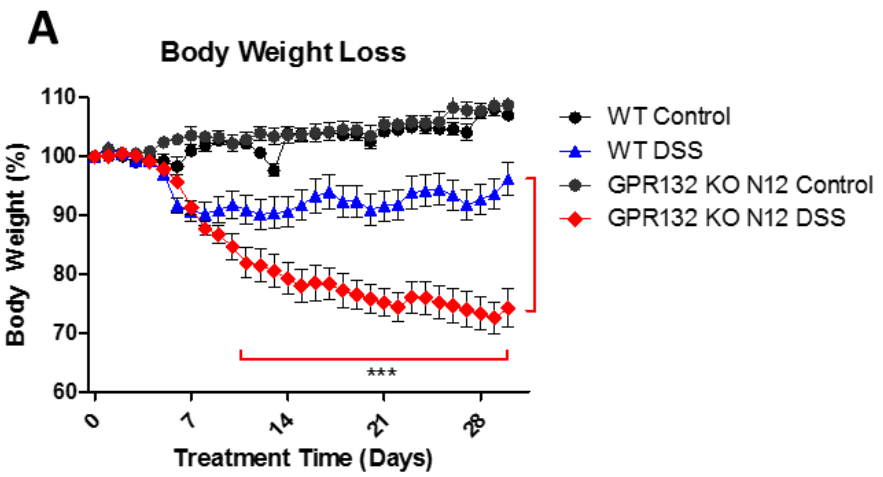
A
Body Weight Loss
Body Weight (%)
110
100
90
80
70
60
0
7
14
21
28
Treatment Time (Days)
***
WT Control
WT DSS
GPR132 KO N12 Control
GPR132 KO N12 DSS

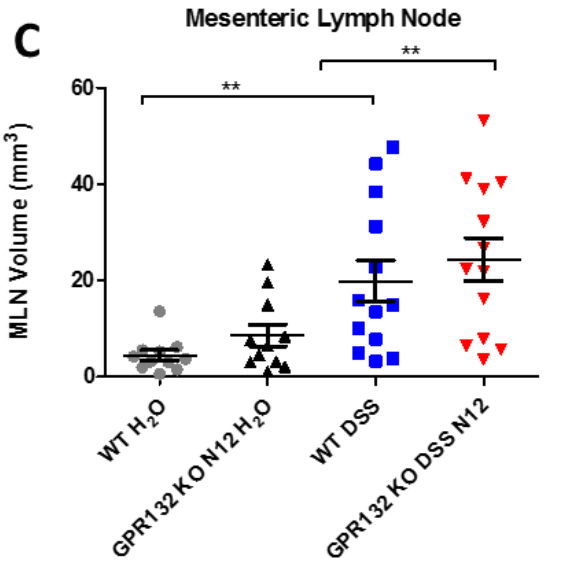
C
Mesenteric Lymph Node
MLN Volume (mm3)
60
40
20
0
**
**
WT H2O
GPR132 KO N12 H2O
WT DSS
GPR132 KO DSS N12

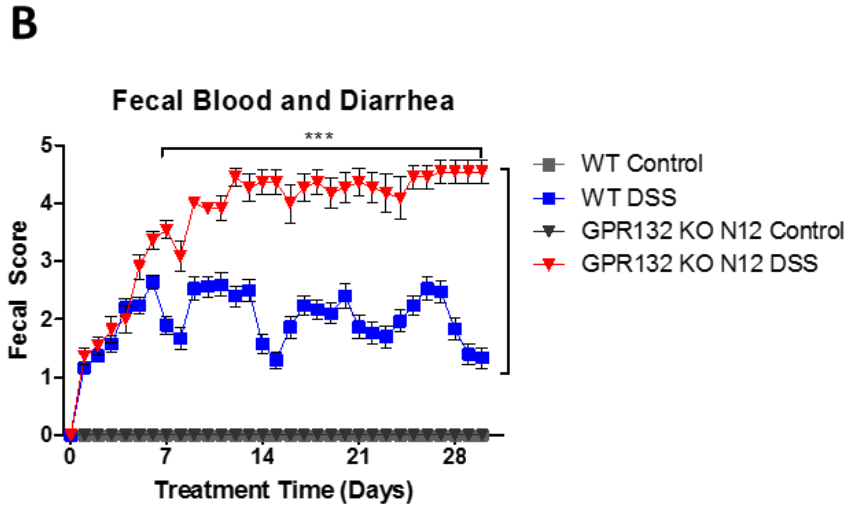
B
Fecal Blood and Diarrhea
Fecal Score
5
4
3
2
1
0
0
7
14
21
28
Treatment Time (Days)
***
WT Control
WT DSS
GPR132 KO N12 Control
GPR132 KO N12 DSS

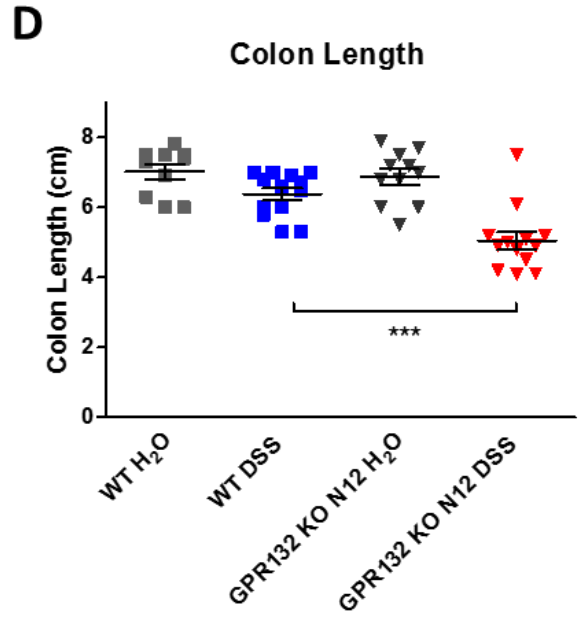
D
Colon Length
Colon Length (cm)
8
6
4
2
0
***
WT H2O
WT DSS
GPR132 KO N12 H2O
GPR132 KO N12 DSS

Figure 5.3: Clinical parameters and macroscopic disease indicators for GPR132 KO N12 mice in the chronic DSS-induced colitis mouse model. The extent of chronic DSS-induced colitis in mice was assessed. (A) body weight, (B) fecal score, (C) mesenteric lymph node volume, and (D) colon length were measured as parameters to gauge the disease severity in mice. We observed GPR132 KO N12-DSS mice had heightened disease severity when compared to WT-DSS mice. WT-control (n=11), WT-DSS (n=13), GPR132 KO N12-control (n=11), and GPR132 KO N12-DSS (n=13) mice. WT mice used in this analysis were randomly assigned for comparison with GPR132 KO N12 mice and were duplicated from analysis used for GPR4 KO and GPR65 KO chronic DSS experiment groups. Each dot represents the data from an individual mouse. Data are presented as mean ± SEM and was analyzed for statistical significance using the two-way or one-way ANOVA followed by Bonferroni post hoc. (*$P < 0.05$, **$P < 0.01$, *** $P< 0.001$).

A

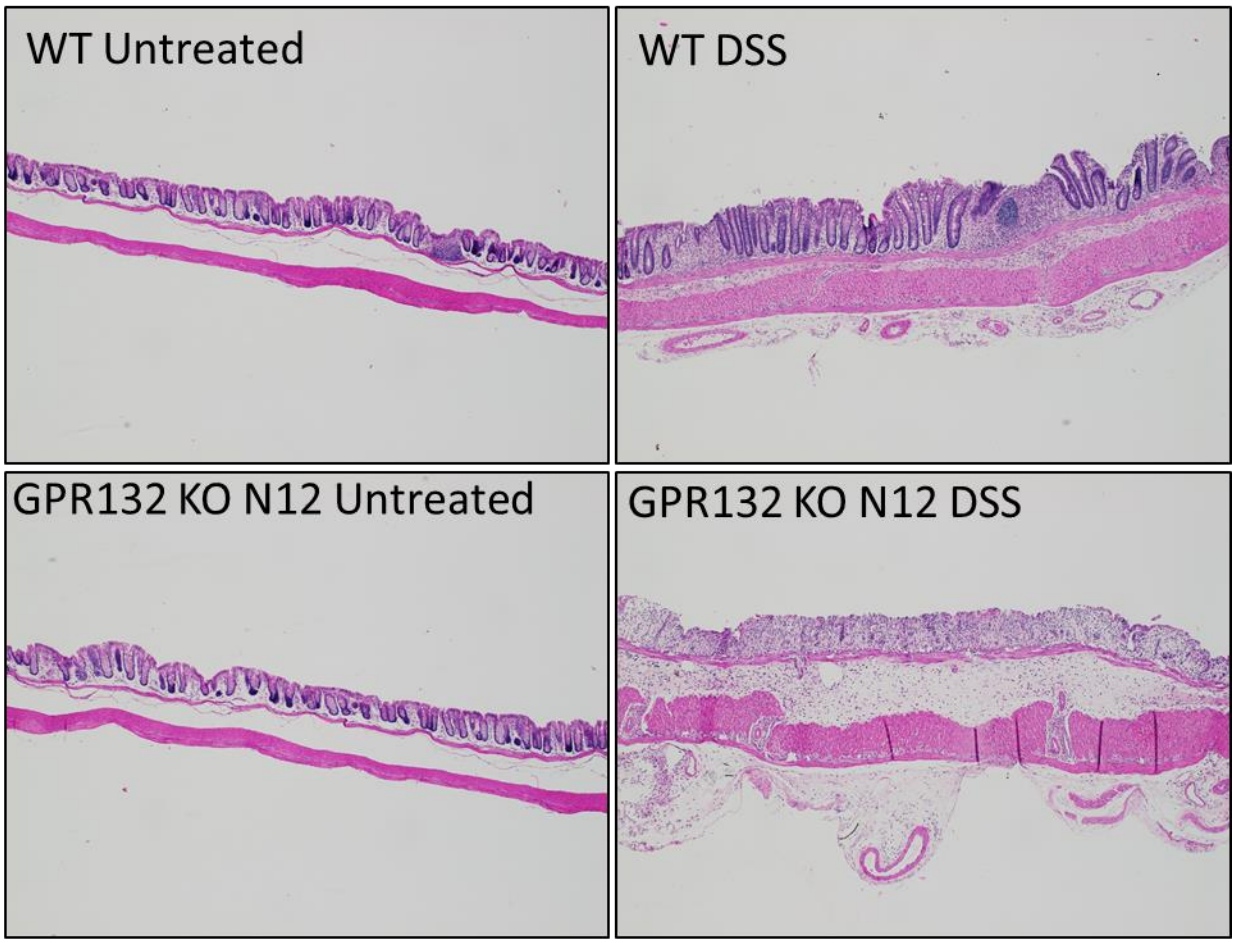
WT Untreated
WT DSS
GPR132 KO N12 Untreated
GPR132 KO N12 DSS

B

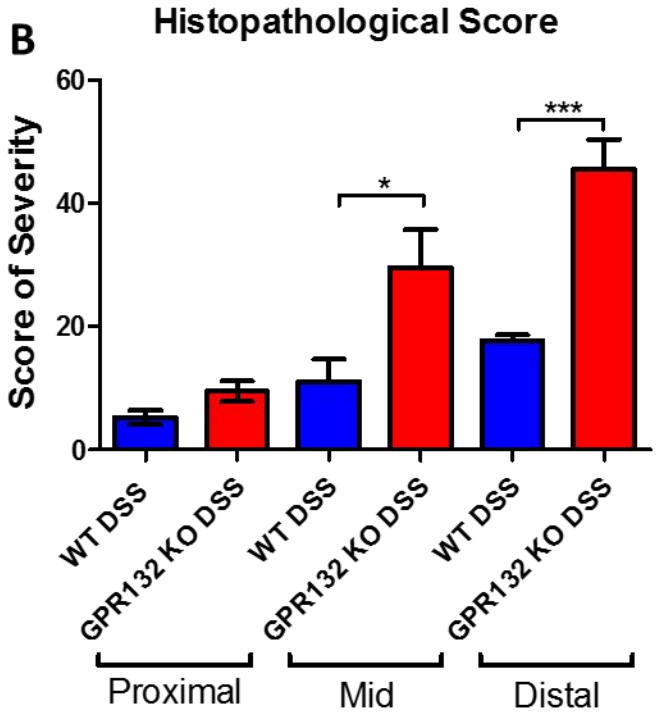
Histopathological Score
Score of Severity
60
40
20
0
*
***
WT DSS
GPR132 KO DSS
WT DSS
GPR132 KO DSS
WT DSS
GPR132 KO DSS
Proximal
Mid
Distal

Figure 5.4: Histopathological analysis of colon tissues. Characteristic histopathological features of colitis were assessed to further characterize the degree of intestinal inflammation. GPR132 KO N12-DSS mice presented elevated disease parameters compared to WT-DSS mice. Representative H&E pictures were taken for (A) WT-control, (B) WT-DSS, (C) GPR132 KO N12 control, and (D) G2A KO N12-DSS mice. Graphical representation of (E) histopathological parameters. WT-control (n=10), WT-DSS (n=10), and GPR132 KO N12-DSS (n=10). WT mice used in this analysis were randomly assigned for comparison with GPR132 KO N12 mice and were duplicated from analysis used for GPR4 KO and GPR65 KO chronic DSS experiment groups. Data are presented as mean ± SEM and was analyzed for statistical significance using the one-way ANOVA followed by Bonferroni post hoc. (*$P < 0.05$, *** $P< 0.001$).

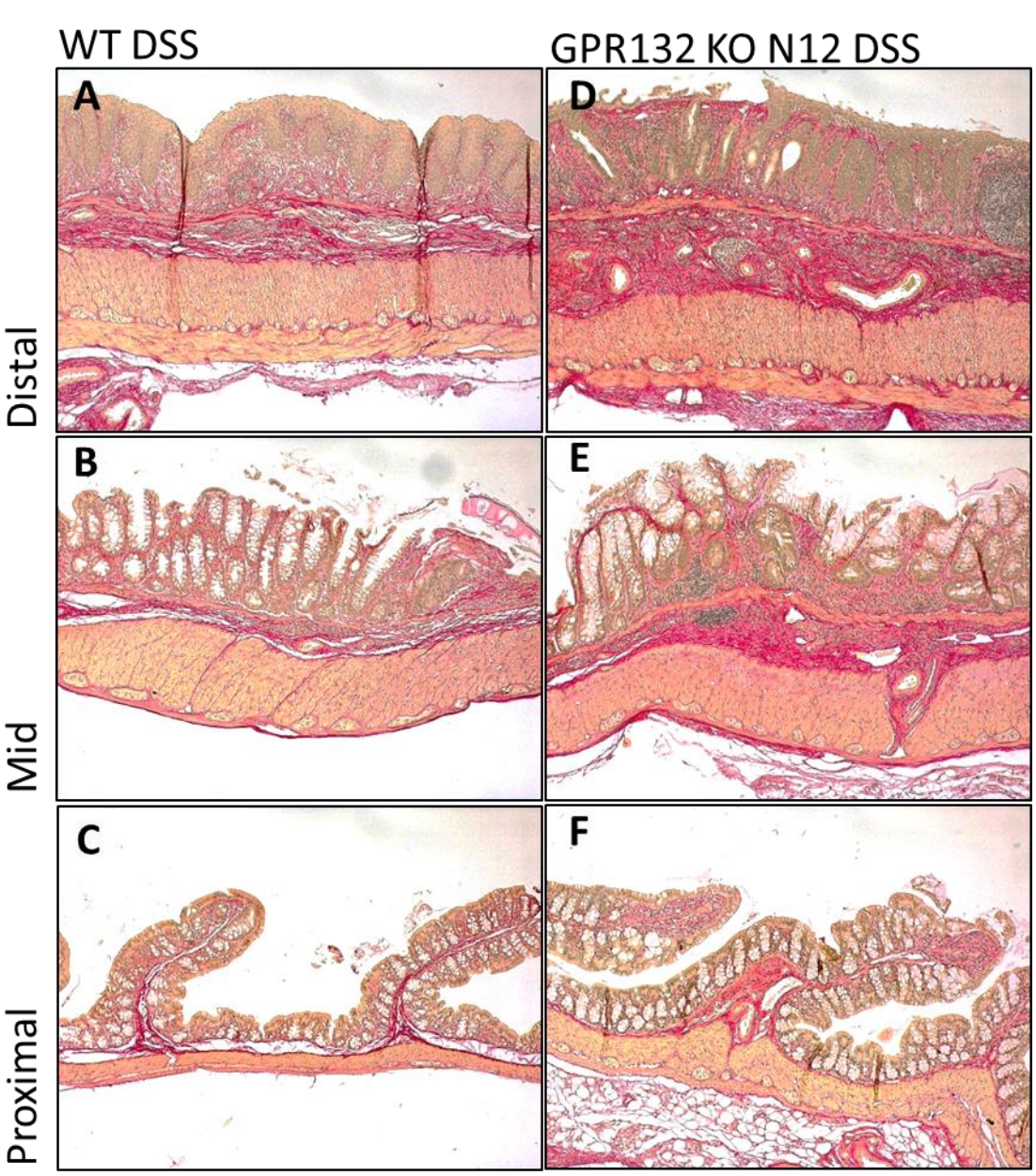
WT DSS
GPR132 KO N12 DSS
A
D
B
E
C
F
Distal
Mid
Proximal

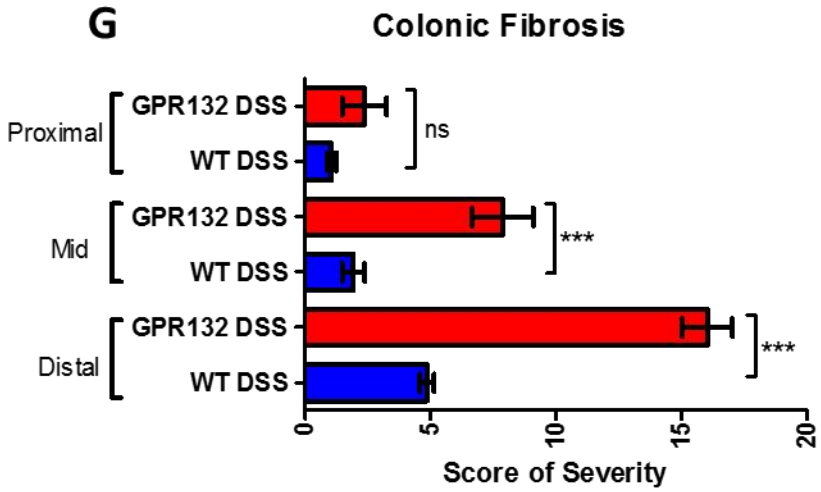
G
Colonic Fibrosis
Proximal
GPR132 DSS
WT DSS
ns
Mid
GPR132 DSS
WT DSS
***
Distal
GPR132 DSS
WT DSS
***
0
5
10
15
20
Score of Severity

Figure 5.5. **Pathological fibrosis quantification of colon tissues**. Colonic fibrosis was assessed to further characterize the degree of inflammation-association intestinal complications. GPR132 KO N12-DSS mice presented elevated fibrosis scores when compared to WT-DSS mice. Representative picrosirius red pictures were taken for (A-C) WT-DSS and (D-F) GPR132 KO N12 DSS-mice from the distal, middle, and proximal colon segments. Graphical representation of (G) fibrosis score. WT-control (n=10), WT-DSS (n=10), GPR132 KO N12-control (n=11), and GPR132 KO N12-DSS (n=9). WT mice used in this analysis were randomly assigned for comparison with GPR132 KO N12 mice and were duplicated from analysis used for GPR4 KO and GPR65 KO chronic DSS experiment groups. Data are presented as mean ± SEM and was analyzed for statistical significance using the student's *t*-test between WT-DSS and GPR132 KO N12 DSS groups. (*** $P < 0.001$).

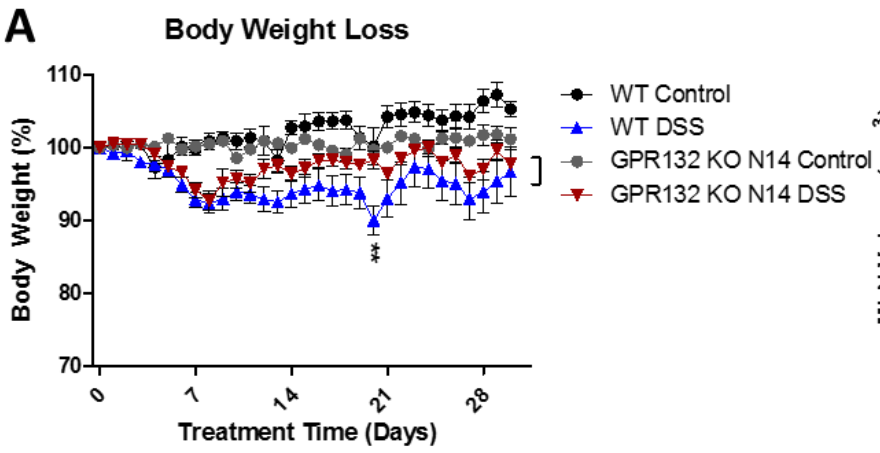
A
Body Weight Loss
Body Weight (%)
Treatment Time (Days)
WT Control
WT DSS
GPR132 KO N14 Control
GPR132 KO N14 DSS

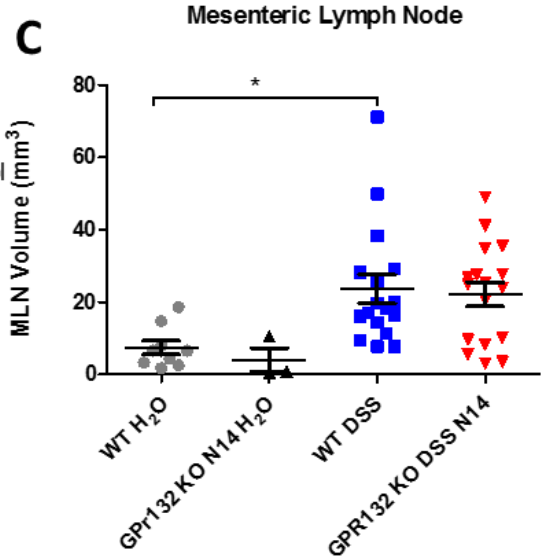
C
Mesenteric Lymph Node
MLN Volume (mm3)
WT H2O
GPr132 KO N14 H2O
WT DSS
GPR132 KO DSS N14

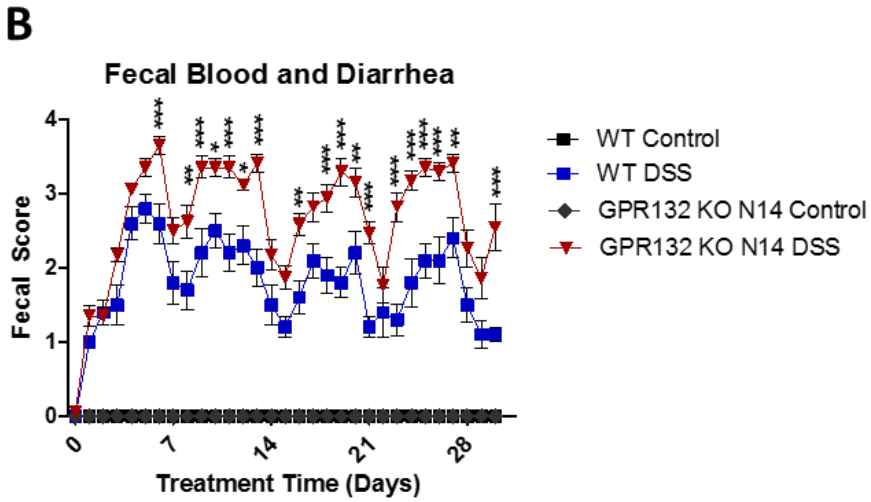
B
Fecal Blood and Diarrhea
Fecal Score
Treatment Time (Days)
WT Control
WT DSS
GPR132 KO N14 Control
GPR132 KO N14 DSS

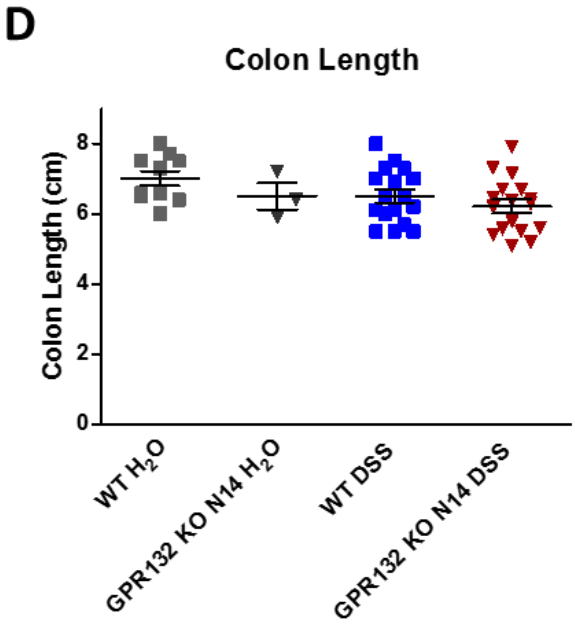
D
Colon Length
Colon Length (cm)
WT H2O
GPR132 KO N14 H2O
WT DSS
GPR132 KO N14 DSS

Figure 5.6. **Clinical parameters and macroscopic disease indicators for the G2A KO N14 generation in the chronic DSS-induced colitis mouse model**. G2A KO N12 mice were backcrossed two generations to establish the G2A KO N14 mouse colony. G2A KO N14 mice display a mild increased severity when compared to WT mice. (A) Body weight, (B) Fecal blood and diarrhea, (C) mesenteric lymph node expansion, and (D) colon length. WT-control (n=9), WT-DSS (n=17), G2A KO N14 control (n=3), and G2A KO N14-DSS (n=17). WT mice used in this analysis were randomly assigned for comparison with G2A KO N14 mice and were duplicated from analysis used for GPR4 KO and GPR65 KO chronic DSS experiment groups. Data are presented as mean ± SEM and was analyzed for statistical significance using the two-way or one-way ANOVA followed by Bonferroni post hoc. (*$P < 0.05$, **$P < 0.01$, *** $P< 0.001$).

D. Discussion

GPR132 is a controversial family member of the pH-sensing GPCRs. Previously, studies have shown protons can activate GPR132; however, the pH-induced activation of GPR132 was described as minimal [83, 91]. Additional studies identified GPR132 as a receptor for oxidized free fatty acids such as 11-hydroxyeicosatetraenoic acid (HETE) and 9-hydroxyoctadecadienoic acid (9-HODE) and also bioactive lipids such lysophosphatidylcholine (LPC). Very recent studies have identified GPR132 can sense and respond to extracellular lactate as well as microbial metabolites such as N-acyl-3-hydroxy-palmitoyl glycine (commendamide) [89, 92, 93].

The aim of our work was to elucidate the functional role of GPR132 in acute and chronic DSS-induced intestinal inflammation. Previous studies suggest GPR132 is a negative regulator of inflammation [85, 91, 95, 96, 98, 193, 194]. As such, we hypothesized that GPR132 genetic deletion would result in more severe intestinal inflammation. We evaluated two generations of GPR132 KO mice (GPR132 KO N12 and GPR132 KO N14) for comparison to WT mice with and without DSS-induced colitis. Interestingly, GPR132 KO N12 mice displayed no significant clinical manifestations of heightened sensitivity to DSS when compared to WT DSS mice in the acute DSS-induced colitis mouse model. A recent study published during the preparation of this dissertation work investigated the effects of the genetic deficiency of GPR132 in the DSS-induced acute colitis mouse model [193]. WT and GPR132 knockout mice were treated for 2-6 days with 3% DSS. GPR132 KO DSS-treated mice displayed exaggerated disease activity, body weight loss, fecal scores, and colon shortening. This anti-inflammatory function of GPR132 observed in the DSS colitis mouse model was attributed to the increased production of IFNɣ whereby monocyte inflammatory programs are reduced, and subsequent eosinophil-mediated tissue injury is blunted.

The central conclusion drawn from this recently published study on the effects of GPR132 deficiency in acute DSS-induced colitis is not consistent with our results obtained from the acute DSS-induced colitis model but is in line with our results from the chronic DSS-induced colitis mouse model. The GPR132 KO N12 DSS mice from this dissertation work displayed exaggerated sensitivity to the DSS insult when compared to WT mice. GPR132 KO N12 DSS mice lost ~27% bodyweight by the final day of the chronic DSS model. Heightened fecal blood and diarrhea scores also accompanied by the dramatic bodyweight loss. Following the course of chronic DSS administration, mouse colon histopathology was evaluated. GPR132 KO N12 mice had a heightened score of severity when compared to WT DSS mice. Furthermore, fibrosis was evaluated and GPR132 KO N12 mice had more pathological colonic fibrosis when compared to WT DSS mice. We next evaluated the GPR132 KO N14 generation in the chronic DSS induced colitis mouse model. We observed no significant differences in mouse bodyweight loss in GPR132 KO N14 mice but enhanced fecal blood and diarrhea scores when compared to WT DSS mice. These results suggest differences in the genetic background of GPR132 KO mice may contribute to the observed phenotype differences between GPR132 KO N12 and GPR132 KO N14 generational sensitivity to the DSS chemical insult. Taking these results together with Frasch et al [193], GPR132 seems to provide an anti-inflammatory role in intestinal inflammation.

However, there are some distinct discrepancies between studies. First, as briefly described above, we observed no clinical indicators of increased severity owing to GPR132 deficiency in the acute DSS-induced colitis model as we observed in the chronic DSS-induced colitis mouse model. Second, minimal information is provided describing the genetic background of the GPR132 KO mice with respect to WT control, which could contribute to

differential DSS sensitivity between this dissertation work and Frasch et al. Other factors, such as microbiome of the mouse colonies, diet, and microenvironments at different animal facilities, could all contribute to the observed differential severity among the GPR132 KO DSS-induced colitis models.

Taking this work in the context of current literature regarding the role of GPR132 in intestinal inflammation, our work suggests GPR132 suppresses intestinal inflammation in the DSS-induced colitis mouse model. However, additional studies are needed to delineate the mechanism of GPR132 in intestinal inflammation.

Chapter VI: General Discussion

This dissertation work aimed to evaluate the functional responses to genetic deficiency of the pH-sensitive GPCRs GPR4, GPR65, and GPR132 in the acute and chronic DSS-induced colitis mouse model. This IBD model closely resembles human UC. Loss of GPR4 resulted in ameliorated parameters of disease severity such as body weight loss and fecal blood and diarrhea in both acute and chronic DSS-induced colitis. In line with reduced clinical disease parameters, GPR4 knockout (KO) mice had reduced mesenteric lymph node expansion and colon shorten. These results are consistent with reduced inflammation in the DSS-induced colitis mouse model. Loss of GPR4 reduced total histopathology in the colon and also significantly impeded neutrophil, T-cell, and macrophage accumulation in the distal colon. We also indirectly assessed GPR4 expression in non-inflamed and inflamed intestinal tissues though visualizing GFP as a surrogate marker for GPR4 in GPR4 KO mice. We confirmed GPR4 is highly expressed in intestinal vasculature. Interestingly, we observed GFP expression in some, but not all, intestinal macrophages. The role of GPR4 in macrophages is currently unknown. We also observed a significant correlation with heightened inflammatory gene expression, such as E-selectin and COX-2, with GPR4 mRNA levels. Since we have previously shown GPR4 mediates acidosis-induced endothelial cell (EC) inflammation and leukocyte-EC interactions, we evaluated EC adhesion molecules VCAM-1 and E-selectin in inflamed tissues. We observed a GPR4 dependent increase of protein expression in intestinal microvascular ECs. We also assessed GPR4 mRNA levels in patients with and without CrD and UC. A notable increase in GPR4 mRNA was observed in IBD samples when compared to non-inflamed intestinal samples. Elevated GPR4 expression in IBD suggest GPR4 is involved in IBD pathology and could serve as a therapeutic target. We investigated a novel GPR4 inhibitor in the acute DSS-induced colitis

mouse model. Mice provided the GPR4 antagonist displayed reduced disease parameters, histopathology, EC-specific adhesion molecule expression, and inflammatory gene expression. Collectively, we provide evidence GPR4 is a pro-inflammatory regulator of intestinal inflammation and is a novel therapeutic target. Though this dissertation work provides valuable insights built upon previous work performed from our group, further investigation into the potential molecular mechanism by which GPR4 regulates intestinal inflammation is warranted.

Following the completion of this project, another group reported similar findings as to the role of GPR4 during intestinal inflammation [195]. This group used both the DSS-induced colitis mouse model and the IL-$10^{-/-}$ spontaneous colitis mouse model. They reported reduced disease severity in mice devoid of GPR4 in both colitis mouse models. Interestingly, they observed a reduced Th1 cellular infiltrate in the intestinal mucosa accompanied by reduced IFNγ mRNA levels. This group also independently confirmed our observations that GPR4 is expressed in some mucosal macrophages using *in situ* hybridization. Provided the role of GPR4 is unknown in macrophages and GPR4 expression is not observed in T cells, further investigation into the role of GPR4 in macrophages are desirable. These observations of GPR4 expression in macrophages and a reduced Th1 response in GPR4 deficient mice suggest there may be a role for GPR4 in the classical activation of macrophages in IBD.

However, most literature seems to indicate the predominate mechanism by which GPR4 regulates intestinal inflammation is likely mediated through EC activation. Our group has recently demonstrated that GPR4 regulates acidosis-induced ER stress responses in vascular endothelial cells [196]. Developing evidence from human IBD genetic risk data and mouse models implicate the endoplasmic reticulum (ER) stress/unfolded protein response (UPR) as a central pathway involved in intestinal inflammation [25, 197, 198]. The UPR is a response to an

increase in unfolded or misfolded proteins in the ER during protein synthesis. Mild ER stress has been shown to provide protective effects and allow cell adaptation, however, prolonged (severe) ER stress can result in cell death and inflammation [199, 200]. There is accumulating evidence suggesting UPR and inflammatory signaling pathways are interconnected in IBD [201]. Genome-wide association studies (GWAS) have provided new IBD susceptibility gene candidates involved in the ER stress/UPR pathways which include *XBP1*, *ORMDL3*, and *AGR2* [202, 203]. Variants in these ER stress related genes could increase risk of IBD development and progression through inhibition of cell stress adaptation. Mice devoid of XBP1 and AGR2 within the intestinal epithelium disrupt ER stress homeostasis and develop spontaneous intestinal inflammation [204]. Additionally, ER stress/UPR genes $Ire1^{-/-}$, $atf6^{-/-}$, and $chop^{-/-}$ knock-out mice have been studied using IBD mouse models and are involved in modulating intestinal inflammation [204]. These animal studies have demonstrated a link between ER stress and intestinal inflammation due to reduced epithelial barrier functions and pro-inflammatory phenotypes of epithelial cells. Based on these evidences, ER stress/UPR appears to be involved in both initiating and maintaining unresolved intestinal inflammation. The link between ER stress and inflammation observed in intestinal inflammation highlights a potential general mechanism of ER stress/Inflammation. Recently, ER stress/UPR has been directly connected to local and systemic inflammation. Initiation of ER stress has resulted in the acute phase inflammatory response, activation of NF-κB nuclear transcription factor, and mitogen-activated protein kinase (MAPK) signaling in a variety of cell types and biological contexts [201]. These observations suggest that ER stress can directly initiate inflammation. Several reports support these observations in vascular endothelial cells as ER stress can increase the inflammatory response leading to complications in several disease states such as atherosclerosis, diabetes

mellitus, and diabetic retinopathy [205, 206]. However, the interaction between ER stress signaling and inflammation has not been studied in intestinal microvascular endothelial cells (IMECs) and has not been implicated in intestinal inflammation. Our group has recently implicated GPR4 as a regulator of ER stress/inflammation in vascular endothelial cells (ECs) [113, 114, 196]. Furthermore, this dissertation work has connected the involvement of this receptor in potentiating intestinal inflammation in a mouse model of acute colitis. We have demonstrated that GPR4 is expressed in a variety of ECs, including intestinal microvascular endothelial cells (IMECs) and can fully activate all three arms of the ER stress response pathways (ATF6, PERK, and IRE1) *in vitro* and increases pro-inflammatory mediators such as vascular adhesion molecules, cytokines, chemokines, and functionally increases adhesion of leukocytes to a variety of EC types [113, 114, 196]. However, the effects of GPR4 mediated ER stress in IBD have not been investigated. GPR4 could be involved in regulating a novel underlying mechanism connecting GPR4 dependent ER stress and inflammatory crosstalk with unresolved vascular dysfunction in IBD. Future mechanistic studies could investigate if GPR4 can sense acidity in the mucosa of inflamed intestinal tissue and subsequently modify the vascular inflammatory function through the ER stress response.

This dissertation work also provided new insights into the role of GPR65 in intestinal inflammation using the acute and chronic DSS-induced colitis model. We compared WT mice with GPR65 KO mice for both acute and chronic mouse models. We observed no significant differences between WT and GPR65 KO mice in mouse body weight loss and fecal blood scores. Macroscopic disease indicators, however, provided confounding results. GPR56 KO mice had less colon shortening, indicating reduced intestinal inflammatory severity. However, GPR65 had a trend in greater mesenteric lymph node expansion. These results suggested GPR65 does not

have a significant role in the DSS-induced acute intestinal inflammation model. To observe the role of GPR65 in a chronic colitis disease state, we used the chronic DSS colitis model. Our results provided GPR65 with an anti-inflammatory role in IBD. Collectively, the mouse body weight, fecal blood scores, mesenteric lymph node volume, and colon length were all more severe in GPR65 KO mice compared to WT. Histopathological features and pathological fibrosis were assessed and GPR65 KO mice were more severe when compared to WT. Additionally, the numbers of neutrophils, T cells, and macrophages were evaluated in GPR65 KO mice. We also used the same approach as above to indirectly assess GPR65 expression in non-inflamed and inflamed intestinal tissues though the visualization of GFP as a surrogate marker for GPR65 in GPR65 KO mice. GFP signal was observed in polymorphonuclear neutrophils, macrophages, and lymphocytes.

Given the broad expression profile of GPR65 in the intestinal infiltrate, proposing a singular potential mechanism of how GPR65 reduces chronic intestinal inflammation proves difficult. As mentioned above, GPR65 has pleiotropic roles in the inflammatory programs among different immune cell populations. Some reports have described GPR65 as a driver of Th17 mediated pathogenesis while others have shown GPR65 reduces macrophage activation and possibly neutrophilic inflammation [82, 103, 104, 106, 207]. It is important to highlight the G-protein activation status for GPR65. Reports have shown that GPR65 couples to Gαs and $G_{12/13}$ [106, 208, 209]. However, the majority of the described acidosis-induced cellular effects have been proposed though the GPR65/Gαs/cAMP/CREB-ATF-1 pathway. The role of cyclic AMP (cAMP) has long been investigated in the role of immune cell function. Interestingly, inhibition of phosphodiesterase 4, which is an intracellular enzyme involved in the degradation of cAMP, has been shown to reduce expression of TNF-α, IL-1β, IL-17, and NF-κB in the mucosa of

patients with IBD [187, 210]. However, both pro- and anti-inflammatory effects have been described for cAMP and these roles are seemingly cell type specific. For example, cAMP can increase Nur77 expression in monocytes, which represses pro-inflammatory cytokines produced from the pro-inflammatory $Ly6C^{high}$ type monocyte and skews monocytes toward the anti-inflammatory $Ly6C^{low}$ type [211-213]. Also, cAMP has shown ability to reduce neutrophilic extracellular traps for bactericidal action [214]. For evaluation of cAMP in professional antigen presenting cells, cAMP reduces dendritic cell (DC) secretion of TNF-α, IL-17, and IFNγ while increasing IL-10 [215, 216]. Also, cAMP likely reduces cyclic nucleotide PDE4 expression in DCs which can subsequently suppress Th17 differentiating cytokines IL-6 and TGFβ. Several studies have shown cAMP is critical for T regulatory activity and involved in reducing TCR activation and subsequent T cell function [217, 218] [181]. Interestingly, however, cAMP appears to provide a pro-inflammatory role during T helper differentiation by driving Th17 and Th1 subsets, but not Th2 [219]. These observations could provide insights as to why GPR65 deficient mice have exaggerated intestinal inflammation in the DSS-induced colitis mouse model. Loss of GPR65 could inhibit the anti-inflammatory role of the Gαs/cAMP/CREB-ATF-1 pathway in macrophages, DCs, and neutrophils. However, since UC is not primarily a Th17 mediated inflammatory disease, though involvement has been demonstrated, the loss of the potential pro-inflammatory role of GPR65 in Gαs/cAMP/CREB would not be observed in mouse disease severity in the chronic DSS-induced colitis mouse model.

Provided the distinct role of cAMP/CREB pathway in regulating immune cell function and the subsequent implication of GPR65 involvement in mediating these effects though the Gαs/cAMP/CREB-ATF-1 pathway, we sought to evaluate the acidosis/GPR65/Gαs activation status in distinct immune cell populations *in vitro*. We differentiated WT and GPR65-deficient

mouse bone marrow progenitor cells to either macrophages or dendritic cells. To assess a heterogenous population of T cells, we isolated WT and GPR65 KO mouse thymocytes. We observed acidosis was capable of inducing CREB and ATF-1 phosphorylation in these immune cell populations and that this increase was due in part to GPR65 as the loss of GPR65 blunted the induction of acidosis-induced CREB and ATF-1 phosphorylation in these cell types. We next centered our evaluation of investigating the functional role of acidosis/GPR65 in bone marrow derived macrophage (BMDM) proliferation and migration. Acidic pH reduced BMDM proliferation and migration toward chemoattractant C5a in WT BMDMs. However, the loss of GPR65 resulted in a recovery of BMDM proliferation and migration suggesting GPR65 reduces these functions in naïve macrophages. We next endeavored to assess the function of acidosis/GPR65 in macrophages polarized to either the pro-inflammatory M1 phenotype or anti-inflammatory M2 phenotype. GPR65 KO M1 BMDMs had elevated TNF-α mRNA expression, but not IL-1β when compared to WT M1 BMDMs. These results suggest GPR65 may have moderate effects in the reduction of M1 macrophage activity. For the M2 macrophage phenotype, loss of GPR65 increased expression of arginase 1 and FIZZ1 mRNA under acidic pH conditions in BMDMs. These results suggest acidosis/GPR65 reduces M2 macrophage activity. These results seem contradictory to the purported anti-inflammatory role of GPR65 in macrophage function. However, the M2 macrophage has pleotropic roles in antibacterial functions. Increased M2 macrophage phenotypes in inflamed tissues have classically been implicated in regulating inflammation through increased anti-inflammatory cytokines and reduced pathogen killing functions [220, 221]. M2 macrophages are also central for the promotion of wound healing following tissue damage. Some reports suggest M2 macrophage function in IBD could promote impaired pathogen clearance and thereby sustain intestinal

inflammation [222-224]. Also, M2 macrophages have been implicated in IBD-associated pathological fibrosis from continual wound repair. In addition to arginase 1 and FIZZ1 expression analysis in acidosis stimulated BMDMs, we also measured IL-10 mRNA levels. At physiological pH, IL-10 mRNA was reduced in GPR65 KO M2 BMDMs when compared to WT. This suggests GPR65 contributes to M2 driven IL-10 secretion. Interestingly, acidosis reduced the IL-10 cytokine expression in M2 BMDMs, however, there was no further reduction of IL-10 mRNA in GPR65 KO BMDMs. We did not, however, evaluate the role of acidosis/GPR65 in M1/M2 macrophage polarization and subsequent immunomodulatory functions.

Taken together, GPR65 appears to protect against DSS-induced chronic colitis. The molecular mechanism, however, has yet to be fully uncovered. The role of GPR65 in the amelioration of colitis may very well involve modulating macrophage inflammatory programs. Future studies should be performed to evaluate the specific contribution of GPR65 in particular immune cells specific to the mucosal immune system. Additional IBD animal models with different mechanisms for colitis induction should also be explored whereby GPR65 contribution could be further delineated. For example, adoptive transfer of WT and GPR65 KO $CD45R^{high}$ T cells into RAG1 deficient hosts or reciprocally adoptive transfer of WT $CD45R^{high}$ T cells to RAG1/GPR65 double knockout mice could provide insights into the GPR65/T-cell contribution to intestinal inflammation.

Provided both GPR132 and GPR65 are highly expressed on leukocytes, and that both have pH-sensing capabilities, we sought to investigate the functional role of the GPR65 proton-sensing family member GPR132 in intestinal inflammation. As previously described, however, the pH-sensing capability of GPR132 is considered moderate. More recent reports indicate

ligands other than protons are the primary mediators of GPR132 activity and subsequent cellular functions. These ligands, in part, include bioactive lipids such as LPC and commendamide. Further ligands include certain oxidized free fatty acids like 9-HODE and HPODE, HETE [59, 83, 86, 89, 93, 189, 190]. Recently, lactate has also been proposed to activate GPR132 [92]. Many of these endogenous ligands are present in the gastrointestinal system and are mediators of the inflammatory response, and in addition to protons, suggest GPR132 could mediate intestinal inflammation though sensing cellular metabolic byproducts (protons and lactate), bioactive lysophospholipids (LPC and commendamide), and oxidized free fatty acids (9-HODE) in the intestinal tissues.

We evaluated GPR132 deficient mice backcrossed into the C57BL/6 genetic background twelve generations during acute and chronic DSS-induced experimental colitis. Mouse body weight loss and fecal blood scores were evaluated daily for seven days. We observed no significant differences in body weight loss or fecal severity scores between WT and GPR132 KO N12 mice. Additionally, no significant differences were observed in mesenteric lymph node expansion and colon length between WT and GPR132 KO N12 mice following the seven-day DSS colitis induction. Interpretation of these results indicate GPR132 deficiency does not affect clinical manifestations of intestinal inflammation in the acute DSS-induced colitis model. We next endeavored to assess the functional role of GPR132 in the chronic DSS colitis model by assessing the disease severity indicators. Initial observations indicated that the genetic deficiency of GPR132 resulted in dramatic disease progression. More than 70% of GPR132 KO N12 mice reached the humane endpoint before the experimental endpoint when compared to 10% in WT mice. These observations suggested GPR132 has a protective role during chronic DSS chemical exposure. In line with the higher mortality events observed in GPR132 KO mice, body weight

loss and fecal blood scores were more severe than observed in WT mice. Histopathological analysis of colon tissues also revealed heightened severity in G2A KO mice compared to WT. We next backcrossed the GPR132 KO N12 generation two additional generations resulting in GPR132 KO N14 mice. We then initiated the GPR132 KO N14 mice in the chronic DSS-induced colitis model. We observed GPR132 KO N14 displayed a modest heightened severity to the DSS chemical insult when compared to WT-DSS induced mice.

The results obtained from the GPR132 KO N14 compared to the GPR132 KO N12 mice were supportive of our overall conclusion that GPR132 provides a protective role during intestinal inflammation. However, the differences in the degree of severity between GPR132 KO N12 and N14 mice were markedly different. Following the completion of these experiments, Frasch et al published a research article whereby WT and GPR132 KO mice were used in the acute DSS-induced colitis mouse model [193]. Results from Frasch et al were supportive of the data we observed from the GPR132 KO N12 and N14 mouse experiments in the chronic DSS-induced colitis mouse model. However, where Frasch et al observed a strong phenotypic sensitivity to the DSS insult in the acute DSS mouse model, our results only presented differences in mouse severity during the chronic DSS model. Frasch et al, however, did not include detailed information regarding the genetic background such as how many generations the GPR132 KO mice were bread into the C57Bl/6 background.

Taking both our results and that of Frasch et al into consideration, it appears the genetic background of the GPR132 KO mice is a contributor to the observed phenotypes in either the acute or chronic DSS-induced colitis mouse models. Other factors, such as DSS potency, microbiome of the GPR132 KO mouse colonies, diet, and microenvironments of different animal facilities could also contribute the differing severities observed. Future directions for the

delineation of the role that GPR132 plays in regulating intestinal inflammation will both center on determining the contribution of the genetic background on the mouse phenotype and also determining the underlying mechanism by which G2A protects against intestinal inflammation. To overcome these complications, alternate animal models can be used with different modes of colitis induction as well as modulating the current genetic background of the GPR132 KO mice. The DSS-induced colitis mechanism of action is broad, namely, the nonspecific damage of the intestinal epithelia and subsequent inflammatory response to infiltrated bacteria and luminal antigen. This presents a greater chance of penetrance of unknown mutations which may have contributed to the heightened sensitivity to DSS chemical (GPR132 KO N12) or mild sensitivity (GPR132 KO N14) observed. As described above, in addition to the inducible modes of colitis induction there are animal models where the spontaneous development of colitis occurs. In particular, the IL-10 knockout model or adoptive transfer models could be useful for the evaluation of spontaneous development of colitis not initially occurring from a chemical insult. However, these animal models will require time, effort, and resources. Furthermore, the genetic contributions of the differing degrees of DSS sensitivities observed between N12 and N14 GPR132 KO generations are unknown and may continue to alter the phenotypes in spontaneous colitis animal models.

Previous publications have described differing sensitivities to the DSS chemical insult based on mouse strains [123]. For example, the C3H and C57BL/6 mouse strains are the most susceptible to DSS-induced colitis showing severe inflammation in the cecum, proximal, middle, and distal colon segments. On the other hand, BALB/C and CBA/H mouse stains show severe inflammation predominately restricted to the distal colon segment. Breeding the C57BL/6 GPR132 KO mice into the less susceptible BALB/C or CBA/H mouse strains for at least six

generations could reduce the penetrance of unknown mutations in either the N12 or N14 GPR132 KO C57BL/6 mice. The WT littermates and GPR132 KO N6 BALB/c or CBA/H mice could be compared in the chronic DSS-induced colitis mouse model. On the other hand, further efforts to continue to backcross the GPR132 KO N14 mice additional generations into the C57BL/6 background could also eliminate potential mutations which provide differing sensitivities to the DSS-chemical insult.

In addition to addressing concerns over the contributions of genetic background to mouse phenotypes, effort must also be made to delineate the mechanism whereby GPR132 reduces severity of intestinal inflammation [116, 117]. Several previous reports provide insights into the potential anti-inflammatory role of GPR132. T regulatory cells are critical for proper immune homeostasis and dysregulation of Tregs have been implicated in IBD. A GPR132 ligand, LPC, was shown to increase human T regulatory immunosuppressive functions [194]. LPC increased Foxp3 expression and also upregulated TGF-β1 mRNA levels. Genetic knockdown of GPR132 in Treg demonstrated that the enhanced LPC-induced Treg immunosuppressive function was mediated through GPR132 activation. This paper presents a possible mechanism for the observed functional role of GPR132 in intestinal inflammation. GPR132 could enhance Treg function in IBD and contribute to dampening mucosal inflammation. Another potential mechanism by which GPR132 could be implicated in suppressing intestinal inflammation is T cell activation and proliferation. As described earlier, GPR132 was originally shown to inhibit cell cycle progression through the G2/M phase. In line with this early observation, a group reported that GPR132 KO mice developed a late-onset autoimmune syndrome characterized by heavy leukocyte infiltration into the liver, lung, and kidney, among others [85]. Furthermore, GPR132 KO mice developed an enlarged spleen with heightened expansion of CD4+ and CD8+ T cells.

T cells isolated from the spleen of GPR132 KO mice were hyperresponsive to anti-CD3/CD28 T cell receptor stimulation and resulted in increased T cell proliferation. These results suggest GPR132 could serve a central role in suppressing T cell activation and proliferation in IBD. These aspects could be further evaluated in future studies to delineate potential mechanisms by which GPR132 suppresses intestinal inflammation.

In conclusion, this dissertation work evaluated the role of proton sensors GPR4, GPR65, and GPR132 in both the acute and chronic experimental colitis mouse models. Previous studies have already provided a pro-inflammatory role for GPR68 in intestinal inflammation. Our results indicate GPR4 potentiates intestinal inflammation likely by mediating leukocyte extravasation into the intestinal mucosa. GPR65, on the other hand, appears to suppress intestinal inflammation likely though reducing immune cell activation. Our results seem to provide an anti-inflammatory role for GPR132 in intestinal inflammation, which is supported by a recent publication by Frasch et al. This report also provides an immunosuppressive role for GPR132 in intestinal inflammation. Taking the collective contribution of the entire family of pH-sensing GPCRs in intestinal inflammation together, there appears to be a balance between inflammatory contribution (GPR4 and GPR68) and protection (GPR65 and GPR132) during intestinal inflammation. Based on the purported equally distributed pro-and anti-inflammatory roles amongst the pH-sensing GPCR family members, one could hypothesize that in the context of the inflammatory loci acidosis/pH-sensing GPCR activation would have no functional consequence. These observations are intriguing when considering the involvement of each pH-sensing GPCR family member within the roles of the cell type in which they are natively expressed. As described above, the intestinal mucosal immune system is in a constant state of "physiological inflammation" whereby bacteria are eliminated and immunoregulatory functions exist to prevent

chronic, uncontrolled inflammation in response to the large number of bacteria in the gut. The colonic interstitial tissue pH is largely within physiological range and thereby provides minimal activation of the pH-sensing GPCRs. The differing roles of each pH-sensing GPCR during intestinal inflammation, whereby local acidosis exists, could manifest based on the current stage of the inflammatory response and whether the pathogenic insult can be effectively removed. For example, following active inflammation whereby leukocytes have accumulated in the site of inflammation, acidosis likely serves as an endogenous danger signal to alert the immune system following bacterial overgrowth or tissue damage. GPR4 will contribute to the initial and continual influx of leukocytes which subsequently augment tissue inflammation by host vasculature. Once the immune cells get to the site of inflammation, they too will exist in the acidic inflammatory loci. GPR65 likely impedes the inflammatory response as a checkpoint to prevent chronic, uncontrolled inflammation and mediate effective resolution following the inflammatory response. However, literature seems to suggest GPR65 has pro-inflammatory roles in Th17 cells which could implicate GPR65 as a driver in Th17 mediated inflammatory diseases. One potential explanation for the dual roles of GPR65 in differing immune cell populations could be due to the evolution of the adaptive immune system. As described previously, GPR65 immunosuppressive role in innate immune cells is consistent with the role of cyclic AMP (cAMP), a downstream second messenger of Gαs, in cells of the innate immune system. Interestingly, bacteria and some fungi have taken advantage of the anti-inflammatory function of cAMP though the introduction of microbial adenylyl cyclases to intoxicate phagocytes with preformed cAMP to suppress inflammation. GPR65 could be conserved in the molecular evolution of the adaptive immune system where cAMP has shown to enhance anti-bacterial functions for these certain bacteria. These collective functions of both GPR4 and GPR65 would

serve for the effective removal of the inflammatory stimuli and resolve inflammation for the maintenance of intestinal homeostasis. However, if these processes are perturbed then the proton-sensing GPCRs could serve as inflammatory mediators.

References

[1] B. Beutler, Innate immunity: an overview, Mol Immunol 40 (2004) 845-859.

[2] S.E. Turvey, D.H. Broide, Innate immunity, J Allergy Clin Immunol 125 (2010) S24-32.

[3] Y. Zhang, W. Gu, L. He, B. Sun, Th1/Th2 cell's function in immune system, Adv Exp Med Biol 841 (2014) 45-65.

[4] P. Kidd, Th1/Th2 balance: the hypothesis, its limitations, and implications for health and disease, Altern Med Rev 8 (2003) 223-246.

[5] D.S. Robinson, The Th1 and Th2 concept in atopic allergic disease, Chem Immunol 78 (2000) 50-61.

[6] A. Raza, W. Yousaf, R. Giannella, M.T. Shata, Th17 cells: interactions with predisposing factors in the immunopathogenesis of inflammatory bowel disease, Expert Rev Clin Immunol 8 (2012) 161-168.

[7] T. Korn, E. Bettelli, M. Oukka, V.K. Kuchroo, IL-17 and Th17 Cells, Annu Rev Immunol 27 (2009) 485-517.

[8] B. Stockinger, S. Omenetti, The dichotomous nature of T helper 17 cells, Nat Rev Immunol 17 (2017) 535-544.

[9] W. Ouyang, J.K. Kolls, Y. Zheng, The biological functions of T helper 17 cell effector cytokines in inflammation, Immunity 28 (2008) 454-467.

[10] K. Matusiewicz, B. Iwańczak, M. Matusiewicz, Th9 lymphocytes and functions of interleukin 9 with the focus on IBD pathology, Adv Med Sci 63 (2018) 278-284.

[11] J. Li, S. Chen, X. Xiao, Y. Zhao, W. Ding, X.C. Li, IL-9 and Th9 cells in health and diseases-From tolerance to immunopathology, Cytokine Growth Factor Rev 37 (2017) 47-55.

[12] S. Malik, V. Dardalhon, A. Awasthi, Characterization of Th9 Cells in the Development of EAE and IBD, Methods Mol Biol 1585 (2017) 201-216.

[13] M.A. Sugimoto, L.P. Sousa, V. Pinho, M. Perretti, M.M. Teixeira, Resolution of Inflammation: What Controls Its Onset?, Front Immunol 7 (2016) 160.

[14] J.M. Kim, Molecular mechanisms of regulatory T cell development and suppressive function, Prog Mol Biol Transl Sci 92 (2010) 279-314.

[15] N. Askenasy, A. Kaminitz, S. Yarkoni, Mechanisms of T regulatory cell function, Autoimmun Rev 7 (2008) 370-375.

[16] W.A. Muller, Leukocyte-endothelial-cell interactions in leukocyte transmigration and the inflammatory response, Trends Immunol 24 (2003) 327-334.

[17] K. Ley, C. Laudanna, M.I. Cybulsky, S. Nourshargh, Getting to the site of inflammation: the leukocyte adhesion cascade updated, Nat Rev Immunol 7 (2007) 678-689.

[18] W.A. Muller, Getting leukocytes to the site of inflammation, Vet Pathol 50 (2013) 7-22.

[19] N. Reglero-Real, D. García-Weber, J. Millán, Cellular Barriers after Extravasation: Leukocyte Interactions with Polarized Epithelia in the Inflamed Tissue, Mediators Inflamm 2016 (2016) 7650260.

[20] D. Vestweber, Novel insights into leukocyte extravasation, Curr Opin Hematol 19 (2012) 212-217.

[21] J.M. Williams, C.A. Duckworth, M.D. Burkitt, A.J. Watson, B.J. Campbell, D.M. Pritchard, Epithelial cell shedding and barrier function: a matter of life and death at the small intestinal villus tip, Vet Pathol 52 (2015) 445-455.

[22] B. Ahluwalia, M.K. Magnusson, L. Öhman, Mucosal immune system of the gastrointestinal tract: maintaining balance between the good and the bad, Scand J Gastroenterol 52 (2017) 1185-1193.

[23] T.T. MacDonald, The mucosal immune system, Parasite Immunol 25 (2003) 235-246.

[24] J.R. McGhee, K. Fujihashi, Inside the mucosal immune system, PLoS Biol 10 (2012) e1001397.

[25] A. Kaser, S. Zeissig, R.S. Blumberg, Inflammatory bowel disease, Annu Rev Immunol 28 (2010) 573-621.

[26] R.J. Xavier, D.K. Podolsky, Unravelling the pathogenesis of inflammatory bowel disease, Nature 448 (2007) 427-434.

[27] H.J. Su, Y.T. Chiu, C.T. Chiu, Y.C. Lin, C.Y. Wang, J.Y. Hsieh, S.C. Wei, Inflammatory bowel disease and its treatment in 2018: Global and Taiwanese status updates, J Formos Med Assoc (2018).

[28] S.R. Brown, L.C. Coviello, Extraintestinal Manifestations Associated with Inflammatory Bowel Disease, Surg Clin North Am 95 (2015) 1245-1259.

[29] F. Rieder, C. Fiocchi, Intestinal fibrosis in inflammatory bowel disease - Current knowledge and future perspectives, J Crohns Colitis 2 (2008) 279-290.

[30] J. Xie, S.H. Itzkowitz, Cancer in inflammatory bowel disease, World J Gastroenterol 14 (2008) 378-389.

[31] S. Chandel, A. Prakash, B. Medhi, Current scenario in inflammatory bowel disease: drug development prospects, Pharmacol Rep 67 (2015) 224-229.

[32] J.H. Park, L. Peyrin-Biroulet, M. Eisenhut, J.I. Shin, IBD immunopathogenesis: A comprehensive review of inflammatory molecules, Autoimmun Rev 16 (2017) 416-426.

[33] Z. Wen, C. Fiocchi, Inflammatory bowel disease: autoimmune or immune-mediated pathogenesis?, Clin Dev Immunol 11 (2004) 195-204.

[34] L. Jostins, S. Ripke, R.K. Weersma, R.H. Duerr, D.P. McGovern, K.Y. Hui, J.C. Lee, L.P. Schumm, Y. Sharma, C.A. Anderson, J. Essers, M. Mitrovic, K. Ning, I. Cleynen, E. Theatre, S.L. Spain, S. Raychaudhuri, P. Goyette, Z. Wei, C. Abraham, J.P. Achkar, T. Ahmad, L. Amininejad, A.N. Ananthakrishnan, V. Andersen, J.M. Andrews, L. Baidoo, T. Balschun, P.A. Bampton, A. Bitton, G. Boucher, S. Brand, C. Buning, A. Cohain, S. Cichon, M. D'Amato, D. De Jong, K.L. Devaney, M. Dubinsky, C. Edwards, D. Ellinghaus, L.R. Ferguson, D. Franchimont, K. Fransen, R. Gearry, M. Georges, C. Gieger, J. Glas, T. Haritunians, A. Hart, C. Hawkey, M. Hedl, X. Hu, T.H. Karlsen, L. Kupcinskas, S. Kugathasan, A. Latiano, D. Laukens, I.C. Lawrance, C.W. Lees, E. Louis, G. Mahy, J. Mansfield, A.R. Morgan, C. Mowat, W. Newman, O. Palmieri, C.Y. Ponsioen, U. Potocnik, N.J. Prescott, M. Regueiro, J.I. Rotter, R.K. Russell, J.D. Sanderson, M. Sans, J. Satsangi, S. Schreiber, L.A. Simms, J. Sventoraityte, S.R. Targan, K.D. Taylor, M. Tremelling, H.W. Verspaget, M. De Vos, C. Wijmenga, D.C. Wilson, J. Winkelmann, R.J. Xavier, S. Zeissig, B. Zhang, C.K. Zhang, H. Zhao, M.S. Silverberg, V. Annese, H. Hakonarson, S.R. Brant, G. Radford-Smith, C.G. Mathew, J.D. Rioux, E.E. Schadt, M.J. Daly, A. Franke, M. Parkes, S. Vermeire, J.C. Barrett, J.H. Cho, Host-microbe interactions have shaped the genetic architecture of inflammatory bowel disease, Nature 491 (2012) 119-124.

[35] K.M. de Lange, L. Moutsianas, J.C. Lee, C.A. Lamb, Y. Luo, N.A. Kennedy, L. Jostins, D.L. Rice, J. Gutierrez-Achury, S.G. Ji, G. Heap, E.R. Nimmo, C. Edwards, P. Henderson, C. Mowat, J. Sanderson, J. Satsangi, A. Simmons, D.C. Wilson, M.

Tremelling, A. Hart, C.G. Mathew, W.G. Newman, M. Parkes, C.W. Lees, H. Uhlig, C. Hawkey, N.J. Prescott, T. Ahmad, J.C. Mansfield, C.A. Anderson, J.C. Barrett, Genome-wide association study implicates immune activation of multiple integrin genes in inflammatory bowel disease, Nat Genet 49 (2017) 256-261.

[36] B. Verstockt, K.G. Smith, J.C. Lee, Genome-wide association studies in Crohn's disease: Past, present and future, Clin Transl Immunology 7 (2018) e1001.

[37] B.D. Ye, D.P. McGovern, Genetic variation in IBD: progress, clues to pathogenesis and possible clinical utility, Expert Rev Clin Immunol 12 (2016) 1091-1107.

[38] L. Antoni, S. Nuding, J. Wehkamp, E.F. Stange, Intestinal barrier in inflammatory bowel disease, World J Gastroenterol 20 (2014) 1165-1179.

[39] B. Ahluwalia, L. Moraes, M.K. Magnusson, L. Öhman, Immunopathogenesis of inflammatory bowel disease and mechanisms of biological therapies, Scand J Gastroenterol 53 (2018) 379-389.

[40] S.H. Lee, J.E. Kwon, M.L. Cho, Immunological pathogenesis of inflammatory bowel disease, Intest Res 16 (2018) 26-42.

[41] G. Bamias, F. Cominelli, Role of type 2 immunity in intestinal inflammation, Curr Opin Gastroenterol 31 (2015) 471-476.

[42] T. Imam, S. Park, M.H. Kaplan, M.R. Olson, Effector T Helper Cell Subsets in Inflammatory Bowel Diseases, Front Immunol 9 (2018) 1212.

[43] D. Cibor, R. Domagala-Rodacka, T. Rodacki, A. Jurczyszyn, T. Mach, D. Owczarek, Endothelial dysfunction in inflammatory bowel diseases: Pathogenesis, assessment and implications, World J Gastroenterol 22 (2016) 1067-1077.

[44] L. Deban, C. Correale, S. Vetrano, A. Malesci, S. Danese, Multiple pathogenic roles of microvasculature in inflammatory bowel disease: a Jack of all trades, Am J Pathol 172 (2008) 1457-1466.

[45] A. Papa, F. Scaldaferri, S. Danese, S. Guglielmo, I. Roberto, M. Bonizzi, G. Mocci, C. Felice, C. Ricci, G. Andrisani, G. Fedeli, G. Gasbarrini, A. Gasbarrini, Vascular involvement in inflammatory bowel disease: pathogenesis and clinical aspects, Dig Dis 26 (2008) 149-155.

[46] M.F. Neurath, Current and emerging therapeutic targets for IBD, Nat Rev Gastroenterol Hepatol 14 (2017) 269-278.

[47] P.S. Dulai, W.J. Sandborn, Next-Generation Therapeutics for Inflammatory Bowel Disease, Curr Gastroenterol Rep 18 (2016) 51.

[48] U. Billmeier, W. Dieterich, M.F. Neurath, R. Atreya, Molecular mechanism of action of anti-tumor necrosis factor antibodies in inflammatory bowel diseases, World J Gastroenterol 22 (2016) 9300-9313.

[49] P.B. Koul, Diabetic ketoacidosis: a current appraisal of pathophysiology and management, Clin Pediatr (Phila) 48 (2009) 135-144.

[50] J.A. Kraut, N.E. Madias, Approach to patients with acid-base disorders, Respir Care 46 (2001) 392-403.

[51] N.S. Krieger, K.K. Frick, D.A. Bushinsky, Mechanism of acid-induced bone resorption, Curr Opin Nephrol Hypertens 13 (2004) 423-436.

[52] J. Lemann, Jr., D.A. Bushinsky, L.L. Hamm, Bone buffering of acid and base in humans, Am J Physiol Renal Physiol 285 (2003) F811-832.

[53] C. Aalkjaer, H.L. Peng, pH and smooth muscle, Acta Physiol Scand 161 (1997) 557-566.

[54] P. De Vito, The sodium/hydrogen exchanger: a possible mediator of immunity, Cell Immunol 240 (2006) 69-85.

[55] J. Fang, Q.J. Quinones, T.L. Holman, M.J. Morowitz, Q. Wang, H. Zhao, F. Sivo, J.M. Maris, M.L. Wahl, The H+-linked monocarboxylate transporter (MCT1/SLC16A1): a potential therapeutic target for high-risk neuroblastoma, Mol Pharmacol 70 (2006) 2108-2115.

[56] H. Izumi, T. Torigoe, H. Ishiguchi, H. Uramoto, Y. Yoshida, M. Tanabe, T. Ise, T. Murakami, T. Yoshida, M. Nomoto, K. Kohno, Cellular pH regulators: potentially promising molecular targets for cancer chemotherapy, Cancer Treat Rev 29 (2003) 541-549.

[57] G. Curley, M.M. Contreras, A.D. Nichol, B.D. Higgins, J.G. Laffey, Hypercapnia and acidosis in sepsis: a double-edged sword?, Anesthesiology 112 (2010) 462-472.

[58] R.A. Gatenby, R.J. Gillies, Glycolysis in cancer: a potential target for therapy, Int J Biochem Cell Biol 39 (2007) 1358-1366.

[59] W.C. Huang, P. Swietach, R.D. Vaughan-Jones, O. Ansorge, M.D. Glitsch, Extracellular acidification elicits spatially and temporally distinct Ca2+ signals, Curr Biol 18 (2008) 781-785.

[60] J.F. Hunt, K. Fang, R. Malik, A. Snyder, N. Malhotra, T.A. Platts-Mills, B. Gaston, Endogenous airway acidification. Implications for asthma pathophysiology, Am J Respir Crit Care Med 161 (2000) 694-699.

[61] J.A. Kellum, Determinants of blood pH in health and disease, Crit Care 4 (2000) 6-14.

[62] J.A. Kellum, M. Song, J. Li, Science review: extracellular acidosis and the immune response: clinical and physiologic implications, Crit Care 8 (2004) 331-336.

[63] A. Lardner, The effects of extracellular pH on immune function, J Leukoc Biol 69 (2001) 522-530.

[64] M. Nedergaard, R.P. Kraig, J. Tanabe, W.A. Pulsinelli, Dynamics of interstitial and intracellular pH in evolving brain infarct, Am J Physiol 260 (1991) R581-588.

[65] S.Y. Park, D.J. Bae, M.J. Kim, M.L. Piao, I.S. Kim, Extracellular low pH modulates phosphatidylserine-dependent phagocytosis in macrophages by increasing stabilin-1 expression, J Biol Chem 287 11261-11271.

[66] H.P. Simmen, J. Blaser, Analysis of pH and pO2 in abscesses, peritoneal fluid, and drainage fluid in the presence or absence of bacterial infection during and after abdominal surgery, Am J Surg 166 (1993) 24-27.

[67] H.P. Simmen, H. Battaglia, P. Giovanoli, J. Blaser, Analysis of pH, pO2 and pCO2 in drainage fluid allows for rapid detection of infectious complications during the follow-up period after abdominal surgery, Infection 22 (1994) 386-389.

[68] F. Barkas, E. Liberopoulos, A. Kei, M. Elisaf, Electrolyte and acid-base disorders in inflammatory bowel disease, Ann Gastroenterol 26 (2013) 23-28.

[69] Z. Lu, H. Gui, L. Yao, L. Yan, H. Martens, J.R. Aschenbach, Z. Shen, Short-chain fatty acids and acidic pH up-regulate UT-B, GPR41, and GPR4 in rumen epithelial cells of goats, Am J Physiol Regul Integr Comp Physiol (2014) ajpregu 00323 02014.

[70] P.B. Mortensen, M.R. Clausen, Short-chain fatty acids in the human colon: relation to gastrointestinal health and disease, Scand J Gastroenterol Suppl 216 (1996) 132-148.

[71] D.F. Evans, G. Pye, R. Bramley, A.G. Clark, T.J. Dyson, J.D. Hardcastle, Measurement of gastrointestinal pH profiles in normal ambulant human subjects, Gut 29 (1988) 1035-1041.

[72] J. Fallingborg, L.A. Christensen, B.A. Jacobsen, S.N. Rasmussen, Very low intraluminal colonic pH in patients with active ulcerative colitis, Dig Dis Sci 38 (1993) 1989-1993.

[73] J. Fallingborg, Intraluminal pH of the human gastrointestinal tract, Dan Med Bull 46 (1999) 183-196.

[74] S.G. Nugent, D. Kumar, D.S. Rampton, D.F. Evans, Intestinal luminal pH in inflammatory bowel disease: possible determinants and implications for therapy with aminosalicylates and other drugs, Gut 48 (2001) 571-577.

[75] A.G. Press, I.A. Hauptmann, L. Hauptmann, B. Fuchs, M. Fuchs, K. Ewe, G. Ramadori, Gastrointestinal pH profiles in patients with inflammatory bowel disease, Aliment Pharmacol Ther 12 (1998) 673-678.

[76] Y. Sasaki, R. Hada, H. Nakajima, S. Fukuda, A. Munakata, Improved localizing method of radiopill in measurement of entire gastrointestinal pH profiles: colonic luminal pH in normal subjects and patients with Crohn's disease, Am J Gastroenterol 92 (1997) 114-118.

[77] K. Ewe, S. Schwartz, S. Petersen, A.G. Press, Inflammation does not decrease intraluminal pH in chronic inflammatory bowel disease, Dig Dis Sci 44 (1999) 1434-1439.

[78] P. Holzer, Acid-sensitive ion channels and receptors, Handb Exp Pharmacol (2009) 283-332.

[79] J.B. Smith, S.D. Dwyer, L. Smith, Lowering Extracellular Ph Evokes Inositol Polyphosphate Formation and Calcium Mobilization, Journal of Biological Chemistry 264 (1989) 8723-8728.

[80] S.D. Dwyer, Y. Zhuang, J.B. Smith, Calcium mobilization by cadmium or decreasing extracellular Na+ or pH in coronary endothelial cells, Exp Cell Res 192 (1991) 22-31.

[81] M.G. Ludwig, M. Vanek, D. Guerini, J.A. Gasser, C.E. Jones, U. Junker, H. Hofstetter, R.M. Wolf, K. Seuwen, Proton-sensing G-protein-coupled receptors, Nature 425 (2003) 93-98.

[82] E.J. Sanderlin, C.R. Justus, E.A. Krewson, L.V. Yang, Emerging roles for the pH-sensing G protein-coupled receptors in response to acidotic stress, Cell Health Cytoskelet 7 (2015) 99-109.

[83] C.G. Radu, A. Nijagal, J. McLaughlin, L. Wang, O.N. Witte, Differential proton sensitivity of related G protein-coupled receptors T cell death-associated gene 8 and G2A expressed in immune cells, Proc Natl Acad Sci U S A 102 (2005) 1632-1637.

[84] Z. Weng, A.C. Fluckiger, S. Nisitani, M.I. Wahl, L.Q. Le, C.A. Hunter, A.A. Fernal, M.M. Le Beau, O.N. Witte, A DNA damage and stress inducible G protein-coupled receptor blocks cells in G2/M, Proc Natl Acad Sci U S A 95 (1998) 12334-12339.

[85] L.Q. Le, J.H. Kabarowski, Z. Weng, A.B. Satterthwaite, E.T. Harvill, E.R. Jensen, J.F. Miller, O.N. Witte, Mice lacking the orphan G protein-coupled receptor G2A develop a late-onset autoimmune syndrome, Immunity 14 (2001) 561-571.

[86] J.H. Kabarowski, K. Zhu, L.Q. Le, O.N. Witte, Y. Xu, Lysophosphatidylcholine as a ligand for the immunoregulatory receptor G2A, Science 293 (2001) 702-705.

[87] L. Wang, C.G. Radu, L.V. Yang, L.A. Bentolila, M. Riedinger, O.N. Witte, Lysophosphatidylcholine-induced surface redistribution regulates signaling of the murine G protein-coupled receptor G2A, Mol Biol Cell 16 (2005) 2234-2247.

[88] N. Murakami, T. Yokomizo, T. Okuno, T. Shimizu, G2A is a proton-sensing G-protein-coupled receptor antagonized by lysophosphatidylcholine, J Biol Chem 279 (2004) 42484-42491.

[89] L.J. Cohen, H.S. Kang, J. Chu, Y.H. Huang, E.A. Gordon, B.V. Reddy, M.A. Ternei, J.W. Craig, S.F. Brady, Functional metagenomic discovery of bacterial effectors in the human microbiome and isolation of commendamide, a GPCR G2A/132 agonist, Proc Natl Acad Sci U S A 112 (2015) E4825-4834.

[90] H. Obinata, T. Hattori, S. Nakane, K. Tatei, T. Izumi, Identification of 9-hydroxyoctadecadienoic acid and other oxidized free fatty acids as ligands of the G protein-coupled receptor G2A, J Biol Chem 280 (2005) 40676-40683.

[91] K. Seuwen, M.G. Ludwig, R.M. Wolf, Receptors for protons or lipid messengers or both?, J Recept Signal Transduct Res 26 (2006) 599-610.

[92] P. Chen, H. Zuo, H. Xiong, M.J. Kolar, Q. Chu, A. Saghatelian, D.J. Siegwart, Y. Wan, Gpr132 sensing of lactate mediates tumor-macrophage interplay to promote breast cancer metastasis, Proc Natl Acad Sci U S A 114 (2017) 580-585.

[93] J.L. Lahvic, M. Ammerman, P. Li, M.C. Blair, E.R. Stillman, E.M. Fast, A.L. Robertson, C. Christodoulou, J.R. Perlin, S. Yang, N. Chiang, P.C. Norris, M.L. Daily, S.E. Redfield, I.T. Chan, M. Chatrizeh, M.E. Chase, O. Weis, Y. Zhou, C.N. Serhan, L.I. Zon, Specific oxylipins enhance vertebrate hematopoiesis via the receptor GPR132, Proc Natl Acad Sci U S A 115 (2018) 9252-9257.

[94] C.G. Radu, L.V. Yang, M. Riedinger, M. Au, O.N. Witte, T cell chemotaxis to lysophosphatidylcholine through the G2A receptor, Proc Natl Acad Sci U S A 101 (2004) 245-250.

[95] D.T. Bolick, M.D. Skaflen, L.E. Johnson, S.C. Kwon, D. Howatt, A. Daugherty, K.S. Ravichandran, C.C. Hedrick, G2A deficiency in mice promotes macrophage activation and atherosclerosis, Circ Res 104 (2009) 318-327.

[96] A.J. Park, G.W. Agak, M. Qin, L.D. Hisaw, A. Pirouz, S. Kao, L.J. Marinelli, H.J. Garbán, D. Thiboutot, P.T. Liu, J. Kim, G2A Attenuates, Ann Dermatol 29 (2017) 688-698.

[97] S.C. Frasch, R.F. Fernandez-Boyanapalli, K.Z. Berry, C.C. Leslie, J.V. Bonventre, R.C. Murphy, P.M. Henson, D.L. Bratton, Signaling via macrophage G2A enhances efferocytosis of dying neutrophils by augmentation of Rac activity, J Biol Chem 286 (2011) 12108-12122.

[98] C. Peter, M. Waibel, C.G. Radu, L.V. Yang, O.N. Witte, K. Schulze-Osthoff, S. Wesselborg, K. Lauber, Migration to apoptotic "find-me" signals is mediated via the phagocyte receptor G2A, J Biol Chem 283 (2008) 5296-5305.

[99] C.W. Huang, J.N. Tzeng, Y.J. Chen, W.F. Tsai, C.C. Chen, W.H. Sun, Nociceptors of dorsal root ganglion express proton-sensing G-protein-coupled receptors, Mol Cell Neurosci 36 (2007) 195-210.

[100] J.W. Choi, S.Y. Lee, Y. Choi, Identification of a putative G protein-coupled receptor induced during activation-induced apoptosis of T cells, Cell Immunol 168 (1996) 78-84.

[101] H. Kyaw, Z. Zeng, K. Su, P. Fan, B.K. Shell, K.C. Carter, Y. Li, Cloning, characterization, and mapping of human homolog of mouse T-cell death-associated gene, DNA Cell Biol 17 (1998) 493-500.

[102] F. Okajima, Regulation of inflammation by extracellular acidification and proton-sensing GPCRs, Cell Signal 25 (2013) 2263-2271.

[103] C. Mogi, M. Tobo, H. Tomura, N. Murata, X.D. He, K. Sato, T. Kimura, T. Ishizuka, T. Sasaki, T. Sato, Y. Kihara, S. Ishii, A. Harada, F. Okajima, Involvement of proton-sensing TDAG8 in extracellular acidification-induced inhibition of proinflammatory cytokine production in peritoneal macrophages, J Immunol 182 (2009) 3243-3251.

[104] X.D. He, M. Tobo, C. Mogi, T. Nakakura, M. Komachi, N. Murata, M. Takano, H. Tomura, K. Sato, F. Okajima, Involvement of proton-sensing receptor TDAG8 in the anti-inflammatory actions of dexamethasone in peritoneal macrophages, Biochem Biophys Res Commun 415 (2011) 627-631.

[105] Y. Onozawa, Y. Fujita, H. Kuwabara, M. Nagasaki, T. Komai, T. Oda, Activation of T cell death-associated gene 8 regulates the cytokine production of T cells and macrophages in vitro, Eur J Pharmacol 683 (2012) 325-331.

[106] Y. Jin, K. Sato, A. Tobo, C. Mogi, M. Tobo, N. Murata, S. Ishii, D.S. Im, F. Okajima, Inhibition of interleukin-1beta production by extracellular acidification through the TDAG8/cAMP pathway in mouse microglia, J Neurochem 129 (2014) 683-695.

[107] A. Nagasaka, C. Mogi, H. Ono, T. Nishi, Y. Horii, Y. Ohba, K. Sato, M. Nakaya, F. Okajima, H. Kurose, The proton-sensing G protein-coupled receptor T-cell death-associated gene 8 (TDAG8) shows cardioprotective effects against myocardial infarction, Sci Rep 7 (2017) 7812.

[108] Y. Onozawa, T. Komai, T. Oda, Activation of T cell death-associated gene 8 attenuates inflammation by negatively regulating the function of inflammatory cells, Eur J Pharmacol 654 (2011) 315-319.

[109] R.C. Wirasinha, D. Vijayan, N.J. Smith, G.P. Parnell, A. Swarbrick, R. Brink, C. King, G. Stewart, D.R. Booth, M. Batten, GPR65 inhibits experimental autoimmune encephalomyelitis through CD4, Immunol Cell Biol 96 (2018) 128-136.

[110] L.C. Kottyan, A.R. Collier, K.H. Cao, K.A. Niese, M. Hedgebeth, C.G. Radu, O.N. Witte, G.K. Khurana Hershey, M.E. Rothenberg, N. Zimmermann, Eosinophil viability is increased by acidic pH in a cAMP- and GPR65-dependent manner, Blood 114 (2009) 2774-2782.

[111] J.T. Gaublomme, N. Yosef, Y. Lee, R.S. Gertner, L.V. Yang, C. Wu, P.P. Pandolfi, T. Mak, R. Satija, A.K. Shalek, V.K. Kuchroo, H. Park, A. Regev, Single-Cell Genomics Unveils Critical Regulators of Th17 Cell Pathogenicity, Cell 163 (2015) 1400-1412.

[112] M.H. Al-Mossawi, L. Chen, H. Fang, A. Ridley, J. de Wit, N. Yager, A. Hammitzsch, I. Pulyakhina, B.P. Fairfax, D. Simone, Y. Yi, S. Bandyopadhyay, K. Doig, R. Gundle, B. Kendrick, F. Powrie, J.C. Knight, P. Bowness, Unique transcriptome signatures and GM-CSF expression in lymphocytes from patients with spondyloarthritis, Nat Commun 8 (2017) 1510.

[113] A. Chen, L. Dong, N.R. Leffler, A.S. Asch, O.N. Witte, L.V. Yang, Activation of GPR4 by acidosis increases endothelial cell adhesion through the cAMP/Epac pathway, PLoS One 6 (2011) e27586.

[114] L. Dong, Z. Li, N.R. Leffler, A.S. Asch, J.T. Chi, L.V. Yang, Acidosis Activation of the Proton-Sensing GPR4 Receptor Stimulates Vascular Endothelial Cell Inflammatory Responses Revealed by Transcriptome Analysis, PLoS One 8 (2013) e61991.

[115] H. Aoki, C. Mogi, T. Hisada, T. Nakakura, Y. Kamide, I. Ichimonji, H. Tomura, M. Tobo, K. Sato, H. Tsurumaki, K. Dobashi, T. Mori, A. Harada, M. Yamada, M. Mori, T.

Ishizuka, F. Okajima, Proton-sensing ovarian cancer G protein-coupled receptor 1 on dendritic cells is required for airway responses in a murine asthma model, PLoS One 8 (2013) e79985.

[116] C. de Valliere, Y. Wang, J.J. Eloranta, S. Vidal, I. Clay, M.R. Spalinger, I. Tcymbarevich, A. Terhalle, M.G. Ludwig, T. Suply, M. Fried, G.A. Kullak-Ublick, I. Frey-Wagner, M. Scharl, K. Seuwen, C.A. Wagner, G. Rogler, G Protein-coupled pH-sensing Receptor OGR1 Is a Regulator of Intestinal Inflammation, Inflamm Bowel Dis 21 (2015) 1269-1281.

[117] S. Hutter, W.T. van Haaften, A. Hunerwadel, K. Baebler, N. Herfarth, T. Raselli, C. Mamie, B. Misselwitz, G. Rogler, B. Weder, G. Dijkstra, C.F. Meier, C. de Valliere, A. Weber, P.H. Imenez Silva, C.A. Wagner, I. Frey-Wagner, P.A. Ruiz, M. Hausmann, Intestinal activation of pH-sensing receptor OGR1 (GPR68) contributes to fibrogenesis, J Crohns Colitis (2018).

[118] A. Mizoguchi, Animal models of inflammatory bowel disease, Prog Mol Biol Transl Sci 105 (2012) 263-320.

[119] H. Laroui, S.A. Ingersoll, H.C. Liu, M.T. Baker, S. Ayyadurai, M.A. Charania, F. Laroui, Y. Yan, S.V. Sitaraman, D. Merlin, Dextran sodium sulfate (DSS) induces colitis in mice by forming nano-lipocomplexes with medium-chain-length fatty acids in the colon, PLoS One 7 (2012) e32084.

[120] B. Chassaing, J.D. Aitken, M. Malleshappa, M. Vijay-Kumar, Dextran sulfate sodium (DSS)-induced colitis in mice, Curr Protoc Immunol 104 (2014) Unit 15 25.

[121] M.L. Clapper, H.S. Cooper, W.C. Chang, Dextran sulfate sodium-induced colitis-associated neoplasia: a promising model for the development of chemopreventive interventions, Acta Pharmacol Sin 28 (2007) 1450-1459.

[122] S. Wirtz, C. Neufert, B. Weigmann, M.F. Neurath, Chemically induced mouse models of intestinal inflammation, Nat Protoc 2 (2007) 541-546.

[123] M. Perse, A. Cerar, Dextran sodium sulphate colitis mouse model: traps and tricks, J Biomed Biotechnol 2012 (2012) 718617.

[124] L. Dong, E. Krewson, D. Bliss, D.A. Tulis, L.V. Yang, Abstract 11587: Acidosis/GPR4 signaling regulates inflammatory and endoplasmic reticulum stress responses in vascular endothelial cells, Circulation 128 (2013) A11587.

[125] L.V. Yang, C.G. Radu, M. Roy, S. Lee, J. McLaughlin, M.A. Teitell, M.L. Iruela-Arispe, O.N. Witte, Vascular abnormalities in mice deficient for the G protein-coupled receptor GPR4 that functions as a pH sensor, Mol Cell Biol 27 (2007) 1334-1347.

[126] C.G. Radu, D. Cheng, A. Nijagal, M. Riedinger, J. McLaughlin, L.V. Yang, J. Johnson, O.N. Witte, Normal immune development and glucocorticoid-induced thymocyte apoptosis in mice deficient for the T-cell death-associated gene 8 receptor, Mol Cell Biol 26 (2006) 668-677.

[127] M.F. Festing, Randomized block experimental designs can increase the power and reproducibility of laboratory animal experiments, ILAR J 55 (2014) 472-476.

[128] E.J. Sanderlin, N.R. Leffler, K. Lertpiriyapong, Q. Cai, H. Hong, V. Bakthavatchalu, J.G. Fox, J.Z. Oswald, C.R. Justus, E.A. Krewson, D. O'Rourke, L.V. Yang, GPR4 deficiency alleviates intestinal inflammation in a mouse model of acute experimental colitis, Biochim Biophys Acta 1863 (2016) 569-584.

[129] U. Erben, C. Loddenkemper, K. Doerfel, S. Spieckermann, D. Haller, M.M. Heimesaat, M. Zeitz, B. Siegmund, A.A. Kuhl, A guide to histomorphological evaluation of intestinal inflammation in mouse models, Int J Clin Exp Pathol 7 (2014) 4557-4576.

[130] W. Wang, J. Li, K. Wu, B. Azhati, M. Rexiati, Culture and Identification of Mouse Bone Marrow-Derived Dendritic Cells and Their Capability to Induce T Lymphocyte Proliferation, Med Sci Monit 22 (2016) 244-250.

[131] W. Ying, P.S. Cheruku, F.W. Bazer, S.H. Safe, B. Zhou, Investigation of macrophage polarization using bone marrow derived macrophages, J Vis Exp (2013).

[132] R.V. Alka Madaan, Anu T Singh, Swatantra Kumar Jain, Manu Jaggi, A stepwise procedure for isolation of murine bone marrow and generation of dendritic cells, Journal of Biological Methods 1 (2014).

[133] C.R. Justus, N. Leffler, M. Ruiz-Echevarria, L.V. Yang, In vitro cell migration and invasion assays, J Vis Exp (2014).

[134] M.S. Mahadevan, S. Baird, J.E. Bailly, G.G. Shutler, L.A. Sabourin, C. Tsilfidis, C.E. Neville, M. Narang, R.G. Korneluk, Isolation of a novel G protein-coupled receptor (GPR4) localized to chromosome 19q13.3, Genomics 30 (1995) 84-88.

[135] L. Dong, Z. Li, L.V. Yang, Function and signaling of the pH-sensing G protein-coupled receptors in physiology and diseases, in: J.T. Chi (Ed.), Molecular Genetics of Dysregulated pH Homeostasis, Springer, New York, 2014, pp. 45-65.

[136] C.R. Justus, L. Dong, L.V. Yang, Acidic tumor microenvironment and pH-sensing G protein-coupled receptors, Front Physiol 4 (2013) 354.

[137] C.R. Justus, E.J. Sanderlin, L. Dong, T. Sun, J.T. Chi, K. Lertpiriyapong, L.V. Yang, Contextual tumor suppressor function of T cell death-associated gene 8 (TDAG8) in hematological malignancies, J Transl Med 15 (2017) 204.

[138] J.P. Liu, T. Nakakura, H. Tomura, M. Tobo, C. Mogi, J.Q. Wang, X.D. He, M. Takano, A. Damirin, M. Komachi, K. Sato, F. Okajima, Each one of certain histidine residues in G-protein-coupled receptor GPR4 is critical for extracellular proton-induced stimulation of multiple G-protein-signaling pathways, Pharmacol Res 61 (2010) 499-505.

[139] I.C. Taracido, E.M. Harrington, R. Hersperger, R. Lattmann, W. Miltz, K. Weigand, Imidazo pyridine derivatives, vol. US 2009/0291942 A1, Novartis Institute for Biomedical Research, Inc., United States, 2009, pp. 1-50.

[140] H. Lum, J. Qiao, R.J. Walter, F. Huang, P.V. Subbaiah, K.S. Kim, O. Holian, Inflammatory stress increases receptor for lysophosphatidylcholine in human microvascular endothelial cells, Am J Physiol Heart Circ Physiol 285 (2003) H1786-1789.

[141] D.W. Edlow, W.H. Sheldon, The pH of inflammatory exudates, Proc Soc Exp Biol Med 137 (1971) 1328-1332.

[142] T.T. Ward, R.T. Steigbigel, Acidosis of synovial fluid correlates with synovial fluid leukocytosis, Am J Med 64 (1978) 933-936.

[143] K.M. Latson, J.E. Nieto, P.M. Beldomenico, J.R. Snyder, Evaluation of peritoneal fluid lactate as a marker of intestinal ischaemia in equine colic, Equine Vet J 37 (2005) 342-346.

[144] P. Vernia, R. Caprilli, G. Latella, F. Barbetti, F.M. Magliocca, M. Cittadini, Fecal lactate and ulcerative colitis, Gastroenterology 95 (1988) 1564-1568.

[145] W.E. Cromer, J.M. Mathis, D.N. Granger, G.V. Chaitanya, J.S. Alexander, Role of the endothelium in inflammatory bowel diseases, World J Gastroenterol 17 (2011) 578-593.

[146] D. Guagnozzi, R. Caprilli, Natalizumab in the treatment of Crohn's disease, Biologics 2 (2008) 275-284.

[147] L.P. McLean, T. Shea-Donohue, R.K. Cross, Vedolizumab for the treatment of ulcerative colitis and Crohn's disease, Immunotherapy 4 (2012) 883-898.

[148] Q.Y. Lean, R.D. Eri, S. Randall-Demllo, S.S. Sohal, N. Stewart, G.M. Peterson, N. Gueven, R.P. Patel, Orally Administered Enoxaparin Ameliorates Acute Colitis by Reducing Macrophage-Associated Inflammatory Responses, PLoS One 10 (2015) e0134259.

[149] S.M. Farooq, R. Stillie, M. Svensson, C. Svanborg, R.M. Strieter, A.W. Stadnyk, Therapeutic effect of blocking CXCR2 on neutrophil recruitment and dextran sodium sulfate-induced colitis, J Pharmacol Exp Ther 329 (2009) 123-129.

[150] T. Vowinkel, M. Mori, C.F. Krieglstein, J. Russell, F. Saijo, S. Bharwani, R.H. Turnage, W.S. Davidson, P. Tso, D.N. Granger, T.J. Kalogeris, Apolipoprotein A-IV inhibits experimental colitis, J Clin Invest 114 (2004) 260-269.

[151] R.G. Lorenz, D.D. Chaplin, K.G. McDonald, J.S. McDonough, R.D. Newberry, Isolated lymphoid follicle formation is inducible and dependent upon lymphotoxin-sufficient B lymphocytes, lymphotoxin beta receptor, and TNF receptor I function, J Immunol 170 (2003) 5475-5482.

[152] R.G. Lorenz, R.D. Newberry, Isolated lymphoid follicles can function as sites for induction of mucosal immune responses, Ann N Y Acad Sci 1029 (2004) 44-57.

[153] M. Tsuji, K. Suzuki, H. Kitamura, M. Maruya, K. Kinoshita, Ivanov, II, K. Itoh, D.R. Littman, S. Fagarasan, Requirement for lymphoid tissue-inducer cells in isolated follicle formation and T cell-independent immunoglobulin A generation in the gut, Immunity 29 (2008) 261-271.

[154] M.M. Yeung, S. Melgar, V. Baranov, A. Oberg, A. Danielsson, S. Hammarstrom, M.L. Hammarstrom, Characterisation of mucosal lymphoid aggregates in ulcerative colitis: immune cell phenotype and TcR-gammadelta expression, Gut 47 (2000) 215-227.

[155] N. Shah, B. Thakkar, E. Shen, M. Loh, P.Y. Chong, W.H. Gan, T.M. Tu, L. Shen, R. Soong, M. Salto-Tellez, Lymphocytic follicles and aggregates are a determinant of mucosal damage and duration of diarrhea, Arch Pathol Lab Med 137 (2013) 83-89.

[156] K. Lauber, E. Bohn, S.M. Krober, Y.J. Xiao, S.G. Blumenthal, R.K. Lindemann, P. Marini, C. Wiedig, A. Zobywalski, S. Baksh, Y. Xu, I.B. Autenrieth, K. Schulze-Osthoff, C. Belka, G. Stuhler, S. Wesselborg, Apoptotic cells induce migration of phagocytes via caspase-3-mediated release of a lipid attraction signal, Cell 113 (2003) 717-730.

[157] B. Vainer, O.H. Nielsen, T. Horn, Expression of E-selectin, sialyl Lewis X, and macrophage inflammatory protein-1alpha by colonic epithelial cells in ulcerative colitis, Dig Dis Sci 43 (1998) 596-608.

[158] T. Ulyanova, L.M. Scott, G.V. Priestley, Y. Jiang, B. Nakamoto, P.A. Koni, T. Papayannopoulou, VCAM-1 expression in adult hematopoietic and nonhematopoietic cells is controlled by tissue-inductive signals and reflects their developmental origin, Blood 106 (2005) 86-94.

[159] M.W. Epperly, C.A. Sikora, S.J. DeFilippi, J.E. Gretton, D. Bar-Sagi, H. Archer, T. Carlos, H. Guo, J.S. Greenberger, Pulmonary irradiation-induced expression of VCAM-I

and ICAM-I is decreased by manganese superoxide dismutase-plasmid/liposome (MnSOD-PL) gene therapy, Biol Blood Marrow Transplant 8 (2002) 175-187.

[160] A. Bajnok, M. Ivanova, J. Rigo, Jr., G. Toldi, The Distribution of Activation Markers and Selectins on Peripheral T Lymphocytes in Preeclampsia, Mediators Inflamm 2017 (2017) 8045161.

[161] S. Harashima, T. Horiuchi, N. Hatta, C. Morita, M. Higuchi, T. Sawabe, H. Tsukamoto, T. Tahira, K. Hayashi, S. Fujita, Y. Niho, Outside-to-inside signal through the membrane TNF-alpha induces E-selectin (CD62E) expression on activated human CD4+ T cells, J Immunol 166 (2001) 130-136.

[162] A. Tobo, M. Tobo, T. Nakakura, M. Ebara, H. Tomura, C. Mogi, D.S. Im, N. Murata, A. Kuwabara, S. Ito, H. Fukuda, M. Arisawa, S. Shuto, M. Nakaya, H. Kurose, K. Sato, F. Okajima, Characterization of Imidazopyridine Compounds as Negative Allosteric Modulators of Proton-Sensing GPR4 in Extracellular Acidification-Induced Responses, PLoS One 10 (2015) e0129334.

[163] D. Lagadic-Gossmann, L. Huc, V. Lecureur, Alterations of intracellular pH homeostasis in apoptosis: origins and roles, Cell Death Differ 11 (2004) 953-961.

[164] B.K. Siesjo, K. Katsura, T. Kristian, Acidosis-related damage, Adv Neurol 71 (1996) 209-233; discussion 234-206.

[165] B.K. Siesjo, K.I. Katsura, T. Kristian, P.A. Li, P. Siesjo, Molecular mechanisms of acidosis-mediated damage, Acta Neurochir Suppl 66 (1996) 8-14.

[166] X. Sun, L.V. Yang, B.C. Tiegs, L.J. Arend, D.W. McGraw, R.B. Penn, S. Petrovic, Deletion of the pH sensor GPR4 decreases renal acid excretion, J Am Soc Nephrol 21 (2010) 1745-1755.

[167] N.N. Kumar, A. Velic, J. Soliz, Y. Shi, K. Li, S. Wang, J.L. Weaver, J. Sen, S.B. Abbott, R.M. Lazarenko, M.G. Ludwig, E. Perez-Reyes, N. Mohebbi, C. Bettoni, M. Gassmann, T. Suply, K. Seuwen, P.G. Guyenet, C.A. Wagner, D.A. Bayliss, PHYSIOLOGY. Regulation of breathing by CO(2) requires the proton-activated receptor GPR4 in retrotrapezoid nucleus neurons, Science 348 (2015) 1255-1260.

[168] A. Franke, D.P. McGovern, J.C. Barrett, K. Wang, G.L. Radford-Smith, T. Ahmad, C.W. Lees, T. Balschun, J. Lee, R. Roberts, C.A. Anderson, J.C. Bis, S. Bumpstead, D. Ellinghaus, E.M. Festen, M. Georges, T. Green, T. Haritunians, L. Jostins, A. Latiano, C.G. Mathew, G.W. Montgomery, N.J. Prescott, S. Raychaudhuri, J.I. Rotter, P. Schumm, Y. Sharma, L.A. Simms, K.D. Taylor, D. Whiteman, C. Wijmenga, R.N. Baldassano, M. Barclay, T.M. Bayless, S. Brand, C. Buning, A. Cohen, J.F. Colombel, M. Cottone, L. Stronati, T. Denson, M. De Vos, R. D'Inca, M. Dubinsky, C. Edwards, T. Florin, D. Franchimont, R. Gearry, J. Glas, A. Van Gossum, S.L. Guthery, J. Halfvarson, H.W. Verspaget, J.P. Hugot, A. Karban, D. Laukens, I. Lawrance, M. Lemann, A. Levine, C. Libioulle, E. Louis, C. Mowat, W. Newman, J. Panes, A. Phillips, D.D. Proctor, M. Regueiro, R. Russell, P. Rutgeerts, J. Sanderson, M. Sans, F. Seibold, A.H. Steinhart, P.C. Stokkers, L. Torkvist, G. Kullak-Ublick, D. Wilson, T. Walters, S.R. Targan, S.R. Brant, J.D. Rioux, M. D'Amato, R.K. Weersma, S. Kugathasan, A.M. Griffiths, J.C. Mansfield, S. Vermeire, R.H. Duerr, M.S. Silverberg, J. Satsangi, S. Schreiber, J.H. Cho, V. Annese, H. Hakonarson, M.J. Daly, M. Parkes, Genome-wide meta-analysis increases to 71 the number of confirmed Crohn's disease susceptibility loci, Nat Genet 42 (2010) 1118-1125.

[169] K.G. Lassen, C.I. McKenzie, M. Mari, T. Murano, J. Begun, L.A. Baxt, G. Goel, E.J. Villablanca, S.Y. Kuo, H. Huang, L. Macia, A.K. Bhan, M. Batten, M.J. Daly, F. Reggiori, C.R. Mackay, R.J. Xavier, Genetic Coding Variant in GPR65 Alters Lysosomal pH and Links Lysosomal Dysfunction with Colitis Risk, Immunity (2016).

[170] G.J. Marlow, D. van Gent, L.R. Ferguson, Why interleukin-10 supplementation does not work in Crohn's disease patients, World J Gastroenterol 19 (2013) 3931-3941.

[171] H. Fukuda, S. Ito, K. Watari, C. Mogi, M. Arisawa, F. Okajima, H. Kurose, S. Shuto, Identification of a Potent and Selective GPR4 Antagonist as a Drug Lead for the Treatment of Myocardial Infarction, ACS Med Chem Lett 7 (2016) 493-497.

[172] J. Velcicky, W. Miltz, B. Oberhauser, D. Orain, A. Vaupel, K. Weigand, J. Dawson King, A. Littlewood-Evans, M. Nash, R. Feifel, P. Loetscher, Development of Selective, Orally Active GPR4 Antagonists with Modulatory Effects on Nociception, Inflammation, and Angiogenesis, J Med Chem 60 (2017) 3672-3683.

[173] P.S. Hosford, V. Mosienko, K. Kishi, G. Jurisic, K. Seuwen, B. Kinzel, M.G. Ludwig, J.A. Wells, I.N. Christie, L. Koolen, A.P. Abdala, B.H. Liu, A.V. Gourine, A.G. Teschemacher, S. Kasparov, CNS distribution, signalling properties and central effects of G-protein coupled receptor 4, Neuropharmacology 138 (2018) 381-392.

[174] I.E. Koutroubakis, G. Tsiolakidou, K. Karmiris, E.A. Kouroumalis, Role of angiogenesis in inflammatory bowel disease, Inflamm Bowel Dis 12 (2006) 515-523.

[175] S. Danese, M. Sans, C. de la Motte, C. Graziani, G. West, M.H. Phillips, R. Pola, S. Rutella, J. Willis, A. Gasbarrini, C. Fiocchi, Angiogenesis as a novel component of inflammatory bowel disease pathogenesis, Gastroenterology 130 (2006) 2060-2073.

[176] P. Liu, Y. Lu, H. Liu, W. Wen, D. Jia, Y. Wang, M. You, Genome-wide association and fine mapping of genetic loci predisposing to colon carcinogenesis in mice, Mol Cancer Res 10 (2012) 66-74.

[177] S. Ishii, Y. Kihara, T. Shimizu, Identification of T cell death-associated gene 8 (TDAG8) as a novel acid sensing G-protein-coupled receptor, J Biol Chem 280 (2005) 9083-9087.

[178] C.R. Justus, E.J. Sanderlin, L.V. Yang, Molecular Connections between Cancer Cell Metabolism and the Tumor Microenvironment, Int J Mol Sci 16 (2015) 11055-11086.

[179] H. Tsurumaki, C. Mogi, H. Aoki-Saito, M. Tobo, Y. Kamide, M. Yatomi, K. Sato, K. Dobashi, T. Ishizuka, T. Hisada, M. Yamada, F. Okajima, Protective Role of Proton-Sensing TDAG8 in Lipopolysaccharide-Induced Acute Lung Injury, Int J Mol Sci 16 (2015) 28931-28942.

[180] F. Rieder, J. Brenmoehl, S. Leeb, J. Scholmerich, G. Rogler, Wound healing and fibrosis in intestinal disease, Gut 56 (2007) 130-139.

[181] V.K. Raker, C. Becker, K. Steinbrink, The cAMP Pathway as Therapeutic Target in Autoimmune and Inflammatory Diseases, Front Immunol 7 (2016) 123.

[182] W. Strober, I.J. Fuss, Proinflammatory cytokines in the pathogenesis of inflammatory bowel diseases, Gastroenterology 140 (2011) 1756-1767.

[183] G. Latella, R. Sferra, S. Speca, A. Vetuschi, E. Gaudio, Can we prevent, reduce or reverse intestinal fibrosis in IBD?, Eur Rev Med Pharmacol Sci 17 (2013) 1283-1304.

[184] F. Rieder, C. Fiocchi, Intestinal fibrosis in inflammatory bowel disease: progress in basic and clinical science, Curr Opin Gastroenterol 24 (2008) 462-468.

[185] R.C. Stone, I. Pastar, N. Ojeh, V. Chen, S. Liu, K.I. Garzon, M. Tomic-Canic, Epithelial-mesenchymal transition in tissue repair and fibrosis, Cell Tissue Res 365 (2016) 495-506.

[186] V. Valatas, E. Filidou, I. Drygiannakis, G. Kolios, Stromal and immune cells in gut fibrosis: the myofibroblast and the scarface, Ann Gastroenterol 30 (2017) 393-404.

[187] M. Spadaccini, S. D'Alessio, L. Peyrin-Biroulet, S. Danese, PDE4 Inhibition and Inflammatory Bowel Disease: A Novel Therapeutic Avenue, Int J Mol Sci 18 (2017).

[188] X.D. Ma, L.H. Hang, D.H. Shao, W.W. Shu, X.L. Hu, H. Luo, TDAG8 activation attenuates cerebral ischaemia-reperfusion injury via Akt signalling in rats, Exp Neurol 293 (2017) 115-123.

[189] M. Bercher, B. Hanson, C. van Staden, K. Wu, G.Y. Ng, P.H. Lee, Agonists of the orphan human G2A receptor identified from inducible G2A expression and beta-lactamase reporter screen, Assay Drug Dev Technol 7 (2009) 133-142.

[190] T. Hattori, H. Obinata, A. Ogawa, M. Kishi, K. Tatei, O. Ishikawa, T. Izumi, G2A plays proinflammatory roles in human keratinocytes under oxidative stress as a receptor for 9-hydroxyoctadecadienoic acid, J Invest Dermatol 128 (2008) 1123-1133.

[191] Z. Kmieć, M. Cyman, T.J. Ślebioda, Cells of the innate and adaptive immunity and their interactions in inflammatory bowel disease, Adv Med Sci 62 (2017) 1-16.

[192] C. Chelakkot, J. Ghim, S.H. Ryu, Mechanisms regulating intestinal barrier integrity and its pathological implications, Exp Mol Med 50 (2018) 103.

[193] S.C. Frasch, E.N. McNamee, D. Kominsky, P. Jedlicka, C. Jakubzick, K. Zemski Berry, M. Mack, G.T. Furuta, J.J. Lee, P.M. Henson, S.P. Colgan, D.L. Bratton, G2A Signaling Dampens Colitic Inflammation via Production of IFN-γ, J Immunol 197 (2016) 1425-1434.

[194] H. Hasegawa, J. Lei, T. Matsumoto, S. Onishi, K. Suemori, M. Yasukawa, Lysophosphatidylcholine enhances the suppressive function of human naturally occurring

regulatory T cells through TGF-beta production, Biochem Biophys Res Commun 415 (2011) 526-531.

[195] Y. Wang, C. de Valliere, P.H. Imenez Silva, I. Leonardi, S. Gruber, A. Gerstgrasser, H. Melhem, A. Weber, K. Leucht, L. Wolfram, M. Hausmann, C. Krieg, K. Thomasson, O. Boyman, I. Frey-Wagner, G. Rogler, C.A. Wagner, The Proton-activated Receptor GPR4 Modulates Intestinal Inflammation, J Crohns Colitis 12 (2018) 355-368.

[196] L. Dong, E.A. Krewson, L.V. Yang, Acidosis Activates Endoplasmic Reticulum Stress Pathways through GPR4 in Human Vascular Endothelial Cells, Int J Mol Sci 18 (2017).

[197] A. Kaser, T.E. Adolph, R.S. Blumberg, The unfolded protein response and gastrointestinal disease, Semin Immunopathol 35 (2013) 307-319.

[198] A. Kaser, A.H. Lee, A. Franke, J.N. Glickman, S. Zeissig, H. Tilg, E.E. Nieuwenhuis, D.E. Higgins, S. Schreiber, L.H. Glimcher, R.S. Blumberg, XBP1 links ER stress to intestinal inflammation and confers genetic risk for human inflammatory bowel disease, Cell 134 (2008) 743-756.

[199] C. Hetz, The unfolded protein response: controlling cell fate decisions under ER stress and beyond, Nat Rev Mol Cell Biol 13 89-102.

[200] P. Walter, D. Ron, The unfolded protein response: from stress pathway to homeostatic regulation, Science 334 (2011) 1081-1086.

[201] K. Zhang, R.J. Kaufman, From endoplasmic-reticulum stress to the inflammatory response, Nature 454 (2008) 455-462.

[202] T. Fritz, L. Niederreiter, T. Adolph, R.S. Blumberg, A. Kaser, Crohn's disease: NOD2, autophagy and ER stress converge, Gut 60 (2011) 1580-1588.

[203] S. Bogaert, M. De Vos, K. Olievier, H. Peeters, D. Elewaut, B. Lambrecht, P. Pouliot, D. Laukens, Involvement of endoplasmic reticulum stress in inflammatory bowel disease: a different implication for colonic and ileal disease?, PLoS One 6 (2011) e25589.

[204] M.A. McGuckin, R.D. Eri, I. Das, R. Lourie, T.H. Florin, ER stress and the unfolded protein response in intestinal inflammation, Am J Physiol Gastrointest Liver Physiol 298 (2010) G820-832.

[205] P.S. Gargalovic, N.M. Gharavi, M.J. Clark, J. Pagnon, W.P. Yang, A. He, A. Truong, T. Baruch-Oren, J.A. Berliner, T.G. Kirchgessner, A.J. Lusis, The unfolded protein response is an important regulator of inflammatory genes in endothelial cells, Arterioscler Thromb Vasc Biol 26 (2006) 2490-2496.

[206] J. Li, J.J. Wang, Q. Yu, M. Wang, S.X. Zhang, Endoplasmic reticulum stress is implicated in retinal inflammation and diabetic retinopathy, FEBS Lett 583 (2009) 1521-1527.

[207] N. Murata, C. Mogi, M. Tobo, T. Nakakura, K. Sato, H. Tomura, F. Okajima, Inhibition of superoxide anion production by extracellular acidification in neutrophils, Cell Immunol 259 (2009) 21-26.

[208] L.H. Hang, J.P. Yang, W. Yin, L.N. Wang, F. Guo, F.H. Ji, D.H. Shao, Q.N. Xu, X.Y. Wang, J.L. Zuo, Activation of spinal TDAG8 and its downstream PKA signaling pathway contribute to bone cancer pain in rats, Eur J Neurosci 36 (2012) 2107-2117.

[209] J.Q. Wang, J. Kon, C. Mogi, M. Tobo, A. Damirin, K. Sato, M. Komachi, E. Malchinkhuu, N. Murata, T. Kimura, A. Kuwabara, K. Wakamatsu, H. Koizumi, T. Uede, G. Tsujimoto, H. Kurose, T. Sato, A. Harada, N. Misawa, H. Tomura, F. Okajima,

TDAG8 is a proton-sensing and psychosine-sensitive G-protein-coupled receptor, J Biol Chem 279 (2004) 45626-45633.

[210] A. Keshavarzian, E. Mutlu, J.P. Guzman, C. Forsyth, A. Banan, Phosphodiesterase 4 inhibitors and inflammatory bowel disease: emerging therapies in inflammatory bowel disease, Expert Opin Investig Drugs 16 (2007) 1489-1506.

[211] M.A. Maxwell, G.E. Muscat, The NR4A subgroup: immediate early response genes with pleiotropic physiological roles, Nucl Recept Signal 4 (2006) e002.

[212] J. Bystrom, I. Evans, J. Newson, M. Stables, I. Toor, N. van Rooijen, M. Crawford, P. Colville-Nash, S. Farrow, D.W. Gilroy, Resolution-phase macrophages possess a unique inflammatory phenotype that is controlled by cAMP, Blood 112 (2008) 4117-4127.

[213] E.A. Wall, J.R. Zavzavadjian, M.S. Chang, B. Randhawa, X. Zhu, R.C. Hsueh, J. Liu, A. Driver, X.R. Bao, P.C. Sternweis, M.I. Simon, I.D. Fraser, Suppression of LPS-induced TNF-alpha production in macrophages by cAMP is mediated by PKA-AKAP95-p105, Sci Signal 2 (2009) ra28.

[214] J.C. Eby, M.C. Gray, E.L. Hewlett, Cyclic AMP-mediated suppression of neutrophil extracellular trap formation and apoptosis by the Bordetella pertussis adenylate cyclase toxin, Infect Immun 82 (2014) 5256-5269.

[215] W. Bäumer, J. Hoppmann, C. Rundfeldt, M. Kietzmann, Highly selective phosphodiesterase 4 inhibitors for the treatment of allergic skin diseases and psoriasis, Inflamm Allergy Drug Targets 6 (2007) 17-26.

[216] S. Oger, C. Méhats, E. Dallot, D. Cabrol, M.J. Leroy, Evidence for a role of phosphodiesterase 4 in lipopolysaccharide-stimulated prostaglandin E2 production and

matrix metalloproteinase-9 activity in human amniochorionic membranes, J Immunol 174 (2005) 8082-8089.

[217] T. Vang, K.M. Torgersen, V. Sundvold, M. Saxena, F.O. Levy, B.S. Skålhegg, V. Hansson, T. Mustelin, K. Taskén, Activation of the COOH-terminal Src kinase (Csk) by cAMP-dependent protein kinase inhibits signaling through the T cell receptor, J Exp Med 193 (2001) 497-507.

[218] K. Liopeta, S. Boubali, L. Virgilio, G. Thyphronitis, G. Mavrothalassitis, G. Dimitracopoulos, F. Paliogianni, cAMP regulates IL-10 production by normal human T lymphocytes at multiple levels: a potential role for MEF2, Mol Immunol 46 (2009) 345-354.

[219] X. Li, F. Murray, N. Koide, J. Goldstone, S.M. Dann, J. Chen, S. Bertin, G. Fu, L.S. Weinstein, M. Chen, M. Corr, L. Eckmann, P.A. Insel, E. Raz, Divergent requirement for Gαs and cAMP in the differentiation and inflammatory profile of distinct mouse Th subsets, J Clin Invest 122 (2012) 963-973.

[220] R.A. Isidro, C.B. Appleyard, Colonic macrophage polarization in homeostasis, inflammation, and cancer, Am J Physiol Gastrointest Liver Physiol 311 (2016) G59-73.

[221] E.C. Steinbach, S.E. Plevy, The role of macrophages and dendritic cells in the initiation of inflammation in IBD, Inflamm Bowel Dis 20 (2014) 166-175.

[222] K. Prame Kumar, A.J. Nicholls, C.H.Y. Wong, Partners in crime: neutrophils and monocytes/macrophages in inflammation and disease, Cell Tissue Res 371 (2018) 551-565.

[223] A.M. Smith, F.Z. Rahman, B. Hayee, S.J. Graham, D.J. Marks, G.W. Sewell, C.D. Palmer, J. Wilde, B.M. Foxwell, I.S. Gloger, T. Sweeting, M. Marsh, A.P. Walker, S.L.

Bloom, A.W. Segal, Disordered macrophage cytokine secretion underlies impaired acute inflammation and bacterial clearance in Crohn's disease, J Exp Med 206 (2009) 1883-1897.

[224] W. Ohashi, K. Hattori, Y. Hattori, Control of Macrophage Dynamics as a Potential Therapeutic Approach for Clinical Disorders Involving Chronic Inflammation, J Pharmacol Exp Ther 354 (2015) 240-250.

APPENDIX A: Animal use protocols

East Carolina University

Animal Care and Use Commitee
212 Ed Warren Life Sciences Building
East Carolina University
Greenville, NC 27834

252-744-2436 office
252-744-2355 fax

June 10, 2014

Kvin Lertpiriyapong, DVM
Department of Comparative Medicine
208 Life Sciences Building
ECU Brody School of Medicine

Dear Dr. Lertpiriyapong:

Your Animal Use Protocol entitled, "Roles of G-Protein Coupled Receptor Genes in Inflammatory Bowel Diseases and Gastrointestinal Carcinogenesis" (AUP #Z157) was reviewed by this institution's Animal Care and Use Committee on 6/10/14. The following action was taken by the Committee:

"Approved as submitted"

Please contact Dale Aycock at 744-2997 prior to hazard use

A copy is enclosed for your laboratory files. Please be reminded that all animal procedures must be conducted as described in the approved Animal Use Protocol. Modifications of these procedures cannot be performed without prior approval of the ACUC. The Animal Welfare Act and Public Health Service Guidelines require the ACUC to suspend activities not in accordance with approved procedures and report such activities to the responsible University Official (Vice Chancellor for Health Sciences or Vice Chancellor for Academic Affairs) and appropriate federal Agencies. **Please ensure that all personnel associated with this protocol have access to this approved copy of the AUP and are familiar with its contents.**

Sincerely yours,

Susan McRae, Ph.D.
Chair, Animal Care and Use Committee

SM/jd

Enclosure

East Carolina University
Tomorrow starts here.

Animal Care and
Use Committee
212 Ed Warren Life
Sciences Building
East Carolina University
Greenville, NC 27834-4354

252-744-2436 office
252-744-2355 fax

April 25, 2017

Li Yang, Ph.D.
Department of Internal Medicine
Brody 3E-127
East Carolina University

Dear Dr. Yang:

Your Animal Use Protocol entitled, "Roles of G-Protein Coupled Receptor Genes in Inflammatory Bowel Diseases and Gastrointestinal Carcinogenesis" (AUP #Z157a) was reviewed by this institution's Animal Care and Use Committee on April 25, 2017. The following action was taken by the Committee:

"Approved as submitted"

Please contact Aaron Hinkle at 744-2997 prior to hazard use

A copy is enclosed for your laboratory files. Please be reminded that all animal procedures must be conducted as described in the approved Animal Use Protocol. Modifications of these procedures cannot be performed without prior approval of the ACUC. The Animal Welfare Act and Public Health Service Guidelines require the ACUC to suspend activities not in accordance with approved procedures and report such activities to the responsible University Official (Vice Chancellor for Health Sciences or Vice Chancellor for Academic Affairs) and appropriate federal Agencies. **Please ensure that all personnel associated with this protocol have access to this approved copy of the AUP and are familiar with its contents.**

Sincerely yours,

Susan McRae, Ph.D.
Chair, Animal Care and Use Committee

SM/jd

Enclosure

APPENDIX B: Biological safety protocols

Laboratory Safety Plan for Dextran Sulfate Sodium Salt (DSS) Administration in mice

***Process**	Dextran Sulfate Sodium Salt (DSS) in water bottles of mice
***Hazardous Chemical/ Chemical Class**	Dextran Sulfate Sodium Salt Hazard Class: Non-hazardous
***Hazardous Equipment**	N/A
***Potential Hazards**	May be harmful if ingested. Slight possibility of irritation to respiratory tract.
***Personal Protective Equipment**	Safety glasses/goggles; chemical resistant gloves (e.g. nitrile), non or low permeation disposable gowns; close toed shoes, long pants
***Engineering and Ventilation Controls**	Handling and preparation from powder to solution should be completed in a certified chemical fume hood/biosafety cabinet. Before removing from hood, wet wipe and ensure container is securely closed.
Designated Use Area for Carcinogens, Reproductive Toxins or Acute Toxins	Substance is considered non-hazardous.
Special Use Procedures	N/A
Special Handling and Storage Requirements	This material should be stored in a tightly sealed container in a cool, dry, well-ventilated area. Store with chemicals of same hazard classification. Store at 15-30°C away from ignition sources.
***Spill and Accident Procedures**	For small spills dilute with water and use absorbent material to clean spill area. Place used material in an appropriate waste container for EH&S pickup and ventilate area. If large spills, contact EH&S for cleanup.
***Waste Minimization Plan**	Use minimum amount of chemicals for each experiment
***Hazardous Waste Disposal**	Diluted amounts of DSS (amounts in water bottles) can be drained disposed with copious amounts of water. If undiluted or powder form, discard through EH&S Hazardous Waste Management.
Decontamination Procedures	If necessary hood will be decontaminated at the end of each work session wiping interior surface from top to bottom then back to front.
Animal Care Precautions	Animal care workers should wear standard PPE.
***Chemical Procurement**	Smallest quantity required will be purchased
***Revision Date**	June 20, 2013

6-10-14

Laboratory Safety Plan for GPR4-Inhibitor Compound 13

***Process**	Oral dose of GPR4-Inhibitor Compound 13
***Hazardous Chemical** **Chemical Class**	GPR4-inhibitor compound 13 Target Organ: GPR4 gene and inflammatory genes
***Hazardous Equipment**	N/A
***Potential Hazards**	Prolonged or repeated contact may cause skin or eye irritation. Harmful if ingested or inhaled. It is a drug that is used to suppress the increase in expression of a number of inflammatory genes regulated by from the ~~encoded~~ GPR4 gene.
***Personal Protective Equipment**	Chemical safety glasses/goggles; chemical resistant gloves (e.g. Nitrile); full buttoned front or back closing lab coat; long pants, closed toed shoes.
***Engineering and Ventilation Controls**	All handling and preparation will be in a certified fume hood/ biosafety cabinet under sterile conditions. The floor of the hood will be covered with plastic backed paper liner. All extraneous equipment will be removed from the hood before work begins. All equipment required for preparing the solutions should be in place before continuing with chemical. Containers containing these materials can only be removed from flume hood if tightly capped and the exterior wet wiped.
Designated Use Area of Carcinogens, Reproductive Toxins or Acute Toxins	N/A
Special Use Procedures	Container of this chemical should be removed from hood only when tightly capped. Store away from incompatibles: Acids, bases, and oxidizers.
Special Handling and Storage Requirements	Avoid prolonged contact with skin or eyes. Wash hands thoroughly after handling. Avoid contact with acids, bases, and oxidizers. Should be kept below 40 degree Celsius at all times. Keep container tightly closed in a dry and well-ventilated place. Keep in a dry place. Keep away from freezing and extreme heat.
***Spill and Accident Procedures**	Clean spills only if proper materials are available and if researcher is properly trained to do so. All other spills should be reported to EH&S for clean-up. Avoid breathing vapors, mist, or gas. Ensure adequate ventilation is present. Prevent further leakage or spillage if safe to do so. Do not let product enter drains. Pick up and arrange disposal in a tightly sealed container. Sweep up and shovel. Keep in suitable, closed containers for disposal. PPE as listed above must be worn during spill and accident procedures.
***Waste Minimization Plan**	Use minimum amount of chemicals for each experiment
***Hazardous Waste Disposal**	Disposable of hazardous waste shall be completed by EH&S Waste Management. Collect and store hazardous waste according to federal, state and university regulations. Empty containers should be rinsed three times with water and disposed as normal trash.
Decontamination Procedures	If necessary hood will be decontaminated by removing the paper liner and wiping the hood interior surfaces from top to bottom then back to front with soap and water. (PPE as listed above must be worn during decontamination.)
Animal Care Precautions	Animal care workers in this area should wear standard required PPE.
***Chemical Procurement**	Smallest quantity required will be purchased
***Revision Date**	July 20, 2017

Kelly S Shook 7/26/17

Appendix C: Elsevier License to Publish